

# Sheffield Hallam University

*Monte Carlo simulations of amphiphilic systems.*

DESPLAT, Jean-Christophe C.

Available from the Sheffield Hallam University Research Archive (SHURA) at:

<http://shura.shu.ac.uk/19557/>

## A Sheffield Hallam University thesis

This thesis is protected by copyright which belongs to the author.

The content must not be changed in any way or sold commercially in any format or medium without the formal permission of the author.

When referring to this work, full bibliographic details including the author, title, awarding institution and date of the thesis must be given.

Please visit <http://shura.shu.ac.uk/19557/> and <http://shura.shu.ac.uk/information.html> for further details about copyright and re-use permissions.

# MONTE CARLO SIMULATIONS OF AMPHIPHILIC SYSTEMS

JEAN-CHRISTOPHE DESPLAT, DUT, BSc, Grad. Inst. Phys.

A thesis submitted in partial fulfilment of the requirements  
of Sheffield Hallam University for the degree of  
Doctor of Philosophy

April 1996

Materials Research Institute, Sheffield Hallam University  
in collaboration with Albright and Wilson UK Ltd., Whitehaven.

ProQuest Number: 10694438

All rights reserved

INFORMATION TO ALL USERS

The quality of this reproduction is dependent upon the quality of the copy submitted.

In the unlikely event that the author did not send a complete manuscript and there are missing pages, these will be noted. Also, if material had to be removed, a note will indicate the deletion.



ProQuest 10694438

Published by ProQuest LLC (2017). Copyright of the Dissertation is held by the Author.

All rights reserved.

This work is protected against unauthorized copying under Title 17, United States Code  
Microform Edition © ProQuest LLC.

ProQuest LLC.  
789 East Eisenhower Parkway  
P.O. Box 1346  
Ann Arbor, MI 48106 – 1346

## Abstract

Results are presented from NVT Monte Carlo simulations of a three-dimensional lattice model of a binary mixture of solvent and surfactant chains in which free self assembly is allowed.

It is demonstrated that the model exhibits a critical micelle concentration together with cluster size distributions consistent with experiment and theory (minimum and maximum in the distribution within the micellar region). The weight average aggregation number,  $N_w$ , increases linearly with the square root of the concentration of micellised surfactant as predicted theoretically. The dilute solution excess chemical potential ( $\mu_n^o - \mu_1^o$ ) is determined from the cluster size distribution. It is found to be a monotonically decreasing function of  $n$  with different functional forms for small and large clusters. A single analytical expression is found to describe the cluster size distribution and the  $X_1$  versus  $X_a$  curve on the concentration range from 0 to 5 *vol. %*. It is necessary to introduce an activity coefficient to accurately describe the behaviour of the model for amphiphile concentrations greater than 5 *vol. %*. The dependence of this expression on temperature and molecular interaction parameters is determined.

Results are also presented for the simulation of longer chains. Following investigation of three of the models free parameters, regions of phase space in which ‘spongy’ structures and vesicles — either spherical or tubular — are successfully identified. A preliminary phase diagram is established by considering the variation in the cavity size distribution function. These results are discussed in relation with experimental data and existing phenomenological studies.

An extension of the Configurational-bias Monte Carlo (CBMC) based on a self-

avoiding walk using sites selected from subsets of sites known *a priori* available for the regrowth is also established. Its theoretical foundation is laid out together with a partial assessment of its efficiency relative to both the classic reptation and CBMC for the simulation of chains lying on a lattice of high coordination number. A methodology for the simulation of polyoxyethylene oxide (POE) surfactants using a cubic lattice of coordination number  $c = 26$  is briefly discussed.

*To the memory of my father,*

*To my mother*

*"Mais je ne craindrai pas de dire que je pense avoir eu beaucoup d'heur de m'être rencontré dès ma jeunesse en certains chemins qui m'ont conduit à des considérations et des maximes dont j'ai formé une méthode, par laquelle il me semble que j'ai moyen d'augmenter par degrés ma connoissance, et de l'élever peu à peu au plus haut point auquel la médiocrité de mon esprit et la courte durée de ma vie lui pourront permettre d'atteindre."*

**René DESCARTES** (excerpt from: *"Discours de la méthode pour bien conduire sa raison, et chercher la vérité dans les sciences"*)

# Contents

List of Figures	vii
List of Tables	xi
<b>1 Introduction</b>	<b>1</b>
1.1 Aims	1
1.2 Overview	3
1.2.1 Chemistry and thermodynamics of surfactant systems	3
1.2.2 Computer models of surfactant systems	4
1.2.3 Simulations results and analysis	4
<b>2 Surfactant systems</b>	<b>6</b>
2.1 Description	6
2.2 Classification	7
2.2.1 Anionic	7
2.2.2 Cationic	7
2.2.3 Non-ionic	8
2.2.4 Zwitterionic	8
2.3 Properties	9
2.3.1 Surface activity	9
2.3.2 Micellisation	10
2.3.3 Solubilisation	12
2.4 Interactions	13
2.4.1 Steric repulsion	13
2.4.2 Coulombic interactions	13
2.4.3 Hydrogen-bonding interactions	14
2.4.4 Van der Waals interactions	15
2.5 Mesophases	15
2.5.1 Limits of the liquid crystal region	16
2.5.2 Well-established phases	19
2.5.3 Other phases	24
2.6 Liposomes and vesicles	25
2.6.1 Description	25
2.6.2 Preparation	27
2.7 Experimental techniques	28
2.7.1 Nuclear magnetic resonance (NMR)- Electron-spin resonance (ESR)	28
2.7.2 Optical microscopy - Electronic microscopy	29

2.7.3	Small angle X-ray scattering (SAXS) - Small angle neutron scattering (SANS) - Light scattering (LS) . . . . .	29
2.7.4	Other techniques . . . . .	29
2.8	Applications . . . . .	30
<b>3</b>	<b>Thermodynamical aspects</b>	<b>31</b>
3.1	Thermodynamics of immiscibility . . . . .	31
3.2	Hydrophobic and entropic effects . . . . .	34
3.3	Mathematical models . . . . .	35
3.3.1	Phase separation model . . . . .	36
3.3.2	Mass-action law model . . . . .	37
3.3.3	Multiple equilibrium model . . . . .	38
3.3.4	Small systems model . . . . .	40
3.4	Driving forces and geometric packing . . . . .	40
3.4.1	Optimal head group area . . . . .	40
3.4.2	Geometric packing considerations . . . . .	42
<b>4</b>	<b>Models of surfactant systems</b>	<b>45</b>
4.1	Phenomenological models . . . . .	46
4.2	Ising-type models . . . . .	47
4.2.1	Spin-1/2 Ising (Widom-type) models . . . . .	47
4.2.2	Spin-1 Ising (Blume-Emery-Griffiths-type) models . . . . .	55
4.2.3	Decorated lattice-gas models . . . . .	59
4.3	Chain models . . . . .	61
4.3.1	Constrained chains . . . . .	62
4.3.2	Self-assembling chains . . . . .	63
4.4	Other models . . . . .	72
4.5	Conclusion . . . . .	73
<b>5</b>	<b>Model</b>	<b>74</b>
5.1	Model . . . . .	74
5.1.1	Description . . . . .	74
5.1.2	The 'basic' implementations . . . . .	76
5.1.3	The 'extended' implementation . . . . .	77
5.2	Sampling the system . . . . .	78
5.2.1	Molecular mechanics . . . . .	79
5.2.2	Molecular dynamics . . . . .	79
5.2.3	Monte Carlo . . . . .	80
5.2.4	Statistical mechanics . . . . .	80
5.2.5	Importance sampling . . . . .	81
5.2.6	Metropolis method . . . . .	82
5.3	Schemes . . . . .	83
5.3.1	Reptation . . . . .	85
5.3.2	Configurational-bias Monte Carlo . . . . .	86
5.4	The observables . . . . .	90
5.4.1	Cluster properties . . . . .	91
5.4.2	Cavity properties . . . . .	94
5.4.3	Chain properties . . . . .	96
5.4.4	Other averages . . . . .	97
5.5	The simulations . . . . .	101

5.5.1	The hardware . . . . .	101
5.5.2	Optimisations and style . . . . .	101
5.5.3	The schemes . . . . .	102
5.6	Conclusion . . . . .	104
<b>6</b>	<b>A novel scheme for the simulation of chain molecules on a lattice</b>	<b>105</b>
6.1	The ‘modified’ configurational-bias Monte Carlo . . . . .	106
6.1.1	The concept . . . . .	106
6.1.2	Acceptance criterion . . . . .	107
6.1.3	Application to the simulation of diblock copolymers: a benchmark . . . . .	111
6.2	Proposed methodology for a more accurate mapping . . . . .	115
6.3	Conclusion . . . . .	119
<b>7</b>	<b>Simulations in the ‘vesicle’ region</b>	<b>121</b>
7.1	Preliminary stage: reproducibility and finite size effects . . . . .	122
7.1.1	Introduction . . . . .	122
7.1.2	Simulation results . . . . .	123
7.1.3	Conclusion . . . . .	125
7.2	Phase diagram of the ‘vesicle’ region . . . . .	127
7.2.1	The simulations . . . . .	127
7.2.2	Simulation data . . . . .	128
7.2.3	Analysis and discussion . . . . .	140
7.3	Concluding remarks . . . . .	145
<b>8</b>	<b>Simulations in the micellar region</b>	<b>147</b>
8.1	Simulation . . . . .	147
8.1.1	Preliminary runs . . . . .	148
8.1.2	Production runs . . . . .	149
8.2	Results and analysis . . . . .	151
8.2.1	Description of the results . . . . .	151
8.2.2	Discrepancies with experiment . . . . .	155
8.3	Thermodynamical treatment . . . . .	157
8.4	Comparison with theory . . . . .	162
8.5	Temperature and hydrophilic strength-dependencies . . . . .	165
8.5.1	Temperature dependency . . . . .	165
8.5.2	Hydrophilic strength dependency . . . . .	169
8.6	Conclusion . . . . .	172
<b>9</b>	<b>Conclusion</b>	<b>174</b>
9.1	Concluding remarks . . . . .	174
9.2	Suggested improvements and further work . . . . .	177
9.3	Conclusion . . . . .	178
	<b>Bibliography</b>	<b>180</b>
<b>A</b>	<b>Appendix</b>	<b>196</b>
A.1	Average number of cavity . . . . .	196
A.2	Average cavity size . . . . .	198
A.3	Average volume fraction of enclosed solvent . . . . .	200
A.4	Normalised average number of external interactions . . . . .	202
A.5	Mean aggregation number . . . . .	209

# List of Figures

1.1	Purpose of computer modelling (from reference [1]) . . . . .	2
2.1	Schematic representation of an amphiphile . . . . .	6
2.2	Variation of some physico-chemical properties around the cmc (from reference [2]) . . . . .	10
2.3	Schematic representation of reverse $L_2$ (left) and normal $L_1$ (right) micelles (from reference [3]) . . . . .	11
2.4	Typical Temperature-Composition limits of liquid crystalline phases (from reference [4]) . . . . .	18
2.5	Phase diagram of $C_{12}EO_6$ (from reference [5]) . . . . .	19
2.6	Schematic representation of a lamellar phase, $L_\alpha$ (from reference [6]) . . . .	20
2.7	Optical texture of a lamellar phase $L_\alpha$ ( $\times \approx 150$ ) . . . . .	21
2.8	Schematic representations of normal $H_1$ (left), and reverse $H_2$ (right) hexagonal phases (from reference [6]) . . . . .	21
2.9	Optical texture of an hexagonal phase $H_1$ ( $\times \approx 150$ ) . . . . .	22
2.10	Proposed structure of the sponge phase, $L_3$ (from reference [7]) . . . . .	24
2.11	Optical texture of a lamellar dispersion $L_\alpha + W$ ( $\times \approx 150$ ) . . . . .	25
2.12	Freeze-fracture electron micrograph of a liposome ( $\times \approx 10^4$ ) (courtesy of Albright & Wilson UK ltd) . . . . .	26
2.13	Schematic representation of a vesicle (from reference [3]) . . . . .	26
3.1	Reduced free energy of mixing for a partially miscible system . . . . .	33
3.2	Schematic distribution of surfactants between monomers and micelles: typical predictions from the mass-action law (plain lines) and the phase separation models (dashed lines) . . . . .	38
3.3	Optimal head group area, $a_0$ (from reference [3]) . . . . .	43
4.1	Mapping of spin 1/2 Ising model into Wheeler and Widom model (from reference [8]) . . . . .	48
4.2	Schematic of phase diagram of ANNNI model on simple-cubic lattice. L is the Lifshitz point, PR is the ferromagnetic-period-6 first-order transition line (from reference [9]) . . . . .	51
4.3	Phase diagram constructed using the spin densities obtained by solving the mean-field equations, for certain selected symmetries of phase (from reference [10]) . . . . .	55
4.4	Mean-field phase diagram (from reference [11]) . . . . .	56

4.5	Phase diagram in two dimensions. Full lines and dashed lines indicate first order and continuous transitions, respectively. Dotted line is the disorder line (from reference [12]) . . . . .	58
4.6	Monte Carlo phase diagram. Dashed lines denote continuous transitions (from reference [13]) . . . . .	61
4.7	Volume fraction of surfactant $H_3T_4$ in aggregates with aggregation number $n$ (from reference [14]) . . . . .	64
4.8	The dependence of the ratio of the smallest to largest principal moments of inertia on reduced temperature and amphiphilic concentration. A, small clusters; B, large cylinders; C, bicontinuous; D, lamellar (from reference [15])	66
4.9	Vesicle formed during the preliminary study with chains of length $s = 6$ ( $\beta^{-1} = 1.10$ , $\gamma = -1.0$ and $X_a = 9.38 \text{ vol. } \%$ ) . . . . .	67
4.10	Castellated bilayer ( $s = 4$ , $\beta^{-1} = 0.90$ , $\gamma = -2.0$ and $X_a = 50.0 \text{ vol. } \%$ ) . . . . .	68
4.11	Micellar size distribution function $f(s)$ . $s$ is the number of surfactants in an aggregate (from reference [16]) . . . . .	71
4.12	Three-dimensional cluster size distribution for total surfactant mole fractions $x = 0.005, 0.01, 0.02, 0.03, 0.04, 0.05, 0.06, 0.08$ respectively (from reference [17]) . . . . .	72
4.13	Polydispersity of the aggregates in the system as a function of the overall concentration (from reference [18]) . . . . .	73
5.1	Chain on a lattice . . . . .	75
5.2	'Folded' and 'straight' conformations . . . . .	77
5.3	Periodic boundary conditions: the actual simulation box is shaded . . . . .	84
5.4	The reptation scheme . . . . .	85
5.5	The configurational-bias Monte Carlo scheme . . . . .	88
5.6	Sites to be checked following a reptation . . . . .	103
6.1	A subset of available sites . . . . .	106
6.2	Comparison of the 'conventional' and 'modified' CBMC: $n_{AS}^*$ for the small system . . . . .	113
6.3	Comparison of the 'conventional' and 'modified' CBMC: $n_{BS}^*$ for the large system (the reptation failed to converge sufficiently rapidly to appear on this graph) . . . . .	113
6.4	$a$ , $b$ and $c$ conformations . . . . .	115
6.5	$aa$ , $ab$ and $ac$ conformations . . . . .	116
6.6	$bb$ , $bc$ and $cc$ conformations . . . . .	117
6.7	Mapping of a basic hydrophobic (left) and hydrophilic (right) unit . . . . .	118
7.1	Rod-like structure ( $\beta^{-1} = 1.20$ , $\gamma = -1.0$ , $N = 512$ ) . . . . .	124
7.2	Vesicles ( $\beta^{-1} = 1.10$ , $\gamma = -1.0$ , $N = 1024$ ) . . . . .	124
7.3	Slice through the vesicles ( $\beta^{-1} = 1.10$ , $\gamma = -1.0$ , $N = 1024$ ) . . . . .	125
7.4	Slice through a 'spongy' structure ( $\beta^{-1} = 0.90$ , $\gamma = -1.0$ , $N = 2048$ ) . . . . .	126
7.5	Average number of cavities ( $\varepsilon = 0.0$ ) . . . . .	129
7.6	Average number of cavities ( $\varepsilon = 1.0$ ) . . . . .	130
7.7	Average number of cavities ( $\varepsilon = 2.0$ ) . . . . .	130
7.8	Average cavity size ( $\varepsilon = 0.0$ ) . . . . .	131
7.9	Average cavity size ( $\varepsilon = 1.0$ ) . . . . .	132
7.10	Average cavity size ( $\varepsilon = 2.0$ ) . . . . .	132
7.11	Average volume fraction of entrapped solvent ( $\varepsilon = 0.0$ ) . . . . .	134

7.12	Average volume fraction of entrapped solvent ( $\epsilon = 1.0$ ) . . . . .	134
7.13	Average volume fraction of entrapped solvent ( $\epsilon = 2.0$ ) . . . . .	135
7.14	Normalised average number of <i>HS</i> interactions, $\overline{n_{HS}^*}$ ( $\epsilon = 1.0$ ) . . . . .	136
7.15	Normalised average number of <i>TS</i> interactions, $\overline{n_{TS}^*}$ ( $\epsilon = 1.0$ ) . . . . .	136
7.16	Mean aggregation number, $N_n$ ( $\epsilon = 1.0$ ) . . . . .	138
8.1	Statistical inefficiency of the external interactions, $s_{n_{HS}}$ and $s_{n_{TS}}$ ( $\beta^{-1} = 1.18$ , $\gamma = -2.0$ ) . . . . .	151
8.2	Monomer concentration, $X_1$ , as a function of the total concentration in surfactant ( $\beta^{-1} = 1.18$ , $\gamma = -2.0$ ). Note the sharp variation around the cmc	152
8.3	Concentration of monomers in clusters of size $n$ , $X_n$ : pre-micellar and micellar distributions ( $\beta^{-1} = 1.18$ , $\gamma = -2.0$ ) . . . . .	153
8.4	Linear-dependence of the average weight aggregation number, $N_w$ ( $\gamma = -2.0$ and $\beta^{-1} = 1.18$ ) . . . . .	154
8.5	Size distribution index, $N_w/N_n$ ( $\gamma = -2.0$ and $\beta^{-1} = 1.18$ ) . . . . .	155
8.6	'Spherical' micelles ( $\beta^{-1} = 1.26$ , $\gamma = -2.0$ , $X_a = 6.25 \text{ vol. } \%$ ) . . . . .	156
8.7	'Cylindrical' micelle ( $\beta^{-1} = 0.90$ , $\gamma = -2.0$ , $X_a = 25.0 \text{ vol. } \%$ ) . . . . .	156
8.8	$h(n, X_a)$ . . . . .	159
8.9	Monomer concentration, $X_1$ , as a function of the total concentration in surfactant, $X_a$ : simulation data and fit ( $\beta^{-1} = 1.18$ , $\gamma = -2.0$ ) . . . . .	160
8.10	Concentration of monomers in clusters of size $n$ , $X_n$ : pre-micellar and micellar distributions: simulation data and fit ( $\beta^{-1} = 1.18$ , $\gamma = -2.0$ ) . . . . .	160
8.11	Slope and intercept of $h(n, X_a)$ : data and fits . . . . .	161
8.12	Temperature-dependence of the cmc ( $\gamma = -2.0$ ) . . . . .	166
8.13	Temperature-dependence of the monomer concentration, $X_1$ , as a function of the total concentration in surfactant, $X_a$ ( $\gamma = -2.0$ ) . . . . .	166
8.14	Temperature-dependence of the concentration of monomers in clusters of size $n$ , $X_n$ ( $\gamma = -2.0$ and $X_a = 4.04 \text{ vol. } \%$ ) . . . . .	167
8.15	Temperature-dependence of $\sqrt{N_n}$ ( $\gamma = -2.0$ ) . . . . .	168
8.16	Temperature-dependence of the exponents of the fits, $c_1$ and $c_2$ ( $\gamma = -2.0$ )	169
8.17	Hydrophilic strength-dependence of the monomer concentration, $X_1$ , as a function of the total concentration in surfactant, $X_a$ ( $\beta^{-1} = 1.18$ ) . . . . .	170
8.18	Hydrophilic strength-dependence of the concentration of monomers in clusters of size $n$ , $X_n$ ( $\beta^{-1} = 1.18$ and $X_a = 4.04 \text{ vol. } \%$ ) . . . . .	171
9.1	Concentration of monomers in clusters of size $n$ , $X_n$ : pre-micellar and micellar distributions (preliminary results, $\beta^{-1} = 1.18$ and $\gamma = -2.0$ ) . . . . .	175
9.2	Micelles forming at $X_a = 4.0 \text{ vol. } \%$ (preliminary results, $\beta^{-1} = 1.18$ and $\gamma = -2.0$ ) . . . . .	176
A.1	Average number of cavity ( $\epsilon = 0.0$ ) . . . . .	196
A.2	Average number of cavity ( $\epsilon = 1.0$ ) . . . . .	197
A.3	Average number of cavity ( $\epsilon = 2.0$ ) . . . . .	197
A.4	Average cavity size ( $\epsilon = 0.0$ ) . . . . .	198
A.5	Average cavity size ( $\epsilon = 1.0$ ) . . . . .	199
A.6	Average cavity size ( $\epsilon = 2.0$ ) . . . . .	199
A.7	Average volume fraction of enclosed solvent ( $\epsilon = 0.0$ ) . . . . .	200
A.8	Average volume fraction of enclosed solvent ( $\epsilon = 1.0$ ) . . . . .	201
A.9	Average volume fraction of enclosed solvent ( $\epsilon = 2.0$ ) . . . . .	201
A.10	Normalised average number of <i>HS</i> interactions ( $\epsilon = 0.0$ ) . . . . .	202

A.11	Normalised average number of <i>HS</i> interactions ( $\varepsilon = 1.0$ )	203
A.12	Normalised average number of <i>HS</i> interactions ( $\varepsilon = 2.0$ )	203
A.13	Normalised average number of <i>HS</i> interactions ( $\varepsilon = 0.0$ )	204
A.14	Normalised average number of <i>HS</i> interactions ( $\varepsilon = 1.0$ )	204
A.15	Normalised average number of <i>HS</i> interactions ( $\varepsilon = 2.0$ )	205
A.16	Normalised average number of <i>TS</i> interactions ( $\varepsilon = 0.0$ )	205
A.17	Normalised average number of <i>TS</i> interactions ( $\varepsilon = 1.0$ )	206
A.18	Normalised average number of <i>TS</i> interactions ( $\varepsilon = 2.0$ )	206
A.19	Normalised average number of <i>TS</i> interactions ( $\varepsilon = 0.0$ )	207
A.20	Normalised average number of <i>TS</i> interactions ( $\varepsilon = 1.0$ )	207
A.21	Normalised average number of <i>TS</i> interactions ( $\varepsilon = 2.0$ )	208
A.22	Mean aggregation number, $N_n(\varepsilon = 0.0)$	209
A.23	Mean aggregation number, $N_n(\varepsilon = 1.0)$	210
A.24	Mean aggregation number, $N_n(\varepsilon = 2.0)$	210
A.25	Mean aggregation number, $N_n(\varepsilon = 0.0)$	211
A.26	Mean aggregation number, $N_n(\varepsilon = 1.0)$	211
A.27	Mean aggregation number, $N_n(\varepsilon = 2.0)$	212

# List of Tables

2.1	Anionic surfactants . . . . .	7
2.2	Cationic surfactants . . . . .	8
2.3	Non-ionic surfactants . . . . .	8
2.4	Zwitterionic surfactants . . . . .	9
3.1	Critical packing parameter and favoured structures (from reference [3]) . . .	43
6.1	Radii of gyration . . . . .	118
7.1	Simulation parameters . . . . .	122
7.2	Simulation parameters . . . . .	128
8.1	Simulation parameters . . . . .	150
8.2	$\beta^{-1}$ -dependence of $fit(n)$ ( $\gamma = -2.0$ ) . . . . .	169
8.3	$\gamma$ -dependence of the cmc ( $\beta^{-1} = 1.18$ ) . . . . .	170
8.4	$\gamma$ -dependence of $fit(n)$ ( $\beta^{-1} = 1.18$ ) . . . . .	171

## Acknowledgements

I would like to thank my supervisors, Prof C.M. Care and Dr J. Haigh for advice and guidance throughout this project; I also wish to acknowledge the support of Albright & Wilson UK Ltd. and in particular of their technical manager, Mr E. T. Messenger, and Dr K. Hatchman for introducing me to the world of surfactant formulation and useful comments on the draft. Dr Hatchman also granted permission for the reproduction of some of the liquid crystal phases schematic representations included in chapter 2.

Hopefully, a few people have also played a very important role in permitting me to carry on working on my PhD whilst doing my national service as a *CSN-Scientifique-Chercheur*. These include the people in charge of my case at the Ministry of Defence and *Services sciences et technologie* of the French Embassy in London as well as Dr D. Roux for his sponsorship letter.

Finally, I wish to express my gratitude to my family and friends whose unreserved and constant moral support made this project achievable.

# Chapter 1

## Introduction

### 1.1 Aims

Surfactant systems are probably amongst the most fascinating compounds to study in physical chemistry. Indeed, the duality in their structure is responsible for the combination of two antagonistic properties giving rise to remarkable characteristic properties (*e.g.* micellisation and surface activity) and to the formation of liquid crystalline phases over a wide range of composition and temperature. These particular properties lead to amphiphilic materials being the main ingredient in many applications, the most famous of which being the detergent industry.

The earliest attempts to model surfactant systems in the late 1960s — such as Wheeler and Widom's [8] who adapted a classic spin-1/2 Ising model to deal with microemulsions — were of very little interest to surfactant manufacturers, but thanks to the ever-increasing in computer power the first simulations of micellisation and liquid crystal formation using more realistic models based on self-assembling chains are now successfully established. There is growing pressure on surfactant manufacturers to make the formulation of new surfactants meet ecological and economical requirements. Computer modelling

is therefore likely to become an important tool at their disposal in the near future.

As described by Allen and Tildesley [1], the purpose of computer modelling is essentially to fill in the gap between the experimental and theoretical approaches by allowing one to solve *exactly* a model of the real systems.

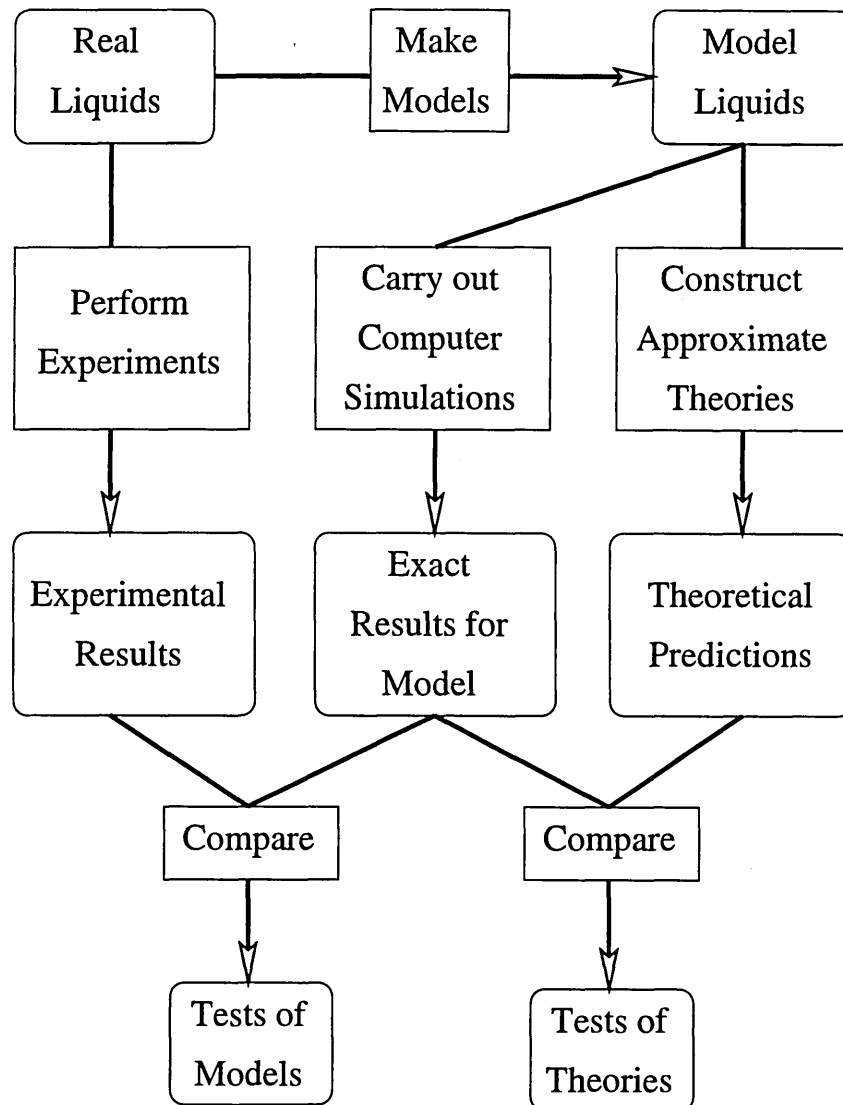


Figure 1.1: Purpose of computer modelling (from reference [1])

The new information thus generated can then be compared to experimental data and theoretical predictions (see figure 1.1). This role will be particularly well illustrated during the study of the micellar phase presented herein (see chapter 8).

## CHAPTER 1. INTRODUCTION

The aims of this project are to undertake simulations in the micellar and ‘vesicle’ regions in order to gain a better understanding of the self-assembly process (*i. e.* of the mechanisms and driving forces involved).

Finally, the studies undertaken during this project must be considered as the latest evolution of a model initially presented by Care in 1987 [19] and later extended by Brindle in three dimensions [15]. This model is currently being modified to allow one more step towards realism.

### 1.2 Overview

The material presented in this thesis is mainly articulated around three topics:

- Chemistry and thermodynamics of surfactant systems.
- Computer models of surfactant systems.
- Results and analysis from the simulations.

#### 1.2.1 Chemistry and thermodynamics of surfactant systems

In chapter 2, basics and general information about surfactants is provided. Thus, their classification, a description of the interactions involved and characteristic physico-chemical properties exhibited are summarised. A description of the most common mesophases has also been undertaken with particular emphasis on the sponge phase and liposomes which have a particular relevance to the results presented in chapter 7.

Complementary information about the thermodynamics of surfactant systems is then presented in chapter 3. The different mathematical models available as well as some theories about the driving forces leading to the formation of micelles is discussed in more

details. The foundations of the analysis of the results from the simulations carried out in the micellar phase is laid out in this chapter.

### 1.2.2 Computer models of surfactant systems

Firstly, an overview of the main models applied for the simulation of microemulsions and liquid crystal phases is presented in chapter 4. In its last section, the case of self-assembling chain models is tackled and most significant results from models *in competition* with the one used for the present study — *i. e.* using slightly different approaches — are presented thus allowing interesting points of comparison.

A description of the model used itself together with the properties computed during those studies is presented in chapter 5.

Finally, a novel scheme derived from Frenkel's generalisation [20] of the classic configurational-bias Monte Carlo CBMC [21] to off-lattice simulations is introduced with a partial assessment of its efficiency and general applicability.

### 1.2.3 Simulations results and analysis

Two main studies have been undertaken:

1. Investigation of the formation of spongy aggregates (vesicles and structures resembling that forming in an asymmetric sponge phase): attempt to characterise the region of phase space where they occur, their structure, possible mechanisms and driving forces.
2. A detailed study of the micellisation process with particular reference to the multiple phase equilibria approach. Characteristic properties such as the variation of the concentration in free monomer as a function of the total concentration in surfactant, the cluster size distribution function, the mean aggregation number, size distribu-

## CHAPTER 1. INTRODUCTION

tion index and excess chemical potential have been monitored as a function of the temperature and hydrophilic strength.

Finally, some overall comments and suggested improvements are presented in the conclusion (chapter 9). Some preliminary results of new simulations currently undertaken with modifications based on the conclusions laid out following the work presented herein have also been included.

# Chapter 2

## Surfactant systems

### 2.1 Description

Amphiphilic molecules are characterised by the possession of two different moieties one of which is polar (and hydrophilic) and the other non-polar (and hydrophobic)<sup>1</sup>. They are often referred as respectively the 'head' and the 'tail' of the amphiphile.

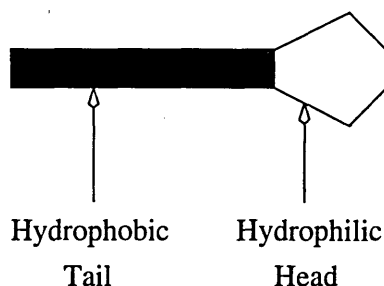


Figure 2.1: Schematic representation of an amphiphile

Whereas the hydrophobic part is usually made of a flexible linear or ramified hydrocarbon (seldom fluorocarbon) chain, the hydrophilic region can be made of a variety of different functional groups, either charged or not. The minimum polarity required is typically found to be just larger than one alcohol group  $-\text{CH}_2\text{OH}$  [22]. Amphiphiles are

<sup>1</sup>The presence (or absence) of polarity does not always guarantee hydrophilicity (or hydrophobicity).

generally classified according to the charge carried by their head group.

## 2.2 Classification

Whereas ionic amphiphiles will dissociate in aqueous solution (the surface active part being the anion for the anionic amphiphiles and the cation for the cationic amphiphiles), non-ionic amphiphiles will retain their integrity. Amongst those latter, a particular type of dipolar compounds known as ‘zwitterionic’ can — depending on factors such as the pH of the solution — be neutral, anionic or cationic.

### 2.2.1 Anionic

Their head group carries a negative charge. The most common functional groups include carboxylates ( $-\text{CO}_2^-$ ), sulphonates ( $-\text{SO}_3^-$ ), sulphates ( $-\text{SO}_4^-$ ) and phosphate esters ( $-\text{OPO}_2^-$ ).

Potassium laurate	$\text{CH}_3(\text{CH}_2)_{10}\text{COO}^-$	$\text{K}^+$
Sodium dodecyl sulphate (SDS)	$\text{CH}_3(\text{CH}_2)_{11}\text{SO}_4^-$	$\text{Na}^+$
Hexadecyl sulphonic acid	$\text{CH}_3(\text{CH}_2)_{15}\text{SO}_3^-$	$\text{H}^+$

Table 2.1: Anionic surfactants

### 2.2.2 Cationic

Their head group carries a positive charge. They are based on quaternary ammoniums such as trimethyl ammonium ( $-\text{N}^+(\text{CH}_3)_3$ ).

## CHAPTER 2. SURFACTANT SYSTEMS

Dodecylamine hydrochloride	$\text{CH}_3(\text{CH}_2)_{11}\text{NH}_3^+$	$\text{Cl}^-$
Hexadecyl trimethylammonium bromide (CTAB)	$\text{CH}_3(\text{CH}_2)_{15}\text{N}^+(\text{CH}_3)_3$	$\text{Br}^-$
Dodecyl pyrimidine chloride	$\text{C}_6\text{H}_5\text{N}^+(\text{CH}_2)_{11}\text{CH}_3$	$\text{Cl}^-$

Table 2.2: Cationic surfactants

### 2.2.3 Non-ionic

The majority of non-ionic surfactants are polyoxyethylene *POE* compounds but other types also include polyhydroxy, group V and group VI oxides ( $\text{N} \rightarrow \text{O}$ ,  $\text{P} \rightarrow \text{O}$ ,  $\text{S} \rightarrow \text{O}$  and  $\text{As} \rightarrow \text{O}$ ), phosphinyl esters and amides as well as ammonioamidates or N-terminal hydrophilic groups.

Polyoxyethylene glycol mono n-alkyl ethers	$\text{C}_n\text{H}_{2n+1}\text{O}(\text{CH}_2\text{CH}_2\text{O})_m\text{H}$
	$3 \leq n < 16$
	$3 \leq m < 15$
Dimethyl dodecyl phosphonate	$\text{C}_{12}\text{H}_{25}(\text{CH}_3)_2\text{P} \rightarrow \text{O}$

Table 2.3: Non-ionic surfactants

### 2.2.4 Zwitterionic

Although strictly speaking they are also part of the non-ionic class, their peculiarity leads them to be treated separately: the ionic functional groups are similar to those previously described.

N-dodecyl-N, N-dimethyl betaine       $C_{12}H_{25}N^+(CH_3)_2COO^-$

Table 2.4: Zwitterionic surfactants

## 2.3 Properties

Due to their particular and seemingly conflicting constitution which makes them partially soluble in oil and partially soluble in water, surfactants exhibit many remarkable properties such as surface activity, micellisation or solubilisation.

### 2.3.1 Surface activity

As their name suggests, the main property characterising surfactants is their surface activity, *i. e.* their ability to adsorb at air-water, oil-water interfaces and the surface of solids.

A complex mechanism involving various repulsive and attractive interactions takes place when surfactants are in aqueous solution (see section 2.4). Essentially, the disruption of the local water network by the surfactant molecules and its reorganisation following a more ordered disposition on the one hand, and the removal of the freedom of motion of the hydrophobic tails in water on the other hand make entropically favourable any mechanism leading to the removal of the surfactant tail from the aqueous solution [23]. As a consequence of that, surfactants will preferentially be located at interfaces with their hydrophobic part out of the aqueous solution. Since the apolar-water interaction is much weaker than the water-water one, this presence of the surfactants at interfaces leads to a major reduction in the surface tension. In some circumstances, the decrease can be such that the emulsification of two immiscible liquids can spontaneously occur.

## 2.3.2 Micellisation

Another important property of surfactant molecules is micellisation. When their concentration reaches a characteristic concentration known as the ‘critical micelle concentration’, *cmc*, surfactant molecules spontaneously aggregate together forming groups of micelles. As illustrated figure 2.2, this change in configuration causes a sudden change in many physical properties such as the equivalent conductivity, the osmotic pressure or the surface tension. The *cmc* can be experimentally determined using either techniques sensitive to a change in monomer concentration (*e.g.* surface tension techniques) or micelle concentration (*e.g.* light scattering techniques) thus yielding potential discrepancies.

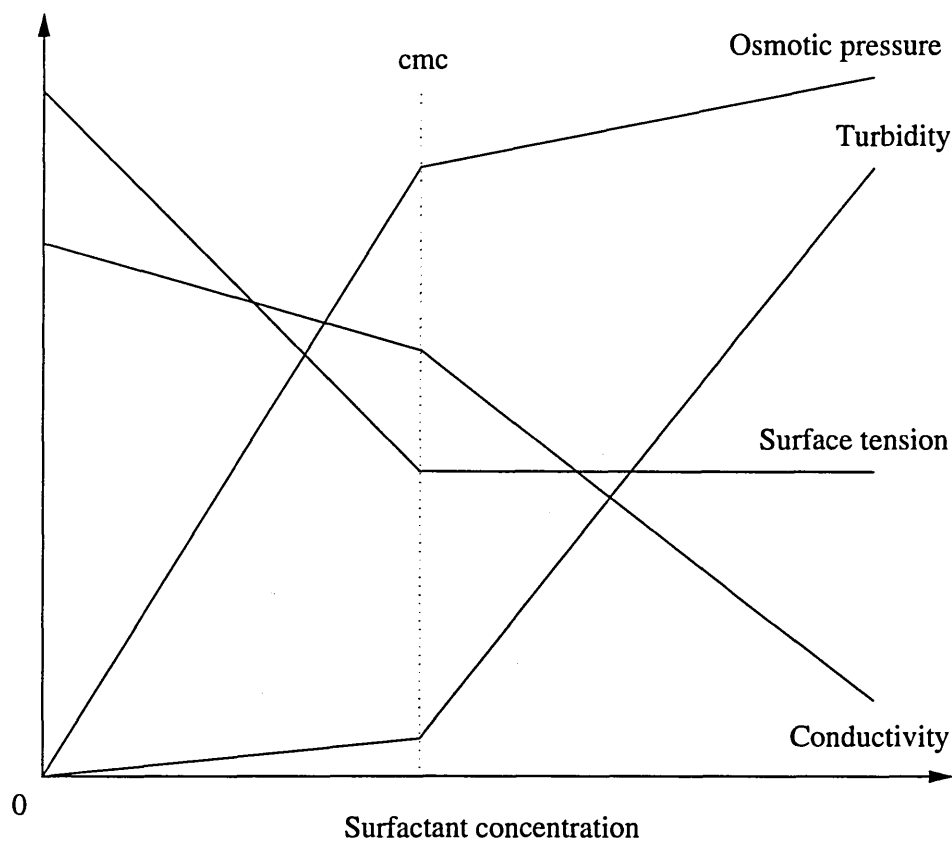


Figure 2.2: Variation of some physico-chemical properties around the *cmc* (from reference [2])

In their ‘normal’ arrangement, the surfactant molecules will dispose themselves so that their polar end lie in the outer region — with some bound water — and their non-

polar tail lie in the micellar core forming an essentially liquid-like phase. Ionic surfactants are also surrounded by an electrical double layer known as the Stern (innermost) and Gouy-Chapman (outermost) layers. An alternative exists where the heads point inwards and the tails form an external hydrocarbon continuum. Such a situation occurs when the total concentration in surfactant is very high or the solvent is apolar. The region over which they form is respectively known as the micellar phase,  $L_1$ , and reverse micellar phase,  $L_2$  (see figure 2.3).

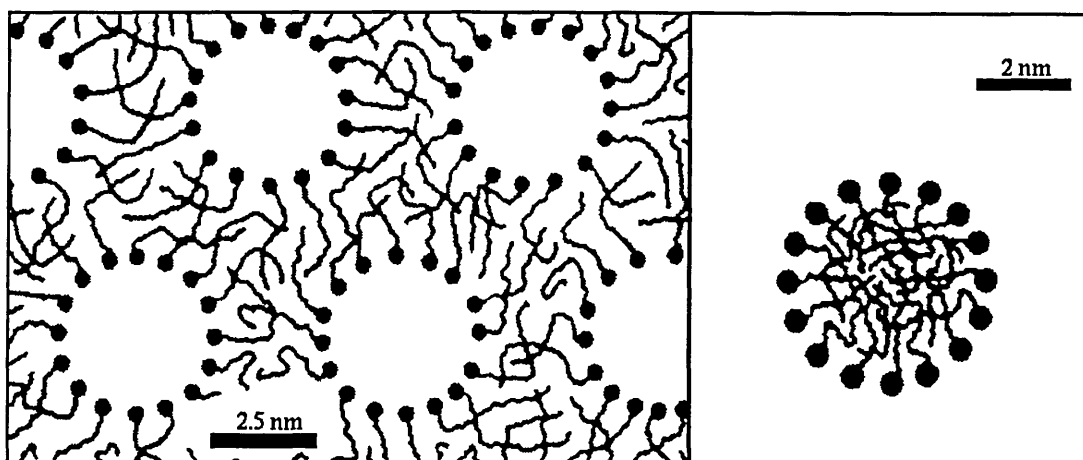


Figure 2.3: Schematic representation of reverse  $L_2$  (left) and normal  $L_1$  (right) micelles (from reference [3])

Although micelles formed near the cmc are spherical in shape, it is also possible to form disk-like, cylindrical or flexible rod-like micelles. The dependence of the shape relative to thermodynamical or geometric packing considerations is discussed in chapter 3 where the most common mathematical models of micellisation are also reviewed. Many experimental studies of micellisation have also been undertaken using various techniques. A survey is also presented in section 2.7.

The phenomenon of micellisation constitutes an alternative to moving to an interface since both factors governing the surfactant surface activity are still fulfilled: micellisation is entropically favourable.

### 2.3.3 Solubilisation

Thanks to their particular structure, micelles provide a liquid-like lipid interior and have therefore the opportunity to dissolve solutes which are barely — if not at all — soluble in water. The detergency properties exhibited by surfactants is a fine example of this. As pointed out by Wennerström [24], solubilisation is more easily understood in the framework of the phase separation model where micelles are assumed to form a phase of their own (see chapter 3). Indeed, experimental evidences [25–27] confirm that the solute behaves as if it is in a liquid-like environment and solubilisation may therefore be regarded as a non-specific dilution in a non-aqueous phase exempt from any specific binding to a particular location or micelle interior.

However, depending on both solute-solvent, solute-surfactant interactions — mostly dependent upon the polarity of the solute — and packing considerations, the solute will preferentially occupy different locations in a micellar interior. The general trend is for apolar solutes to stay in the hydrocarbon liquid-like interior whereas polar solutes prefer occupying a more external position in the micelle where they decrease both the water-hydrocarbon tail contact area and the number of gauche conformations in the surrounding hydrophobic tails. The extent of this process is closely related to the length of the surfactant hydrophobic tail. As a general trend, solubilisation is improved by increasing the tail length. An exponential  $n$ -dependence has been reported by Birdi [28].

Solubilisation is the most important property for the use of surfactants in pharmaceutical applications where they are used to solubilise some otherwise insoluble drugs.

## 2.4 Interactions

Amongst all the usual interactions arising in solution, some forces appear to be of primary importance in promoting the formation of liquid crystalline phases and physico-chemical properties characteristic to surfactant systems. Those forces are namely steric repulsions, Coulombic interactions (for ionic amphiphiles), H-bonds and Van der Waals interactions.

The relative strength of those interactions is the following:

$$\begin{array}{ccccc} \text{Van der Waals} & \longrightarrow & \text{H-bonding} & \longrightarrow & \text{Coulombic} \\ (\approx 1\text{kJ.mol}^{-1}) & & (\approx 10 - 40\text{kJ.mol}^{-1}) & & (\approx 500\text{kJ.mol}^{-1}) \end{array}$$

### 2.4.1 Steric repulsion

The steric repulsion has a quantum mechanical origin: it stems from the overlap of electron clouds from neighbouring atoms. It is characterised by a very short range and very steep repulsive interaction as the atoms get closer. Since no expression of the distance dependence of this potential exists yet, a series of empirical expressions such as the hard sphere or power-law potentials have been proposed through the years.

The total intermolecular pair potential may be expressed with a 6-12 potential such as the Lennard-Jones or Gay-Berne potentials.

### 2.4.2 Coulombic interactions

The Coulombic interactions are amongst the strongest physical forces in chemical interactions. They arise between two charged atoms of ionic valencies  $z_1$  and  $z_2$  separated by a distance  $r$  so that:

$$F = \frac{z_1 z_2 e^2}{4\pi\epsilon_0\epsilon r^2}$$

where  $e$  is the elementary charge,  $\epsilon_0$  the permittivity of free space and  $\epsilon$  the relative permittivity. The interaction is attractive between unlike charges and repulsive otherwise. One may notice the apparent long-range — inverse-square distance dependence — of such forces. However, a phenomenon of screening rapidly occurs as ions get surrounded by ions of opposite charge thus causing Coulombic interactions to drop-off much more rapidly. An exponential decay with distance has been reported for long distance [3].

### 2.4.3 Hydrogen-bonding interactions

When an H atom is covalently bond to an electronegative atom  $X$  (*e.g.* O, N, F, ...), it gets depleted from its electron and thus gains a partial positive charge,  $\delta^+$ . This charge is responsible for the formation of a particular type of dipole-dipole interaction known as the ‘hydrogen bond’ with another electronegative atom  $Y$ . Is is usually represented as  $X - H \cdots Y$ . One must emphasise that although this type of interaction has sometimes been misinterpreted as some sort of weak covalent bond due to its remarkable strength (for a dipole-dipole interaction) and directionality, it is now accepted that the H atom is not shared between the two electronegative atoms but remains covalently bonded to its original neighbour [29]. H-bonds can therefore be regarded as an effective H-mediated ‘bond’ between two electronegative atoms [3].

The relative strength and directionality of those interactions are mainly responsible for increasing the cohesion and range of the order of some *associated liquids* such as water thus yielding unexpected physico-chemical properties such as a high boiling point.

Comprehensive studies of the H-bonding interactions are widely available in the literature (*e.g.* [30]).

#### 2.4.4 Van der Waals interactions

The Van de Waals forces actually involve contributions from three different types of interactions [3]:

- The orientation interaction (also known as Keesom or angle-averaged dipole-dipole interaction) is a Boltzmann-averaged interaction between two permanent dipoles.
- The induction interaction (also known as Debye interaction) is a dipole-induced dipole interaction.
- The dispersion interaction (also known as Landau interaction) is a dipole-induced dipole-induced interaction. It is the most important contribution.

All three contributions have an inverse-sixth power distance dependence. Whereas the first two are only existent for certain molecules with particular properties of polarisation or polarity, the dispersion interaction exists for all atoms and molecules. Particular features of the Van der Waals interactions are their pairwise non-additivity, relative long-range ( $0.2 \rightarrow 10\text{nm}$ ) and non-specificity (are either repulsive or attractive). Dispersion forces also have a weak orienting effect.

## 2.5 Mesophases

If the concentration in surfactant is progressively increased from a dilute micellar solution, a series of size and shape transitions will first take place (see chapter 3). However, as the concentration is increased, so are intermicellar repulsive forces arising from the water-head group binding and — if applicable — electrostatic forces between micelles. For a given temperature below the azeotropic point, a critical composition exists at which a disorder  $\rightarrow$  order transition will take place and a liquid crystal will form from the micellar

solution.

Liquid crystals are a class of phase structures which is characterised by the existence of an orientational order and some — but unlike crystals not complete — positional order. Thus they exhibit a significant degree of long-range order along at least one direction in space. Amongst those liquid crystals, two different categories can be identified:

**Thermotropic liquid crystals:** form liquid crystal phases solely by the action of thermal energy (or of electrical or magnetic fields). The presence of a solvent is not required. They have applications in liquid crystal display devices.

**Lyotropic liquid crystals:** form liquid crystals which depend for their existence upon the presence of a solvent.

The liquid crystals formed by amphiphilic molecules are of the second type and must therefore not be confused with the others. The difference between them lies in the fact that both solvation and thermal energies are required to form lyotropic liquid crystals, while thermal energy alone suffices for thermotropics. The occurrence of those phases is constrained to a finite range of composition and temperature and will therefore have both upper and lower composition and temperature limits (see figure 2.4).

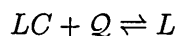
### 2.5.1 Limits of the liquid crystal region

#### Temperature limits of liquid crystalline region

The maximum temperature at which most liquid crystalline regions exist may be regarded as an azeotropic point. Indeed, it is required that at this point both the liquid ( $L$ ) and liquid crystal ( $LC$ ) boundaries touch asymptotically at a unique temperature and composition: a liquid and liquid crystalline phase of the same composition coexist at this point. The following reversible reaction may therefore take place at this temperature along

## CHAPTER 2. SURFACTANT SYSTEMS

the isopleth passing through the composition:



At the opposite, the lower temperature limit occurs at an eutectic where the following reaction occurs:



where '*dilute fluid*' can be a liquid or another liquid crystal, and *C* a crystal phase.

Whereas the azeotropic point of the upper temperature limit is approximately centered within the region, the eutectic composition at the lower temperature limit invariably lies near the most dilute composition limit of the region (see figure 2.4).

Although the upper limit can be qualitatively understood as arising from the higher entropy of the liquid (with respect to the liquid crystalline phase), the lower limit is governed by the balance between the sum of the thermal energy plus water free energy on the one hand, and the crystal free energy on the other hand [4]. The disruption of the crystal is opposed by its low enthalpy, while thermal and solvation energies favour its disruption.

### Composition limits of liquid crystalline phases

The sequence of reactions occurring along isothermal mixing paths is an alternating succession of irreversible stoichiometric phase reactions (within miscibility gaps) and dilution processes (within phase region).

As a summary, the principal factors which govern the dependance of surfactant phase behaviours on system variables are [4]:

- The enthalpies of crystal phases.

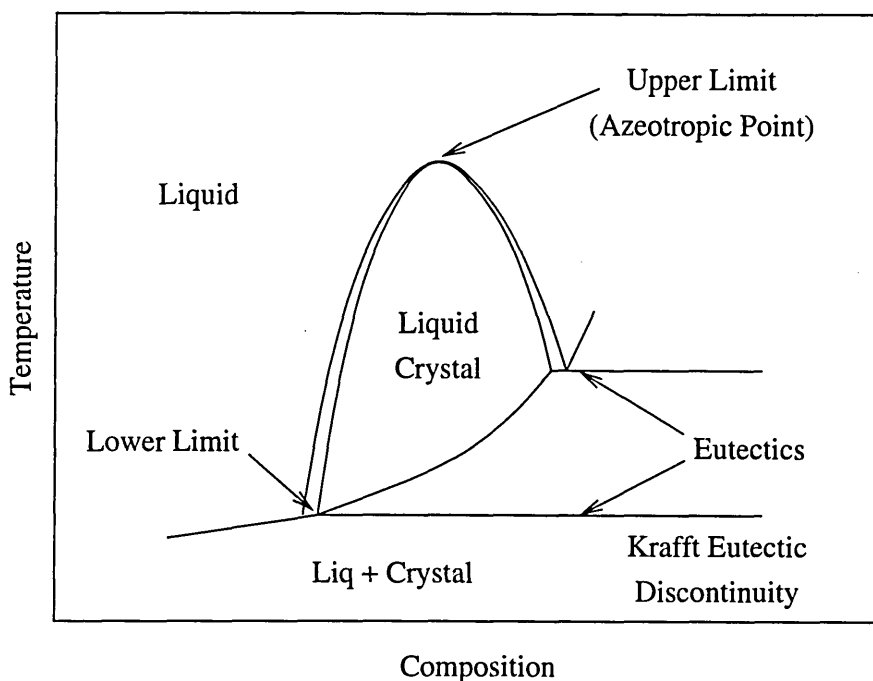


Figure 2.4: Typical Temperature-Composition limits of liquid crystalline phases (from reference [4])

- The numerical values of water free energies (which depend on both the thermodynamic activity of water and the water composition).
- The ambient level of thermal energy (which is dictated by the temperature).

The phase behaviour of binary mixtures of surfactant and solvent is usually represented by plotting a Temperature-Composition phase diagram. A simple example is that of  $C_{12}EO_6$  (see figure 2.5).

Amongst those phases, only a few of them have been clearly established with experimental evidence whilst many others remain hypothetical explanations of otherwise unexplained experimental results or theories. An exhaustive description of these phases goes beyond the scope of the present work; many articles and textbooks provide such a review [4, 5, 31, 32].

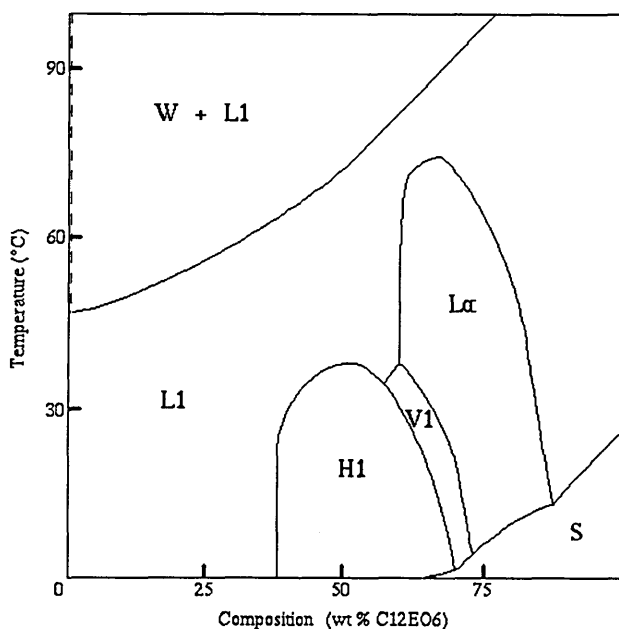


Figure 2.5: Phase diagram of C<sub>12</sub>EO<sub>6</sub> (from reference [5])

## 2.5.2 Well-established phases

### The lamellar phase ( $L_{\alpha}$ )

The lamellar phase — also known as the *neat phase* ( $G$ ) — is certainly the most common of all liquid crystalline phases. It consists of stacks of ordered bilayers separated by water layers (see figure 2.6). Whereas the thickness of this latter appears to be pretty sharply defined (2 – 200Å), the conformations of the chains within the bilayers appear to continuously fluctuate. The bilayer thickness is typically  $0.8 - 1.6L_{trans}$  where  $L_{trans}$  is the all-trans chain length. The bilayers typically extend over a micron [5].

Due to obvious packing arguments (see chapter 3), lamellar phases are preferentially formed by amphiphiles with small head groups and/or bulky tails.

The range of composition within which this phase can form is typically about 40wt% – 90wt%. It is often the most concentrated liquid crystalline phase and as such,

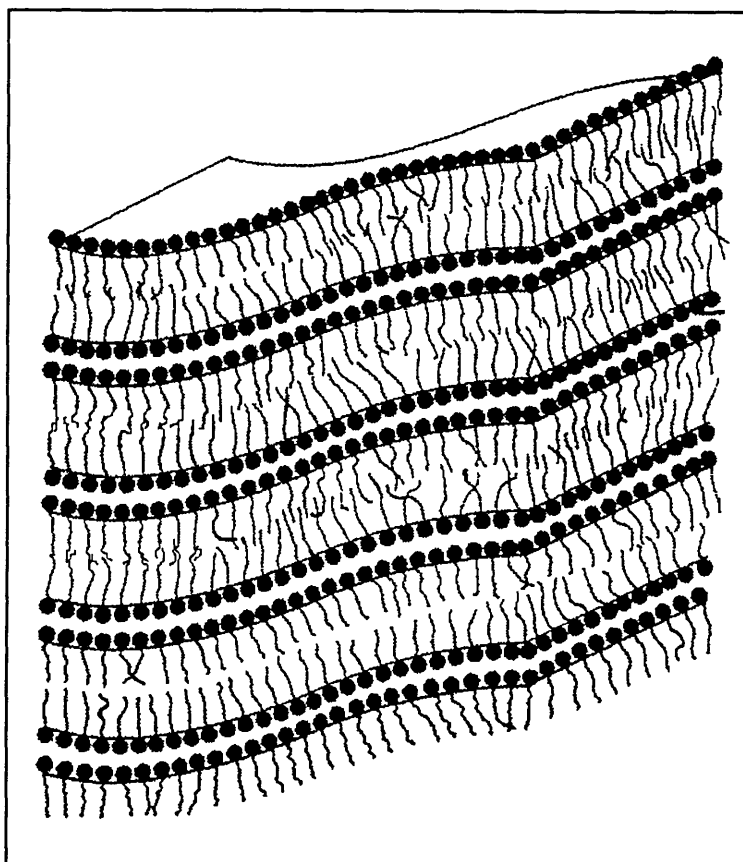


Figure 2.6: Schematic representation of a lamellar phase,  $L_\alpha$  (from reference [6])

occurs at higher temperatures and is the least tolerant of hydration energy of other liquid crystalline phases.

This phase can easily be identified by optical microscopy under crossed-polars thanks to its characteristic optical textures (the most common of which being the mosaic and oily streaks textures).

### The hexagonal phase ( $H_1$ , $H_2$ )

This phase — also known as the *middle phase (M)* — is the second most common liquid crystalline phase forming. It consists of hexagonal arrays of parallel long rod micelles. Their diameter is  $1.5 - 2.0L_{trans}$  and the intermicellar separation lies in the range

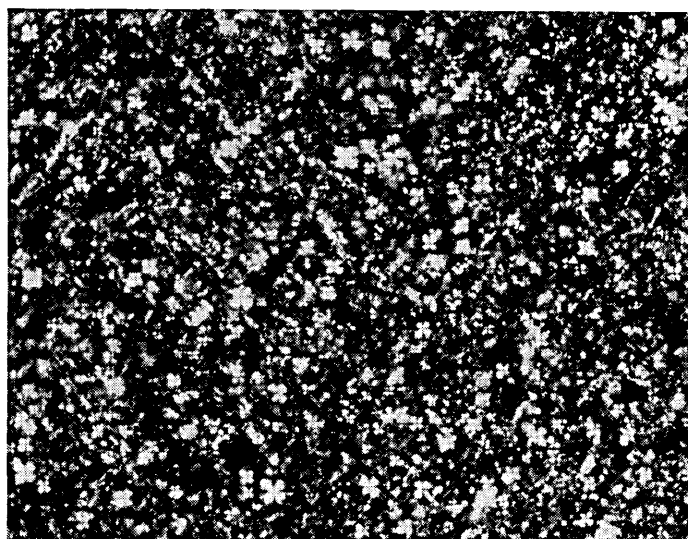


Figure 2.7: Optical texture of a lamellar phase  $L_\alpha$  ( $\times \approx 150$ )

8 – 50Å [5].

Whereas for the ‘normal’ hexagonal phase  $H_1$  the head groups lie at the micelle surface with a continuum of water region separating adjacent micelles, the reversed phase  $H_2$  is composed of water cylinders packed in an hexagonal array surrounded by a continuum hydrocarbon environment. The diameter of the water cylinder is typically 10 – 20Å.

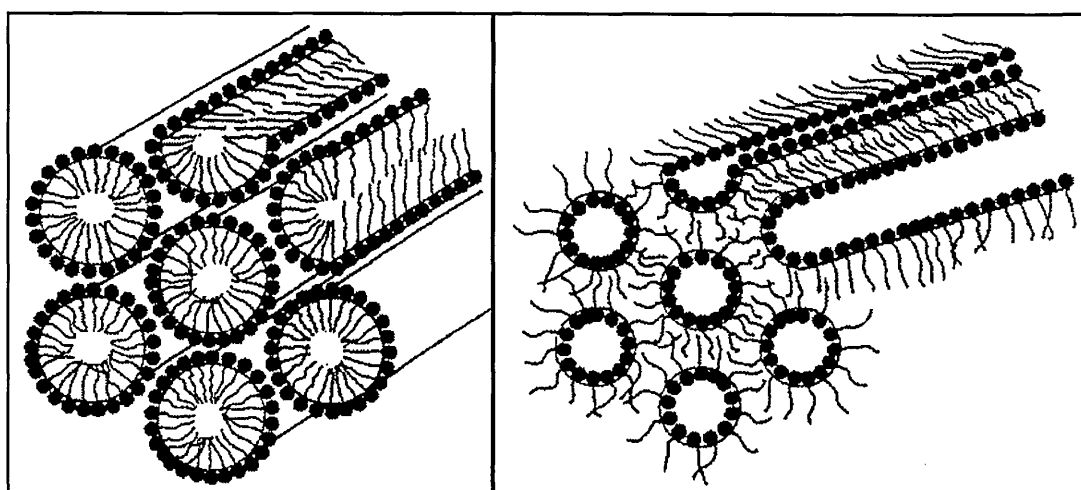


Figure 2.8: Schematic representations of normal  $H_1$  (left), and reverse  $H_2$  (right) hexagonal phases (from reference [6])

## CHAPTER 2. SURFACTANT SYSTEMS

Like the lamellar phase, the hexagonal phases also possess a single axis of symmetry and are therefore optically bi-refringent. They can easily be identified from optical microscopic observations as fan-like textures.



Figure 2.9: Optical texture of an hexagonal phase  $H_1$  ( $\times \approx 150$ )

Their viscosity is much higher than that of the lamellar phase.

### The cubic phase ( $I_1$ , $I_2$ , $V_1$ , $V_2$ )

The discontinuous ( $I_1$ ,  $I_2$ ) and bicontinuous ( $V_1$ ,  $V_2$ ) cubic phases are much less common than the previous two. They only tend to occur over a very narrow range of concentration and their structures still remain to be fully elucidated [33].

Whilst the discontinuous phases occur at composition between the micellar solutions and hexagonal phase ( $L_1 \leftrightarrow I_1 \leftrightarrow H_1$  and  $H_2 \leftrightarrow I_2 \leftrightarrow L_2$ ) the bicontinuous phases occur between the hexagonal and lamellar phases ( $H_1 \leftrightarrow V_1 \leftrightarrow L_\alpha \leftrightarrow V_2 \leftrightarrow H_2$ ).

The structure of  $I_1$  and  $I_2$  is known to consist of a cubic close packed array of small globular micelles, the micelle shapes and array arrangements still remaining to be fully established.  $V_1$  and  $V_2$  are thought to consist of a three-dimensional bicontinuous network with both surfactant and water forming continuous zones [34].

## CHAPTER 2. SURFACTANT SYSTEMS

The discontinuous cubic phases are more viscous than the bicontinuous ones which are themselves more viscous than the hexagonal phases. Cubic phases are optically isotropic.

### **The nematic phase ( $N_C$ , $N_D$ )**

First established in 1967 [35], they only occur for a very few systems between  $L_1$  and  $H_1$ , and  $L_1$  and  $L_\alpha$  phases. They are optically bi-refringent and exhibit a very low viscosity. They are mostly uniaxial phases of ordered small cylindrical micelles ( $N_C$ ) or small disc micelles ( $N_D$ ).

### **The sponge phase ( $L_3$ )**

An isotropic phase constituted of multiply connected bilayer structures has also been identified [22]. This phase typically occurs over a narrow region — typically at relatively high temperature (50–80°C) — of both binary and ternary mixtures of surfactant-oil-water when the mean curvature at the hydrophile-lipophile interface bends towards the solvent [33]. The driving force responsible for the preferential formation of the sponge phase — rather than a lamellar phase — appears to be the prospect of altering the surfactant bilayer curvature towards its optimal value more than the underlying increase in entropy.

The sponge phase can be seen as a continuous two-dimensional film of bilayers partitioning three-dimensional space into two volumes [36]. Two different categories of sponge phase can thus be discerned: the symmetrical — containing similar amounts of solvent in both sub-volumes — and the asymmetrical sponge phases. A structure of the symmetric sponge phase is proposed figure 2.10.

The sponge phase is rather viscous and scatters light strongly [33].

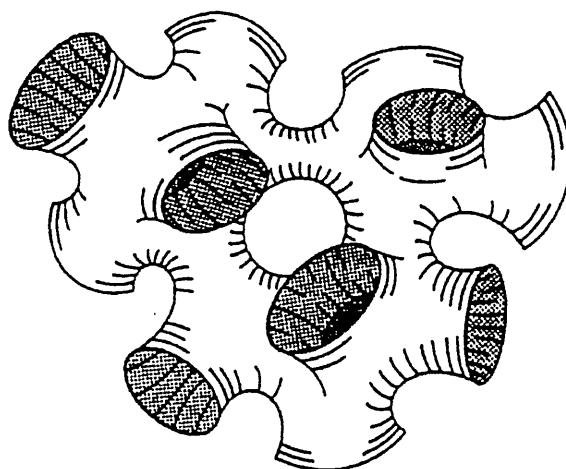


Figure 2.10: Proposed structure of the sponge phase,  $L_3$  (from reference [7])

### 2.5.3 Other phases

In addition to those main phases which have been thoroughly studied and characterised, several intermediate phases have also been proposed. Most of them are still hypothetical or not well characterised and their occurrence is often restricted to a limited class of compounds. These phases can be classified according to their degree of relation to  $H_1$  (rod-like structures),  $L_\alpha$  (layer structures) or  $V_1/V_2$  phases (three-dimensional structures) [31].

Amongst those phases, one may mention the existence of the biaxial nematic ( $N_{Bx}$ ) [37], some lamellar phases with highly ordered amphiphiles occurring at higher concentrations (gel phase  $L_{\alpha\beta}$ ,  $L_\beta$ ,  $L'_\beta$ ) [38] or lower temperatures ( $P_{\alpha\beta}$ ,  $P'_\beta$ ) [39] than  $L_\alpha$ , as well as the variations of the hexagonal phase known as the rectangular (R) [40], monoclinic ( $M_\alpha$ ) [41], deformed ( $H_{1d}$ ) and complex hexagonal ( $H_c$ ) [42] phases, and finally, the "K" phase [43].

## 2.6 Liposomes and vesicles

### 2.6.1 Description

It is possible by mixing a lamellar phase with excess water to obtain preferentially a lamellar dispersion made of elements known as liposomes rather than a micellar solution. This appears to be the case for the particles that exist in colloidal dispersions of insoluble surfactants such as polar lipids (*e. g.* phospholipids such as lecithin) or surfactants with a short head [4]. These liposomes are actually spherically concentric multi-layer vesicles (MLV) with an internal water-filled cavity. The region where they form is often referred as the lamellar dispersions region or ‘spherulitic phase’ ( $L_{\alpha} + W$ ).

When observed under an optical microscope with crossed-polars, liposomes appear as small spherical spheres with a characteristic maltese cross (see figure 2.11).

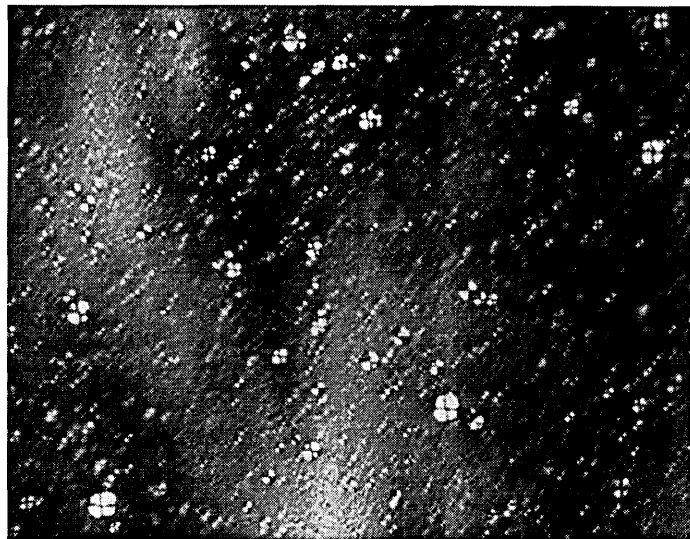


Figure 2.11: Optical texture of a lamellar dispersion  $L_{\alpha} + W$  ( $\times \approx 150$ )

Techniques such as photon correlation spectroscopy (PCS), small angle X-ray scattering (SAXS) or freeze fracture microscopy (see figure 2.12) [44, 45] have been used to obtain precise measurements of the size and arrangement of those structures. Whereas

## CHAPTER 2. SURFACTANT SYSTEMS

the liposome diameter is typically in the range  $0.1 - 5\mu\text{m}$  with an average of 25 layers for a diameter of  $0.5\mu\text{m}$ , vesicles prepared by ultrasonication may be as small as  $20\text{nm}$ . A vesicle of  $50\text{nm}$  typically contains up to 25,000 molecules [4]. The thickness from the active layers and water layers have been measured to be respectively  $2.5\text{nm}$  and 5 to  $10\text{nm}$  [46].

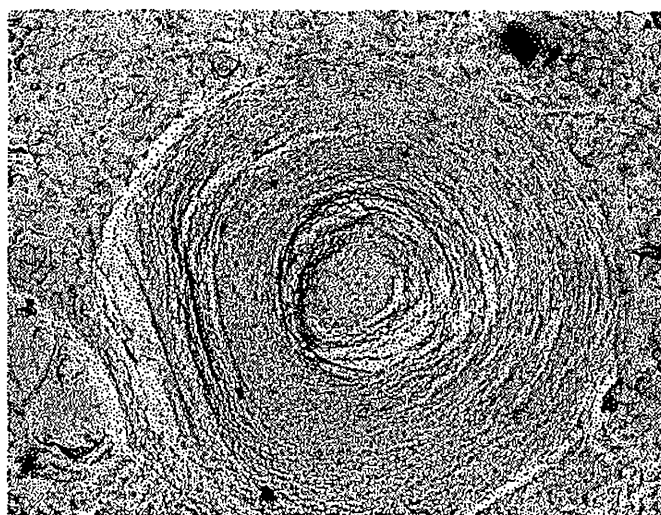


Figure 2.12: Freeze-fracture electron micrograph of a liposome ( $\times \approx 10^4$ ) (courtesy of Albright & Wilson UK ltd)

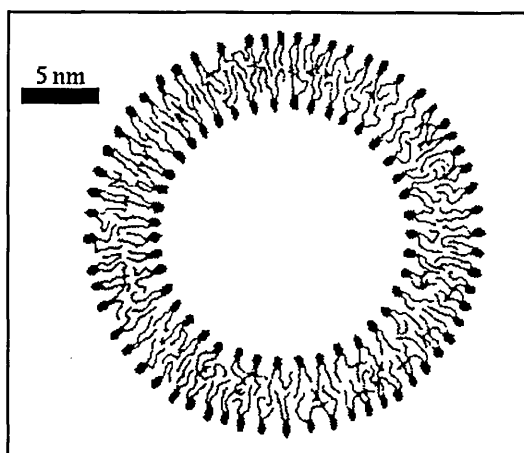


Figure 2.13: Schematic representation of a vesicle (from reference [3])

Because of their particular structure, both hydrophilic and hydrophobic sub-

stances can be solubilised respectively in the internal aqueous regions or within the lipid bilayers. These encapsulation capabilities make them of primary importance as delayed drug delivery systems in the pharmaceutical and cosmetic industries. Liposomes are also used for the manufacture of highly concentrated detergents where they combine unique features, allowing a high concentration of surfactant and suspending or solubilising otherwise immiscible components such as phosphate or zeolite builders whilst retaining a low viscosity. Latest developments include the use of deflocculating side branched polymers with lateral hydrophobic arms — often similar to the surfactant tail — anchored in the outermost layer of the liposome [47].

Although some liposomes have been reported to remain stable over more than two years, no evidence exist *a priori* that they constitute a genuine thermodynamically stable state [4], but they can however be regarded as one phase [5]. The vesicles are also often described as originating from dilution of a sponge phase  $L_3$  by a continuous transition. They appear to be stabilised by both a gain in entropy and enthalpic contributions arising from a favourable packing energy as the bilayers Gaussian curvature rigidity  $\bar{\kappa}$  is decreased towards its stability limit. The influence of the curvature rigidities and critical packing parameter on the stability of the vesicles has been discussed respectively by Cates [36] and Israelachvili [3] (see chapter 3).

### 2.6.2 Preparation

Although liposomes may naturally occur by addition of electrolyte [45], they are usually prepared with suitable preparation techniques to get a greater control over their structure, composition and encapsulation contents. Most techniques used for the preparation of liposomes or vesicles can be divided in two main categories [48]: those based on the mechanical disruption of hydrated lipids (*e.g.* ultrasonication or high-speed homogeni-

sation) and those based on the solvent evaporation from two-phase solvent systems. A new approach more suitable to bulk production is based on the spontaneous formation of liposomes by simple addition of water to a solution of pro-liposome [49].

## 2.7 Experimental techniques

A variety of experimental techniques has been used for the investigation of the phase structure. Most popular include X-ray diffraction, NMR spectroscopy and optical microscopy. As pointed out by Tiddy [31], the use of more than one technique is often required in order to get sufficiently unambiguous information.

### 2.7.1 Nuclear magnetic resonance (NMR)- Electron-spin resonance (ESR)

NMR is probably one of the most popular techniques of investigation because both static and dynamic information can be obtained from it. Indeed, whereas the order parameter  $S$  can be calculated from measurements of the splitting in absorption peaks, information about both rotational and translational molecular motions can be obtained from relaxation time measurements (through estimations of the correlation time  $\tau_c$ ).

That technique is applicable to surfactants, water and counter-ions thanks to the wide range of nuclei that can be traced ( $^1\text{H}$ ,  $^2\text{H}$ ,  $^{13}\text{C}$ ,  $^{23}\text{Na}$ , ...).

ESR allows one to obtain similar information to NMR but its sensitivity is much higher therefore making it particularly suitable for the study of small samples. However, discrepancies in values of the order parameter would suggest that the presence of the magnetic spin-probe causes interferences thus limiting the usefulness of this technique.

### 2.7.2 Optical microscopy - Electronic microscopy

As previously mentioned, the most common phases are optically birefringent under crossed-polars and can therefore be identified by their characteristic optical textures. A useful procedure for the determination of a phase diagram is the phase penetration scan experiment [50] where pure surfactant is placed at one end of a cover slip and some solvent at the other end thus establishing a concentration gradient over the full composition range. Microscopic observations reveal a succession of bands corresponding to the phases occurring at the current temperature. Isotropic phases can often be identified by their viscosity and the phases surrounding them.

Freeze-fracture electronic microscopy is a technique commonly used to study particular structures such as liposomes.

### 2.7.3 Small angle X-ray scattering (SAXS) - Small angle neutron scattering (SANS) - Light scattering (LS)

Unlike the spectroscopic techniques herein described, (low angle) scattering techniques allow the collection of direct information about the dimension of the liquid crystal unit cell. Characteristic diffraction line patterns also give valuable information about the relative lattice arrangement of these units.

### 2.7.4 Other techniques

Spectroscopic techniques such as Raman or infra-red (IR) spectroscopy can also be used to study hydrocarbon conformations and water-hydrogen bonding.

## 2.8 Applications

Thanks to their remarkable physico-chemical properties, surfactants are nowadays being used for a myriad of different applications. This includes:

**Agrochemical surfactants:** emulsifiers, dispersants, hydrotopes or wetting agents.

**Textile and leather processing:** bleaching agents, detergents, dispersants, emulsifiers, flame retardants, softeners, pigment dispersants.

**Foundry and construction chemicals:** plasticisers, retarders or catalysts.

**Polymers and plastics manufactures, coatings:** dispersants for emulsion and suspension polymerisations, catalysts, foaming agents, compounding aids or antistatic agents.

**Pharmaceuticals:** bactericides, disinfectants, foaming agents or compounding aids.

**Oilfield chemicals:** emulsifiers-enhanced oil recovery.

**Ore flotation:** flotation aids.

**Fire fighting:** foam boosters.

**Cutting fluids:** lubricants, emulsifiers, corrosion inhibitors, dispersants or wetting agents.

**Cosmetics and toiletries, industrial and domestic detergents.**

## Chapter 3

# Thermodynamical aspects

### 3.1 Thermodynamics of immiscibility

Like any other system, surfactants obey the fundamental principles of thermodynamics. In order to get an overall understanding of the phenomena taking place, it appears necessary to consider the phase behaviour of surfactants at a macroscopic level and spell out the basic principles of particular relevance to them.

The most useful partial molar quantity used to characterise self-aggregation is undoubtedly the chemical potential  $\mu$ . In a mixture, each component  $i$  is characterised by its chemical potential  $\mu_i$  with:

$$\mu_i = \left( \frac{\partial G_t}{\partial n_i} \right)_{T,P,n_{j \neq i}}$$

where  $G_t$  is the total Gibbs free energy of the system. The chemical potential  $\mu_i$  can thus be seen as representing the change in free energy which would stem from the variation  $\delta n_i$  in quantity of a component  $i$ , at constant pressure, temperature, the composition of other components remaining unchanged. The free energy  $G^{Ph}$  of a particular phase  $Ph$  can be expressed as a function of the chemical potential of all the species  $i$  present in this phase,  $\mu_i^{Ph}$ :

$$G^{Ph} = \sum_i n_i^{Ph} \mu_i^{Ph}$$

Applying this relation to a binary mixture of surfactant in water leads to [51]:

$$G = n_W \mu_W + n_S \mu_S$$

The main interest with this approach is to differentiate between contributions to the free energy arising from the water  $W$  and the surfactant  $S$ . For simplicity those contributions are often referred as respectively the water and surfactant free energies.

In the *ideal mixing approach* where the components are considered fully miscible within each other, the ideal free energy of mixing between two components is:

$$\Delta G_t = (n_1 \mu_1 + n_2 \mu_2) - (n_1 \mu_1^0 + n_2 \mu_2^0)$$

where the reference states  $\mu_i^0$  are taken to relate to the pure compounds.

Since we consider ideal mixtures, the activities  $a_i$  are equal to the mole fractions  $x_i$  (Raoult's law):

$$\mu_i = \mu_i^0 + RT \ln a_i = \mu_i^0 + RT \ln x_i$$

and one can define the dimensionless *reduced free energy of mixing*,  $\Delta G_r$ , as:

$$\Delta G_r = \frac{\Delta G_t}{(n_1 + n_2)RT} = x_1 \ln x_1 + x_2 \ln x_2$$

and the *entropy of mixing*,  $S_m$ , is:

$$S_m = -R\Delta G_r$$

It can be pointed out that the reduced free energy of mixing  $G_r$  is negative over all the composition range of the mixture (except at the boundaries where  $x_i = 0$  or  $x_i = 1$ )

### CHAPTER 3. THERMODYNAMICAL ASPECTS

and therefore the entropy of mixing positive: in the absence of any enthalpic contribution, all compounds have a natural tendency to mix.

However, like many other compounds, surfactants prove to be only partially miscible in water, the most flagrant example of this being the *cloud point* phenomenon exhibited by most nonionic surfactants where they exhibit a closed miscibility loop. Though, their behaviour may often be quantitatively described using the laws of ideal systems and assessing how much it deviates from them. This approach involves the use of quantities known as *thermodynamic activities* in place of compositions.

One of the condition for equilibrium of different phases is that the field variables ( $T$ ,  $p$  and  $\mu$ ) must be identical. No such requirements exist for density variables — like the free energies — which are typically different. The principle known as the ‘*double tangent construction*’ states that in order for coexisting phases of different compositions to have identical chemical potentials, the tangent to the free energy mixing curve at the first composition must also be tangential at the second composition. This construction is illustrated figure 3.1.

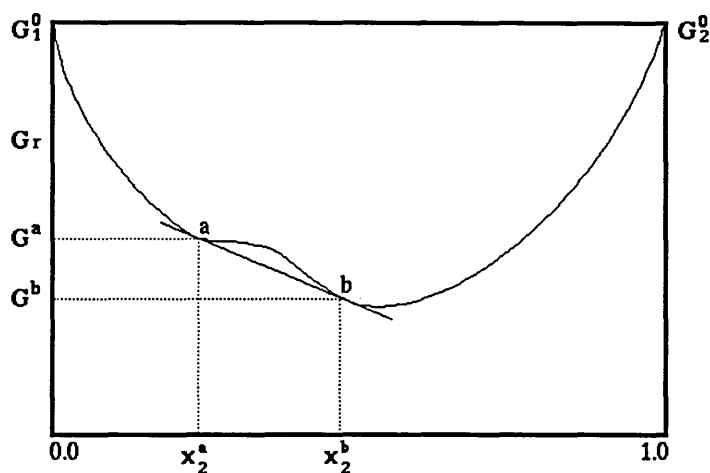


Figure 3.1: Reduced free energy of mixing for a partially miscible system

It follows that for any composition  $x_2$  falling within this miscibility gap ( $x_2^a < x_2 < x_2^b$ ) the system will separate into two distinct phases of different compositions known as the *dilute* and *concentrated* phases, the relative amount of which being so that the total composition remains equal to  $x_2$  (lever rule). A typical composition plot of  $G_r$  for a simple partially miscible system (*i. e.* with a single miscibility gap between  $x_2^a$  and  $x_2^b$ ) is represented in figure 3.1.

The number of phases formed at a given temperature, pressure and composition,  $P$ , only depends upon the number of components,  $C$ , and the degree of freedom of the system,  $F$ ; this dependency is described by a law known as the *Gibbs phase rule*:

$$P + F = C + 2 \quad (3.1)$$

where the degree of freedom (also known as variance) is defined as being ‘the number of system variables that must be specified in order to define fully the state of a mixture that is held under a particular set of conditions’ [4].

The phase rule implies that provided the number of components does not change throughout an experiment (*e. g.* by chemical reaction), the sum  $P + F$  remains constant and fixed to  $C + 2$ .

## 3.2 Hydrophobic and entropic effects

One of the main driving forces responsible for the particular behaviour of surfactants in water is related to the disruption of the water network by their apolar tail.

Indeed, water molecules are known to have the remarkable property of being arranged with each oxygen atom tetrahedrally coordinated with four other oxygen atoms, and a hydrogen atom being situated between each pair [3]. This linearity is principally

caused by the directionality of the H-bonds (see chapter 2). Each water molecule has thus the opportunity of forming an average of  $\approx 3.0 - 3.5$  H-bonds with its neighbours.

When an apolar compound such as an alkyl chain is placed in water, its inability to participate in the formation of any such bond leads the surrounding water molecules to adopt a different arrangement thus minimising the number of lost H-bonds. Although the tetrahedral coordination of water molecules allows them to succeed in finding such an arrangement, this latter appears to impose a much more ordered disposition of the water molecules surrounding the apolar compound thus being entropically very unfavourable. The magnitude of this effect is known to be proportional to the surface area of the apolar compound in contact with water molecules.

This effect responsible for the immiscibility of apolar compounds is known as the *hydrophobic effect* [51]. It is mainly entropic in origin since dispersion forces between apolar compounds and water are actually attractive.

### 3.3 Mathematical models

The phenomenon of micellar aggregation has been the subject of extensive experiments and theoretical models in an attempt to gain a better understanding of the accompanying changes taking place. Amongst those treatments, mathematical models have been long known [52] and proved to be successful in providing quantitative information. Four main different approaches have been used so far [23, 24]: the phase separation model, the mass action law model, the multiple equilibrium model and the small systems model; only the latter two allow a rigorous treatment.

### 3.3.1 Phase separation model

In this approach, the assumption is made that micelles do constitute a proper phase of their own. When the monomer concentration reaches the cmc, the chemical potential of the monomers existing as free monomers is equal to that of those in the ‘micellar pseudo-phase’ and the system is treated as if it underwent a real phase transition. If the chemical potential of the surfactants in the micellar phase is considered constant at constant temperature:

$$\mu_m^0 = \mu_1^0 + RT \ln a_1$$

where  $a_1 = f_1 x_1$  is the monomer activity,  $f_1$  the monomer activity coefficient and  $x_1$  the dimensionless mole fraction. Since the monomer activity is assumed constant above the cmc, the standard free energy of micellisation,  $\Delta G_m^0$ , can be expressed as:

$$\Delta G_m^0 = \mu_m^0 - \mu_1^0 = RT \ln(f_1 x_1) \quad (3.2)$$

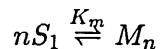
Or assuming that the concentration of free monomers in the presence of micelles is constant and equal to the cmc and the activity coefficients are equal to unity:

$$\Delta G_m^0 = RT \ln cmc$$

This model of micellisation is easy to understand and can be used to calculate quantitative values but does not allow to get any information about the micelles size or shape. It appears to provide better results in the post-micellar region for long chain surfactants [53, 54] (*i. e.* having a low cmc). However, comparisons with experimental results clearly show some obvious discrepancies with predicted values derived from this model. This mainly arises because of the oversimplifications made by assuming that a ‘true’ phase transition occurred at the cmc on the one hand, and that the monomer activity remained constant above the cmc on the other hand [24].

### 3.3.2 Mass-action law model

A different approach is to assume that the monomers are in dynamic association-dissociation equilibrium with micelles of a fixed number of monomers,  $n$ :



Since the equilibrium constant  $K_m$  is:

$$K_m = \frac{f_n x_n / n}{(f_1 x_1)^n}$$

The standard free energy of micellisation is thus:

$$\Delta G_m^0 = -\frac{RT}{n} \ln K_m = -\frac{RT}{n} \ln \left( \frac{f_n x_n}{n} \right) + RT \ln(f_1 x_1) \quad (3.3)$$

Assuming that the activity coefficients are independent of the total concentration of surfactant and equal to unity, the system can be fully described by only one parameter:

$$\ln cmc \approx -\frac{1}{n} \ln K_m$$

Although slightly more difficult to use than the phase separation model, the mass action law model is more successful with short chain surfactants and works over a larger range of concentration than the phase separation model (it can also be used for pre-micellar concentrations). The different predictions from both approaches is illustrated figure 3.2. One may note that both become equivalent when  $n \rightarrow \infty$ , *i. e.* the phase separation approach is equivalent to the formation of a micelle of infinite size.

Both phase separation and mass-action law models fail to explain all sources of non-ideality. Long-range coulombic forces between ionic species and hydrophobic interactions between monomers can be accounted for through activity coefficients in the equilibrium equations and through second virial coefficients (as will be all sources of non-ideality in the post-micellar region) [55, 56].

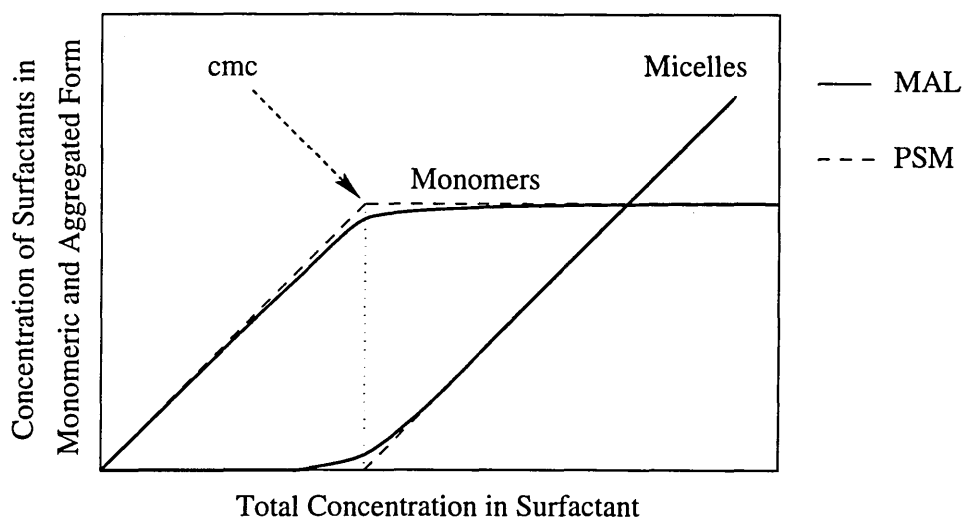
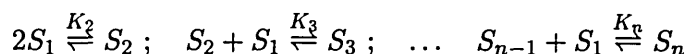


Figure 3.2: Schematic distribution of surfactants between monomers and micelles: typical predictions from the mass-action law (plain lines) and the phase separation models (dashed lines)

### 3.3.3 Multiple equilibrium model

Although the mass-action law model provides a more realistic description of the micellisation, its assumption that the micelles are monodisperse constitutes an oversimplification which prevents it from describing both the actual polydispersity of the micellar size distribution and its variation with the total concentration of surfactant or the temperature. In the extension of the mass-action law model known as *the multiple equilibrium model*, the original unique single-step association/dissociation is replaced by a series of association reactions of monomers:



which may be expressed differently as:



it follows that:

$$K'_n = \frac{a_n/n}{a_1^n} = \prod_{i=2}^n K_i$$

### CHAPTER 3. THERMODYNAMICAL ASPECTS

Equilibrium thermodynamics requires that in a system of molecules which form aggregates in solution the chemical potential of all identical species be the same. Considering quantities per molecules instead of molar quantities, this implies that:

$$\mu = \mu_1^0 + kT \ln a_1 = \mu_2^0 + \frac{kT}{2} \ln \left( \frac{a_2}{2} \right) = \dots = \mu_n^0 + \frac{kT}{n} \ln \left( \frac{a_n}{n} \right) \quad (3.4)$$

where  $\mu_n^0$  is the mean interaction free energy per molecule in micelle of aggregation number  $n$ . Equation 3.4 may be rewritten to express the excess chemical potential as:

$$\mu_n^0 - \mu_1^0 = kT \ln(f_1 x_1) - \frac{kT}{n} \ln \left( \frac{f_n x_n}{n} \right) \quad (3.5)$$

Together with the conservation relation  $x_{tot} = \sum_{n=1}^{\infty} x_n$ , this equation completely defines the model. It can be expressed under a more convenient form as:

$$x_n = n \frac{(f_1 x_1)^n}{f_n} \exp \left[ \frac{-n(\mu_n^0 - \mu_1^0)}{kT} \right] \quad (3.6)$$

Depending on how the chemical potentials are defined [57], the dimensionless concentration  $x_n$  may be also expressed as a volume fraction or mole fraction.

Ben-Shaul *et al.* [58] have extended this model by incorporating the influence of the aggregate shape in addition to its size. Their expression of the chemical potential  $\mu_{n,s}$  for an aggregate of size  $n$  and shape  $s$  is thus:

$$\mu_{n,s} = \mu_{n,s}^0 + \frac{kT}{n} \ln \left( \frac{x_{n,s}}{n} \right) + \chi_{n,s} \quad (3.7)$$

where  $\chi_{n,s}$  is a corrective term accounting for the non-ideality of the system. This approach has the merit of giving a better description of the system thus allowing the analysis of transitions like the micellar sphere-to-cylinder transition by decomposing the free energy

of a rod-like micelle,  $\mu_{rod}$ , into contributions from the amphiphiles contained at the semi-spherical end caps,  $\mu_{sph}$ , and from the cylindrical centre,  $\mu_{cyl}$ .

### 3.3.4 Small systems model

As pointed out by Wennerström [24], the phase separation and mass-action law models fail to relate any change in micellar size or shape and would require some alterations in order to incorporate them. The most rigorous approach is probably that of Hall and Pethica [59] who modified the theory of small system thermodynamics [60] to extend the phase separation model of classic thermodynamics. In this model, the micelles are considered as ‘small systems’ in dynamic equilibrium with each other and surrounded by a bath defining the environment variables. This theory allows the maximum number of independent intensive variables to be increased by one (relative to that of a corresponding macroscopic system) and therefore to express the micellar size distribution function  $x_n$  as a function of the temperature  $T$ , the pressure  $p$ , and the free monomer chemical potential  $\mu_1$ .

Although the most rigorous, this approach has not been very popular and often regarded as unnecessarily complicated [24].

## 3.4 Driving forces and geometric packing

### 3.4.1 Optimal head group area

The mechanism behind the formation of micellar systems and crystalline phases may also be understood [5, 51] by decomposing the interactions responsible for the self-aggregation process as including contributions from intra and inter-aggregates components.

Assuming that the amphiphiles are aggregated and fully hydrated:

$$G_{total} = G_{intra} + G_{inter}$$

where  $G_{total}$  is the relative free energy of aggregation in a particular structure,  $G_{intra}$  and  $G_{inter}$  respectively its contributions from intra and inter-aggregate interactions. Those latter can also be decomposed as:

$$G_{intra} = G^{elec} + G^{surf} + G^{conf}$$

$$G_{inter} = G^{elec} + G^{vdW} + G^{hydr}$$

where  $G^{elec}$ ,  $G^{surf}$ ,  $G^{conf}$ ,  $G^{vdW}$  and  $G^{hydr}$  are the respective contributions from electrostatic, surface, conformational, van der Waals interactions and hydration forces.

In diluted micellar systems, contributions from the inter-aggregate interactions can be neglected (*i. e.*  $G_{intra} \ll G_{inter}$ ) and two conflicting driving forces oppose each other:

- A repulsive hydrophilic interaction between the head groups: those latter try to remain solvated and will therefore tend to repel each other in order to maximise the interfacial surface area  $a$  with the water.
- An attractive hydrophobic forces between the tail groups: it arises following the necessity to minimise the interfacial surface area  $a$  with the water.

The first type of interactions is steric and electrostatic — if applicable — in origin; contributions from hydration forces are also present. It will favour the formation of spherical or — to less extent — of cylindrical micelles as opposed to disk-like micelles or bilayers. This contribution is expected to be inversely proportional to the surface area  $a$ ,  $\propto K/a$  [57].

On the other hand, the second type favours the formation of those structures in the reverse order (bilayers  $\rightarrow$  disks  $\rightarrow$  cylinders  $\rightarrow$  spheres). It may be expressed as  $\gamma a$  where  $\gamma$  is the interfacial free energy per unit area.

The former influence appears to be predominant in most cases for diluted micellar systems — *i. e.* when packing constraints do not prevent it and no electrolyte is added — thus explaining the preferential formation of spherical micelles. This approach can be extended further [5] to attempt predicting the formation of liquid crystalline phases.

Following Israelachvili, the interfacial free energy of a molecule in an aggregate can therefore be written as the sum of those two terms:

$$\mu_n^0 = \gamma a + \frac{K}{a} \quad (3.8)$$

where  $K$  is a constant.

$\mu_n^0$  is minimised for a value of  $a$  known as the ‘optimal surface area’,  $a_0 = \sqrt{K/\gamma}$  (see figure 3.3).

It must be pointed out that although important influences such as the effect of the surface curvature have been neglected in this approach, it still succeeds in giving a good account of the hydrocarbon interactions in aggregates.

### 3.4.2 Geometric packing considerations

The previous arguments can be extended further to predict which structures will be favoured [61]. In addition to the optimal headgroup area  $a_0$ , both the ‘critical chain length’,  $l_c$ , and the hydrocarbon chain volume,  $v$  must be considered.  $l_c$  is defined as ‘a semi-empirical parameter beyond which hydrocarbon chains can no longer be represented as fluid’ [3]; it is actually slightly smaller than the all-trans chain length. Tanford [51] has established a simple linear relation between those two properties and the number of

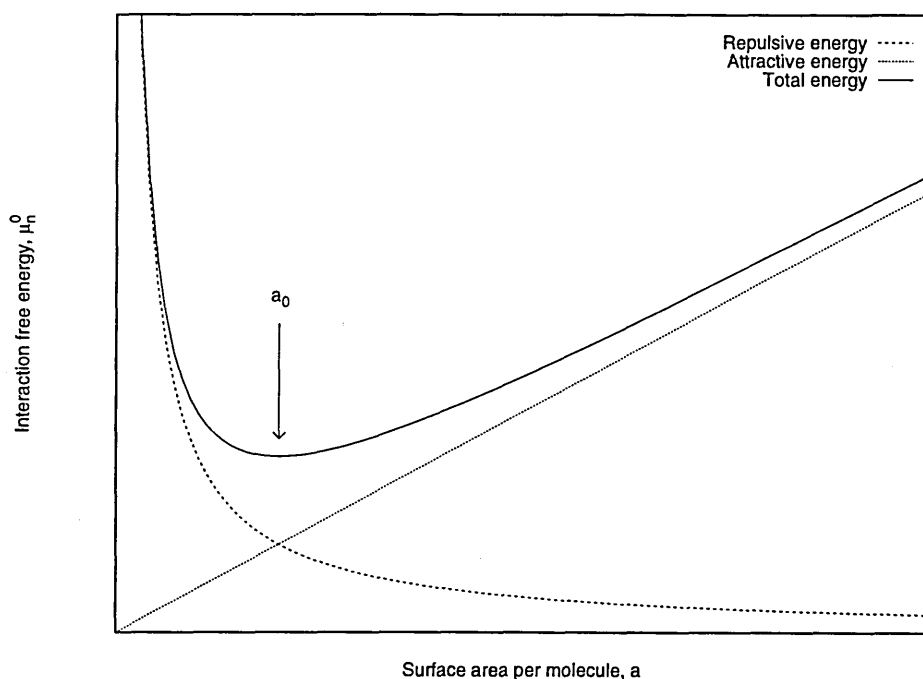


Figure 3.3: Optimal head group area,  $a_0$  (from reference [3])

carbon atoms in the hydrophobic tail.

For convenience, one can define a new dimensionless quantity known as the *critical packing parameter* or *shape factor* as  $v/a_0l_c$ . Israelachvili has demonstrated that this parameter alone could suffice to predict the type of aggregate preferentially formed.

Critical packing parameter $v/a_0l_c$	Critical packing shape	Structures formed
$< 1/3$	Cone	Spherical micelles
$1/3 - 1/2$	Truncated cone	Cylindrical micelles
$1/2 - 1$	Truncated cone	Vesicles, flexible bilayers
$\approx 1$	Cylinder	Planar bilayers
$> 1$	Inverted truncated cone	Inverted micelles

Table 3.1: Critical packing parameter and favoured structures (from reference [3])

Any factor affecting the value of  $v$ ,  $a_0$  or  $l_c$  will therefore have an influence on the type of structure formed. The main factors can be classified in one of the following categories [3]:

### CHAPTER 3. THERMODYNAMICAL ASPECTS

- Factors affecting the headgroup area,  $a_0$  (*e. g.* the pH or addition of electrolyte).
- Factors affecting the chain packing (*e. g.* degree of branching or unsaturation of the hydrocarbon chain): influence both  $l_c$  and  $v$ .
- Temperature: influence both  $a_0$  and  $l_c$ .

If two competing structures appear to have an identical interfacial free energy, the one with the smallest aggregation number will be favoured for entropic reasons.

Another essential parameter is the way the chemical potential varies with the size of the aggregate. A simple dependency has been proposed by Israelachvili for different structures:

$$\mu_n^0 = \mu_\infty^0 + \frac{\alpha kT}{n^p} \quad \text{where} \quad \begin{cases} p = 1/3 & \text{for a sphere} \\ p = 1/2 & \text{for a disk} \\ p = 1 & \text{for a rod} \end{cases} \quad (3.9)$$

## Chapter 4

# Models of surfactant systems

The modelling of liquids may be approached from two opposing points of view. On the one hand one can try to simulate the behaviour of very few particles with some very detailed and realistic potentials, or on the other hand one can take the opposite route and choose to simulate a whole system of particles — typically several thousands — with some idealised and simplified interactions. The choice depends mainly on the phenomenon under investigation and whether estimates of the entropy and free energies are needed.

These two families of models can also be subdivided according to the basic model they originate from. Neglecting the first category which is mostly irrelevant for the modelling of surfactant systems since a large number of chains are involved in the phenomena typically studied (*i. e.* micellisation or phase transitions), the second one is essentially composed of Ising-like and chain-type models — which can themselves be subdivided as lattice *or* off-lattice simulations and constrained-chains *or* self-assembling chains.

An extensive review of lattice models of surfactant systems has been presented by Care, Desplat and Brindle [62].

## 4.1 Phenomenological models

The first phenomenological models for disordered microemulsions have been devised by Talmon and Prager in 1978 [63] and later extended by De Gennes and co-workers [64–66]. One of the most active group in this area has probably been that of Andelman, Cates, Roux and Safran [67] who created a simple model describing the phase equilibria and structural properties of microemulsions. This model is a lattice model in which each site is occupied by pure oil or water. Oil and water are regarded as continuum liquids whereas the interfacial surfactant layer is treated as a flexible sheet characterised by a size-dependent bending constant. The presence of salt or alcohol can be accounted for through the energy parameters of the interfacial sheet. The following methodology had then to be used in order to generate the phase diagram of this ternary mixture: once the volume fraction of oil, water and surfactant has been fixed, the free energy of a hypothetical homogeneous phase could be calculated from the amount of surfactant in the system. This process is repeated for each new composition.

Andelman *et al.* were thus able to build ternary phase diagrams with a middle-phase microemulsion which coexists with dilute phases of surfactant in oil and surfactant in water, and two regions of two-phase equilibrium involving upper and lower-phase microemulsions coexisting with either almost pure water or almost pure oil.

These phenomenological models yield a reasonably realistic picture of the behaviour of microemulsions. However, as pointed out by Sturgeon and Reiss [68], an approach in which the random mixing approximation is used leads to some errors in the calculation of the entropy of mixing arising from the influence of the underlying lattice on the counting of configurations. Furthermore, one may consider the inadequacy of this approach to describe the formation of lyotropic phases.

Other types of phenomenological studies have been undertaken specifically to

deal with micellar systems (*e. g.* Benedek and Blankschtein [69, 70]) and proved to be reasonably successful in describing the sphere-to-rod transition which influences the cluster size distribution and the growth of micelles into aggregates of different size and shape . A model proposed by Goldstein [71] provides an expression for the dependency of the free energy of aggregation with the cluster size and as such is particularly relevant to the study in the micellar region presented in chapter 8.

## 4.2 Ising-type models

An interesting alternative to the phenomenological approach has been provided by the microscopic approach, the most famous examples of which are the Ising-type models. The main advantage of Ising models is that they have been extensively studied. Some authors decided to adapt them so that they could model microemulsions and lyotropic liquid crystals, the excellent knowledge and huge amount of data about these models still being relevant for their purposes.

These are very coarse grained models in which details of chains and statistics of chain packing are essentially ignored.

### 4.2.1 Spin-1/2 Ising (Widom-type) models

The first attempt to carry out simulations of an oil-water-surfactant system using an Ising-type model was as early as 1968 by Wheeler and Widom [8]. Indeed, although many other simulations had already been carried out on decorated lattice models, this one was the first to have explicitly included the mechanism of bifunctionality as a physical basis. This system was composed of three types of bifunctional molecules  $AA$ ,  $AB$  and  $BB$  lying on a regular lattice so that its bonds were completely filled (see figure 4.1). Infinite potentials were used to prevent them from being occupied by more than one molecule and

ensuring that only similar ends (either all-*A* or all-*B*) lie on the same lattice site. In other words, the  $c$  molecular ends ( $c$  being the coordination number of the lattice) associated with a given site are all the same: similar ends may associate, but different ones repel each other infinitely. Every lattice site may thus be identified as all-*A* or all-*B* site allowing a direct transcription to a spin 1/2 Ising model.

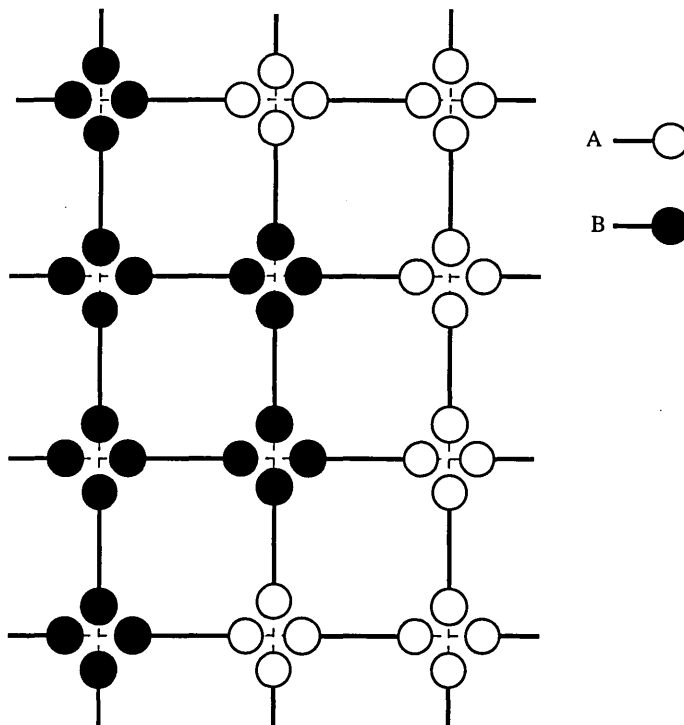


Figure 4.1: Mapping of spin 1/2 Ising model into Wheeler and Widom model (from reference [8])

The energy associated with such a system is thus :

$$E = J (N_{\uparrow\downarrow} - N_{\uparrow\uparrow} - N_{\downarrow\downarrow}) - H (N_{\uparrow} - N_{\downarrow})$$

where  $J$  is the constant spin-spin coupling parameter and  $H$  the product of the magnetic field strength to the constant magnetic moment per spin.  $N_{\uparrow\downarrow}$ ,  $N_{\uparrow\uparrow}$ ,  $N_{\downarrow\downarrow}$ ,  $N_{\uparrow}$ , and  $N_{\downarrow}$  are respectively the number of antiparallel, parallel up, parallel down, up and down spins on the lattice.

The Hamiltonian can alternatively be expressed as:

$$\mathcal{H} = -J \sum_{i,j} S_i S_j - H \sum_i S_i$$

where  $S_i = \pm 1$  and  $\sum_i S_i = M$ .

This model exhibits a phase separation into  $AA$  and  $BB$ -rich phases for low concentrations of  $AB$  with this latter forming a film at the interface. As its concentration is increased,  $AA$  and  $BB$  become mutually soluble up to a point where the solution is then in equilibrium as a single phase. For high concentrations in  $AB$ , a phase transition to an ordered *anti-ferromagnetic* phase may also be observed.

Widom later studied this model in the mean-field approximation [72]. Both the interfacial profiles in  $AA$ ,  $AB$  and  $BB$  and the structure of the bulk phases have been considered. He was thus able to establish the profile of the density of species  $AB$  at the interface and its preferred molecular orientation: the  $A$  ends are pointing towards the  $A$ -rich region whereas the  $B$  ends pointed towards the  $B$ -rich phase. This preferential orientation becomes less and less significant as one gets further from the interface. Similar calculations for the bulk phases yielded micellar and bicontinuous structures analogous to those found in microemulsions and surfactant solutions.

This model was later refined by the addition of a splay energy [9]. This additional interaction was included in order to favour the formation of flat films as they occur experimentally and to give more realistic properties to the microemulsion such as an osmotic compressibility or the ability to be in equilibrium with almost pure oil and water phases simultaneously. A similar approach is used in phenomenological models. This splay energy may depend on whether the curvature is concave to the  $A$  phase or to the  $B$  phase (oil-in-water or water-in-oil). The energy associated with the meeting of two  $A$  ends of an amphiphile was  $K(1 - \lambda)$  and  $K(1 + \lambda)$  for two  $B$  ends where  $K$  is analogous to the rigidity parameter of the phenomenological theories;  $K$  was kept positive throughout the

simulations and  $\lambda$  could be of either sign but was kept null in order to make the bending energy independent of the direction of bending. The Hamiltonian of this system is thus:

$$\mathcal{H} = \sum_{\{i,j,k\}} \left[ \frac{1}{4}K - \frac{1}{4}\lambda K(\sigma_i - \sigma_j + \sigma_k) - \frac{1}{4}K(\sigma_i\sigma_j + \sigma_j\sigma_k - \sigma_i\sigma_k) + \frac{1}{4}\lambda K\sigma_i\sigma_j\sigma_k \right]$$

where  $\sigma_i$ ,  $\sigma_j$  and  $\sigma_k$  are the spins associated with three consecutive sites and  $\{i, j, k\}$  denotes the sum over all distinct triplets; each  $\sigma_x = \pm 1$ . This model is shown to be equivalent to an Ising model with competing first and second-neighbour interactions and three-spin interactions. An equivalence table between the Ising and microemulsions models parameters was established. The symmetrical version of this model in which the activity in  $AA$  and  $BB$  are equal was also studied under the mean-field approximation. It reveals that layered phases and the ferromagnetic and paramagnetic phases are apparently the only stable states when  $J > 0$  and  $M < 0$  (where  $J$  and  $M$  are respectively the ferromagnetic nearest-neighbour and antiferromagnetic next-nearest-neighbour interaction constants), which implies that this model would be equivalent to the anisotropic next-nearest-neighbour Ising  $ANNNI$  model. The modulated phases from its phase diagram — *i. e.* with an oscillatory correlation function — were identified as microemulsion phases whereas the ferromagnetic phases are equivalent to bulk oil or water with some amphiphiles solubilising the other material (see figure 4.2).

The main problem with this model was the occurrence of layered structures even in the macroscopic phases identified as microemulsions and this would probably not exist in a corresponding continuum model. This phenomenon is believed to be an artefact of the underlying lattice. Both the correlation and scattering functions were calculated in the mean-field approximation [73] and appeared to be qualitatively consistent with those of microemulsions.

Dawson [74] undertook a detailed study of the interface generated using the orig-

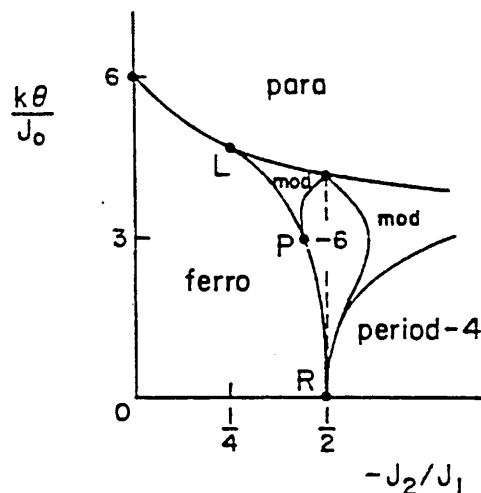


Figure 4.2: Schematic of phase diagram of ANNNI model on simple-cubic lattice. L is the Lifshitz point, PR is the ferromagnetic-period-6 first-order transition line (from reference [9])

inal Widom model [72]. The surface tension at the interface between the oil-rich and water-rich region was calculated using a variational method by subtracting the bulk free energy from the free energy when the interface is present, this latter being itself computed by summing up the free energy density. Qualitative results were in good agreement with experimental data as well as quantitative results for  $M = 0$  (*i. e.* equivalent to a simple nearest-neighbour Ising model) with earlier calculations by Widom. Both the interfacial profiles and surface tensions can be computed with a high numerical accuracy. In order to characterise the appearance of non-monotonic density profiles due to the surface aggregation, an analytical description was also undertaken which included a fourth-gradient term. The bulk phase densities were used as the zeroth approximation in an iterative solution. One may note that for the particular case where  $M = 0$ , the density profile is monotonic. The wetting phenomenon was also studied in the mean-field theory by comparing the surface tensions between the oil-rich and water-rich phases and either of these with the microemulsion phase. As it occurs experimentally, the oil-rich and water-rich regions

appeared not to be wet by microemulsions in the symmetrical region.

More recently, Dawson, Walker and Berera [75] used a simplified version of the model to account for the various liquid crystalline phases. Contributions from Monte Carlo simulations, low-temperature series and renormalisation group analysis generated a complete phase diagram. The Monte Carlo simulations were carried out using a single-spin-flip MC algorithm and either the Metropolis or heat-bath algorithms without any noticeable difference. However, some discrepancies between the results obtained by the mean-field theory and the Monte Carlo simulations were reported by the authors. Indeed, whereas the mean-field approach appeared to be ambiguous for some parts of the phase diagram — especially for higher temperatures — due to its inability to deal with fluctuations, the Monte Carlo simulations suffered from the frustration of the Ising spins and from a strong hysteresis. Although the overall results were in qualitative agreement, there was an obvious difference in the shift of the order-disorder phase boundaries. A different sized lattice was used to assess the strength of the finite-size effect.

The pair correlation functions and structure factors were also computed and some interfacial properties characterised. They appeared to be in good qualitative agreement with the experiment. The phase diagram exhibited disordered *paramagnetic* phases identified as a microemulsions phase, a ferromagnetic phase equivalent to micellar oil and water phases, with a lamellar phase in equilibrium between both these and the microemulsions. The transitions between the disordered phase and the lamellar phases is first-order whereas that between the disordered fluid and the oil-rich and water-rich phases is continuous.

Dawson [76] proposed a closely related model in which the energy contributions arising from the edges and corners of the amphiphilic film were made dissimilar. The idea behind this model was to take into account the energy due to the bends of isolated films (thus with a difference for edges and corners), from two proximate flat pieces of film and to

differentiate between the hydrophilic and hydrophobic ends. The Hamiltonian was then:

$$\mathcal{H} = H \sum_i \sigma_i + \sum_{\{i,j\}} J_{i,j} \sigma_i \sigma_j + \sum_{\{i,j,k\}} L_{i,j,k} \sigma_i \sigma_j \sigma_k + \sum_{\{i,j,k,l\}} P_{i,j,k,l} \sigma_i \sigma_j \sigma_k \sigma_l$$

A set of restrictions for which  $M_2 = 2M_1 = 2M$  ( $M_1$  and  $M_2$  being respectively the two-body spin interactions for diagonal neighbours and linear next-nearest-neighbours) and  $L_1 = L_2 = P = 0$ , made this model analogous to Widom's apart from the presence of a four-body term that reflects the selection of an independent energy corner. This model was studied with both mean-field theory and Monte Carlo simulations. Interfacial tensions were computed and the structure of the interface was characterised through density profile calculations.

This model and its extensions thus appear to give rather good results if we bear in mind that they are amongst the simplest conceivable. However, Stauffer and Jan [77] used the model in a Monte Carlo experiment in both two and three dimensions and experienced some problems due to the interface energy being exactly zero; phases suffer from a lack of stability and no long-range order exists at finite temperature. Dawson, Lipkin and Widom [78] acknowledged the lack of stability of layered phases in two dimensions but claimed that the equivalent phases were likely to be stable in a three-dimensional model. Furthermore, as pointed out by Hansen, Schick and Stauffer [79], this model only allows continuous transitions between the disordered fluid and the water-rich and oil-rich regions; as a consequence of that, no example of three-phase coexistence as found experimentally is observable. In order to overcome this, the previous group presented a 'generalised' version of Widom's model in which an additional two-particle interaction is introduced. Indeed, by introducing an attractive interaction between two collinear amphiphiles separated by

## CHAPTER 4. MODELS OF SURFACTANT SYSTEMS

two lattice sites the model produces a first-order transition between the disordered phase and the ordered water-rich and oil-rich phases, and a disordered line which intersects this line of transitions. The following part was therefore added to the Hamiltonian:

$$-Q \sum_{\{i,j,k,l\}} \sigma_i \sigma_j \sigma_k \sigma_l$$

where  $\{i, j, k, l\}$  denotes a set of four adjacent colinear sites.

This model was studied under mean-field analysis (including the calculation of the free energy for each site) and used to carry out MC simulations. The results from both approaches — order parameters, interfacial tensions and concentration profiles — were consistent and confirmed that the original aim of this model had been reached.

Dawson and Kurtovic [10] created a new model which kept some of the features offered by the Widom's but made it much more realistic by allowing arbitrary orientations of the amphiphiles; the location of the center of mass was still discretised. This improvement aimed to promote self-assembly. Each site  $i$  of the lattice was thus characterised by an Ising-like variable which could take the value  $+1$  or  $0$  depending on whether the site was occupied by an amphiphile or not. If such a molecule is present, its orientation is then given by an Heisenberg spin vector. One of the direct consequences of this new feature was to allow single molecules of amphiphile in water, thus making possible to carry out some simulations near the cmc.

This model was studied under the mean-field theory. Some phase diagrams were obtained for the effective chemical potential versus the temperature by using the spin densities calculated by solving the mean-field equations for all symmetries appearing at zero temperature. They are easily convertible to more classic temperature vs concentration phase diagrams. Those latter exhibit several phases identified as cubic, tubular, isotropic, lamellar or combinations of them as well as two triple points (see figure 4.3).

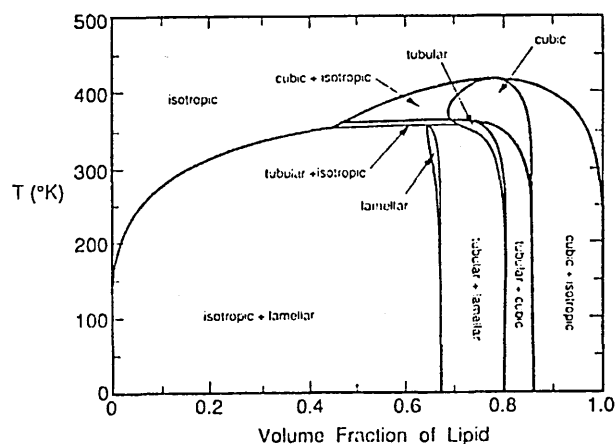


Figure 4.3: Phase diagram constructed using the spin densities obtained by solving the mean-field equations, for certain selected symmetries of phase (from reference [10])

#### 4.2.2 Spin-1 Ising (Blume-Emery-Griffiths-type) models

The model so far described used a spin variable with only two possible values. This was later extended by Gunn and Dawson [11] to study a ternary mixture of oil-water-amphiphiles. Its alteration consisted in changing the discrete variable  $\sigma_i$  so that it can take the values  $-1, 0$  or  $+1$  depending on the nature of the species. The model becomes thus a three-state spin model equivalent to a Blume-Emery-Griffiths model [80]. The main improvement over Widom's type models is the existence of a finite oil-water interaction energy thus allowing direct contact between them. The Hamiltonian of this model is:

$$\mathcal{H} = \sum_{\langle n, n' \rangle} \sum_{i, j = -1, 0, 1} \rho_{i, n} \rho_{j, n'} E_{ij}(S_n, S_{n'}, \Delta_n)$$

where  $E_{ij}(S_n, S_{n'}, \Delta_n)$  is the interaction energy between species  $i$  at site  $n$  with species  $j$  at site  $n'$ .

This model was analysed with both the mean-field theory and Monte Carlo simulations. Some phase diagrams were obtained from the calculation of the free energy. Phases such as micellar, bilayer, cubic, lamellar, water, oil, amphiphile and lamellar phases were successfully identified (see figure 4.4). Results provided by those two approaches were rela-

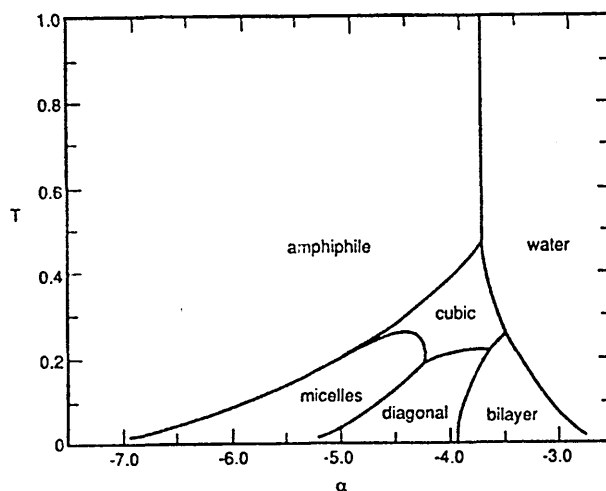


Figure 4.4: Mean-field phase diagram (from reference [11])

tively consistent apart from a microemulsions region which was considerably enhanced in the Monte Carlo simulations; that discrepancy is attributed to the inability of the mean-field theory to deal with the large-scale fluctuations associated with the microemulsions. The Monte Carlo simulations themselves provided results in very good agreement with the experiment both qualitatively — and to less extent — quantitatively (notably the water-water structure factor). We may point out that the MC simulations have been carried out on different lattices ( $24 \times 24 \times 24$  and  $48 \times 48 \times 48$ ) in order to monitor the lattice size effect.

Schick and Shih [81] introduced a new three dimensional spin-1 model of microemulsions for a ternary mixture of oil-water-surfactant, each lattice site being completely filled by water, oil or surfactants; this was represented by a statistical variable  $S_i$  which could take the values of 1,  $-1$  or 0 respectively. The surfactant is made responsible for inducing an attractive interaction between molecules of a different nature at a distance equal to the size of the surfactant molecule. This model is an extrapolation of the *BEG* model. Its Hamiltonian is thus:

$$\mathcal{H} = - \frac{1}{2} \sum_{i,j} [J_{i,j} S_i S_j + K_{i,j} S_i^2 S_j^2 + C_{i,j} (S_i S_j^2 - S_i^2 S_j)] - \sum_i (H S_i - \Delta S_i^2)$$

$J$  and  $K$  were made positive for nearest-neighbour in order to account for the stability of oil and water in absence of surfactants and  $C_{i,j} = H = 0$  (*i. e.* the concentration in oil and water were equal).

The *BEG* model has some specific features which allows it to overcome some of the limitations peculiar to the *ANNNI*. For instance the *BEG* model, being isotropic, describes some phases such as closely-packed tubes or cubes that the *ANNNI* is unable to reproduce. Whereas transitions from the disordered phase were all continuous with the *ANNNI*, only transitions to the uniform ordered phases (oil-rich and water-rich) were continuous with the *BEG* model; the transitions to the microemulsions region is first-order. Another important property of this model is that the lines of first-order transitions separating the phases meet at a single point. This behaviour is much more consistent with the experiment than the *ANNNI* model.

A phase diagram was generated in the temperature-surfactant chemical potential plane using the mean-field theory. Coexisting oil-rich and water-rich phases, disordered fluid, and a bicontinuous phase analogous to that described by other groups were observed. The surface tension between oil-rich and water-rich regions was also calculated as a function of the concentration in surfactant using mean-field calculations.

This model was later used by Gompper and Schick [12] to undertake a study of the three independent density-density correlation functions of the microemulsions. Those latter appeared to be in qualitative good agreement with the experiment. This model was solved exactly using a transfer-matrix method, used for a MC simulation in two-dimensions

and also studied under the mean-field approximation in three-dimensions. The results from these different methods were relatively consistent. A phase diagram was generated in which a triple line ending in critical endpoints which — by raising the temperature — coalesce in a tricritical point (see figure 4.5). This study was presented in greater details in 1990 [82].

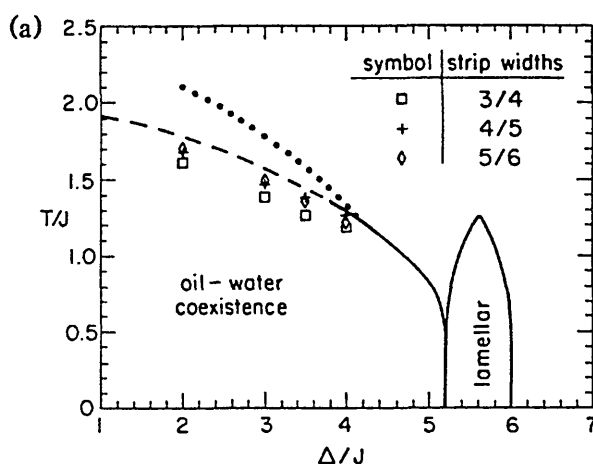


Figure 4.5: Phase diagram in two dimensions. Full lines and dashed lines indicate first order and continuous transitions, respectively. Dotted line is the disorder line (from reference [12])

Laradji, Guo, Grant and Zuckermann [83] studied a simple two-dimensional model of a ternary mixture of oil-water-surfactants. They carried out Monte Carlo simulations for a wide range of concentrations and temperatures. In this model, each site was occupied by either water, oil or surfactants. This was represented by a three-component spin variable  $S_i$  which could take the value  $+1$ ,  $-1$  and  $0$  respectively. In order to take into account the anisotropic nature of the surfactant molecules, a vector operator  $\mathbf{m}_i$  was associated with each of them. The four possible directions along the bonds of the lattice were allowed. Only the case in which an equal amount of oil and water was present has been considered. The Hamiltonian is thus:

$$\mathcal{H} = -J_1 \sum_{i,j} S_i S_j - J_2 \sum_{i,j} (S_j \mathbf{m}_i \cdot \mathbf{r}_{ij} + S_i \mathbf{m}_j \cdot \mathbf{r}_{ij}) + \Delta \sum_i S_i^2$$

where  $\Delta = \mu_s - \frac{1}{2}(\mu_w + \mu_o)$ . One may note that the only free parameter is the interaction ratio  $J_2/J_1$ .

A phase diagram was generated by computing the equilibrium probability distribution of energy and surfactant concentration; this allows us to get thermodynamic functions such as the specific heat or the compressibility. This model exhibits a rich phase behaviour with both microemulsions and liquid crystal phases in good agreement with experiment and with the work of Gompper and Schick: with increasing concentrations, one observes a phase coexistence of oil-rich and water-rich, a disordered (microemulsions) phase, and a lamellar and square phase (believed to be homologous to a cubic phase in three dimensions) with quasi long-range order. The microemulsions, disordered, lamellar, oil-rich and water-phases meet at a tricritical point. The effect of fluctuations has been studied by developing a local mean-field theory for the microemulsions region. The water-water structure factor  $S(q)$  has also been computed in this region.

### 4.2.3 Decorated lattice-gas models

Alexander [84] proposed a decorated lattice-gas model for microemulsions. With some approximations, it maps exactly onto a spin 1/2 Ising model. The phase diagram, correlation functions and the free energy could thus be deduced from those of the corresponding Ising model. Even if some of its features were consistent with those of microemulsions and some mesophases were observed, this model suffers from some serious limitations such as the absence of interactions between surfactants and the symmetry between the two curvatures of the interface.

It was later generalised by Chen, Ebner, Jayaprakash and Pandit [13, 85] who

CHAPTER 4. MODELS OF SURFACTANT SYSTEMS

carried out both mean-field study and Monte Carlo simulations on two — and more rarely three — dimensions of an oil-water-surfactant mixture. Their Hamiltonian was:

$$\mathcal{H} = - H \sum_i \sigma_i - J \sum_{\langle i,j \rangle} \sigma_i \sigma_j - \mu \sum_{\langle ij \rangle} \tau_{ij} - V \sum_{\langle ij,kl \rangle} \tau_{ij} \tau_{kl} - V_1 \sum_{\langle\langle ij,kl \rangle\rangle} \tau_{ij} \tau_{kl} - J_1 \sum_{\langle i,j \rangle} \sigma_i \sigma_j \sigma_{ij}$$

where  $\sigma_i = \pm 1$  indicates the presence of water or oil molecules,  $\tau_{ij} = 1$  when a surfactant molecule lies on sites  $\langle ij \rangle$  and  $\langle i, j \rangle$ ,  $\langle ij, kl \rangle$  and  $\langle\langle ij, kl \rangle\rangle$  are respectively nearest-neighbour pairs of sites and pairs of links that meet at vertices at 90 and 180.

One may note that for  $V = V_1 = 0$ , this Hamiltonian reduces to that of Alexander. Those parameters will however be kept different from zero in order to allow for a first-order phase boundary along which all three of the oil-rich, water-rich and microemulsions coexist. MC simulations were carried out in the grand canonical ensemble using the Glauber single-spin-flip dynamics and in the canonical ensemble using the Kawasaki spin-exchange dynamics.

This model exhibited a disordered paramagnetic phase homologous to a microemulsions phase at high temperature, oil-rich, water-rich, low-period lamellar, low-period crystals and uniform phases at lower temperatures as well as coexistence of two and even three phases (any combination of oil-rich, water-rich and/or microemulsions) and many long-lived metastable phases (lamellar, super anti-ferromagnetic and inhomogeneous). The phase diagram is represented figure 4.6. The structure factor  $S(q)$  and mean-droplet lifetime were also computed;  $S(q)$  appeared to be consistent with other models for low values of  $q$ .

The main weaknesses of this model are its inability to reproduce the large variety of long-period lamellar phases and complicated cubic phases. Furthermore, the concen-

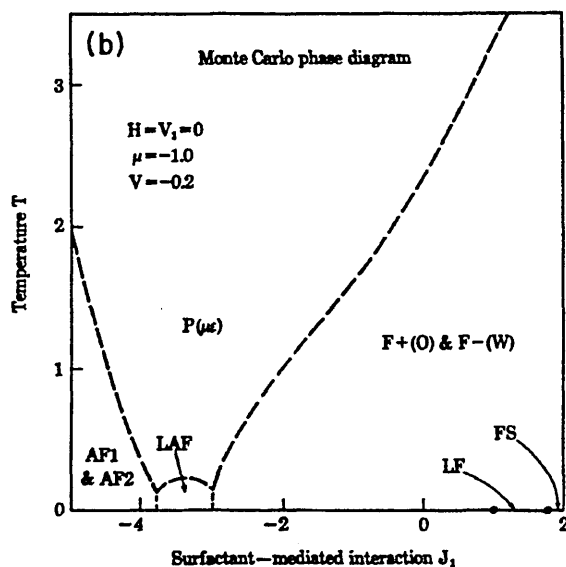


Figure 4.6: Monte Carlo phase diagram. Dashed lines denote continuous transitions (from reference [13])

tration in amphiphile necessary to reach the oil-water-surfactant coexistence is much too high compared to that of experimental microemulsions. Those limitations from this model arose from the fact that oil and water were considered the same way (*e. g.* of similar size), that surfactant molecules were structureless (no head and tail), and that no attempt to use realistic potentials was possible in any way. The effect of the underlying lattice is also believed to be very strong.

Many other groups have worked on the computer modelling of surfactant systems and have brought their own contributions. However, to the best of the author's knowledge, all the major works using Ising-type models have been presented. Most of them have been essentially designed to model microemulsions.

### 4.3 Chain models

As it was previously emphasised, both phenomenological and Ising-type models are unable to account for the different amphiphile conformations. As this factor appears to

be of primary importance for the formation of micelles and may be important in lyotropic liquid crystals, models based on chain molecules appear to be more suitable for modelling such phenomena. Rather than making the distinction on the presence or absence of an underlying lattice, a new classification based on whether the aggregation process is controlled or not appears more appropriate.

### 4.3.1 Constrained chains

The first of these models was that of Haan and Pratt [86] who aimed to study the structure of micelles. They considered aggregates of  $N = 20, 30$  and  $50$  chains of length  $s = 4$  (one of the end being the hydrophilic head and the remaining of the chain the hydrophobic tail) of surfactant molecules in water lying on a diamond lattice. Those chains were moved using a combination of kink-jumps and the reptation scheme [87] but were forced to remain part of the micelle. The Hamiltonian was:

$$\mathcal{U} = \varepsilon_{tt}n_{tt} + \varepsilon_{th}n_{th} + \varepsilon_{hh}n_{hh} + \nu_g g$$

where  $n_{tt}$ ,  $n_{th}$  and  $n_{hh}$  are respectively the number of tail-tail, tail-head and head-head interactions and  $g$  the total number of gauche bonds in the aggregate,  $\varepsilon_{tt}$ ,  $\varepsilon_{th}$ ,  $\varepsilon_{hh}$  and  $\nu_g$  being the associated energy parameters. This model has been reported to give some values of density profile of the heads in relative disagreement with experimental data.

The work carried out by Karaborni and O'Connell [88, 89] also deserves to be mentioned. Extensive sets of simulations have been performed to characterise micellar aggregates. The model used is in essence relatively close to Haan and Pratt's in that the chains are confined to the micelle but differs by the choice of molecular dynamics instead of the Monte Carlo technique. Realistic potentials were applied in order to mimic bond stretch, bend and rotation. The chain conformations, bond order parameters, principal moments of inertia, aggregate radii, group probability distributions, time correlation func-

tion and many others were computed and appear to be in relative good agreement with results from both other simulations and experimental studies (SANS and NMR). The only noticeable discrepancy came from the dynamics of the chains, the bond relaxations being somewhat too fast.

Many other attempts to model ‘constrained micelles’ have been attempted.

### 4.3.2 Self-assembling chains

Other groups have decided to extend this concept further by allowing the self-assembly of the surfactant chains rather than imposing a given microstructure. This new concept of self-assembly is essential and constitutes the main difference with the simulations previously described. Amongst those groups, the most significant advances have been done by that of Larson, Smit and Care — this latter being the one selected to perform the simulations presented in the following chapters.

Larson [90] has first used a square lattice to study a mixture of oil, water and surfactants. In this early model, surfactant molecules were represented as a string of oil and water, *i. e.* the hydrophilic and hydrophobic segments were assumed as interacting in a similar way that respectively water and oil units. Energy parameters are thus reduced to the lipophile-lipophile  $E_{ll}$ , hydrophile-hydrophile  $E_{hh}$  and lipophile-hydrophile  $E_{lh}$  interactions. The moves were performed using a combination of chain reptation, chain twisting and interchange of oil and water units. Both energies and free energies were computed and compared to the values predicted by the quasichemical theory [91]. Although some discrepancies in the free energies were observed, the global phase behaviour appeared to be relatively similar. The influence of the hydration of the head segments on the solubilisation was also studied. This model was later extended in three dimension [92] with a cubic lattice of coordination number  $c = 26$ . The scheme used keeps most of the original

two dimensional one, adding only interactions between two units lying diagonally. A phase diagram has been established from estimates of the free energy of mixing of the two species for different ratios.

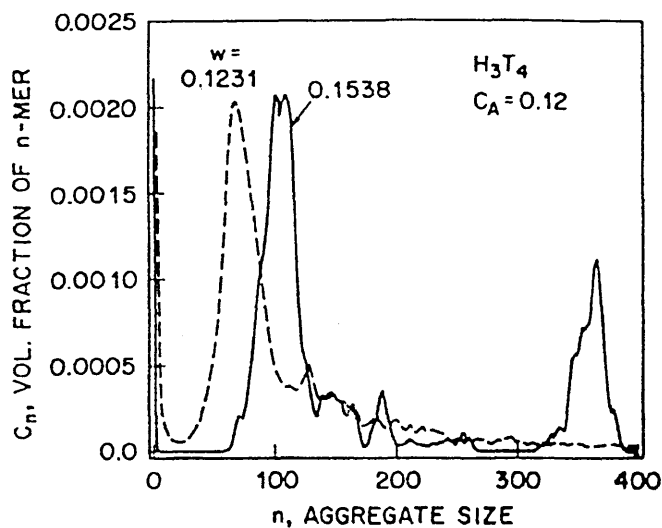


Figure 4.7: Volume fraction of surfactant  $H_3T_4$  in aggregates with aggregation number  $n$  (from reference [14])

Three sets of simulations carried out on lattices of different sizes (from  $10 \times 10 \times 10$  up to  $40 \times 40 \times 40$ ) also allow the extent of the bias resulting from finite-size effects to be quantified. The behaviour of both alcohol-like  $H_1T_1$ , surfactant-like  $H_4T_4$  [92] and asymmetrical chains  $H_2T_6$  [93] was investigated. Various microstructures and phase transitions were generated including some composition-dependent transitions from lamellar to cylindrical to spherical analogous to those observed in the block copolymer systems. This model gives a good account of the solubilisation and low interfacial tensions (significant interfacial free energy). In his latest simulations [14], Larson tackles the influence of the size of the two moieties of the chains on the shape of the micelles formed (spherical, cigar-shaped or cylindrical) and gets the cluster size distribution. Some bicontinuous phases formed by intersecting cylindrical micelles and a symmetric sponge-like phase are also observed. The

phase diagram generated was interpreted as being consistent with the experimental one presented by Kekicheff and Tiddy for lithium perfluorooctanoate in water [94].

Care also carried out simulations using a similar type of model. It was first analysed in the quasi-chemical approximation [19] in order to determine the influence of the different model parameters necessary to reproduce the essential features exhibited by surfactant systems (namely self-aggregation in micelles). Simulations were then performed in two-dimensions using 512 fully flexible chains of three segments (one of which being the hydrophilic head and the remaining the hydrophobic tail) which corresponded to a total volume concentration in amphiphile of 9.4%. The chains were moved using the reptation scheme and the configurations were sampled using the standard Metropolis sampling algorithm. Only nearest-neighbour interactions between head and solvent  $HS$ , and tail and solvent  $TS$  were considered. Thus, the Hamiltonian of the system was written as:

$$\mathcal{H} = n_{HH}E_{HH} + n_{TS}E_{TS} + n_{HS}E_{HS} + \sum_i E_i^c$$

where  $n_{HH}$ ,  $n_{TS}$  and  $n_{HS}$  are respectively the number of head-head, tail-solvent and head-solvent bonds and  $E_{HH}$ ,  $E_{TS}$  and  $E_{HS}$  the corresponding interaction energies;  $E_i^c$  is the energy associated with the conformation of the  $i^{th}$  chain. The chains were assumed fully flexible (*i. e.*  $E_i^c = 0$ ) and the head-head interactions — appearing to be non-compulsory for self-association and of little influence on the aggregate size — were neglected (*i. e.*  $E_{HH} = 0$ ) for those early simulations.

A full cluster size distribution function was derived together with the number average cluster size and rms deviation of the distribution function. A micellar-like phase was observed for a sufficiently hydrophilic head and the cluster size distribution were consistent with those observed experimentally although presumed too polydisperse. There was also evidence of the formation of interdigitated bilayer-type structures.

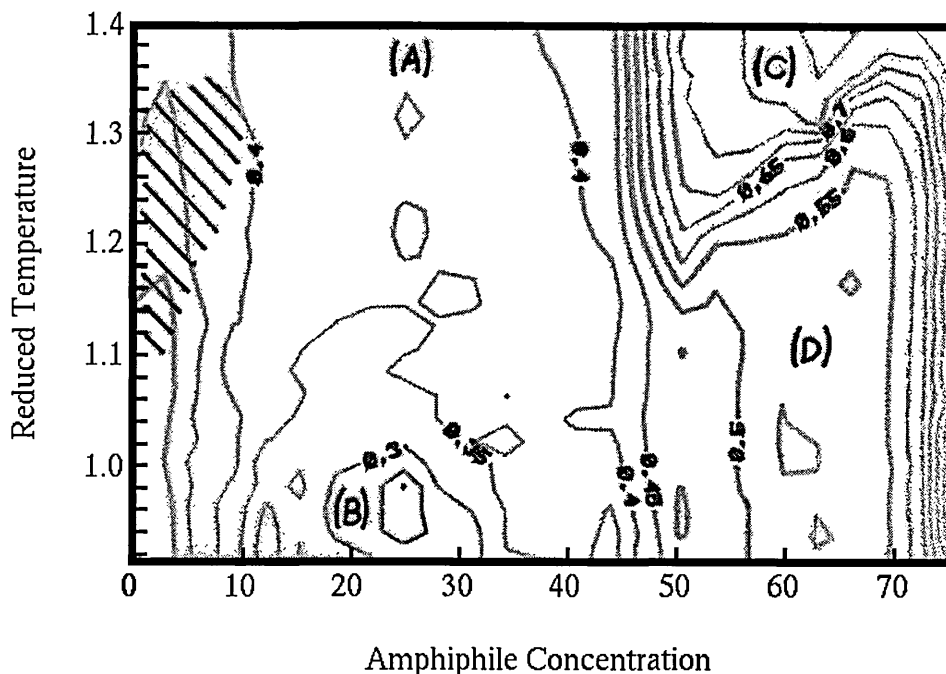


Figure 4.8: The dependence of the ratio of the smallest to largest principal moments of inertia on reduced temperature and amphiphilic concentration. A, small clusters; B, large cylinders; C, bicontinuous; D, lamellar (from reference [15])

This model was later extended in three-dimensions [15], most of its characteristics being kept identical to the previous two-dimensional implementation. The influence of the hydrophobic part length (3, 4, 5 and 7 segments) and head-solvent interaction was investigated. Simulations were carried out for  $\gamma = E_{HS}/E_{TS} = -1.0$  and  $-1.5$  starting from a disordered high temperature phase at a reduced temperature  $\beta^{-1} = kT/E_{TS} = 2.50$  reduced by step  $\Delta\beta^{-1} = 0.10$ . A more detailed study was then undertaken for chains of 4 segments spanning a volume concentration range of 0.78% to 75.0% (22 concentrations investigated). The system was cooled down to  $\beta^{-1} = 0.80$  from a reduced temperature of 1.50 by steps of  $\Delta\beta^{-1} = 0.02$ . Various averages were computed throughout the simulations including the mean principal moment of inertia, the cluster size distribution function, the number average cluster size, the cluster surface roughness and the head and tail roughness.

## CHAPTER 4. MODELS OF SURFACTANT SYSTEMS

A complete temperature vs concentration phase diagram was derived from the equilibrium value of the ratio of the smallest to largest principal moments of inertia of the clusters (see figure 4.8).

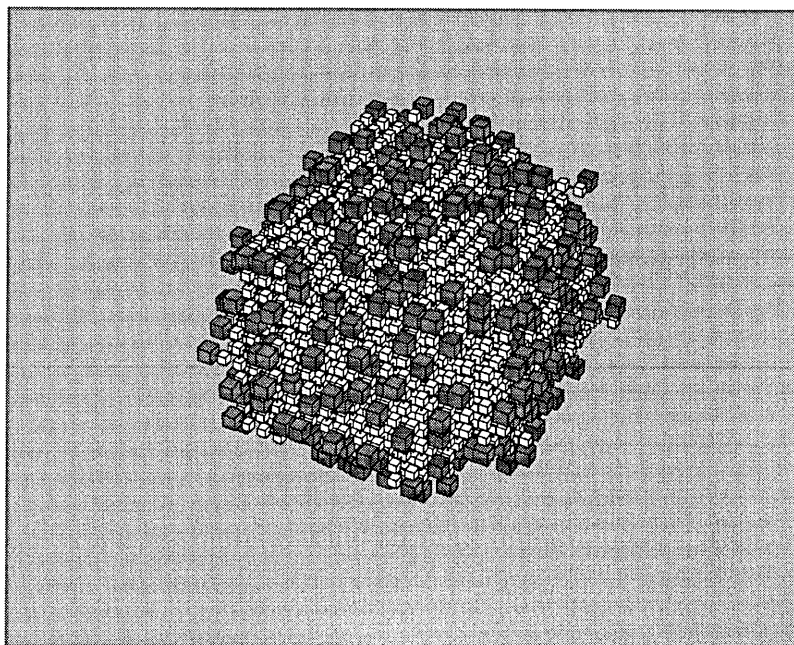


Figure 4.9: Vesicle formed during the preliminary study with chains of length  $s = 6$  ( $\beta^{-1} = 1.10$ ,  $\gamma = -1.0$  and  $X_a = 9.38 \text{ vol. } \%$ )

This model gave some results in good agreement with experimental data such as the growth of micelles in cylinders above the cmc and the self-assembly in complex microstructures at low temperature such as a vesicle in which some solvent was enclosed (see figure 4.9) or castellated bilayers with fully-solvated heads (see figure 4.10). A transition from a bicontinuous to a lamellar phase was reported as the system was cooled down at high concentration. This system also exhibited a relatively sharp cmc. The main discrepancy with experimental data remains a higher polydispersity and weaker minimum in the cluster size distribution than usually assumed; it was believed to be caused by the underlying lattice and/or idealised potential used.

Some aspects of this model will be discussed in more detail chapter 5. Some

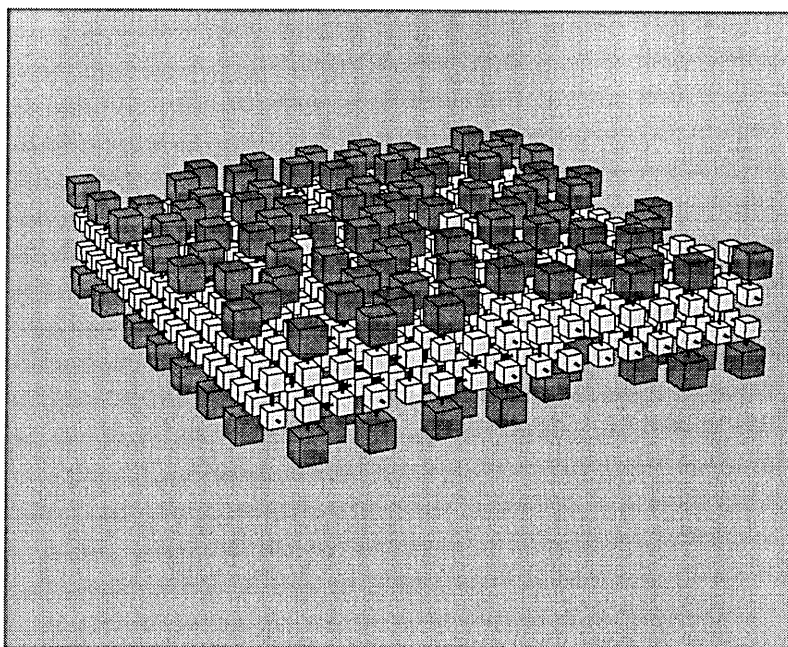


Figure 4.10: Castellated bilayer ( $s = 4$ ,  $\beta^{-1} = 0.90$ ,  $\gamma = -2.0$  and  $X_a = 50.0 \text{ vol. } \%$ )

modifications will be proposed in order to overcome the side-effects caused by the lattice and improve the sampling at low temperature (see chapter 6 and 8).

This type of model appears to be increasingly popular recently and many other related models have been designed. Amongst those, one may mention that of Bernardes [95] who performed two-dimensional lattice simulations of a binary mixture of surfactants and water in the canonical ensemble. The surfactants were represented as chains composed of one hydrophilic segment  $w$  — identical to a water site — connected to two hydrophobic segments  $o$ . In order to reproduce the behaviour of surfactant systems, both nearest-neighbour interactions between alike species,  $oo$  and  $ww$ , were made attractive whereas interactions between unlike species,  $wo$ , were repulsive; a supplementary interaction parameter was also introduced to differentiate between straight and folded conformations ( $E_{straight} = 0$  and  $E_{folded} = \epsilon$ ):

$$E_{ww} = E_{oo} = -E_{wo} = -\epsilon \quad (\epsilon > 0)$$

## CHAPTER 4. MODELS OF SURFACTANT SYSTEMS

The simulations were carried out on lattices of size  $L = 100, 200$  and  $400$  in order to assess finite-size effects. Results were obtained for both the  $X_1^{free}$  vs  $X_{amph}$  curve and the cluster size distribution functions at different temperatures. Unlike the first set of results which are in good agreement with theoretical predictions and experimental data, the cluster size distributions in the micellar region yield unrealistic features, namely the lack of any real minimum in the distribution and too low a mean aggregation number. These discrepancies are likely to vanish if the simulations are extended to three-dimensions.

Unlike the previous groups, Smit *et al.* chose to carry out MD simulations of both binary water-surfactants and ternary oil-water-surfactants [96] mixtures. In their first models, surfactants were modelled as a linear chain of seven segments (two water-like  $w$  and five oil-like  $o$  units) bound to their neighbours by a strong harmonic force. All the particles interact through a truncated and shifted Lennard-Jones potential. The simulations were carried out with 39,304 particles (*i. e.* surfactant concentration in the range 1 – 3%). The spontaneous formation occurred of both a monolayer at the oil/water interface and micelles in the water phase. The density profiles of oil, water and surfactant units were also investigated. Large oscillations in the water density profile were observed and provided an explanation to unexpected results from recent specular neutron reflection experiments. More results have been extracted later [97] including tangential and normal components of the pressure tensor (study of the interfacial tension), bond order parameters (average angle between two successive bonds) and segment distribution in the micelle. The results are in good agreement with experimental data.

Results from a model restricted to a water-surfactants system has been presented more recently [98]. Interactions have been kept essentially similar in this modified model: the different units still interact through a truncated and shifted LJ potential and two consecutive units of a surfactant chain are still bound with a strong harmonic potential;

however, the hydrophilic units are no longer considered as water-like units. As a consequence of that, three different types of units are now to be taken into account: water  $w$ , head  $h$  and tail  $t$ . Some interesting observations have been made from those simulations including the fusion of two micelles, the slow breakdown of a micelle and surfactant chains joining and leaving a micelle. Smit also derived a complete micellar size distribution function which exhibited a maximum for 20 – 25 chains and a polydispersity on the range 15 – 30 chains (see figure 4.11). The long-range repulsive  $hh$  interactions and H-bonding were reported not to be essential for the formation of micelles for these simulations.

Even more recently [16], some more work have been done to characterise the influence of the hydrophobic tail length and head group interaction, and investigate the relationship between the shape of the surfactant and the morphology of the micellar aggregate. The model used was essentially similar with four different types of unit: oil  $o$ , water  $w$ , head  $h$  and tail  $t$ . Small systems of 512 particles with surfactants of hydrophobic length 1, 3 or 5 units was first used. The results were in general agreement with experimental data: the longer the hydrophobic part, the more successfully the surfactant decreased the interfacial tension. Larger systems (39,304 particles) were then studied to measure the influence of the head group interaction and dimension of the head group on the size and shape of the micellar aggregates. Once again, the results obtained appear to be in fairly good agreement with experimental data: more bulky head groups favoured the formation of spherical micelles.

According to that group, these types of simulations would also give a good account of the dynamics of the bilayer-like and spherical micelles. However, this claim must be considered with caution and is most likely unrealistic since MD simulations allow one to simulate phenomena taking place over a typical time scale of up to a nanosecond whereas the processes involved with the dynamics of micelles are believed to be in the range  $10^{-6}$ s

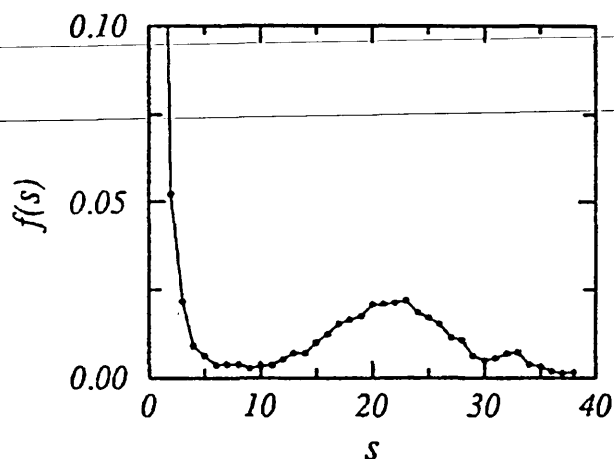


Figure 4.11: Micellar size distribution function  $f(s)$ .  $s$  is the number of surfactants in an aggregate (from reference [16])

(surfactant entering or leaving a micelle) to  $10^{-1}s$  (breakdown of a micelle).

More recently, simulations using a similar type of model have been undertaken by Henderson *et al.* [17]. They studied a binary mixture of solvent and surfactants where those latter were represented as chains of two LJ sites — *i. e.* the head and the tail — connected by a non-harmonic spring. The parameters of the LJ were chosen so that the head site,  $h$ , was identical to the solvent molecules and the tail,  $t$ , was of a smaller diameter in order to favour the formation of spherical aggregates. Simulations were carried out in two and three dimensions. Both the cluster size distribution and chemical potential were determined as a function of the total concentration in surfactants. The values of the surfactant and solvent chemical potentials obtained using Widom's particle insertion method were compared to those from  $NpT$  MD simulations and appeared to be in good agreement.

Although this model proved to reproduce some of the features exhibited by surfactant systems such as a cmc, the cluster size distributions (see figure 4.12) yielded unrealistic peculiarities such as too weak a minimum — if none at all — in the micellar

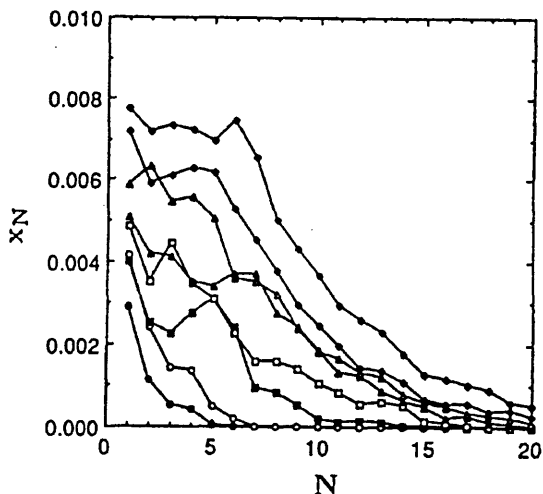


Figure 4.12: Three-dimensional cluster size distribution for total surfactant mole fractions  $x = 0.005, 0.01, 0.02, 0.03, 0.04, 0.05, 0.06, 0.08$  respectively (from reference [17])

region, too wide a polydispersity, as well as a very small mean aggregation number ( $\approx 4$  chains in two-dimensions and  $\approx 10$  in three-dimensions). Amongst other causes, those discrepancies are likely to be a consequence of the criterion used for the cluster counting: a cut-off distance between two tails.

#### 4.4 Other models

Many other simulations have been carried out on surfactant systems, most of them aiming at studying monolayers (*e.g.* Kramer *et al.* [99] or Harris and Rice [100]) and hence offering little or no interest for the present project. The mean-field calculations of Ben-Shaul *et al.* [101] and Dill *et al.* [102] on constrained lattice models and of Mattice *et al.* on diblock copolymers also deserve to be mentioned [18, 103].

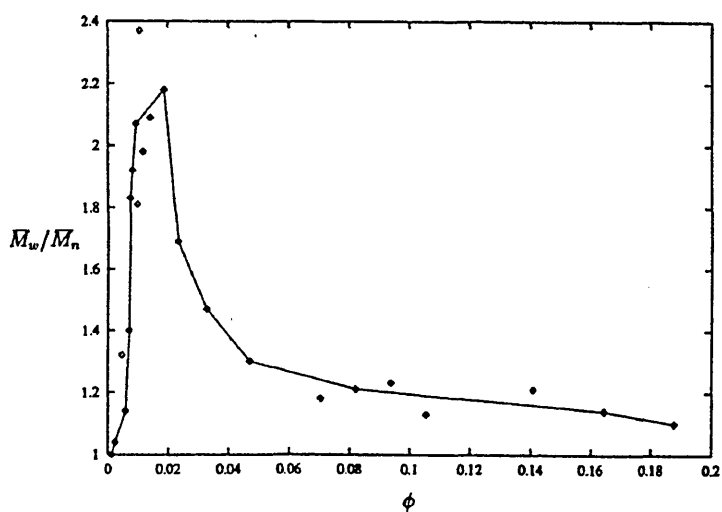


Figure 4.13: Polydispersity of the aggregates in the system as a function of the overall concentration (from reference [18])

## 4.5 Conclusion

The present research project aims to investigate the formation of structures such as micelles and vesicles and will therefore involve the participation of many molecules thus making the approach requiring detailed realistic potentials untractable.

Following the same concern of tractability and pushing it a step forward leads us to favour lattice models over their counterparts, the off-lattice models. Indeed, they allow the use of quicker and smarter algorithms (*e. g.* avoid problems similar to those experienced by Henderson for a cluster-counting algorithm) but despite their simplicity achieve in many circumstances results with more accurate statistics consistent with experimental data or theoretical studies.

# Chapter 5

## Model

### 5.1 Model

The models used for the studies presented herein are extensions of a model initially devised by Care to study amphiphilic self-aggregation in pseudo-micellar aggregates in 1987 [19, 104] (see chapter 4).

#### 5.1.1 Description

The amphiphiles are represented as  $N$  chains of  $s$  connected segments,  $t$  ( $1 \leq t < s$ ) of which representing the hydrophilic part, and the remaining ( $s - t$ ) the hydrophobic part, lying on a lattice of coordination number  $c$  with periodic boundary conditions. All the sites not occupied by an amphiphile segment are considered to be filled with solvent so that the number of solvent sites is  $(M - Ns)$  where  $M$  is the total number of lattice sites. It has previously been demonstrated [19] that all possible interactions (*i. e.* head-head, head-tail, head-solvent, tail-tail, tail-solvent and solvent-solvent) could be accounted for by only considering three of them. For reasons of convenience, these were chosen to be head-head ‘ $HH$ ’, head-solvent ‘ $HS$ ’ and tail-solvent ‘ $TS$ ’.

CHAPTER 5. MODEL

The Hamiltonian for the system can therefore be expressed as a function of those interactions:

$$\mathcal{H} = n_{HH}E_{HH} + n_{HS}E_{HS} + n_{TS}E_{TS} + \sum_{i=1}^N E_i^c \quad (5.1)$$

where  $n_{HH}$ ,  $n_{HS}$  and  $n_{TS}$  are respectively the total number of head-head, head-solvent and tail-solvent interactions,  $E_{HH}$ ,  $E_{HS}$  and  $E_{TS}$  being the corresponding interaction energies and  $E_i^c$  the conformational energy associated with the  $i^{th}$  chain. It is possible to reformulate the total potential energy of the system under a more practical dimensionless form as:

$$\frac{U}{kT} = \beta \left( n_{TS} + \gamma n_{HS} + \eta n_{HH} + \sum_{i=1}^N \sum_{j=1}^{s-2} \varepsilon_{ij} \right) \quad (5.2)$$

where  $\beta = E_{TS}/kT$ ,  $\gamma = E_{HS}/E_{TS}$ ,  $\eta = E_{HH}/E_{TS}$  and  $\sum_{j=1}^{s-2} \varepsilon_{ij} = E_i^c/E_{TS}$ .  $\varepsilon_{ij}$  is the rigidity parameter associated with the  $j^{th}$  triplet of successive segments of the  $i^{th}$  chain and  $\beta^{-1}$  is the reduced temperature for the model.

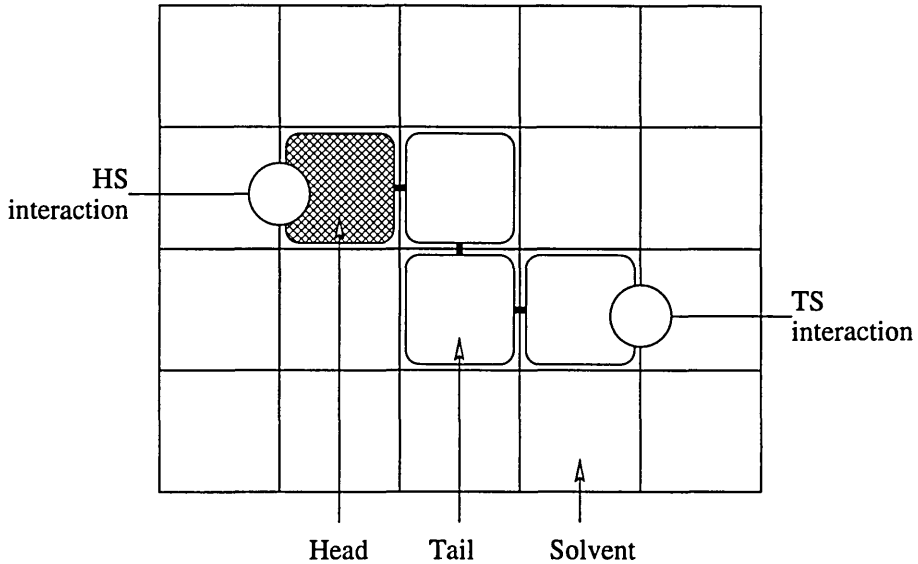


Figure 5.1: Chain on a lattice

It must be pointed out that those ‘segments’ actually correspond to  $\approx 3\text{-CH}_2\text{-}$  groups in volume and as such are responsible for some form of intrinsic partial rigidity of the chain model resulting in a coarse graining procedure. In order to keep the model tractable and because the pseudo-micellar aggregation has been demonstrated to take place without long-range interactions, only short range interactions were considered — although longer range interactions may easily be incorporated — making it more suitable for the modelling of non-ionic surfactants or ionic surfactants in the presence of electrolyte (*i. e.* with screened long-range electrostatic interactions). Typical amphiphilic behaviour was reproduced by keeping  $\beta$  positive and setting-up the hydrophilic strength  $\gamma$  to a negative value. This particular choice of parameters does indeed result in making  $TS$  interactions repulsive whilst  $HS$  ones are attractive.

### 5.1.2 The ‘basic’ implementations

The core of this work aims to study in greater detail preliminary observations made by Brindle and Care [15] in the micellar and ‘vesicle’ regions (see respectively chapter 8 and 7). It therefore appeared judicious to keep as a starting point a similar set of parameters for which the model was well-characterised. For both studies, a cubic lattice of coordination number  $c = 6$  was used where only interactions with nearest-neighbour sites were allowed. The  $HH$  interactions — which proved to be of little influence in previous simulations [19, 104] — were also neglected (*i. e.*  $E_{HH} = 0$ ), and only  $t = 1$  segment was made hydrophilic.

The only differences between the models used for those studies lie in the length of the chains which were made longer for the study in the vesicle region ( $s = 6$  units versus only 4 in the micellar region) and their flexibility; whereas the relative shortness of the chains used in the micellar region allowed us to make them fully-flexible (*i. e.*  $E_i^c = 0$ ),

those used for the study in the vesicle region on the other hand required some form of rigidity to avoid unrealistic folded conformations. The influence of the rigidity on the phase behaviour of the system and the type of aggregates formed has been investigated by making  $\epsilon_{ij} \geq 0$ .

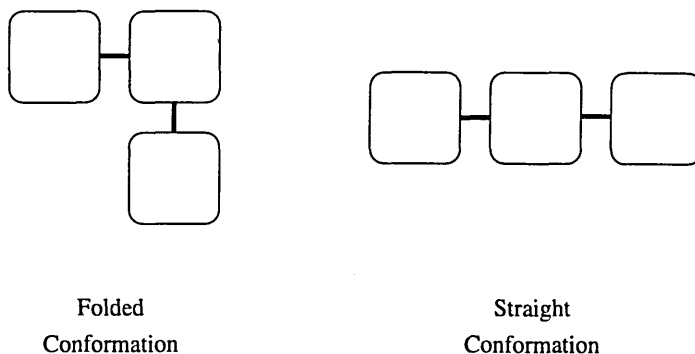


Figure 5.2: ‘Folded’ and ‘straight’ conformations

The mechanism by which chains are inclined to favour straight conformations is similar to that used by Bernardes [95] (see chapter 4): an energy parameter  $\epsilon_{ij}$  is associated to each pair of bonds separating a triplet  $j$  of successive chain segments;  $\epsilon_{straight} = 0$  whilst  $\epsilon_{folded} > 0$ . Since the chains have only one  $H$  segment, no distinction is thought to be necessary between the triplets exclusively made of  $T$  segments and those comprising the unique  $H$ . This simplification has to be removed if a more realistic mapping is looked for (see chapter 6 for a fuller discussion on this topic).

### 5.1.3 The ‘extended’ implementation

This basic implementation suffers from a series of limitations essentially arising from the presence of an underlying cubic lattice. These limitations include the preferential growth of non-spherical aggregates along axis parallel to the  $x$ ,  $y$  or  $z$ -axis, too high a cost for bending a layer of amphiphile resulting in cubic-like cavities, and too few distinct

conformations thus making the coarse-graining procedure very approximate. The obvious step is to change the underlying cubic lattice for a lattice with increased coordination number and/or different symmetry (*e. g.* diamond lattice). Such an extended implementation of the model has been proposed in chapter 6 with the possible simulation of ‘real’ surfactants in mind. In order to achieve a better mapping, it appeared necessary to also allow diagonal and next-nearest neighbour bonds still on a cubic lattice thus increasing its coordination number to  $c = 26$  [93].

When the simulation of ‘real’ surfactants is aimed at, the particular characteristics of the chains (length, number of hydrophobic and hydrophilic units, conformational energy) have to be chosen following a particular methodology detailed in chapter 6. A new scheme aimed at improving the sampling efficiency of such chain molecules lying on a lattice of high coordination number is also presented.

## 5.2 Sampling the system

Three main methods can be used to perform computer simulations of molecules and liquids:

- Molecular mechanics.
- Molecular dynamics.
- Monte Carlo.

Each of these methods offers specific features and suffers from their own characteristic limitations; they will therefore have distinct ‘natural’ domains of application.

### 5.2.1 Molecular mechanics

In this approach, detailed inter-atomic potentials are used. It is the technique commonly chosen by commercial softwares such as *Cerius2* to perform minimisations, conformational analysis of polymers or many others processes involving a unique or very few particles. Indeed, because of its heavy computational requirements, this technique is only applicable to small systems of particles thus making it unsuitable for our purpose.

### 5.2.2 Molecular dynamics

Molecular dynamics — *MD* for short — is a technique which allows one to obtain dynamic properties of many-body systems by solving the Newton equation of motion [1, 105]. The Hamiltonian of a system of  $N$  particles interacting via a potential  $\mathcal{V}$  is:

$$\mathcal{H}(\mathbf{p}, \mathbf{q}) = \sum_i \dot{q}_i p_i - \mathcal{L}(\mathbf{q}, \dot{\mathbf{q}})$$

where  $\mathbf{p}_i$  is the generalised molecular momentum,  $\mathbf{q}_i$  is the generalised coordinates and  $\mathcal{L}(\mathbf{q}, \dot{\mathbf{q}})$  is the Lagrangian function. Its main asset is to allow the calculation of dynamic as well as static properties, thus allowing non-equilibrium simulations (*e. g.* measurement of transport coefficients).

Like molecular mechanics, the main problem with this technique also stems from its computational requirements thus limiting its applicability to phenomena having a typical timescale of  $10^{-9}$ s. Since most of the phenomena taking place in a micellar solution exceed this timescale by several orders of magnitude (typically from  $\approx 10^{-1}$ s for the breakdown of a micelle to  $\approx 10^{-6}$ s for a chain entering or leaving a micelle), it also appears unsuitable for the present studies. However, it must be pointed out that other groups such as that of Smit or Henderson have performed MD simulations of surfactant systems with success (see chapter 4).

### 5.2.3 Monte Carlo

The first Monte Carlo simulation was performed by Metropolis *et al.* back in 1953 [106] on a two-dimensional rigid-sphere system. Before tackling concepts such as the *importance sampling* or the *Metropolis criterion*, it appears necessary to bear in mind the problems encountered in statistical mechanics.

### 5.2.4 Statistical mechanics

If a system is in equilibrium with  $n$  possible states of energy  $E_i$  ( $i = 1, 2, \dots, n$ ), the probability  $P_i$  of the system being in a state  $i$  in the canonical ensemble is [107]:

$$P_i = \frac{\exp(-\beta E_i)}{\sum_{j=1}^n \exp(-\beta E_j)} \quad (5.3)$$

where  $\beta = 1/kT$  and  $\sum_{j=1}^n \exp(-\beta E_j)$  is the canonical partition function  $Q$ .

The average of a thermodynamic observable is given by [108]:

$$\langle \mathcal{A} \rangle = \frac{1}{Q} \sum_{|i\rangle} \exp(-\beta E_i) \langle i | \mathcal{A} | i \rangle$$

where  $|i\rangle$  is a state of energy  $E_i$ .

If the partition function is reformulated under its most familiar form as:

$$Q = a \int d\mathbf{p}^n d\mathbf{q}^n \exp(-\beta \mathcal{H}(\mathbf{q}^n, \mathbf{p}^n))$$

where  $a$  is a constant of proportionality,  $\mathbf{q}^n$  and  $\mathbf{p}^n$  are respectively the coordinates and momenta of the system of  $n$  particles and  $\mathcal{H}(\mathbf{q}^n, \mathbf{p}^n)$  is the Hamiltonian of the system.

The average on  $\mathcal{A}$  becomes:

$$\langle \mathcal{A} \rangle = \frac{\int d\mathbf{p}^n d\mathbf{q}^n \mathcal{A}(\mathbf{q}^n, \mathbf{p}^n) \exp(-\beta \mathcal{H}(\mathbf{q}^n, \mathbf{p}^n))}{\int d\mathbf{p}^n d\mathbf{q}^n \exp(-\beta \mathcal{H}(\mathbf{q}^n, \mathbf{p}^n))} \quad (5.4)$$

As pointed out by Frenkel [108], the main difficulty resides in solving analytically multi-dimensional integrals over the particle coordinates and shows the need for a statistical technique capable of providing a numerical solution of those multi-dimensional integrals; the Monte Carlo technique is such a technique. Note that for velocity independent potentials, the momentum integrals cancel to give the ‘configurational’ integral.

### 5.2.5 Importance sampling

In its most basic form, *the Monte Carlo method for many-dimensional integrals consists simply of integrating over a random sampling of points instead of over a regular array of points* [106]. This is known as *random sampling* (one may point out that the Monte Carlo technique gets its name from the the importance of the role played by random numbers).

Whilst the approach works satisfactorily with uniformly distributed functions, it is relatively inefficient with most integrals encountered in statistical mechanics where most functions to be integrated are sharply peaked functions. It is therefore necessary to modify this technique so that more time is spent sampling states making a significant contribution to the thermodynamic averages — *i. e.* with a large Boltzmann weight — rather than those bringing little contribution. By contrast, this form of sampling is called *importance sampling*.

Thus, if one wishes to integrate a function  $f(x)$  between  $a$  and  $b$  so that:

$$I = \int_a^b f(x) dx \quad (5.5)$$

using the random sampling approach would yield:

$$I = (b - a) \langle f(x) \rangle_{[a,b]} \quad (5.6)$$

whereas the importance sampling would require the reformulation equation 5.5 as:

$$I = \int_a^b w(x) \frac{f(x)}{w(x)} dx \quad (5.7)$$

where  $w(x)$  is a distribution function allowing to concentrate the sampling to those region of phase space with a high Boltzmann weight. As demonstrated by Frenkel [108], the variance  $\sigma_L^2$  thus becomes:

$$\sigma_L^2 = \frac{1}{L} \left[ \left\langle \left( \frac{f}{w} \right)^2 \right\rangle - \left\langle \frac{f}{w} \right\rangle^2 \right] \quad (5.8)$$

which can be made small by choosing  $w(x)$  so that  $f(x)/w(x)$  is a smooth function of  $x$ .

### 5.2.6 Metropolis method

In the Metropolis method, a Markov chain is constructed whose limiting distribution has the canonical distribution; this can be shown to be equivalent to importance sampling. It can be demonstrated (*e.g.* [1,108]) that in order to lead to the correct distribution, the transition matrix  $\pi$  of the Markov chain must be such that the number of transitions from any state  $i$  to any other state  $j$  is equal to the number of transitions from  $j$  to  $i$ . This can be achieved by applying the unnecessary strong condition of *detailed balance*:

$$\rho_i \pi_{ij} = \rho_j \pi_{ji} \quad (5.9)$$

where  $\rho_i$  and  $\rho_j$  are the respective limiting distribution for the states  $i$  and  $j$ , and  $\pi_{ij}$  and  $\pi_{ji}$  are the transition matrices from states  $i$  to state  $j$  and  $j$  to  $i$  respectively.

Many matrices can satisfy such a condition. The most familiar is the Metropolis solution (also known as the *symmetric solution*) [1]:

$$\begin{aligned}
\pi_{mn} &= \alpha_{mn} & \rho_n \geq \rho_m & \quad m \neq n \\
\pi_{mn} &= \alpha_{mn} \frac{\rho_n}{\rho_m} & \rho_n < \rho_m & \quad m \neq n \\
\pi_{mm} &= 1 - \sum_{n \neq m} \pi_{mn} & & \quad (5.10)
\end{aligned}$$

where  $\alpha$  is probability of performing a trial move from a state  $i$  to another state  $j$ ;  $\alpha$  is known as the *underlying matrix of the Markov chain*.

Details on how to construct a more efficient transition matrix have been discussed by Owicki *et al.* [109, 110], a gentle introduction to the application of the Monte Carlo technique to simulations in physics has been presented by Binder [111] and fuller discussions on the Monte Carlo methods can also be found in the literature (*e. g.* [1, 108]).

The principal limitation of the Monte Carlo technique compared to MD is its inability to perform non-equilibrium simulations; only equilibrium thermodynamic averages can be computed.

### 5.3 Schemes

It is common practice when simulating *bulk* systems to use so-called periodic boundary conditions. This technique allows one to increase the apparent box size by assuming that the system can be represented by a set of identical unit cells of smaller dimensions. Its main benefit is to eliminate the effect of free surfaces. This is achieved by obliging the chains leaving the simulation box to re-enter it by its opposite side (see figure 5.3) and making the particles interact with the nearest periodic population. Note that this implies that the phenomenon under investigation must have a correlation length smaller than the size of the smallest box side a bias being otherwise introduced.

Thanks to a constant increase in computer performance, several schemes have

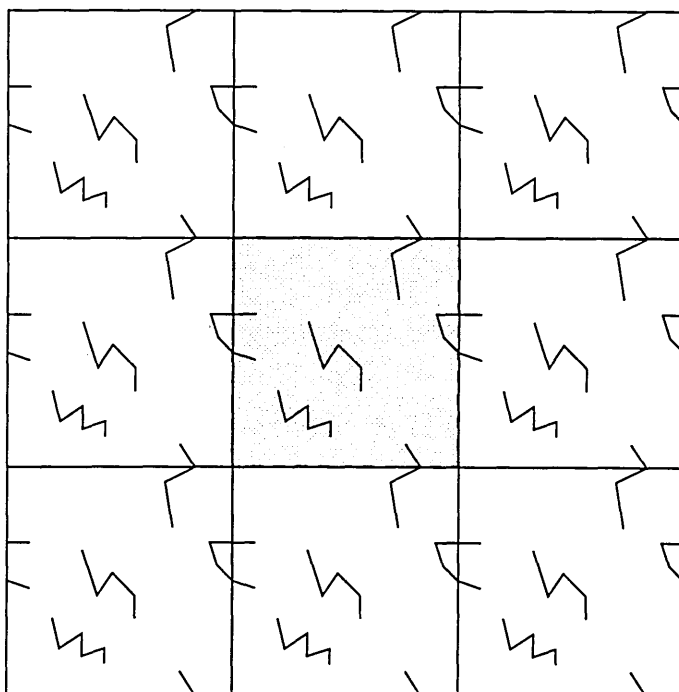


Figure 5.3: Periodic boundary conditions: the actual simulation box is shaded

been recently developed for the simulations of chain molecules — most of them being applicable to both surfactant-like or polymer-like chains. Various schemes such as the *bond-fluctuation* [112, 113] or the *pivot algorithm* [114] have been considered but judged inadequate for the kind of simulations undertaken here. The former has been rejected because of the difficulty of explicitly including the solvent and the latter because of the lack of information about its efficiency and applicability. Another scheme worth mentioning is the *Gibbs Monte Carlo* method devised by Panagiotopoulos [115], mostly applicable to off-lattice simulations of phase equilibria. A lattice implementation has also been presented by Mon *et al.* [116]. The most common schemes used for the simulation of chain molecules have been reviewed by several authors (*e.g.* [117–119]). The schemes selected here are the reptation and configurational-bias Monte Carlo described hereafter.

## 5.3.1 Reptation

This scheme was first described by Wall and Mandel [87]. The chains are being moved along their former contour in the a fashion similar to a 'slithering snake' using the sequence presented figure 5.4.

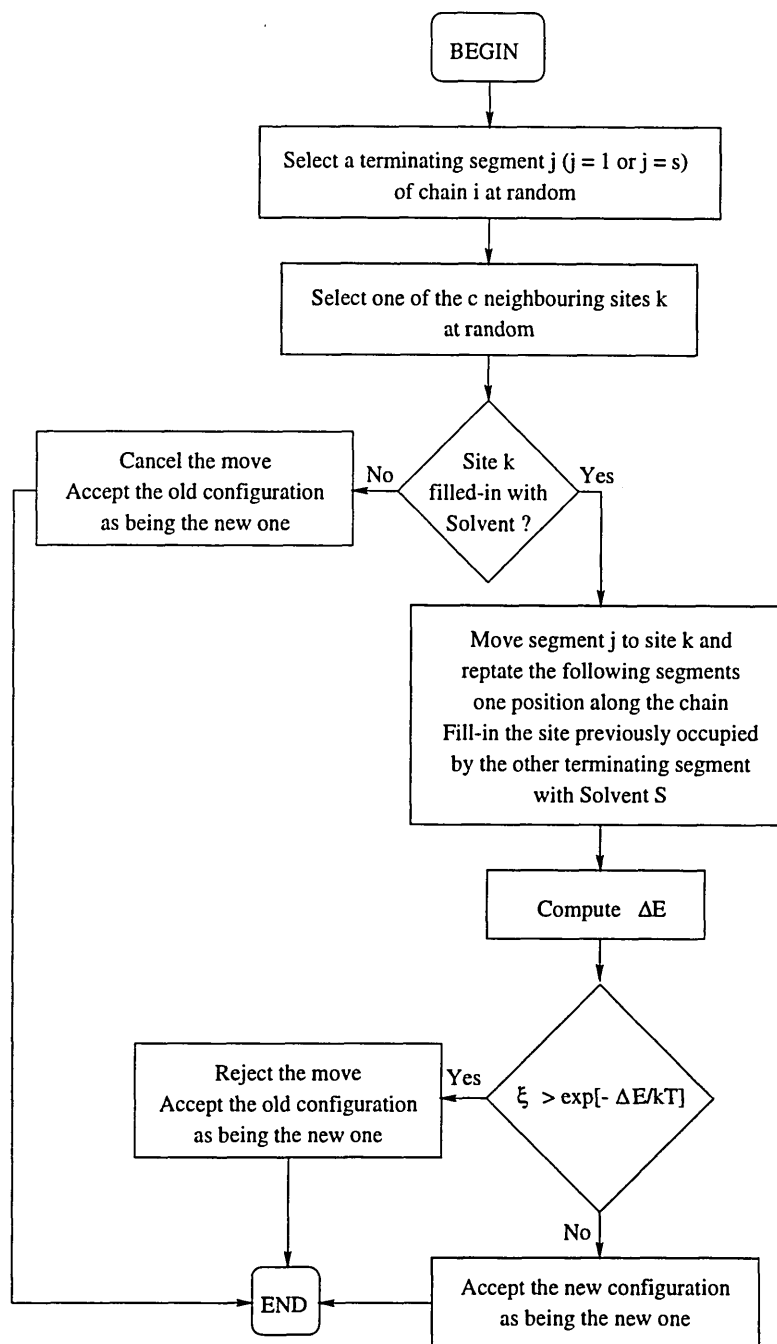


Figure 5.4: The reptation scheme

Once a chain  $i$  has been selected to be moved by reptation, the first step consists in choosing one of its two end segments  $j$  ( $j = 1$  or  $j = s$ ) to be the *head* of the *snake*<sup>1</sup>. The next step consists in choosing at random a site  $k_l$  ( $l = 1, 2, \dots, c$ ) in the neighbourhood of the snake head and attempt to move it to this site. If the site  $k_l$  is already occupied by an amphiphilic segment — exclusive of the other terminating segment which will be moved during the reptation and thus not considered — the move has to be rejected for excluded volume interaction, otherwise the chain will be reptated to its new position by moving each segment one position ahead along the chain — *i. e.* in the direction of the move, towards the *head* of the *snake*. The site freed by the last segment to be moved is filled-in with solvent.

The ‘classic’ Metropolis sampling procedure is then applied: the change in energy between the configurations prior to and following the attempted move  $\Delta E$  is computed and the move is accepted with a probability  $P_{acc} = \text{MIN}[1, \exp(-\Delta E/kT)]$ . If the attempted move is rejected, the ‘old’ configuration is kept and counted as being the new one in the Markov chain.

### 5.3.2 Configurational-bias Monte Carlo

The ‘basic’ schemes used in Monte Carlo simulations (*e. g.* the reptation) generate trial configurations at random and then accept them according to their Boltzmann weight (Metropolis criterion). The main problem with such an approach is that each trial configuration has the same probability of being generated regardless of its Boltzmann weight. When simulations are performed in a region of phase space where most trial configurations have to be rejected because of excluded volume interactions (*e. g.* at high densities) or unfavourable energetics ( $\Delta E > 0$ ), these schemes suffer from a chronic

---

<sup>1</sup>Not to be confused with the hydrophilic head of the amphiphile: the *head* of the *snake* can be either a head  $H$  or tail  $T$  segment

sampling inefficiency due to the high rejection rates.

An alternative exists in the form of the so-called *smart Monte-Carlo techniques*: these latter aim to generate moves which have a higher probability of being accepted. Whatever the mean used to achieve it, all those schemes incorporate some sort of weighting factor which will rectify the bias introduced in the distribution.

A fairly recent sampling scheme designed to improve the sampling efficiency of polymer-like chains on a lattice has been proposed by Siepmann [21]. This scheme is based on the self-avoiding walk (SAW) of Rosenbluth and Rosenbluth [120]. The concept behind this scheme is to discard part of a chain  $i$  from a segment  $j$  to either end and then fully regrow the chain using a SAW according to the sequence illustrated in figure 5.5.

Several variations of this scheme have already been implemented. In its most basic implementation, only excluded volume interactions are taken into account during the regrowth: the site  $k_l$  ( $l = 1, 2, \dots, c'$ ) chosen for the regrowth is chosen with a probability  $1/c'$  (*i. e.* at random) where  $c'$  is the number of neighbouring sites available for regrowth (*i. e.* solvent sites  $S$ ). The Rosenbluth weight associated with the  $m^{\text{th}}$  regrowth,  $W_m$ , is given by  $W_m = [c'/(c-1)]W_{m-1}$ . The configuration at the end of the regrowth process is accepted with a probability  $P_{acc} = \text{MIN}[1, W_{\text{trial}}]$ .

The implementation used for the current studies differs in three ways (see figure 5.5):

1. All the interactions are taken into account during the regrowth (*i. e.* conformational energies and external interactions are also included): the site  $k_l$  is chosen with a probability:

$$P_k = B_k / \sum_{l=1}^{c'} B_l \quad (5.11)$$

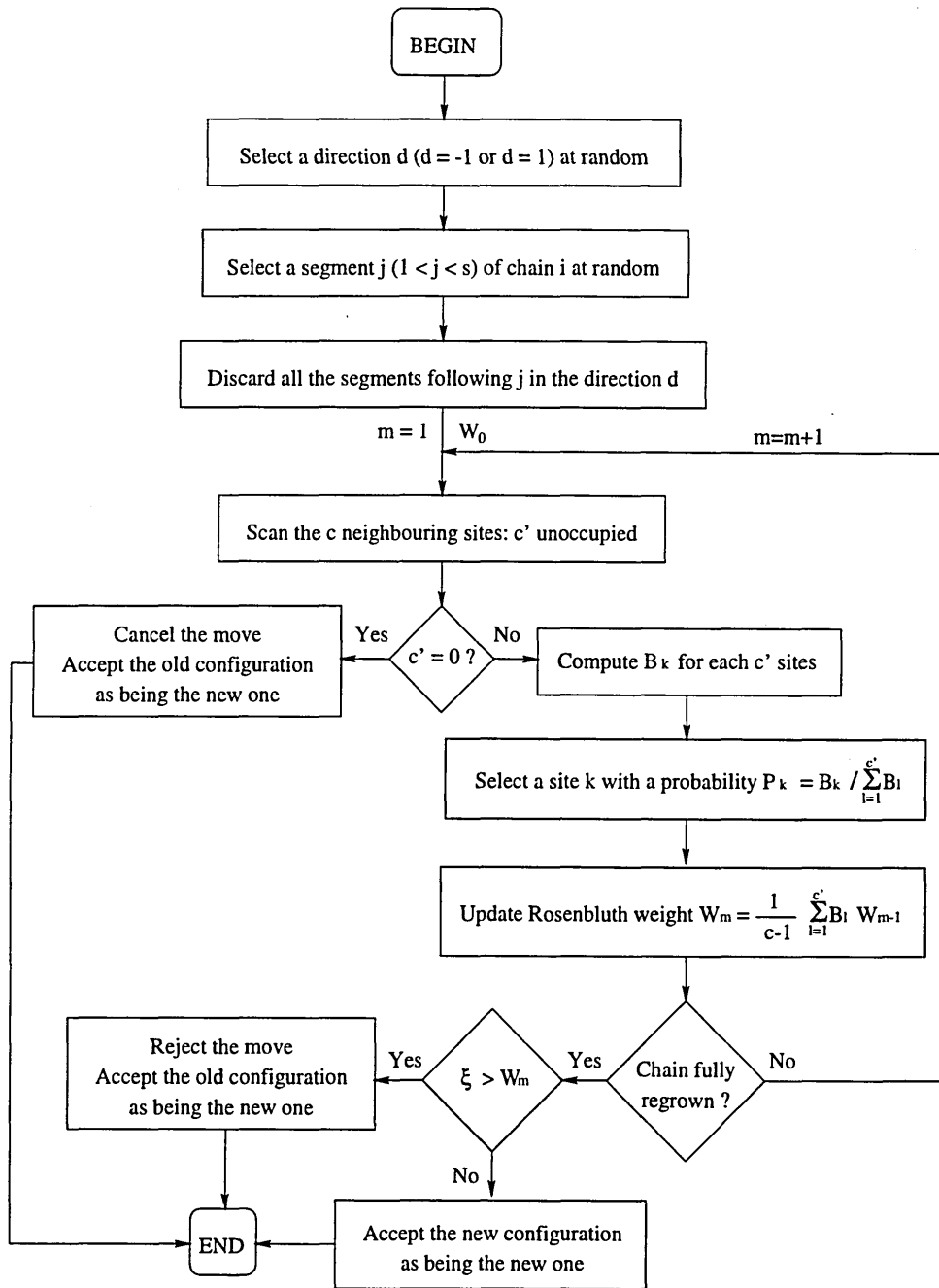


Figure 5.5: The configurational-bias Monte Carlo scheme

where  $B_k = \exp(-\beta\Delta U_{k_l})$  is the Boltzmann weight associated to the attempted insertion of a segment in the site  $k_l$ , and  $\sum_{l=1}^{c'} B_l$  the sum over all the  $c'$  sites available for regrowth.

2. The Rosenbluth weight associated to the  $m^{\text{th}}$  regrowth  $W_m$  becomes:

$$W_m = W_{m-1} \sum_{l=1}^{c'} B_l / (c - 1) \quad (5.12)$$

3. The acceptance criterion has been modified to increase the acceptance rate: the trial configuration is now accepted with a probability:

$$P_{acc} = \text{MIN}[1, W_{trial}/W_{old}]$$

where  $W_{old}$  is the Rosenbluth weight obtained for the regrowth of the old configuration

This scheme has been originally presented as a new method to compute the chemical potential of chain molecules [121]. Contrary to Widom's particle insertion method [122] in which the chains are grown prior to their attempted insertion and regardless of this latter, this new scheme aims to insert only one segment and then regrow the whole chain using a SAW. The bias thus introduced is corrected by multiplying the excess chemical potential by the Rosenbluth weight at the end of the regrowth,  $W$ . An off-lattice implementation of the CBMC has also been recently presented by Frenkel *et al.* [20]. This extension is discussed in more details in chapter 6.

Let us summarise the pros and cons offered by the two schemes detailed above:

**Reptation:**

- + Very straightforward to implement.
- + Computationally cheap.
- + Ensures the displacement of the chain centre of gravity.

but

- Not strictly ergodic.

- Becomes very inefficient at low temperatures and/or high densities.
- Only minor changes between two successive states in the Markov chain.

**Configurational-bias Monte Carlo:**

- + Still reasonably easy to implement.
- + Remains efficient at low temperatures and/or high densities.
- + Can be used for chains with a fixed extremity.
- + Allows important changes between two successive configurations.

but

- Computationally demanding: need to compute the Boltzmann weight of all the empty neighbouring sites for each segment to be regrown.
- Requires medium to long chain (*i. e.* 6 units onwards) to be worth being implemented.

Thus the two schemes presented above have their own advantages and limitations leading one to believe that using them in combination with each other may lead to a more efficient sampling. Depending on the particular properties of the system under consideration (mainly the chain length, temperature range and density), moves were performed using either simple reptation, configurational-bias, or a combination of both schemes.

## 5.4 The observables

In order to characterise the system and in particular its dependency on the different simulation parameters, it appears necessary to measure a series of observables throughout the simulations. As has been previously emphasised, Monte Carlo simulations are

unable to study non-equilibrium and dynamic properties: equilibrium thermodynamic averages are the only ones available. These later can be classified according to the class of properties they aim to measure, namely those relating to the aggregates, to the cavities in the structures, to the chains themselves, or to more general properties associated to the whole system such as the chemical potential or distribution functions.

### 5.4.1 Cluster properties

Cluster properties are used to characterise the aggregation of the chains in clusters. Whereas the number average cluster size and the size distribution index provide valuable information about the average cluster size and their polydispersity, the principal moments of inertia give information about the preferred shape of those aggregates. Finally, the cluster size distribution function proves to be the most important of all when dealing with systems in the micellar region since estimates of the excess chemical potential can be derived from it.

#### The number average cluster size

The number average cluster size,  $\bar{n}$  is:

$$\bar{n} = \frac{\sum_{i=2}^N i n_i}{\sum_{i=2}^N n_i} \quad (5.13)$$

where  $n_i$  is the number of clusters of  $i$  chains. Its root-mean-square deviation  $\sigma_{\bar{n}}^2$  is:

$$\sigma_{\bar{n}}^2 = \frac{\sum_{i=2}^N i^2 n_i}{\sum_{i=2}^N n_i} - \bar{n}^2 \quad (5.14)$$

It must be pointed out that chains in a monomeric state (often referred as ‘free monomers’) are excluded from the summations. This property gives a good insight into

the aggregation but starts failing as the total number of clusters decreases below a certain value.

This property is also referred to as the *mean aggregation number*,  $N_n$ .

### The size distribution index

The size distribution index is defined as being the ratio of the weight number average,  $N_w$ , to the mean aggregation number  $N_n$ , where:

$$N_w = \frac{\sum_{i=2}^N i^2 n_i}{\sum_{i=2}^N i n_i}$$

Thus:

$$\text{Size distribution index} = \frac{\sum_{i=2}^N i^2 n_i / \sum_{i=2}^N i n_i}{\sum_{i=2}^N i n_i / \sum_{i=2}^N n_i} \quad (5.15)$$

This property is commonly used in polymer science to characterise the polydispersity of a solution (*e.g.* see figure 4.13). It is  $\approx 1$  when the polydispersity is very weak and can typically reach values of 2 or higher for micellar solutions near the cmc.

### The cluster size distribution function

The cluster size distribution function gives the volume fraction of amphiphiles  $X_i$  in clusters of size  $i$  ( $1 < i \leq N$ ). Thus:

$$X_i = \frac{1}{M} i n_i s \quad (5.16)$$

where  $M$  is the total number of lattice sites.

The excess chemical potential ( $\mu_n^0 - \mu_1^0$ ) can be calculated from this distribution using the multiple equilibrium approach presented chapter 3.

### The principal moments of inertia

Depending on the region of phase space where the simulations are undertaken, the amphiphiles will spontaneously aggregate in clusters of various size and shape. Whereas the properties previously described give a good account of the cluster size distribution and its polydispersity, the shape of the aggregates can be indicated by computing their principal moments of inertia. The inertia tensor,  $\mathbf{I}$ , has the following components:

$$\mathbf{I} = \begin{pmatrix} I_{xx} & I_{xy} & I_{xz} \\ I_{xy} & I_{yy} & I_{yz} \\ I_{xz} & I_{yz} & I_{zz} \end{pmatrix}$$

where its diagonal components  $I_{\alpha\alpha}$  for clusters of  $i$  chains are:

$$I_{\alpha\alpha} = \sum_{j=1}^{is} m_j (r_j^2 - \alpha_j^2) \quad \alpha = x, y, z$$

and its off-diagonal components  $I_{\alpha\beta}$ :

$$I_{\alpha\beta} = - \sum_{j=1}^{is} m_j \alpha_j \beta_j \quad \begin{array}{l} \alpha = x, y, z \\ \beta = x, y, z \\ \alpha \neq \beta \end{array}$$

There exists a set of eigenvalues of the inertia tensor known as the principal moments of inertia  $I_x$ ,  $I_y$ ,  $I_z$ , for which the inertia tensor will be diagonal; they can be obtained by solving the following characteristic equation:

$$\begin{vmatrix} I_{xx} - \lambda & I_{xy} & I_{xz} \\ I_{xy} & I_{yy} - \lambda & I_{yz} \\ I_{xz} & I_{yz} & I_{zz} - \lambda \end{vmatrix} = 0$$

## CHAPTER 5. MODEL

The principal moments can be sorted and normalised so that:

$$I_l + I_m + I_s = 1 \quad I_l \geq I_m \geq I_s$$

where  $I_l$ ,  $I_m$  and  $I_s$  are respectively the largest, medium and smallest normalised principal moments of inertia.

The mean principal moments of inertia are weighted by the cluster size,  $n_i$ . Thus for a system containing  $n_{clus}$  clusters:

$$\bar{I}_\alpha = \frac{\sum_{i=1}^{n_{clus}} n_i I_{\alpha i}}{\sum_{i=1}^{n_{clus}} n_i} \quad \alpha = l, m, s \quad (5.17)$$

The values taken by the principal moments of inertia can be compared to the following characteristic values:

$$Sphere \quad \longrightarrow \quad I_s = I_m = I_l = 1/3$$

$$Rod \quad \longrightarrow \quad I_s = I_m = 0, \quad I_l = 1$$

$$Disk \quad \longrightarrow \quad I_s = I_m = 1/4, \quad I_l = 1/2$$

Following Brindle [15], the ratio of the smallest to the largest principal moment of inertia has also been computed.

### 5.4.2 Cavity properties

For particular sets of simulation parameters, large aggregates with cavities filled-in with solvent — a cavity being defined as a group of  $i$  ( $i \geq 1$ ) connected solvent sites distinct from the continuum bulk solvent — spontaneously occur (see chapter 7). In order to characterise those structures, it is important to have some measure of the size and shape

of those cavities. The properties used for that purpose are in essence similar to those used for the characterisation of the clusters of amphiphile if one substitutes the amphiphile segments constituting the aggregate by the solvent sites enclosed in the cavities. Thus, the following properties can easily be measured throughout the simulations:

- The mean cavity size.
- The mean number of cavities.
- The mean volume fraction of trapped solvent.
- The cavity size distribution function.
- The cavity principal moments of inertia.

One may note that the first three properties can be easily derived from the cavity size distribution function. For computational cost related reasons, the moments of inertia were not measured.

### Mean cavity size

The mean cavity size is simply defined as the the mean number of solvent sites enclosed in the cavities. Thus:

$$\text{Mean Cavity Size} = \frac{1}{n_{cav}} \sum_{i=1}^{n_{cav}} n_{EncSol_i} \quad (5.18)$$

where  $n_{cav}$  is the number of cavities and  $n_{EncSol_i}$  the number of enclosed solvent sites in the  $i^{th}$  cavity.

### Mean volume fraction of trapped solvent

The mean volume fraction of trapped solvent is easily calculated from the total number of enclosed solvent sites,  $\sum_{i=1}^{n_{cav}} n_{EncSol_i}$ :

$$\text{Mean volume fraction in trapped solvent} = \frac{1}{M} \sum_{i=1}^{n_{cav}} n_{EncSol_i} \quad (5.19)$$

### The cavity size distribution function

The cavity size distribution is measured in a similar manner to the cluster size distribution. Thus the volume fraction of solvent sites  $X_{s_i}$  enclosed in cavities of size  $i$  is:

$$X_{s_i} = \frac{1}{M} i n_{cav_i} \quad (5.20)$$

where  $n_{cav_i}$  is the number of cavities of size  $i$ .

### 5.4.3 Chain properties

Three main properties are generally used to characterise chain conformations whether experimentally or through simulations:

- The end-to-end distance,  $r$ .
- The radius of gyration,  $R_g$ .
- The bond order parameter,  $S_k$ .

The first two only have been measured during this study.

#### End-to-end distance

The end-to-end distance,  $r$ , is simply defined as the sum of the chain bond vectors  $\mathbf{I}_i$ . Thus for a chain of  $(s - 1)$  bonds:

$$\mathbf{r} = \sum_{i=1}^{s-1} \mathbf{I}_i$$

where  $\mathbf{I}_i$  is the bond vector between the  $i^{\text{th}}$  and  $(i+1)^{\text{th}}$  units. Since the orientation of the chain is of little interest for our purpose, the quantity actually computed is the average square of the end-to-end distance  $\bar{r}^2$ :

$$\bar{r}^2 = \frac{1}{N} \sum_{i=1}^N \mathbf{r}_i \cdot \mathbf{r}_i \quad (5.21)$$

### Radius of gyration

The radius of gyration,  $R_g$ , is a quantity mostly used in polymer science as a means to characterise the chain conformations by providing a measure of the spatial domain percolated by the chain. It is defined as ‘the root-mean-square distance of the collection of atoms — or groups — from their common centre of gravity’ [123]. Thus by definition, the average radius of gyration is:

$$\overline{R_g^2} = \frac{1}{N_s} \sum_{i=1}^N \sum_{j=1}^s d_{ij-cm}^2 \quad (5.22)$$

where  $d_{ij-cm}$  is the distance separating the  $j^{\text{th}}$  unit of the  $i^{\text{th}}$  chain from its center of mass; this equation may also be expressed as a function of the inter-segment distance:

$$\overline{R_g^2} = \frac{1}{N_s^2} \sum_{i=1}^N \sum_{1 \leq j < k \leq s} d_{ijk}^2$$

where  $d_{ijk}$  is the distance between the  $j^{\text{th}}$  and  $k^{\text{th}}$  segments of the  $i^{\text{th}}$  chain.

#### 5.4.4 Other averages

##### Site-site distribution function

By definition, the distribution function  $g(r)$  is the probability of finding a pair of atoms a distance  $r$  apart, relative to the probability expected for a completely random

distribution at the same density [1]. The main asset of this property is that it can be calculated from experimental data of the structure factor obtained from small-angle scattering studies. Thus for a system of volume  $V$  containing  $N$  molecules at a density  $\rho$  [124]:

$$g(\mathbf{r}) = \frac{1}{\rho^2} \left\langle \sum_i \sum_{j \neq i} \delta(\mathbf{r}_i) \delta(\mathbf{r}_j - \mathbf{r}) \right\rangle = \frac{V}{N^2} \left\langle \sum_i \sum_{j \neq i} \delta(\mathbf{r} - \mathbf{r}_{ij}) \right\rangle \quad (5.23)$$

where  $\delta()$  the Dirac delta function,  $\mathbf{r}$  the molecular position,  $\mathbf{r}_{ij}$  the position of molecule  $i$  relative to molecule  $j$ .

Since the simulations are performed on a lattice, the distribution function is actually a site-site distribution function  $g_{ss}(i)$ .

$$g_{ss}(i) = \frac{M}{Ns(Ns-1)} \frac{\sum_{j=1}^{Ns} \sum_{k \neq j} \delta(i-1/2 < \mathbf{r}_j - \mathbf{r}_k \leq i+1/2)}{P_{i-1/2 < \mathbf{r}_{ij} \leq i+1/2}} \quad i = 1, 2, \dots, l_{max} \quad (5.24)$$

where  $P_{i-1/2 < \mathbf{r}_{ij} \leq i+1/2}$  is the probability of finding two segments a distance  $i-1/2 \dots i+1/2$  apart for a system at similar density with a random distribution and  $l_{max}$  is half the size of the smallest side of the simulation box.

Other distribution functions such as the centre of mass-center of mass,  $HH$ ,  $TT$  or cluster-cluster distribution functions can be computed in a similar manner. The principal drawback of this property is that its range is limited to half the smallest size of the simulation box thus requiring very large lattices.

### External interactions count

The mean number of external interactions,  $\overline{n_{HS}}$  and  $\overline{n_{TS}}$ , can be measured throughout the simulation to gain a better understanding of how the aggregation process takes place. Information such as the degree of hydration of the head segments can be

deduced from them. They are normalised by the maximum number of possible interactions so that:

$$\overline{n_{HS}}^* = \frac{n_{HS}}{(c-1) + (t-1)(c-2)} \quad (5.25)$$

and:

$$\overline{n_{TS}}^* = \frac{n_{TS}}{(c-1) + (s-t-1)(c-2)} \quad (5.26)$$

where  $\overline{n_{HS}}^*$  and  $\overline{n_{TS}}^*$  are respectively the normalised average number of *HS* and *TS* interactions.

### Rejection rates

Unlike the other properties which are relevant to the system, the rejection rates are useful indicators of the sampling efficiency. For both the reptation and configurational-bias Monte Carlo schemes, contributions from different causes can be measured, namely:

- $R_{excl.vol.}$ : Moves rejected for excluded volume interactions.
- $R_{Metro}$ : Moves rejected by the Metropolis criterion.

with:

$$R_{total} = R_{excl.vol.} + R_{Metro}$$

Note that the fraction of identical successive configurations generated by the configurational-bias Monte Carlo scheme is also measured.

### Statistical inefficiencies

The statistical inefficiency  $s_x$  can be used in conjunction with any of the properties  $x$  previously described in order to assess their correlation and the underlying bias

on the statistics. It is calculated by dividing a run of  $\tau$  Monte Carlo steps in  $n_b$  blocks of size  $\tau_b$  so that  $\tau = n_b \tau_b$ . The average on each block is thus:

$$\langle x \rangle_b = \frac{1}{\tau_b} \sum_{\tau=1}^{\tau_b} x(\tau)$$

and the variance on those averages:

$$\sigma^2(\langle x \rangle_b) = \frac{1}{n_b - 1} \sum_{b=1}^{n_b} (\langle x \rangle_b - \langle x \rangle_{run})^2$$

$\sigma^2(\langle x \rangle_b)$  is expected to become inversely proportional to the block size when this latter is made sufficiently large. The statistical inefficiency provides a measure of this constant of proportionality; it is thus defined as [1, 125]:

$$s_x = \lim_{\tau_b \rightarrow \infty} \frac{\tau_b \sigma^2(\langle x \rangle_b)}{\sigma^2(x)} \quad (5.27)$$

Whilst this method is too computationally demanding to be systematically computed for all the simulations undertaken, it is good practice to use it for a few ‘typical’ runs in order to get a rough estimate of the correlation time.

### Statistical error

It is common practice in computer modelling to assume that the samples are distributed following a Gaussian distribution and are uncorrelated. In such a case, the standard error  $\delta_{1\bar{x}}$  for a set of  $n$  samples  $x_i$  ( $i = 1, 2, \dots, n$ ) is simply:

$$\delta_{1\bar{x}} = \left( \frac{1}{n(n-1)} \sum_{i=1}^n (x_i - \bar{x})^2 \right)^{1/2} \quad (5.28)$$

Whilst the absence of correlation can be checked through the calculation of the statistical inefficiency, the nature of the distribution cannot sometimes be established with certainty. For many properties like the cluster size distribution, the probabilities of

occurrence of some states were so low that their distribution actually obeyed a Poisson distribution. For such distributions the error must be calculated as [126]:

$$\delta_{1\bar{x}} = \left(\frac{1}{n\bar{x}}\right)^{1/2} \quad (5.29)$$

When doubts about the distribution arose, both standard errors were computed and the highest of them was considered. The standard deviation and standard error were also computed for all the observables previously described.

## 5.5 The simulations

### 5.5.1 The hardware

Apart from the explicit declaration of variables — *e. g.* INTEGER\*i and REAL\*j where  $i = 2, 4$  and  $j = 4, 8$  used in place of the standard INTEGER and REAL statements — and the use of an include file to declare the constants, the simulations have been coded in pure ANSI Fortran77 in order to retain full portability. Indeed, different platforms had to be used throughout those studies including an IBM 386DX compatible, an Apollo workstation, Silicon Graphics Iris, Indy or Power Challenge and two 4 and 16-node arrays of Intel iPSC860 connected to a host Sun Sparc station2. The bulk of the simulations were performed on those arrays.

### 5.5.2 Optimisations and style

The algorithmic and programming style was in line with common sense and ‘classic’ optimisation techniques. Thus wherever appropriate, look-up tables and dummy variables were used to avoid unnecessary calculations: *e. g.* the Boltzmann weights were calculated at the beginning of each temperature step and then stored in a three-dimensional

array (the first index being  $\Delta n_{HS}$ , the second one  $\Delta n_{TS}$  and the last one  $\Delta n_{folded}$ ). Reliability, portability and maintainability were the prime concern and prevailed over optimisation. Since the simulations had to be fully portable, no machine or compiler-dependent optimisations (*e. g.* vectorisation-oriented programming) were performed. The optimisation was only performed at compilation time by the compilers according to the local architecture.

Great care has also been taken in ensuring a total modularity of the program *i. e.* each task (*e. g.* setting-up the starting configuration, moving a chain using a particular scheme, measuring an observable, . . .) was self-contained in a module. It was thus possible, depending on the simulation performed, to select a set of observables to be investigated, set-up the *Makefile* to compile the corresponding units and link them together to produce the simulation executable.

A transcript of the code is available in the second volume of this thesis.

### 5.5.3 The schemes

Although some effort was made to optimise the calculation of the observables, most of the efforts were used to optimise the Monte Carlo moves since profiling has shown that most of the CPU time is being spent attempting to move the chains.

#### The reptation

The reptation was particularly susceptible to optimisation since only three sites were subject to a change in occupancy:

- The site to which the *head* of the *snake* will be moved:  $S \rightarrow H$  (or  $S \rightarrow T$  for a backward move).

CHAPTER 5. MODEL

- The site freed by the reptation of the last segment:  $T \rightarrow S$  (or  $H \rightarrow S$  for a backward move).
- The site at the junction between the hydrophilic and hydrophobic part of the chain:  $H \rightarrow T$  (or  $T \rightarrow H$  for a backward move).

Those three sites are respectively **B2**, **D4** and **B4** for the forward move example provided figure 5.6.

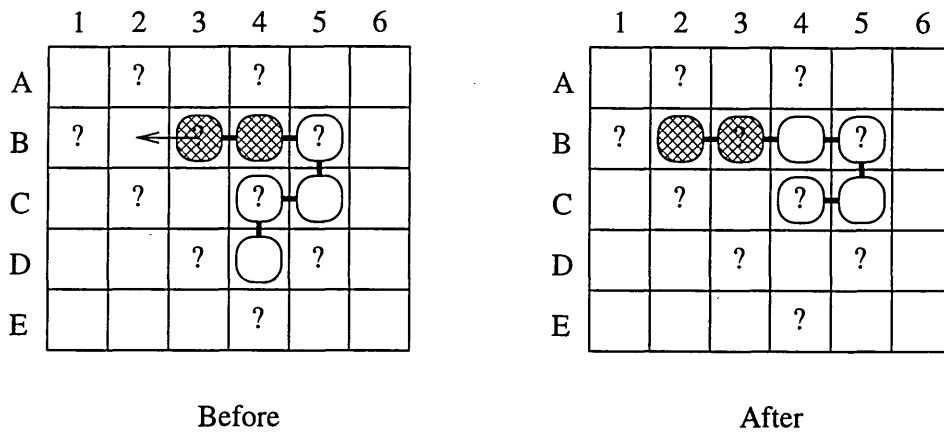


Figure 5.6: Sites to be checked following a reptation

Since only those three sites change occupancy following such a move, it is sufficient to investigate their neighbourhood in order to count  $\Delta n_{HS}$  and  $\Delta n_{TS}$  and therefore deduce  $\Delta E$  (provided  $\Delta n_{folded}$  has already been determined).

However, it can be seen on the typical example provided in figure 5.6 that some particular cases must be considered when the neighbourhood of those three sites overlap each other. These cases can easily be spotted and appropriate corrective terms applied to the interactions count.

## The Configurational-bias Monte Carlo

No particular trick could be implemented. The code is a straightforward implementation of the CBMC algorithm previously described.

## 5.6 Conclusion

Although the model used is very close to the original implementation by Care, one may point out a few modifications aimed at overcoming some limitations reported during previous simulations. The most obvious is probably the use of the Configurational-bias Monte Carlo which, combined with the classic reptation, is thought to improve the overall sampling efficiency at low temperatures or when large aggregates (such as vesicles) do form. The second most important concerns the implementation of some form of chain stiffness. Contrarily to the previous studies, the rigidity parameter  $\varepsilon$  will be set to a value different to zero.

Finally, the observables measured through the simulations are also believed to provide sufficient information to investigate the phenomena of interest, *i. e.* the micellisation process (see chapter 8) and the characterisation of sponge-like structures (see chapter 7). The site-site distribution function and radius of gyration were not extensively used respectively because of the requirements it would place on the system size (the distribution can be obtained for distances less than half the size of the smallest side of the simulation box) and because it provided redundant information by following trends essentially similar to that exhibited by the end-to-end distance.

## Chapter 6

# A novel scheme for the simulation of chain molecules on a lattice

Most computer simulations of chain molecules presented so far (*e. g.* [93, 98, 104]) aim to reproduce the generic behaviour of a ‘typical’ surfactant rather than that exhibited by a particular compound. This is caused by the difficulty of:

1. Achieving a sufficiently accurate mapping of the ‘real molecules’ onto the lattice chain.
2. Using more realistic potentials whilst retaining an overall tractability.

Whereas discussing the use of more realistic potentials would go beyond the scope of the current project, a methodology is proposed for how to achieve a more accurate coarse graining using a Flory-type model.

## 6.1 The ‘modified’ configurational-bias Monte Carlo

### 6.1.1 The concept

Prior to considering the proposed methodology for the mapping, one must realise the increase in computational cost likely to be engendered by such a procedure thus making most conventional Monte Carlo schemes such as the reptation inadequate. Smarter schemes like the configurational-bias Monte Carlo CBMC introduced earlier in chapter 5 proved to be a significant advance but still suffer from a rather high computational cost. For instance in the most elaborate variant of the CBMC proposed by Siepmann, the Boltzmann weights  $b_{ij}$  of all the  $j$  sites available for regrowth of the  $i^{th}$  segment must be calculated. This implies calculations of the contributions from both variations in external interactions  $\Delta E_{extij}^i$  and internal conformations  $\Delta E_{intij}$ .

Thus for lattices of high enough coordination number  $c$ , an alternative approach analogous to that proposed by Frenkel in his extension of the CBMC to off-lattice chain models would be to choose the site for the regrowth of the  $i^{th}$  segment from a subset  $\{m\}_i$  of  $k_i$  sites extracted at random from the  $j_i$  sites available for the regrowth (see figure 6.1).

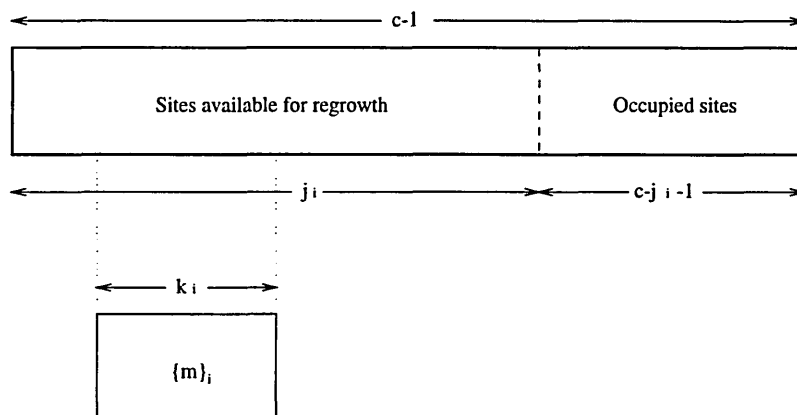


Figure 6.1: A subset of available sites

Provided the size of the subsets  $k_i$  is kept sufficiently large to ensure that most

regrowths can be successfully completed — and with an acceptable Boltzmann weight —, this should ensure a significant speed increase over the conventional CBMC without sacrificing too much of the sampling efficiency. The sampling criterion used by the conventional CBMC to sample the configurations must be modified in order to correct for the new bias thus introduced by the selection of the subsets. One aims first to demonstrate the correctness of the underlying Markov chain by applying the classic criterion for Monte Carlo schemes (*e.g.* [1, 110] and chapter 5).

### 6.1.2 Acceptance criterion

Before describing the author's new approach, let us first consider the original implementation for lattice systems proposed by Siepmann [21] and the continuum generalisation by Frenkel [20].

#### The 'original' CBMC

In this implementation, part or all of a chain is regrown using a self-avoiding walk, *SAW* [120]. At each step of the regrowth, a segment is chosen amongst the neighbouring sites  $n$  in a manner similar to a non-reversible random walk, *NRRW*, *i.e.*  $n = c$  for the regrowth of the second segment and  $n = (c - 1)$  otherwise (see chapter 5 for more details).

If one considers the most sophisticated variant of the original CBMC, the probability,  $P_j$ , of selecting a site  $j$  at the  $i^{\text{th}}$  step of the regrowth is:

$$P_j = \frac{b_j}{Z_i} \quad (6.1)$$

where  $b_j = \exp(-\beta u_{\Gamma_j})$  is the Boltzmann weight of the site  $j$ , and  $Z_i = \sum_{k=1}^n b_k$ . The corresponding Rosenbluth weight,  $W_i$ , is:

$$W_i = \frac{Z_i}{n} W_{i-1} \quad (6.2)$$

The probability of fully growing a chain of length  $s$  in a conformation  $\Gamma$ ,  $P_\Gamma$ , is therefore:

$$P_\Gamma = \prod_{i=1}^{s-1} \frac{\exp(-\beta u_{\Gamma_i})}{Z_i} \quad (6.3)$$

and the Rosenbluth weight at the end of the regrowth,  $W_\Gamma$ , is:

$$W_\Gamma = \prod_{i=1}^{s-1} \frac{Z_i}{n} W_0 \quad (6.4)$$

where  $W_0$  is the Rosenbluth weight at the start of the regrowth.

As was explained in chapter 5, a good acceptance criterion fulfilling the detailed balance criterion for this scheme is:

$$P_{acc} = \text{MIN} \left[ 1, \frac{W_{trial}}{W_{old}} \right] = \text{MIN} \left[ 1, \prod_{i=1}^{s-1} \frac{Z_{trial_i}}{Z_{old_i}} \right] \quad (6.5)$$

This scheme is computationally expensive due to the necessity of computing the Boltzmann weights of all the sites available for the regrowth. This becomes particularly noticeable for lattices of high coordination number.

### The 'continuum' CBMC

Frenkel has shown that it is possible to generalise the CBMC to apply it to off-lattice systems. Instead of selecting the new position of insertion from  $n$  neighbouring sites, a set  $\{m\}_i$  of  $k_i$  positions is generated at each step  $i$  of the regrowth. The probability of generating a particular conformation  $\Gamma$  thus becomes:

$$P_{\Gamma} = \prod_{i=1}^{s-1} k_i P_{\Gamma_i} \frac{\exp(-\beta u_{\Gamma_i})}{Z_{\{m\}_i}} \quad (6.6)$$

where  $P_{\Gamma_i}$  represents the probability of generating a set of positions  $\{m\}_i$ .

The Rosenbluth weight at the end of the regrowth,  $W_{\Gamma}$ , is:

$$W_{\Gamma} = \prod_{i=1}^{s-1} \frac{Z_{\{m\}_i}}{n} W_0 \quad (6.7)$$

### The ‘modified’ CBMC

Let us now consider a chain lying on a lattice of coordination number  $c$ ,  $j_i$  sites of which being not occupied and hence available for the regrowth of the  $i^{\text{th}}$  segment. A subset  $\{m\}_i$  of  $k_i$  sites is extracted at random from the  $j_i$  available sites with an equal probability  $P_{\{m\}_i}$ :

$$P_{\{m\}_i} = \frac{k_i!(j_i - k_i)!}{j_i!} \quad (6.8)$$

The probability of growing a conformation  $b$  using the conventional Rosenbluth SAW algorithm would be:

$$P_b = \prod_{i=1}^{s-1} \sum_{\{m\}_i} P_{\{m\}_i} \frac{\exp(-\beta u_{b_i})}{Z_{\{m\}_i}} \quad (6.9)$$

where

$$Z_{\{m\}_i} = \sum_{j=1}^{k_i} \exp(-\beta u_{m_{i,j}})$$

and the summation over  $\{m\}_i$  includes all the subsets of  $k_i$  unoccupied sites containing the orientation  $b_i$ .

As demonstrated by Frenkel *et al.* [20], one can fulfill the detailed balance criterion by imposing a stronger condition known as the *super-detailed balance*. By definition,

the super-detailed balance criterion is satisfied if:

$$K(a|b)\{m\}_i\{m'\}_i = K(b|a)\{m\}_i\{m'\}_i \quad (6.10)$$

where  $K(a|b)\{m\}_i\{m'\}_i$  is the rate at which configurations  $a$  are transformed into configurations  $b$  using a set of subsets  $\{m\}_i$  and  $K(b|a)\{m\}_i\{m'\}_i$  is the rate at which configurations  $b$  are transformed into configurations  $a$  using a set of subsets  $\{m'\}_i$ .

Thus the probability of regrowing a chain into configuration  $b$  using a set of subsets  $\{m\}_i$  and generating a set  $\{rest'\}$  of  $(k_i - 1)$  orientations  $\{m'\}$  excluding orientations  $a_i$  around configuration  $a$  is:

$$P_b = \prod_{i=1}^{s-1} P_{\{m\}_i} P_{\{rest'\}_i} \frac{\exp(-\beta u_{b_i})}{Z_{\{m\}_i}} \quad (6.11)$$

If one substitutes  $P_a$  and  $P_b$  into the standard acceptance criterion used in Metropolis Monte Carlo (cf [1]):

$$acc(a|b) = MIN \left( 1, \frac{P_a / \exp(-\beta U_{\Gamma_a})}{P_b / \exp(-\beta U_{\Gamma_b})} \right) \quad (6.12)$$

for our problem:

$$P_{\{m\}_i} = 1 / \binom{j_i}{k_i} = \frac{k_i!(j_i - k_i)!}{j_i!}$$

and

$$P_{\{rest'\}_i} = 1 / \binom{j_i - 1}{k_i - 1} = \frac{(k_i - 1)!(j_i - k_i)!}{(j_i - 1)!}$$

equation 6.12 thus becomes:

$$acc(a|b) = MIN \left( 1, \frac{\exp(-\beta U_{\Gamma_{b_1}}) \prod_{i=1}^{s-1} \frac{j_i}{k_i} Z_{\{m\}_i}}{\exp(-\beta U_{\Gamma_{a_1}}) \prod_{i=1}^{s-1} \frac{j'_i}{k'_i} Z_{\{m'\}_i}} \right) \quad (6.13)$$

which can be rewritten as:

$$acc(a|b) = MIN \left( 1, \frac{W_b}{W_a} \right) \quad (6.14)$$

where the corresponding Rosenbluth weights for configurations  $a$  and  $b$  are found to be:

$$\begin{aligned} W_b &= \exp(-\beta U_{\Gamma_{b_1}}) \prod_{i=1}^{s-1} \frac{j_i}{k_i} Z_{\{m\}_i} \\ W_a &= \exp(-\beta U_{\Gamma_{a_1}}) \prod_{i=1}^{s-1} \frac{j'_i}{k'_i} Z_{\{m'\}_i} \end{aligned} \quad (6.15)$$

Note that the only constraint on the subset size  $k_i$  is that  $k_i \leq j_i$ ; its value can be modified at each step of the regrowth. A complete study of the  $k$ -dependence<sup>1</sup> of the sampling efficiency for the case of the continuum implementation has been presented by Frenkel *et al.* [127].

Finally, one must notice that:

1. If all the available sites are considered during the regrowth (*i. e.*  $k_i = j_i$ ), the acceptance criterion expressed in equation 6.13 becomes equivalent to the case described by Siepmann in his original implementation of the CBMC [21] (see equation 6.5).
2. If the set of sites considered becomes very large (*i. e.*  $j_i \rightarrow \infty$ ) and includes occupied sites (*i. e.*  $j_i = c$ ), then this scheme becomes identical to the continuum implementation described by Frenkel [20, 127].

### 6.1.3 Application to the simulation of diblock copolymers: a benchmark

In order to assess the effect of this procedure, this new scheme has been implemented to perform short simulations of diblock copolymers  $A_8 - B_8$ . The solvent was

---

<sup>1</sup>In the continuum implementation,  $k$  represents the size of the set of positions considered for the regrowth of the next segment; their occupancy is not *a priori* known.

made good for the  $A$  monomers and a poor for the  $B$  monomers. This type of compound can be seen as being essentially similar to surfactants with the  $A$  and  $B$  monomers being homologous respectively to hydrophilic and hydrophobic units.

Two sets of simulations were carried out for medium concentrations of 20.0 *vol. %* and 25.0 *vol. %* by placing respectively  $N = 410$  and  $N = 64$  chains of length  $s = 16$  units (8A and 8B) on lattices of size  $32 \times 32 \times 32$  and  $16 \times 16 \times 16$ . The Hamiltonian used was that from equation 5.2. The chains were made fully flexible (*i. e.*  $E_i^c = 0$ ) but the coordination number of the cubic lattice was extended to  $c = 26$  by also allowing moves to and interactions with next-nearest and diagonal neighbours.

Simulations were undertaken to compare the relative performance of the modified configurational-bias Monte Carlo  $MCBMC_k$  with different subset sizes ( $k = 4, 8, 12, \dots, 20$ ) to the classic CBMC and the reptation. One must point out that those values are actually maximum values  $k_{max}$ , the condition  $k_i \leq j_i$  remaining so that at each step of the regrowth  $i$ ,  $k_i = MIN[k_{max}, j_i]$ . The aim of these simulations were twofold:

1. Validating the algorithm by checking that similar limiting distributions were obtained.
2. Assessing the speed improvement of the modified scheme over its conventional counterpart.

### Simulation results

The simulations were performed at constant temperatures of  $\beta^{-1} = 2.0$  (larger system) and  $\beta^{-1} = 2.2$  (smaller system) with  $\gamma = -0.50$ . The starting configurations were random disordered and no thermalisation took place. Both the average square end-to-end distance,  $\bar{r}^2$ , and the normalised external interaction counts,  $n_{AS}^*$  and  $n_{BS}^*$  have been used as indicator of the speed at which the system started fluctuating around its equilibrium

state.

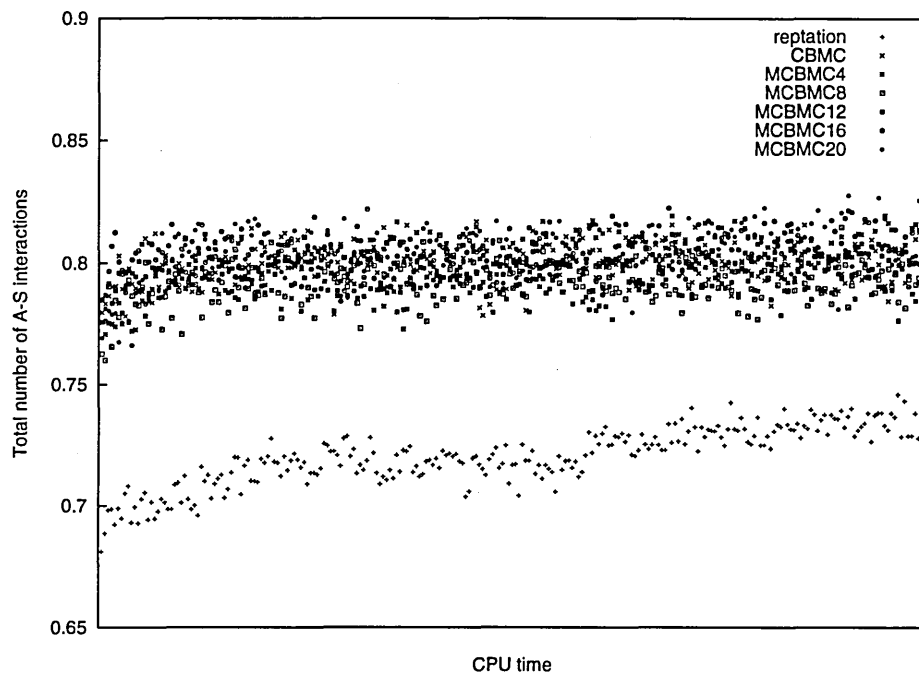


Figure 6.2: Comparison of the 'conventional' and 'modified' CBMC:  $n_{AS}^*$  for the small system

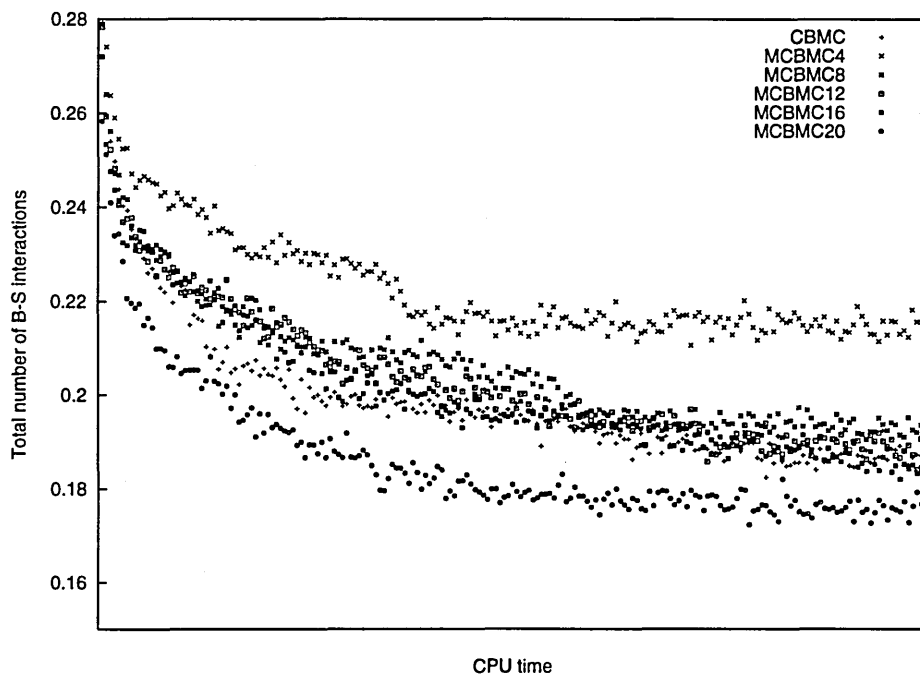


Figure 6.3: Comparison of the 'conventional' and 'modified' CBMC:  $n_{BS}^*$  for the large system (the reptation failed to converge sufficiently rapidly to appear on this graph)

Some results of the normalised external interactions are presented for both the small (figure 6.2) and large (figure 6.3) systems. The total CPU duration of the simulations were of respectively 19h and 40h for the small and large systems. It should be noted that the system using the reptation scheme failed to reach equilibrium for large systems. Other properties including the radius of gyration or the end-to-end distance exhibited a behaviour essentially similar. More information could also be obtained from the rejection rates (excluded volume interaction and sampling criterion) and fraction of successive identical configurations generated. This issue is discussed next section.

### Discussion

All the tests performed agreed on the ability of the modified scheme to provide similar equilibrium values to those of the conventional CBMC thus validating it. However, no quantitative information about a  $k$ -dependent law could be derived from these preliminary tests; only general trends emerged.

Apart from allowing considerable speed up of the regrowth, another important fact making smaller  $k_i$  attractive is that they avoid regrowing the same configuration as it often happens with the CBMC at low temperatures and/or high densities.

This scheme deserves to be studied more thoroughly and characterised using a more systematic methodology such as that followed by Frenkel for the off-lattice implementation of the CBMC [127]. One must point out that although both schemes have a lot in common, they differ in that the sets are composed of positions which may have to be rejected for excluded volume interaction in the off-lattice variant whereas this case never arises for the CBMC since  $k_i \leq j_i$  (*i. e.* it is known *a priori* that the sites are available for the regrowth). However, general trends for the influence of  $k_i$  are roughly the same for both schemes:

- A decrease in the subset size  $k_i$  leads to a loss in sampling efficiency (not enough sites with a ‘sufficiently’ high Boltzmann weight are available throughout the regrowth) and subsequently an increase in the simulation length.
- An increase in  $k_i$  also increases the computational cost (up to the point where there is no advantage over the conventional CBMC).

## 6.2 Proposed methodology for a more accurate mapping

As is emphasised in chapters 5 and 7, a simple cubic lattice of coordination number  $c = 6$  allows only two different types of conformations (folded and straight) thus introducing an unrealistic representation for the bending of amphiphilic structures. Extending the underlying lattice to a coordination of  $c = 26$  by also including next-nearest and diagonal neighbours allows one to partially overcome this by distinguishing three different types of bonds between two neighbouring sites (see figure 6.4):

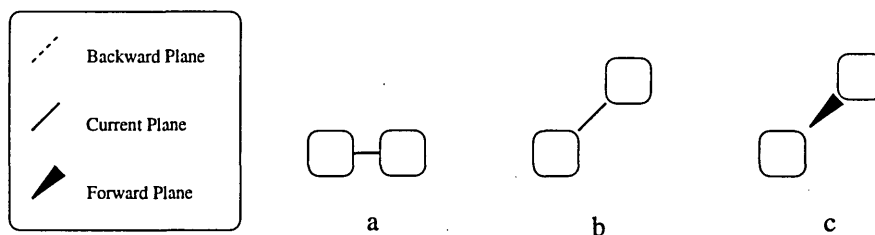


Figure 6.4: *a*, *b* and *c* conformations

- **a:** between two nearest neighbours (6 bonds).
- **b:** between two next-nearest neighbours (12 bonds).
- **c:** between two diagonal neighbours (8 bonds).

Thus if one considers the basic conformational units as being constituted of three consecutive segments (*i. e.* two consecutive basic bonds), there exists  $c \times (c - 1) = 650$  different units. When symmetry is taken into account the number of non equivalent structures is only 17. They can be classified according to their elementary constituents and the square of their end-to-end distance: *e. g.* *ab5* is constituted of a *a* bond connected to a *b* bond in such a manner that their end-to-end distance is  $\sqrt{5}$ . The 17 unique structures are shown in figures 6.5 and 6.6.

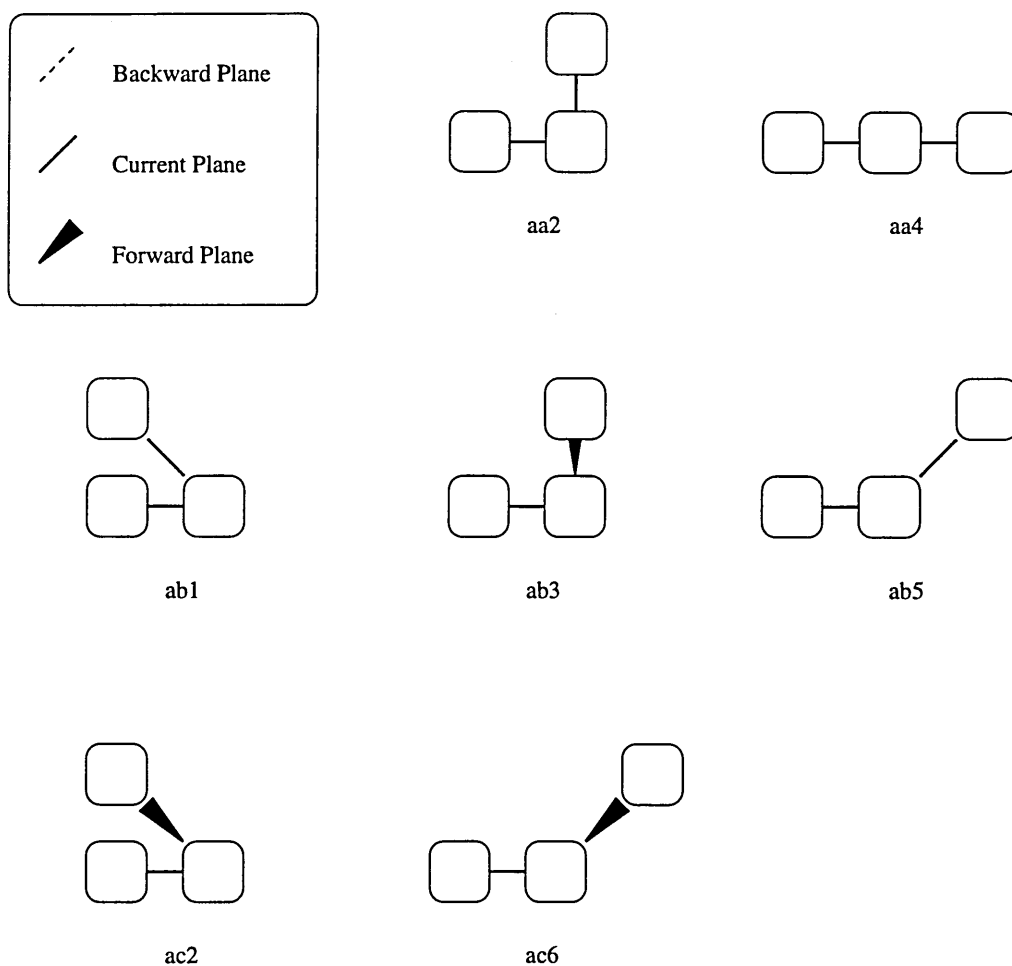


Figure 6.5: *aa*, *ab* and *ac* conformations

It must be pointed out that two conformations from the same category *aa*, *ab*,... have always a distinct end-to-end distance. This remark is also applicable to the

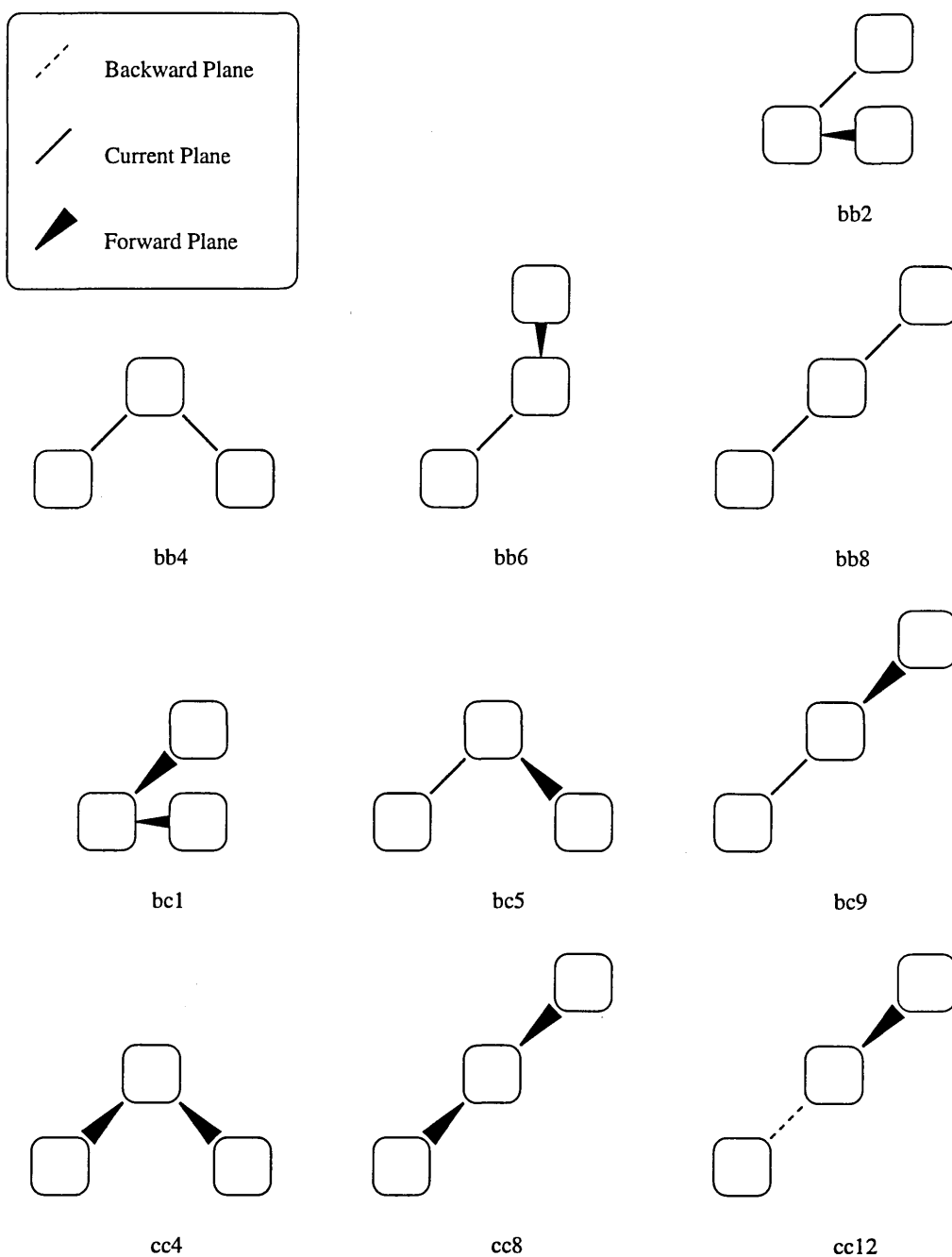


Figure 6.6: *bb*, *bc* and *cc* conformations

radius of gyration (see table 6.1), thus making the coding and design of smart algorithms particularly straightforward to implement.

The potential applications of such a model would include the mapping of block copolymers as well as surfactant made up of basic hydrophilic and hydrophobic units of

Radius of Gyration, $R_g$ (in lattice units)	Conformations
0.667	aa2 ab1
0.816	aa4 ab3 ac2 bb2 bc1
0.943	ab5 bb4
1.05	ac6 bb6 bc5 cc4
1.15	bb8
1.25	bc9 cc8
1.41	cc12

Table 6.1: Radii of gyration

roughly similar dimensions. The most obvious of those types of surfactants is probably the nonionic  $C_xEO_y$  which can be decomposed as a succession of hydrophobic  $-CH_2-$  and hydrophilic  $-CH_2CH_2O-$  units. If one makes a *Head* segment equivalent to this hydrophilic unit, the *Tail* segment therefore has to represent three hydrophobic units  $-(CH_2)_3-$  in order to have similar dimensions (see figure 6.7). With such a model, a surfactant such as  $C_{12}EO_6$  would therefore be represented as a chain of four *T* and six *H* segments.

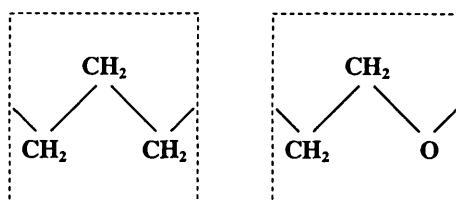


Figure 6.7: Mapping of a basic hydrophobic (left) and hydrophilic (right) unit

A following step would then consist in using a molecular mechanics package such as *Cerius2* which could be used in order to obtain the distribution of geometrical properties such as the radius of gyration and end-to-end distance for both basic hydrophilic and hydrophobic conformational units (*i. e.*  $H - (CH_2CH_2O)_3 - OH$  and  $C_9H_{20}$  respectively) from a MC or MD simulation. A minimisation procedure can then be undertaken in order

to determine an appropriate set of weights (entered through the conformational energy parameters  $\epsilon$ ) to be associated to each of the 17 basic conformations of the chain model for both type of segments in order to obey the same distribution.

The main limitation with such an approach remains its excessive memory and processing power requirements thus limiting the size of the system under investigation. This problem will progressively vanish as the high-performance computers become more affordable and similar types of models are likely to become increasingly popular in the near future. However, high-coordination lattices are already commonly applied for the simulation of polymers and proteins which require a very accurate mapping but only involve one or very few chains. A review of high-coordination number lattices for the mapping of *RIS* polymer chains has been presented by Rapold and Mattice [128] who discuss in detail the features offered by a new lattice named the *second-nearest-neighbour diamond lattice*. This latter has been designed in order to overcome the failure of other popular high-coordination lattices mostly based on an underlying cubic lattice to deal with chains with interdependent bonds such as polyethylene — although they already proved to be successful at mapping proteins.

### 6.3 Conclusion

Although the material presented herein is likely to be useful for future extensions of the model, one must emphasize that it was not applicable to the current project:

1. The modified CBMC certainly offers some improvements of the sampling efficiency over conventional schemes, but its intrinsic requirements (*i. e.* only worth applying to chains of sufficient length, say  $s \geq 8$ ) imply the study of a larger simulation box for a fixed number of chains,  $N$ , hence resources not yet available for such a project.

2. For essentially similar reasons, although a more accurate mapping of real molecules is quite common place for some simulations of polymers and proteins, it is still unpractical for the simulation of surfactant systems which typically require the study of several hundreds — or even thousands — of chains. However, the methodology presented remains valid and it is the author's belief that it will be used for further studies.
3. Some unexpected 'missing features' in the design of *Cerius2* made the mapping of the basic conformational units  $\text{H} - (\text{CH}_2\text{CH}_2\text{O})_3 - \text{OH}$  and  $\text{C}_9\text{H}_{20}$  a much more delicate affair than originally thought. Further versions of this software — or a competitor's product — may correct this and provide more adequate conformational search modules.

## Chapter 7

# Simulations in the ‘vesicle’ region

During his preliminary investigations, Brindle [129] noticed the formation of a vesicle-like structure (see figure 4.9) for a system of  $N = 512$  fully-flexible chains of length  $s = 6$  (total concentration  $X_a = 9.38 \text{ vol. } \%$ ) with a very short hydrophilic head of  $t = 1$  segment. This structure occurred for a relatively weak hydrophilic strength ( $\gamma = -1.0$ ) and ‘medium’ to low temperatures (*i. e.*  $\beta^{-1} < 1.30$ ). The chains were entangled following a bilayer-type arrangement with their head pointing either towards the ‘external’ bulk solvent or the solvent entrapped in an internal cavity.

The present part of this study of amphiphilic systems aims to investigate the occurrence of such vesicle-like structures in a much more detailed way. The obvious first steps consist in checking that the previous observations are reproducible and then to assess the magnitude of the finite size effect. During a second stage, a ‘phase diagram’ is established mostly by measuring the volume fraction of entrapped solvent as a function of the simulation parameters ( $\beta^{-1}, \gamma$ ).

## 7.1 Preliminary stage: reproducibility and finite size effects

### 7.1.1 Introduction

One should bear in mind that the configurations generated by Monte Carlo simulations can be strongly influenced by the sampling scheme used although in principle the thermal averages should be the same. In the particular case of Brindle's simulations, the random configurations were produced by moving the chains using the reptation algorithm and sampled following the conventional Metropolis criterion (by contrast to a so-called *smart MC scheme* such as the CBMC described in chapters 5 and 6); this combination has been reported on many occasions to produce a low quality sampling due to an excessive rejection rate and too small a change between two consecutive configurations. It is thus essential to refrain from drawing hasty conclusions from such preliminary observations about the stability or the probability of occurrence of a particular configuration. Moreover, the magnitude of the finite size effect for a system in which all the chains are involved in the formation of a single aggregate is clearly significant. Indeed, if all the chains are part of a same cluster, we do not have equilibrium clusters. These two preoccupations led to undertaking a preliminary study for a system of parameters identical to those chosen by Brindle, but for a set of system size ranging from  $N = 512$  up to  $N = 4096$  chains (see table 7.1).

Number of chains $N$	Lattice size	Concentration $X_a$ (vol. %)
512	$32 \times 32 \times 32$	9.375
768	$37 \times 37 \times 36$	9.350
1024	$41 \times 40 \times 40$	9.366
1536	$46 \times 46 \times 46$	9.468
2048	$51 \times 51 \times 50$	9.449
4096	$64 \times 64 \times 64$	9.375

Table 7.1: Simulation parameters

The simulations were carried out starting from random disordered configurations at a temperature  $\beta^{-1} = 2.50$  and then cooled down by steps  $\Delta\beta^{-1} = 0.10$  to a final temperature of  $\beta^{-1} = 0.50$ . The model used was the simplest described in chapter 5 with the ‘classic’ reptation moving the chains. At each temperature step, 50,000 Monte Carlo steps were discarded for thermalisation, and the system was sampled over 200,000 MC steps. The starting configuration at the beginning of each temperature step is that which ended the previous step.

### 7.1.2 Simulation results

The observables measured to characterise the system were the usual cluster properties described in chapter 5. No valuable information could be extracted from them. Indeed, both the mean aggregation number and cluster size distribution function are unable to account for any geometrical variation in the shape of an aggregate of fixed size. Thus, visual observations constituted during this preliminary stage the sole mean used to check the reproducibility of Brindle’s findings.

The first simulation with  $N = 512$  chains yielded unexpected results: instead of forming a vesicle, the chains aggregated in a structure which could be described as a rod of fluctuating radius with internal cavities of irregular size and shape filled in with solvent (see figure 7.1). This rod goes through the simulation box and is therefore of ‘infinite’ length (by application of the periodic boundary conditions). This result confirms the reserves expressed earlier concerning the likelihood of an excessive finite size effect.

Similar type of structures formed for all the other systems apart from the simulation undertaken with 1024 chains for which two vesicles of different size appeared (see figure 7.2).

Whereas the smallest vesicle is similar to that described in the original observation

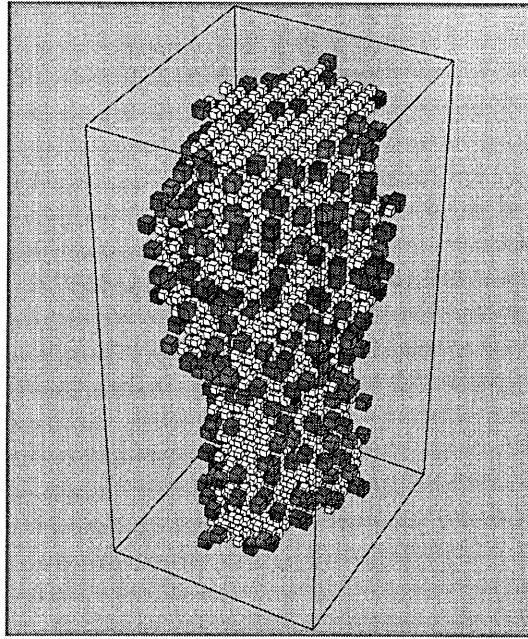


Figure 7.1: Rod-like structure ( $\beta^{-1} = 1.20$ ,  $\gamma = -1.0$ ,  $N = 512$ )

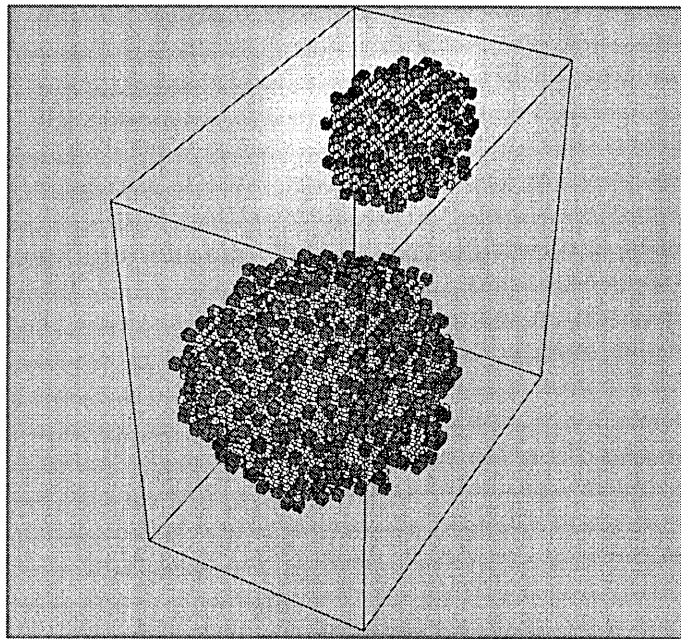


Figure 7.2: Vesicles ( $\beta^{-1} = 1.10$ ,  $\gamma = -1.0$ ,  $N = 1024$ )

with a single central pseudo-spherical cavity, the largest is significantly different in that it contains two communicating cavities. Furthermore, a detailed observation of the perimeter of a slice cut through its smallest side reveals a shape resembling that of a '8'. Those two

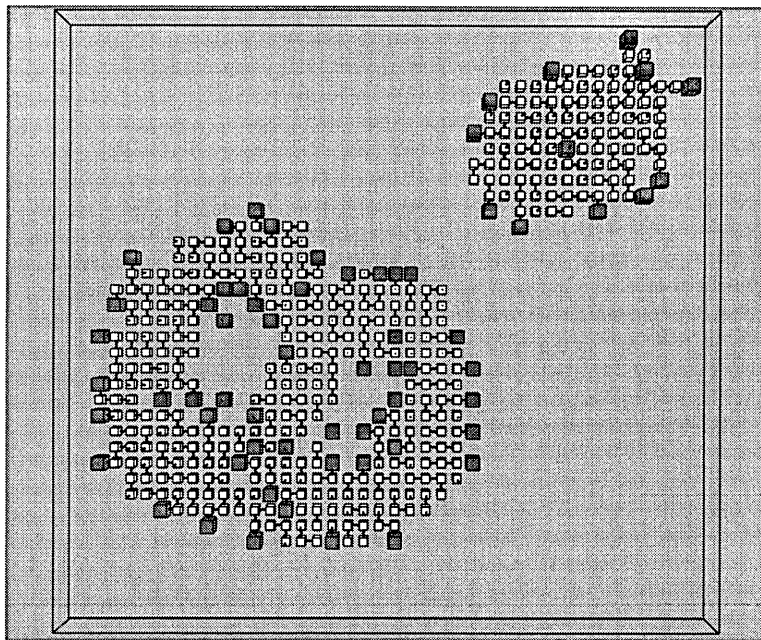


Figure 7.3: Slice through the vesicles ( $\beta^{-1} = 1.10$ ,  $\gamma = -1.0$ ,  $N = 1024$ )

observations would suggest that the number of chains belonging to this vesicle may be close to a critical value for which the large vesicle would break-up into two smaller vesicles.

Similar remarks can also be drawn for the rod-like structures: provided the system is large enough to minimise the finite-size effect, some part of the structures could be identified as some vesicles having just merged — or being close to break-up from the main aggregate (see figure 7.4).

### 7.1.3 Conclusion

The conclusions to be drawn from this preliminary study are rather ambiguous and speculative. The most important can be summarised as follows:

- The magnitude of the finite size effect is important, even for the largest systems.
- Previous observations have been partially reproduced: vesicles occurred for a single simulation whereas the others produced ‘spongy rod-like’ structures which present

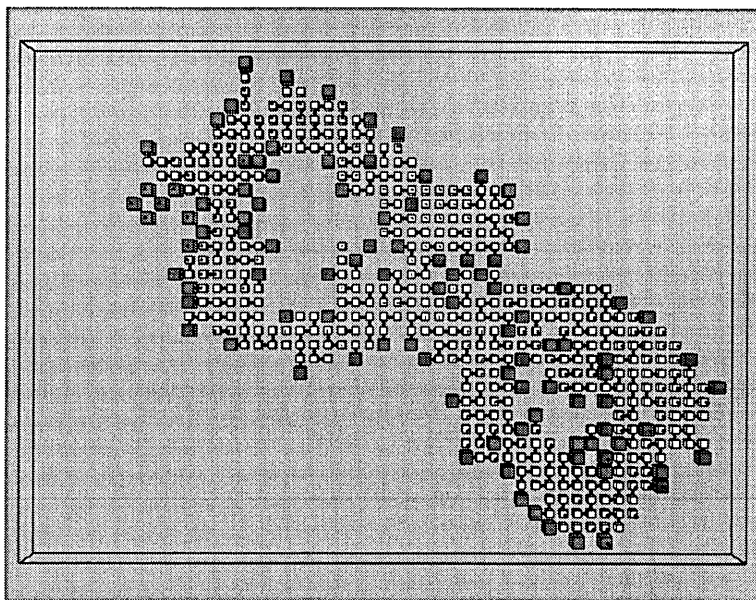


Figure 7.4: Slice through a ‘spongy’ structure ( $\beta^{-1} = 0.90$ ,  $\gamma = -1.0$ ,  $N = 2048$ )

related features. This would suggest that those structures are in equilibrium with each other and possibly with others.

- The reptation scheme seems once more to be inefficient at sampling such configurations where the terminating ends of the chains are often surrounded by occupied sites.
- The most promising way of characterising the structures formed in that region of phase space are the cavities, whether it is by their number, size or shape.
- A plot of the normalised observables measured through the simulations such as the normalised average number of external interactions,  $\overline{n_{HS}^*}$  and  $\overline{n_{TS}^*}$ , and the aggregate properties exhibited no noticeable system-size or structure-type dependence.

## 7.2 Phase diagram of the ‘vesicle’ region

### 7.2.1 The simulations

A series of simulations was undertaken for various values of  $(\beta^{-1}, \gamma, \epsilon)$ . The system consists of  $N = 1536$  chains of  $s = 6$  segments ( $t = 1$  of which representing the hydrophilic head and the remaining segments the hydrophobic tail) lying on a cubic lattice of coordination number  $c = 6$  and size  $47 \times 46 \times 46$ . The total volume concentration in surfactant was therefore  $X_a = 9.27 \text{ vol. } \%$ . This choice of system size is dictated by a trade-off between keeping the magnitude of the finite size effects at an acceptable level whilst still retaining an overall tractability of the problem (the ‘typical timescale’ is  $24h$  per temperature step although it could vary from  $11h$  up to  $38h$  depending on the rejection rates).

In order to achieve a better sampling at lower temperatures and high ‘local’ density<sup>1</sup>, a 1 : 1 combination of reptation and classic CBMC was utilised. The correctness of this procedure was checked by carrying out a set of simulations using pure reptation, pure CBMC, and a combination of them, verifying that they converged to the same limiting distributions. This proved to be true within statistical error. The contribution from the CBMC is very important since it does not require both extremities of the chains to be displaced and allows much larger changes between two consecutive steps whilst retaining a higher acceptance ratio than the reptation at low temperatures and/or high density (see chapter 5).

Although the  $HH$  interactions were still neglected (*i. e.*  $\eta = 0$ ), unlike simulations in the micellar region, chains were made only partially flexible. Thus, rigidity parameters of  $\epsilon = \{0.0; 0.5; 1.0; 2.0\}$  were investigated.

The simulations were started from a high temperature of  $\beta^{-1} = 2.10$  with a ran-

---

<sup>1</sup>*i. e.* for chains belonging to the aggregate(s)

Hydrophilic strength, $\gamma$	Rigidity parameter, $\varepsilon$				Hydrophilic strength, $\gamma$	Rigidity parameter, $\varepsilon$			
-2.00	0.0	1.0	2.0		-1.03	0.0	0.5	1.0	2.0
-1.50	0.0	1.0	2.0		-1.00	0.0	0.5	1.0	2.0
-1.28	0.0	1.0			-0.97	0.0	0.5	1.0	2.0
-1.20	0.0	0.5	1.0	2.0	-0.92	0.0	0.5	1.0	2.0
-1.13	0.0	0.5	1.0	2.0	-0.85	0.0	0.5	1.0	2.0
-1.10	0.0	0.5	1.0	2.0	-0.70	0.0		1.0	
-1.07	0.0	0.5	1.0	2.0	-0.50	0.0		1.0	2.0

Table 7.2: Simulation parameters

dom disordered configuration. The system was then cooled down to a final temperature of  $\beta^{-1} = 0.60$  by steps  $\Delta\beta^{-1} = 0.10$ . The configuration at the end of each temperature step constituted that at the beginning of the next one. At each step, 40,000 MC steps were discarded for thermalisation, and observables were sampled and averaged over 200,000 MC steps. The cavity size distribution function was measured 200 times per temperature step, the external interactions, chain end-to-end distance and radius of gyration 50 times. The average number of cavities, average cavity size and average volume fraction of entrapped solvent could be directly calculated from the cavity distribution function. Whereas the volume fraction of entrapped solvent is the main property used to plot the phase diagram, the chain geometric properties and external interactions help gaining a better understanding of the mechanisms and driving forces involved in the reorganisation of the chains.

### 7.2.2 Simulation data

Unlike the study in the micellar region for which the determination of the cluster size distribution and principal moments of inertia are sufficient to describe the system, the study of the vesicle region requires detailed information about the cavity distribution. However, although the volume fraction of entrapped solvent,  $X_{sol}$ , is sufficient to give

a good account of the level of porosity of the spongy aggregates, it is also necessary to consider the size and number of those cavities to distinguish between the aggregates forming in the different regions of the phase space under investigation — *i. e.* ( $0.60 \leq \beta^{-1} \leq 2.10$ ) and ( $-2.0 \leq \gamma \leq -0.5$ ).

Much of the simulation data is placed in Appendix.

### Number of cavities

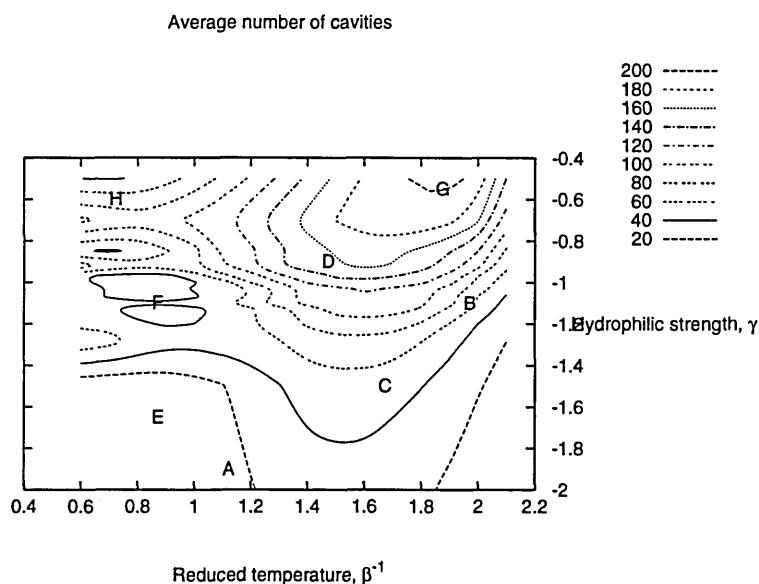


Figure 7.5: Average number of cavities ( $\epsilon = 0.0$ )

As illustrated in figure 7.6, the maximum number of cavities,  $\overline{n_{cav}}$ , occurs for relatively high temperatures ( $\beta^{-1} \simeq 1.90$ ) and for the weakest hydrophilic strength ( $\gamma = -0.50$ ). This average maximum number is greater than 200; it then decreases in a roughly linear manner — *i. e.* the isocontours are roughly concentric — as the temperature is varied and/or the heads are made more hydrophilic.

One can notice the discontinuity in the isosurface caused by the simulation at

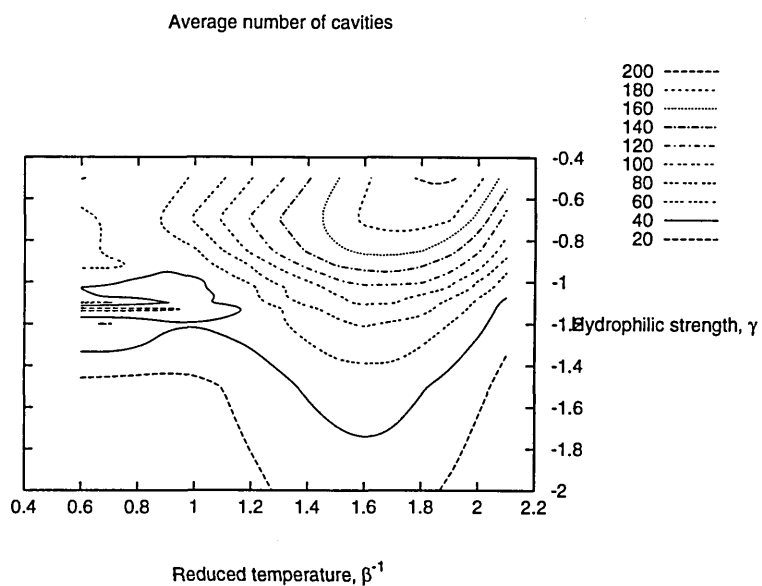


Figure 7.6: Average number of cavities ( $\varepsilon = 1.0$ )

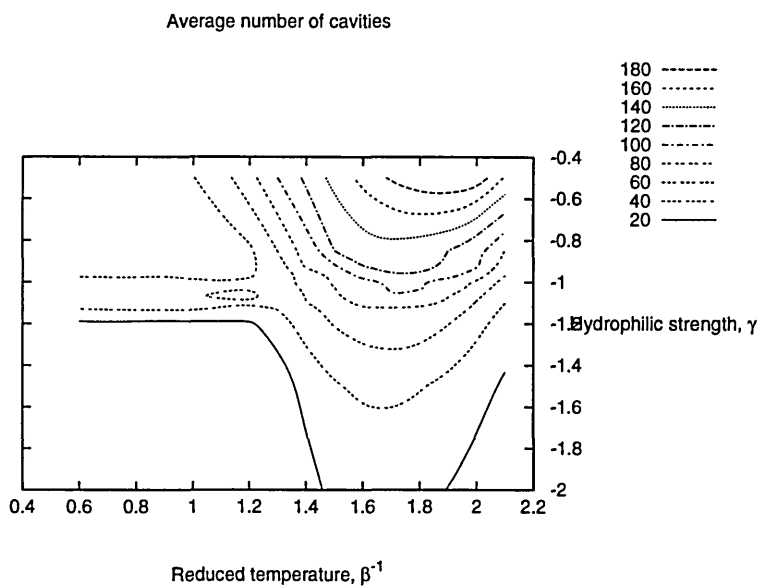


Figure 7.7: Average number of cavities ( $\varepsilon = 2.0$ )

$\gamma = -0.70$ . This was first thought to be a consequence of the relatively poor statistical quality of the data, but the fact that this discontinuity also occurs for a second, totally independent, set of simulations (for both  $\varepsilon = 0.0$  and  $\varepsilon = 1.0$ ) seems to dismiss this explanation and would rather suggest a genuine break in the behaviour of this observable. This latter follows a different regime for low temperatures ( $\beta^{-1} < 0.90$ ) and high hydrophilic strength ( $\gamma < -1.40$ ). The influence of the rigidity does not appear to be of great importance both qualitatively and quantitatively.

### Cavity size

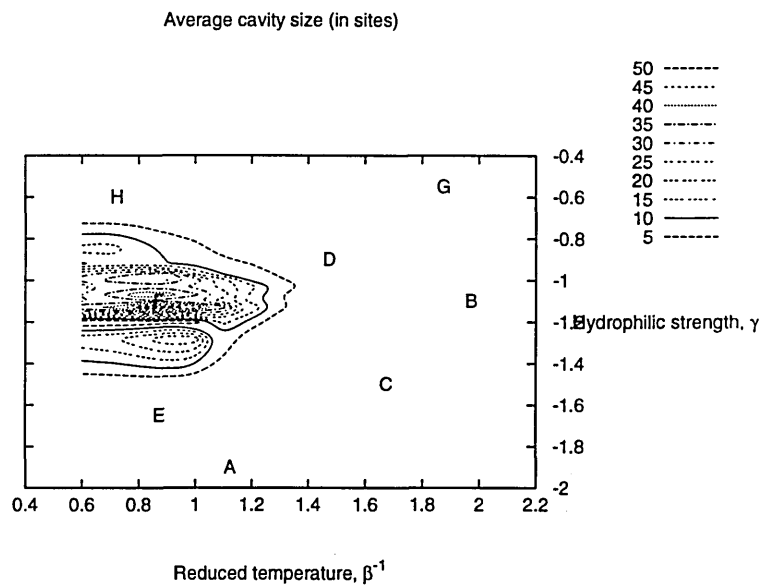


Figure 7.8: Average cavity size ( $\varepsilon = 0.0$ )

The average cavity size can be described as exhibiting noticeably different behaviour in two regions:

1. For medium to low temperatures ( $\beta^{-1} < 1.40$ ) and an hydrophilic strength in the range  $0.75 < \gamma < 1.40$ , the cavities are on average over 10 sites big; this figure can

CHAPTER 7. SIMULATIONS IN THE 'VESICLE' REGION

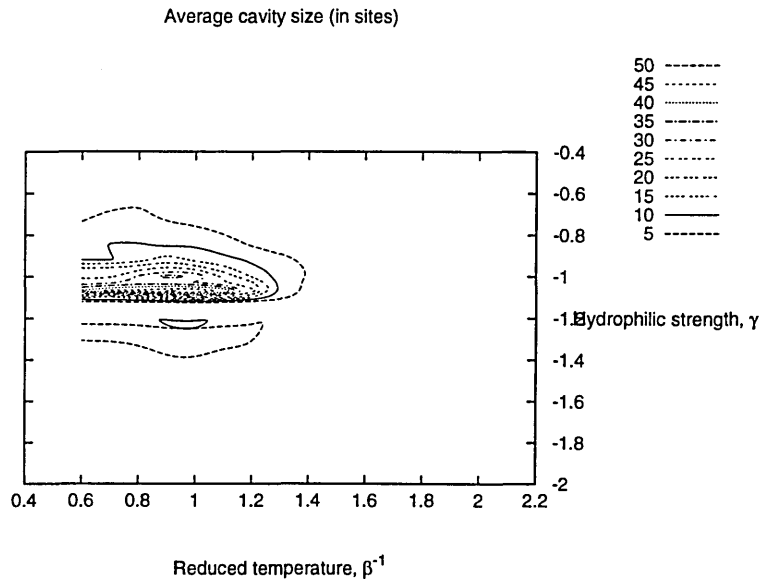


Figure 7.9: Average cavity size ( $\epsilon = 1.0$ )

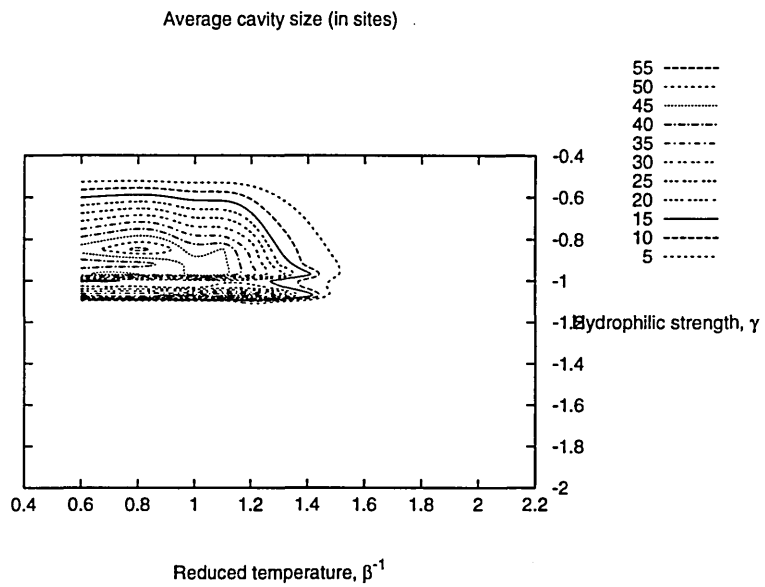


Figure 7.10: Average cavity size ( $\epsilon = 2.0$ )

go over 50 sites for the maximum ( $\gamma = -1.10$  and  $\beta^{-1} = 0.90$ ).

2. For the remaining regions, only small cavities, if any, will form.

One can notice the influence of the rigidity which sharpens considerably the change in cavity size as the heads get more hydrophilic (sharp transition at  $\gamma = -1.20$  when  $\varepsilon = 2.0$ ). The poor statistical quality of the data is mostly responsible for the magnitude of the discontinuities in the measurement of the observables. Indeed, one must point out that the mechanism of the algorithm used for the identification of the cavities is essentially similar to the *ant in the labyrinth* described in chapter 5. This algorithm proved to be unable to account for the presence of partly open pores and communicating cavities which were more common at the boundaries of the 'spongy regions'. This phenomenon can also be observed when measuring the volume fraction of entrapped solvent.

### Volume fraction of entrapped solvent

The total volume concentration of entrapped solvent,  $X_{sol}$ , remains low (*i. e.*  $X_{sol} < 0.25 \text{ vol. } \%$ ) in the regions characterised by highly hydrophilic heads ( $\gamma \leq -1.50$ ) and/or moderate to high temperatures ( $\beta^{-1} \geq 1.40$ ), with the noticeable exception of the region of very weak hydrophilic strength ( $\gamma \approx -0.50$ ) and high temperatures where the occurrence of aggregates featuring a very large number of tiny cavities results in an overall larger concentration in entrapped solvent.

The main region where this quantity becomes significantly larger is localised to medium hydrophilic strength (*i. e.*  $-1.13 \leq \gamma \leq -0.80$ ) and medium to low temperatures (*i. e.*  $\beta^{-1} < 1.30$ ). The discontinuities observed in the data (*e. g.* split peak) results from both poor statistics and the existence of different types of long-lived metastable aggregates (tubular and spherical vesicles).

CHAPTER 7. SIMULATIONS IN THE 'VESICLE' REGION

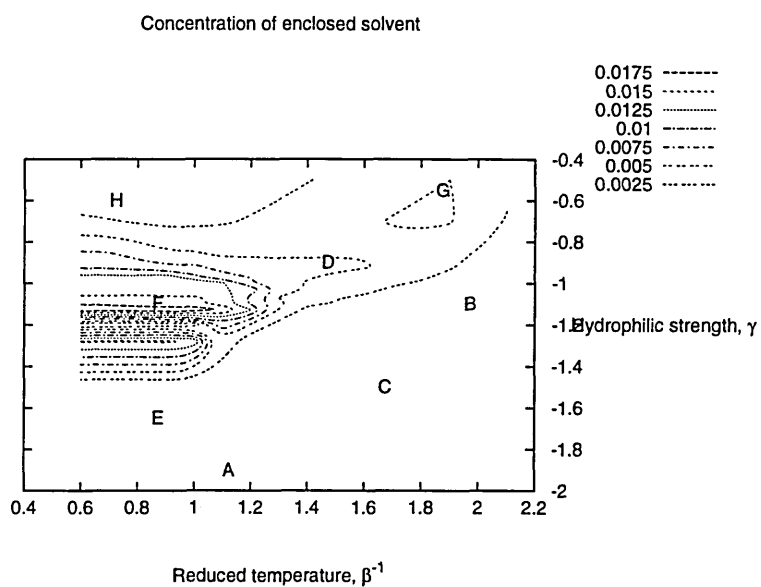


Figure 7.11: Average volume fraction of entrapped solvent ( $\epsilon = 0.0$ )

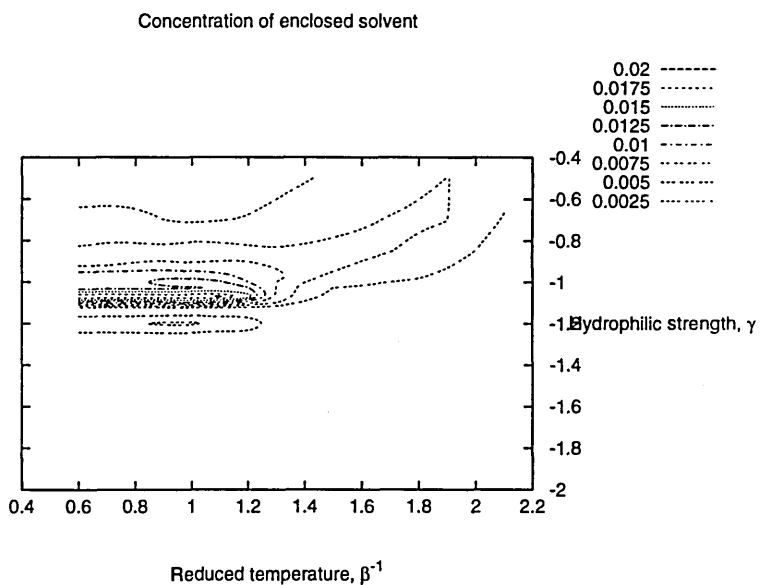


Figure 7.12: Average volume fraction of entrapped solvent ( $\epsilon = 1.0$ )

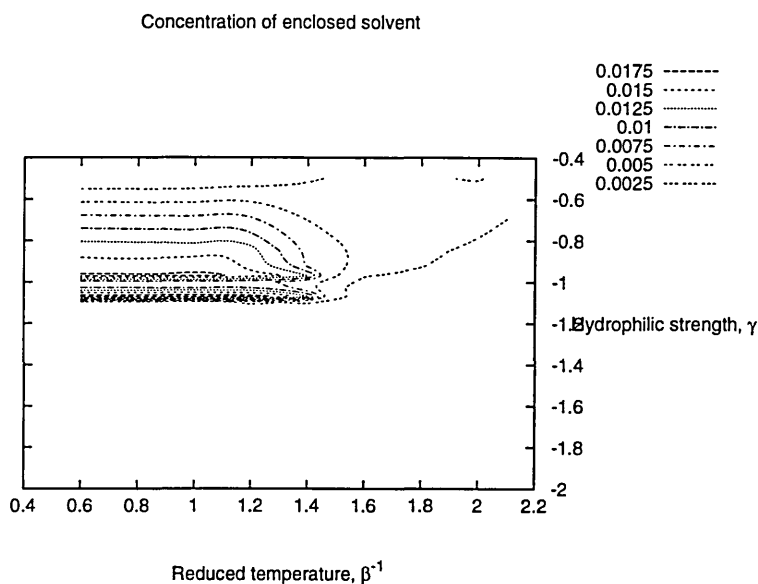


Figure 7.13: Average volume fraction of entrapped solvent ( $\varepsilon = 2.0$ )

### Other observables

Amongst the other observables measured, the one providing the most valuable information has been the normalised average number of external interactions,  $\overline{n_{HS}^*}$  and  $\overline{n_{TS}^*}$  represented respectively figure 7.14 and 7.15.

The variation of  $HS$  interactions follows a ‘non-linear’ behaviour. Surprisingly, the number of  $HS$  interactions first decreases with temperature when cooling down the system from the disordered configuration. This energetically unfavourable change is explained by the fact that the energy can be more effectively decreased by removing the hydrophobic segments out of solution rather than hydrating the unique hydrophilic segment. However, a minimum is rapidly reached at a medium temperature of  $\beta^{-1} \approx 1.50$  from which this variation will get inverted in an almost symmetric manner (see figure 7.14). Logically, the magnitude of this variation as well as the degree of hydration are larger if the heads are made more hydrophilic. The rigidity has also a strong influence on this observable: above

CHAPTER 7. SIMULATIONS IN THE 'VESICLE' REGION

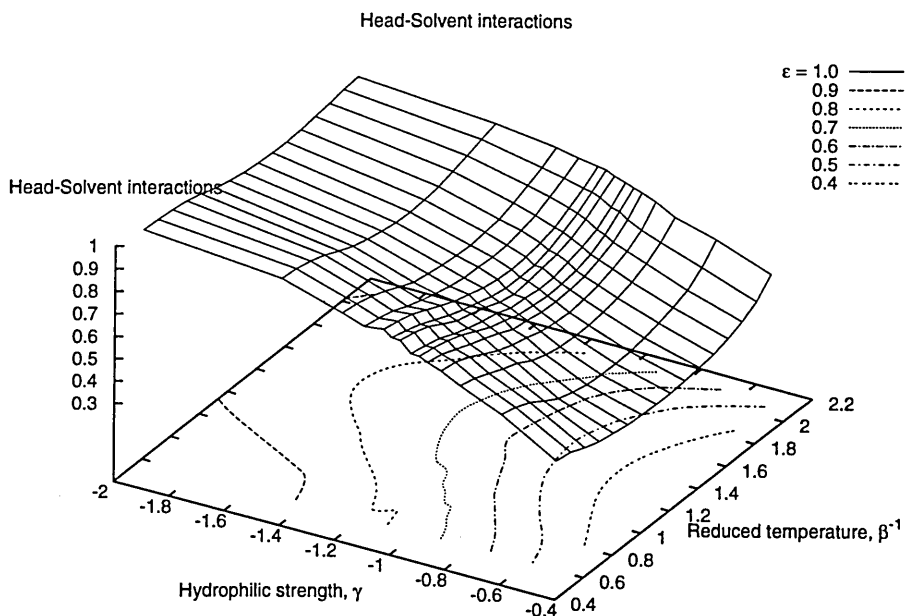


Figure 7.14: Normalised average number of *HS* interactions,  $\overline{n_{HS}}^*$  ( $\epsilon = 1.0$ )

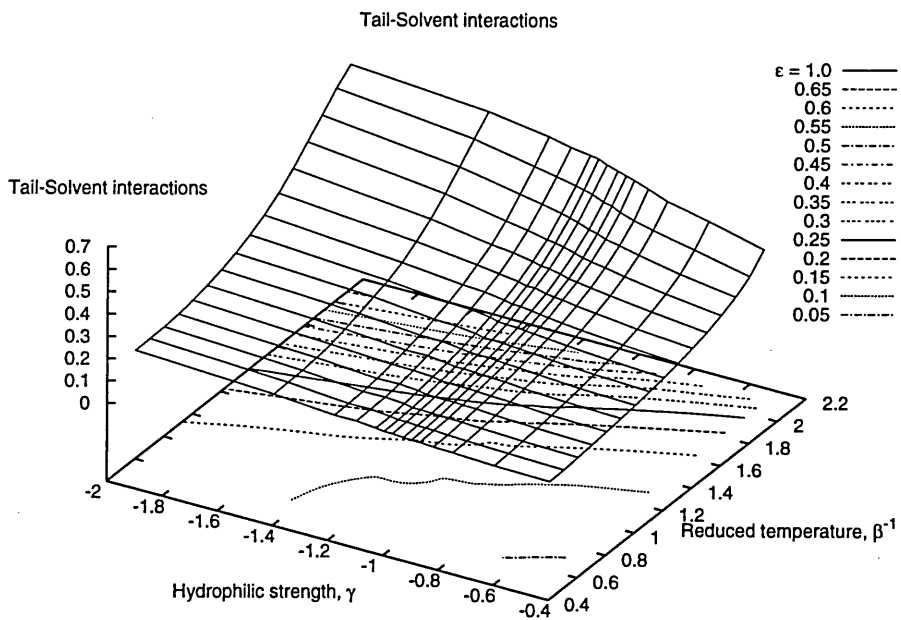


Figure 7.15: Normalised average number of *TS* interactions,  $\overline{n_{TS}}^*$  ( $\epsilon = 1.0$ )

a certain value of rigidity ( $\epsilon \geq 2.0$ ), the symmetry in the behaviour previously reported disappears: whereas the number of *HS* interactions remains roughly identical to what it was for fully flexible or weakly rigid chains down to temperatures at which the minimum degree of hydration occurs, its behaviour at lower temperatures significantly differs: the increase in hydration following the minimum is much steeper in a first time, and then quickly flattens out and settles at the value reached at  $\beta^{-1} \approx 1.00$ .

On the contrary, the variation in *TS* interactions has a weakly 'non-linear' and regular behaviour: the number of interactions drops with decreasing the temperature or increasing the hydrophilic strength. No discontinuities have been observed (see figure 7.15) and this  $(\beta^{-1}, \gamma)$ -dependency is only weakly influenced by the rigidity (surprisingly enough since the hydrophobic section constitutes by far the largest part of the chain).

The remaining observables include the cluster properties described in chapter 5. The principal moments of inertia, very important when describing systems of clusters with simple geometries like plain spheres (micelles) or planes (layers), failed to cope with the complicated structures of the aggregates forming during this study and did not provide any reliable information.

The cluster size distribution also proved to be inadequate for the characterisation of such systems where only very few aggregates co-exist. On the other hand, the mean aggregation number provided a good account of the amphiphiles degree of association. As the system is cooled down, the chains slowly aggregate, up to the point ( $\beta^{-1} \approx 1.40$ ) where the rate of aggregation sharply increases until a single aggregate is formed ( $\beta^{-1} = 1.00$ ). The only behaviour not following this pattern is that in a region later described as the 'micellar region'. The hydrophilic strength-dependency of this phenomenon is very weak (see figure 7.16) although generally slightly higher for less hydrophilic chains.

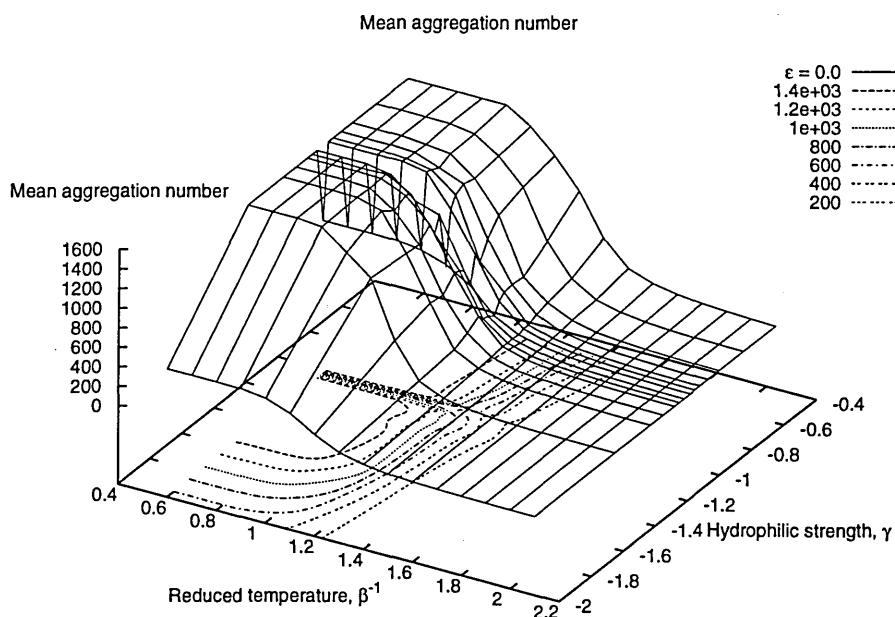


Figure 7.16: Mean aggregation number,  $N_n$  ( $\epsilon = 1.0$ )

### Phase diagram

Several type of aggregates can be identified from the data previously presented thus allowing the characterisation of different regions separated by transitional areas. Thus, one can distinguish (see figure 7.5, 7.8 and 7.11):

1. **Micellar region (A):** for strong hydrophilic strength ( $\gamma = -2.00$ ), spherical micelles with few small cavities form from the initial disordered system; they gradually grow into larger cylindrical cavity-free micelles as the temperature decreases.
2. **Disordered isotropic region (B):** for high temperatures ( $\beta^{-1} > 1.80$ ) and medium hydrophilic strength ( $-1.50 < \gamma < -0.85$ ), the system remains fairly disordered with a low degree of aggregation. Chains principally exist as free monomers.
3. **Spongy disordered region (C):** for high to medium temperatures ( $1.40 \leq \beta^{-1} \leq 1.80$ ) and for medium hydrophilic strength ( $-2.00 < \gamma < -1.20$ ), monomers start

## CHAPTER 7. SIMULATIONS IN THE 'VESICLE' REGION

aggregating and form a bicontinuous but still relatively disordered phase. This region is characterised by the presence of a large number of small cavities and pores.

4. **Spongy ordered region (D):** for weakly hydrophilic heads ( $-0.70 \leq \gamma < -0.85$ ) and medium temperatures ( $1.40 \leq \beta^{-1} \leq 1.80$ ) the system exhibits a region similar to the region (C) previously described but with a higher degree of order. One can report the presence of communicating cavities and cavities open on the bulk solvent.
5. **Discoid region (E):** occurs for medium to low temperatures ( $\beta^{-1} < 1.30$ ) and strong to moderately hydrophilic heads ( $-2.0 < \gamma < -1.20$ ). The aggregates forming in that region are discoid structures with very few but large cavities. The size of the cavities increases with decreasing  $\gamma$ , *i. e.* the aggregate evolves from a bilayer plate or flat rod to a discoid vesicle type of structures.
6. **Vesicle region (F):** is characterised by a large volume fraction of entrapped solvent. The system is in equilibrium between tubular vesicles going across the simulation box and large spherical vesicles containing two or three large cavities. Depending on the temperature, the cavities can be closed, connected, or unique. By creating two separate regions of solvent (the 'inside' and 'outside'), these structures are thought to resemble the structures formed by an asymmetric sponge phase (see chapter 2). This region is located for medium to low temperatures ( $1.30 < \beta^{-1}$ ) and moderately hydrophilic heads ( $-1.13 \leq \gamma \leq -0.80$ ).
7. **Highly-spongy region (G):** this small region is characterised by a highly porous structure *i. e.* a very large number of tiny cavities. It only occurs for high to medium temperatures ( $1.80 < \beta^{-1} < 2.0$ ) and for the weakest hydrophilic strength ( $\gamma = -0.50$ ).

8. **Large cluster region (H):** occurs when the system previously described is cooled down to lower temperatures (*i. e.*  $\beta^{-1} < 1.00$  and  $\gamma = -0.50$ ). All the amphiphiles aggregate in a large single cluster with the head segments only partially solvated.

### 7.2.3 Analysis and discussion

The system clearly undergoes a series of changes when  $(\beta^{-1}, \gamma, \varepsilon)$  is varied. Although ‘quantitative’ characterisation of the phenomena taking place is difficult because it would require significantly more detailed simulations and hence very large CPU time, one can identify qualitative evolutions and attempt to formulate an hypothesis about the likely mechanisms and driving forces by considering the set of observables studied as a whole.

#### Influence of the chain rigidity

The influence of the rigidity appears to remain negligible for values of  $\varepsilon \leq 1.0$  but has a more dramatic effect for higher values. By favouring straight conformations, and therefore increasing the cost of bending, one restricts the freedom of chains to adopt conformations allowing a more efficient packing. Although the motivation behind a non-zero rigidity parameter was to limit the occurrence of unrealistic folded conformations, the side effects are actually an increasing influence of the underlying lattice, *i. e.* the growth of aggregates occurs preferentially parallel to the axis and the cost of bending prevents the formation of spherical structures. The most noticeable phenomena caused by those side effects include:

- The preferential formation of perfectly interdigitated bilayers with fully elongated chains: when bilayer-type structures form, the thickness of the bilayer increases and becomes equal to the length of the fully elongated chain plus one site (*i. e.* fully

elongated overlapping tails plus fully hydrated heads).

- When a vesicle form, the excessive cost of bending result in the formation of a cubic-like aggregate in place of a spherical one.
- For reasons essentially linked to the cost of bending, not only the shape of the cavities is similarly cubic-like rather than spherical, but also fewer larger cavities will be favoured.
- The excessive cost of bending results in the formation of perfectly flat bilayers, and little or no fluctuation in the radius of the tubular vesicles.

The side effects caused by an increase in the chain rigidity appear to have a more negative effect on system than that caused by the unrealistic folded conformations they aim to prevent. However, although the results are dominated by lattice effects, they are qualitatively in agreement with the author’s expectations.

### **Tubular vesicle and ‘onion’ phase**

Two of the structures forming in the ‘vesicle’ region particularly attracted the author’s attention and would deserve further attention:

1. The tubular vesicles: the occurrence of a tubular vesicle is in contradiction with the conclusions of Israelachvili’s theory of self-assembly of hydrocarbon amphiphiles [61]. Indeed, using solely thermodynamic arguments — *i. e.* excluding packing constraints —, Israelachvili demonstrated by minimising the vesicle free energy per unit length that the formation of such structures was disfavoured both entropically and energetically, thus resulting in the preferential formation of bilayers or spherical vesicles.
2. The large spherical vesicle: this type of structures has been reported for low rigidities only (*i. e.*  $\epsilon \leq 1.0$ ). This structure is relatively close to forming the first two bilayers

of an onion shaped structure and could be interpreted as being the precursor of a multilamellar vesicle (see chapter 2).

However, it is not clear whether those aggregates are genuine equilibrium or — more possibly — metastable structures. No conclusion can be drawn until similar simulations are run for much larger systems.

### Structures reorganisation

It is possible by simple observation of the system to trace the reorganisation of the chains leading to the formation of the spherical vesicles.

As the system is cooled down, the amphiphiles first try to minimise the number of Tail-Solvent interactions by aggregating together. Thus, the amphiphiles quickly reach a certain degree of association, aggregating into a very porous but still highly disordered aggregate. By further decreasing the temperature, the hydrophilic heads reorient themselves to achieve a higher degree of hydration. This leads to the formation of small cavities from some of the pores. The aggregate will also see its density increased as the tail segments minimise their interaction with the solvent by achieving a more efficient packing. Some larger cavities will gradually appear following the fusion of smaller ones. This hypothesis is confirmed by the relatively large occurrence of communicating vesicles in that region of phase space. Finally, some of the cavities still open on the 'external' bulk solvent will later close, thus inducing a sharp increase in the volume fraction of entrapped solvent.

### Driving forces

Recalling that the Helmotz free energy of a system,  $F$ , is given by:

$$F = E - TS \tag{7.1}$$

## CHAPTER 7. SIMULATIONS IN THE ‘VESICLE’ REGION

where  $E$  is the internal energy,  $T$  the temperature and  $S$  the entropy of the system, it is apparent that a phase transition can be driven by either a decrease in internal energy or increase in entropy (or most of the time a combination of both). As was previously emphasised, the variation in external interactions do not exhibit any sharp change and therefore dismisses the occurrence of purely energy-driven transitions. This leads us to conclude that most of the transitions observed during this study are entropy-driven — or at least have a large entropic contribution. A discussion of such entropy-driven transitions has been presented in greater detail by Frenkel [130] whilst the particular case of entropic forces between amphiphilic surfaces in liquids is described with great length by Israelachvili and Wennerström [131].

It is possible to gain a better understanding of the mechanisms and driving forces brought into play by widening the context to include results from related experimental and phenomenological studies. Thus, most of the structures reported in this study have been characterised experimentally. For instance, Uchegbu [132] successfully identified multi-lamellar vesicles, micelles, open vesicles, long flexible cylindrical micelles and large metastable disk-shaped structures retaining encapsulated solvent named *discomes*. The following succession of transitions:

vesicles  $\rightarrow$  open vesicles  $\rightarrow$  bilayer sheets  $\rightarrow$  cylindrical micelles  $\rightarrow$  spherical micelles

was induced by addition of a suitable co-surfactant.

The study of the phases formed by bilayer-forming surfactants — and in particular the sponge phase,  $L_3$  — has also been widely undertaken using a phenomenological approach and models mostly based on the Ginzburg-Landau theory (*e. g.* [133–135]).

The most popular hypothesis proposed by those groups to explain the formation of the sponge phase is based on the dilution of a lamellar phase,  $L_\alpha$ : if such a phase is diluted beyond the point where the bilayer separation exceeds the persistence length,

the bilayers would melt into a sponge-like structure which would itself break-up in small vesicles if further dilution is carried out. The occurrence of those phases depends upon the competition between the curvature energy of the bilayers (favouring flat films) and entropic contributions [36]. The sponge phase itself is stabilised by entropic undulation interactions [134]. Structures requiring defects such as edges or seams (*e.g.* disks) are believed to be unstable due to the excessive cost of the defects on the aggregate free energy.

Another related problem is the stability of a phase of diluted non-interacting large vesicles known as  $L_4$  and of the onion phase. Indeed, the formation of such vesicles is possible provided the energy of curvature is made sufficiently small to be compensated by the translational entropy [135]. Simons derived the limit of stability by plotting the free energy of the vesicle and onion phase as a function of the mass fraction in amphiphile for a fixed value of bending energy. The following succession of transitions takes place as the total concentration in amphiphile is increased:

vesicle  $\longrightarrow$  onion  $\longrightarrow$  lamellar phase  $\longrightarrow$  sponge phase.

The mean number of layers in the onion phase has also been calculated as a function of the mass fraction in amphiphile. 'Small onions' of 2 to 5 layers have been demonstrated to be thermodynamically feasible.

Finally, one may also report a Molecular Dynamics study of self-assembling chains in vesicles by Drouffe *et al.* [136] who paid a particular attention to the fluctuation in shape of vesicles.

### 7.3 Concluding remarks

The main difficulties arising during this study are associated to the limitation in computational power. Indeed, three of the simulation parameters ( $\beta$ ,  $\gamma$  and  $\varepsilon$ ) were varied and the availability of only 16Mb of memory per processor limited the system size ( $N < 4096$  chains).

Although the conclusions which can be drawn from this study remain highly speculative, it is reassuring to gather so much evidence of behaviour qualitatively similar to that of real systems of bilayer-forming surfactants. Thus, structures resembling that of a non-symmetric sponge phase, vesicles (open and closed), spherical and long cylindrical micelles, disks and tubular vesicles have, amongst others, been successfully identified. However, serious drawbacks have also to be urgently addressed before a more detailed study can be undertaken. The main points are:

1. Study larger systems ( $N > 4096$ ) in order to decrease finite size effects and get more reliable statistics.
2. Use a non-cubic lattice: the implementation of a chain rigidity proved to enhance the influence of the underlying cubic lattice (see comments in chapter 6). The rigidity is known to play an important role and must be implemented in further work. This could also be achieved by studying slightly smaller chain ( $s = 5$ ) which would have the merit of allowing a larger number of chains to be included for a lattice of fixed size.
3. Study the extent of any hysteresis, and get confirmation of the results by carrying out simulation at fixed temperature but varying the hydrophilic strength.
4. Studies of dilutions at fixed ( $\beta^{-1}$ ,  $\gamma$ ) should also be investigated since it could be more easily related to experimental and phenomenological studies.

5. Use a more efficient sampling scheme.

Clearly, the conditions for the thermodynamical feasibility of some of the structures observed is still open to discussion and it would be very interesting to concentrate in a smaller region of the phase space where particular transitions are known to take place. The model could thus be tuned and the influence of the different model parameters on the stability of the different phases and transitions could be analysed. Further work should be attempted to make such simulations closer to the work undertaken by the phenomenological groups.

## Chapter 8

# Simulations in the micellar region

In previous simulations, Brindle and Care [15] obtained preliminary results consistent with the onset of a micellar phase. The aim of the present chapter is to study in much greater detail these observations and attempt to test them against accepted thermodynamical models. As has been emphasised in chapter 3, the multiple phase equilibrium model is the most realistic thermodynamical model of the micellisation process, and will therefore constitute the model against which data from the simulations will be tested.

### 8.1 Simulation

The simulations were carried out in the canonical ensemble using the simplest implementation — *i. e.* with simple reptation and fully flexible chains — of the model previously described chapter 5. Depending on various conditions such as the total concentration in surfactant or the temperature, the micellisation process is known to produce a whole range of micelles with size  $n$  which can exceed two hundred chains. It appeared necessary to work with a relatively large number of chains in order to capture the behaviour of essential equilibrium properties such as the cluster size distribution or the chemical potential. Indeed, reasonable statistics on clusters of a given size  $i$  can only be obtained

if the system size is noticeably larger. As happens with all computer simulations, the size of the system is also constrained by the processing power available as well as by memory limitations (16Mb on the Paramid Intel i860).

The following strategy was necessary to keep this project tractable, and simulations were carried out in two distinct stages:

### 8.1.1 Preliminary runs

The aims of this first stage were threefold:

- Optimising the simulations by running on small systems of  $N = 512$  chains.
- Identifying the parameter sets ( $\beta^{-1}$ ,  $\gamma$ ,  $X_a$ ) which would exhibit a behaviour consistent with micellisation.
- Generating and saving conformations which could be used as starting configurations for the second stage.

The first stage consisted of a set of 17 Metropolis Monte Carlo simulations carried out in the  $NVT$  ensemble for systems of 512 chains and concentrations  $X_a$  ranging from 0.249 *vol. %* up to 25.6 *vol. %*. The starting configurations were randomly disordered at a high temperature of  $\beta^{-1} = 1.50$ . The system was then cooled down to  $\beta^{-1} = 0.90$  by steps of  $\Delta\beta^{-1} = 0.02$ . At each temperature step, 50,000 Monte Carlo steps were discarded for thermalisation and sampling was carried out for 200,000 Monte Carlo steps. A Monte Carlo step, MC step, is chosen to be an average of one attempted move per chain. One of the main problems with such simulations happens to be the high correlation between successive states generated. A rigorous way of ensuring the adequation of the sampling frequency is to study a property known as the statistical inefficiency [1, 125] as described chapter 5.

The aim of this stage was mainly to generate configurations at the end of each temperature which could be used as a starting configuration for larger simulations. Thermodynamic averages such as the total potential energy of the system, or physical properties such as the mean aggregation number,  $N_n$ , were monitored but never used in thermodynamic treatment because of problems arising from the finite size effect (statistically low-quality data for large clusters).

### 8.1.2 Production runs

The second stage consists of large scale isothermal Metropolis Monte Carlo simulations. The systems were made as large as possible, ranging from 1024 chains for lower concentrations up to 4096 chains for the higher concentrations. This was achieved by replicating the configurations of 512 chains previously saved. One must emphasise that provided the system is being thermalised for long enough at startup, the periodicity and finite size effect induced by these peculiar starting configurations can be made negligible; thus 20,000 Monte Carlo steps were rejected for thermalisation and configurations were sampled every 1,000 steps over a total run of 1,000,000 steps. The properties directly measured were the cluster size distribution function, the number average cluster size and the total number of external interactions (HS and TS interactions).

The methodology was first set-up for a temperature  $\beta^{-1} = 1.18$  and a hydrophilic strength  $\gamma = -2.0$  which appeared to provide the best compromise between sampling efficiency of the phase space and micellar-like behaviour. Other parameter sets were later studied in order to assess the temperature and hydrophilic strength-dependencies (see section 8.5). Thus, temperatures  $\beta^{-1} = \{0.98, 1.08, 1.18, 1.22, 1.28, 1.32, 1.38\}$  were studied at a fixed value of  $\gamma = -2.0$  whereas values of  $\gamma = \{-1.0, -2.0, -3.0, -4.0\}$  were examined at a fixed temperature of  $\beta^{-1} = 1.18$ .

CHAPTER 8. SIMULATIONS IN THE MICELLAR REGION

The particular parameters of the simulations are presented table 8.1

Concentration (vol. %)	Number of chains	Lattice size
0.249	1024	188× 94× 93
0.499		148× 74× 75
0.757		130× 65× 64
0.997		118× 59× 59
1.49	2048	104× 104× 51
1.97		94× 94× 47
2.25		90× 90× 45
2.52		86× 86× 44
2.76	4096	84× 84× 84
2.97		82× 82× 82
3.54		78× 78× 76
4.04		74× 74× 74
5.06		68× 68× 70
10.0		54× 54× 56
14.8		48× 48× 48
20.1		44× 44× 42
25.6		40× 40× 40

Table 8.1: Simulation parameters

Both finite size effects and correlations were monitored for this set of parameters.

The statistical inefficiency  $s_X$  was measured for the total number of external interactions  $n_{TS}$  and  $n_{HS}$ ; typical results for pre-micellar, micellar near the cmc and higher concentrations are illustrated in figure 8.1.

As has to be expected from the higher number of tail segments,  $n_{TS}$  suffers the most from correlation at a fixed concentration. Whereas  $s_{n_{HS}}$  remains at acceptable levels over all the range of concentrations investigated with correlations up to  $\approx 5000$  Monte Carlo steps,  $s_{n_{TS}}$  fails to remain below 10000 MC steps for concentrations exceeding 5 vol.%. Indeed, as illustrated in figure 8.1, the statistical inefficiency plateau was not attained after 40000 MC steps for  $X_a = 20.1$  vol.% thus making the data sets for such high concentrations unsuitable for analysis.

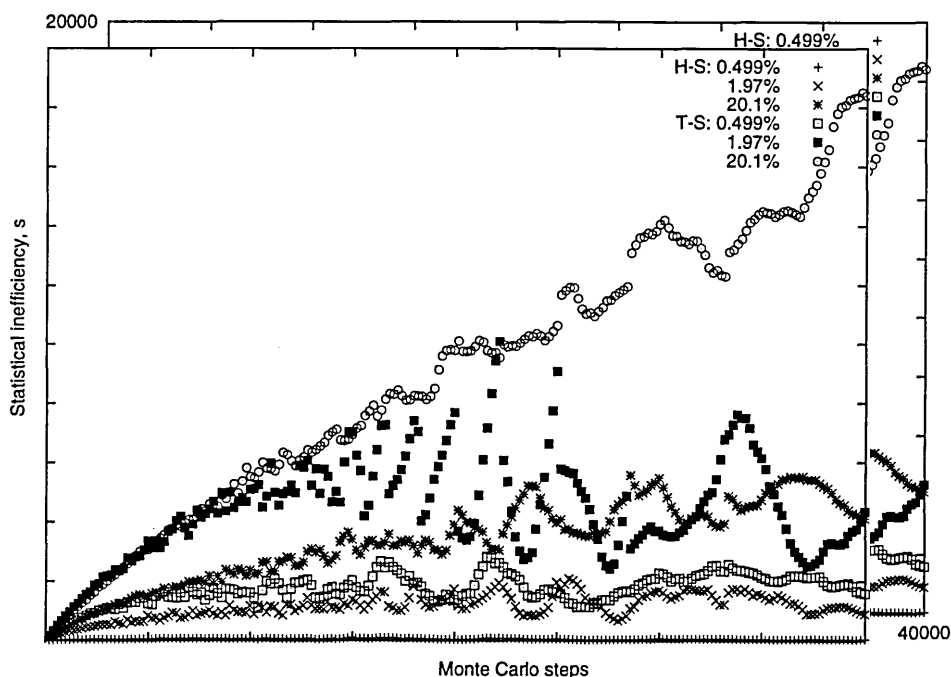


Figure 8.1: Statistical inefficiency of the external interactions,  $s_{n_{HS}}$  and  $s_{n_{TS}}$  ( $\beta^{-1} = 1.18$ ,  $\gamma = -2.0$ )

## 8.2 Results and analysis

### 8.2.1 Description of the results

For this particular choice of parameters ( $\beta^{-1} = 1.18$  and  $\gamma = -2.0$ ), the results appear to be in reasonably good agreement with both experimental observations and theories described chapters 2 and 3:

1. As the total concentration in surfactant  $X_a$  is increased, the monomer concentration  $X_1$  rises almost linearly along a line of slope unity and undergoes a sharp variation when it reaches the cmc for  $(0.79 \pm 0.06) \text{ vol. } \%$  (or  $(0.59 \pm 0.01) \text{ vol. } \%$  depending on the method used for its determination) where it settles down to a constant value (see figure 8.2).

Depending on the model used [55], the cmc can indeed be defined as:

- The maximum concentration of monomers.

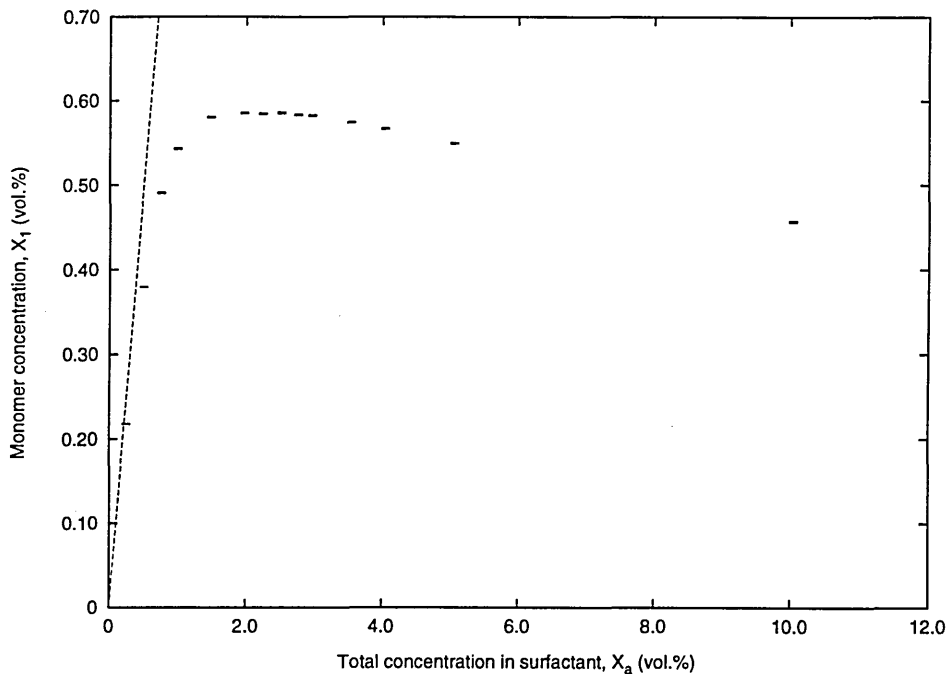


Figure 8.2: Monomer concentration,  $X_1$ , as a function of the total concentration in surfactant ( $\beta^{-1} = 1.18$ ,  $\gamma = -2.0$ ). Note the sharp variation around the cmc

- The sharp change in a physical property.
  - The maximum curvature in the variation of the degree of dissociation  $\alpha$  of a micelle with concentration.
  - The inflection point of  $\alpha$ .
2. Similarly, the cluster size distributions appeared to be consistent with accepted theories (see chapter 3). For concentrations lower than the cmc, almost all the surfactants existed as free monomers and one seldom observed clusters larger than  $n = 4$  (and never larger than 20). The distribution is monotonically decreasing with a very sharp slope. As the total concentration is increased towards the cmc, the tail of the distribution lengthens and a minimum and maximum appear in the distribution. The magnitude of these extrema will increase with  $X_a$  until the system undergoes a phase transition towards a lamellar phase.

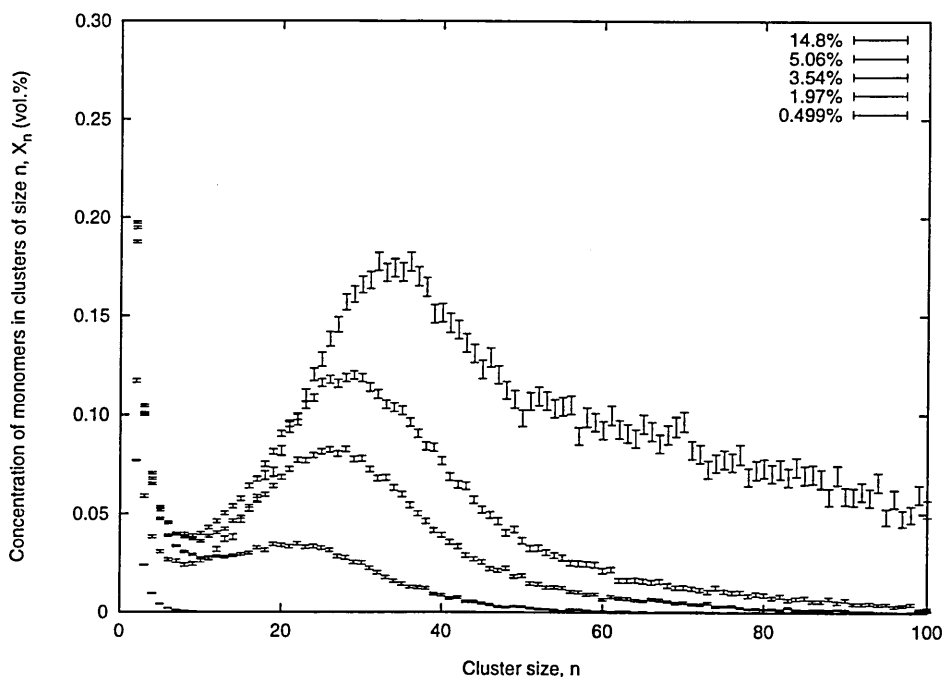


Figure 8.3: Concentration of monomers in clusters of size  $n$ ,  $X_n$ : pre-micellar and micellar distributions ( $\beta^{-1} = 1.18$ ,  $\gamma = -2.0$ )

3. In a closely related work, Mukerjee [137] adapted general procedures for dealing with multiple equilibria in step-wise self-association when all species are in rapid association-dissociation equilibrium to micellar systems. The mean aggregation number,  $N_n$ , was determined from the concentration dependence of the weight average number,  $N_w$ , and made it possible to calculate the size distribution index  $N_w/N_n$ . This latter property gives an indication of the aggregate size polydispersity. Close to unity for small spherical micelles, it increases up to  $N_w/N_n \approx 2$  when larger asymmetric — most likely rod-like — micelles appear.

For nonionic micelles, the formation and growth of micelles is driven by the free energy change due to the self-interaction of the hydrophilic groups at the surface of the aggregates. Thus:

$$-RT \ln K_q = \Delta G_{HC} + \Delta G_{HG} \quad (8.1)$$

where  $\Delta G_{HC}$  and  $\Delta G_{HG}$  are respectively the hydrophobic and the head group self-interaction contributions to the free change due to the introduction of a monomer into a micelle of  $(q - 1)$  monomers and  $K_q$  is the step-wise association constant.

It follows that:

$$N_w = K \sqrt{\frac{C - [b_1]}{[b_1]}} \quad (8.2)$$

where  $[b_1]$  is the concentration of free monomers,  $C$  is the equivalent concentration, and  $K$  a constant including the ratio of the two equilibrium constants from this model of step-wise association.

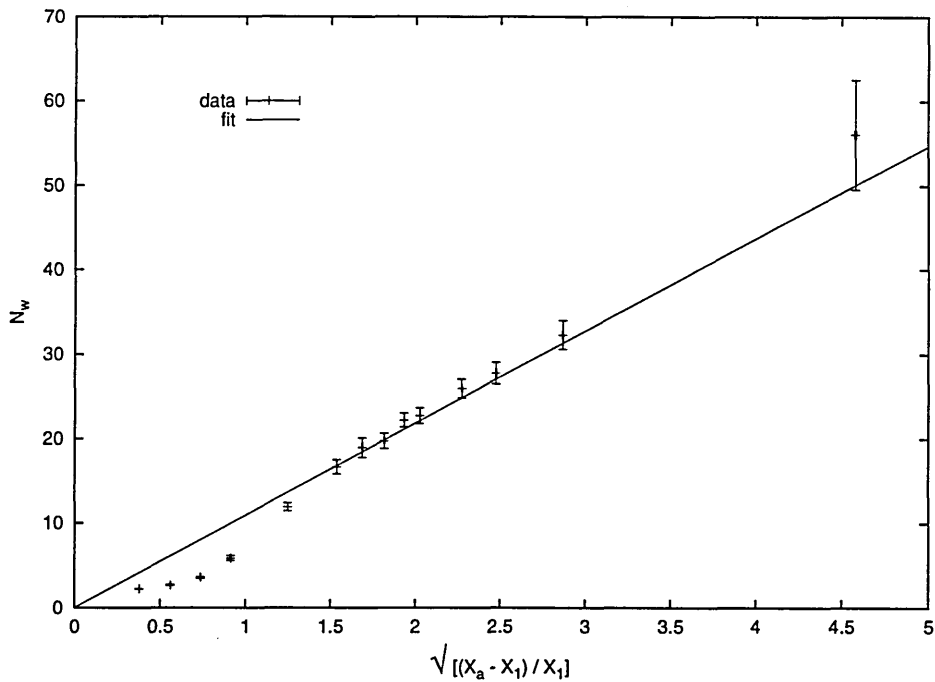


Figure 8.4: Linear-dependence of the average weight aggregation number,  $N_w$  ( $\gamma = -2.0$  and  $\beta^{-1} = 1.18$ )

The relationship expressed in equation 8.2 has been applied to the simulation data and proved to be in very good agreement with it, only failing at pre-micellar concentrations where this expression of the concentration dependence of  $N_w$  is not ap-

plicable.

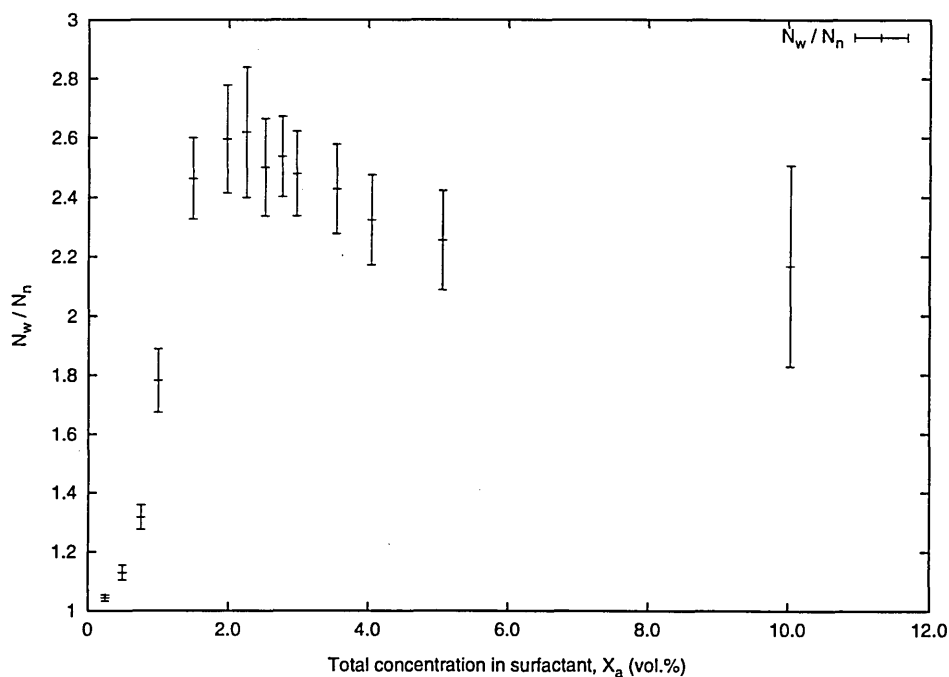


Figure 8.5: Size distribution index,  $N_w/N_n$  ( $\gamma = -2.0$  and  $\beta^{-1} = 1.18$ )

The size distribution index  $N_w/N_n$  appears to grow rapidly (see figure 8.5) from an initial value of 1 — typical of the formation of small monodisperse aggregates — at low concentrations to values above 2 more consistent with the growth of polydisperse elongated aggregates.

- Graphical visualisations of the configurations also confirmed the growth of ‘pseudo-spherical’ clusters into cylindrical micelles as the total concentration in surfactant is increased (see figures 8.6 and 8.7).

### 8.2.2 Discrepancies with experiment

Although in general agreement with most common theories, a few discrepancies must be pointed out. The most noticeable is probably the slightly negative slope of the  $X_1$  vs  $X_a$  curve usually acknowledged as being null for non-ionic surfactants [138]; the slope is

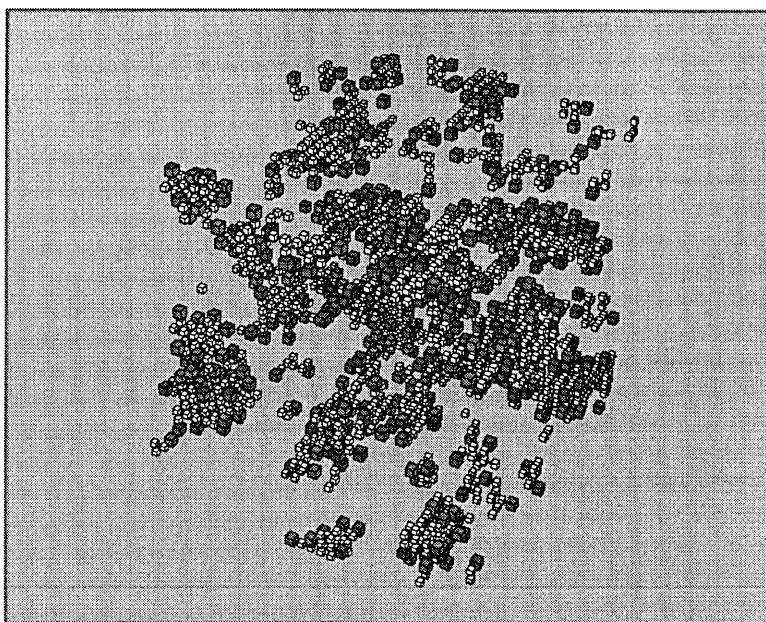


Figure 8.6: 'Spherical' micelles ( $\beta^{-1} = 1.26$ ,  $\gamma = -2.0$ ,  $X_a = 6.25 \text{ vol. } \%$  )

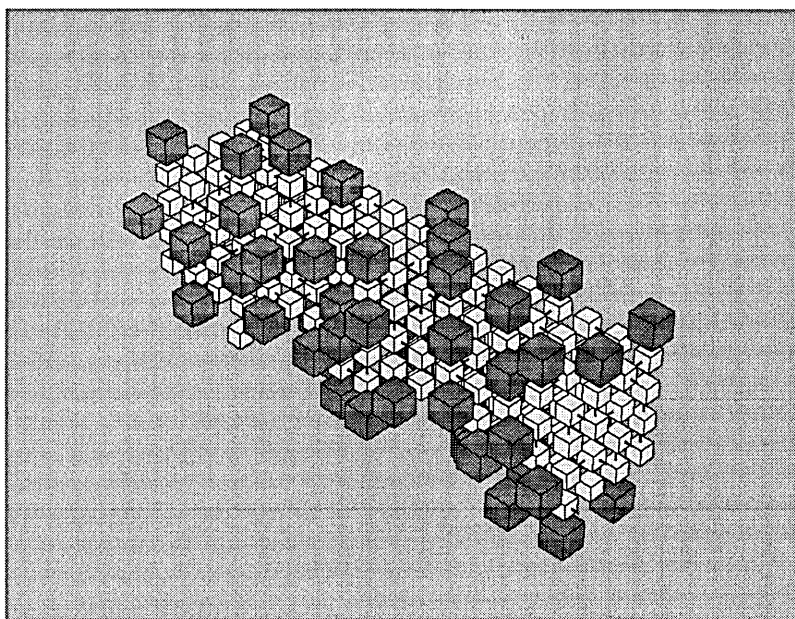


Figure 8.7: 'Cylindrical' micelle ( $\beta^{-1} = 0.90$ ,  $\gamma = -2.0$ ,  $X_a = 25.0 \text{ vol. } \%$  )

known to be slightly negative for most ionic surfactants because of increasing electrostatic interactions as  $X_a$  is increased [139, 140]. The cmc is also believed to be even sharper than observed here.

Other discrepancies include a wider polydispersity in the cluster size distribution than usually assumed (*e. g.*  $N_w/N_n \approx \sqrt{2}$  for a system of large polydisperse cylindrical micelles [24]), a less pronounced minimum and a preferred cluster size  $n_{max}$ , lower than usually observed for non-ionic surfactants (see chapter 2 and 3). The size distribution index,  $N_w/N_n$ , is expected to undergo a sharp change from  $\approx 1$  to  $\approx 2$  near the cmc as the polydispersity at this point is important (micelles start forming but a lot of amphiphiles still remain as free monomers) and then to decrease relatively quickly towards intermediate values (*i. e.*  $\approx < 1.2$ ) as the micellar size distribution becomes less polydisperse. Although the simulation exhibits similar trends (see figure 8.5), one can notice the lack of sharpness in the decrease in the micellar region and its failure to reach such a low value. The ‘ideal’ behaviour resembles that shown figure 4.13. Both lattice effects (enhanced by the cluster counting algorithm) and the excessive width over length ratio of the chains (1 : 4) appear to be responsible for this latter. The steps believed to be necessary in order to lessen those discrepancies are discussed in greater detail in the conclusion.

### 8.3 Thermodynamical treatment

We have seen in chapter 3 that it was possible to reformulate equ. 3.4 under a more convenient form:

$$X_n = n \frac{(f_1 X_1)^n}{f_n} \exp \left[ -n\beta(\mu_n^0 - \mu_1^0) \right] \quad (8.3)$$

where  $X_n$  is the concentration of monomers in clusters of size  $n$ ,  $f_1$  and  $f_n$  the activity coefficients for respectively a free monomer and a monomer belonging to a cluster of size  $n$ , and  $(\mu_n^0 - \mu_1^0)$  the infinite dilution excess chemical potential for chains in clusters of size  $n$ . The reference state is generally either taken as being that at infinite dilution or for a

CHAPTER 8. SIMULATIONS IN THE MICELLAR REGION

cluster of infinite size. For reasons of convenience, the former case has been chosen. It must be pointed out that the activity coefficients are usually neglected (assumption known as the *dilute solution approximation*) and therefore concentrations are approximated as being equivalent to activities. However, as will be demonstrated further in this chapter, such an approximation appears unsuitable for concentrations above 5 *vol. %* where inter aggregate interactions become non-negligible [141].

The activity coefficients are expected to be functions of  $X_a$  with the property that:

$$\lim_{X_a \rightarrow 0} f_1(X_a) = \lim_{X_a \rightarrow 0} f_n(X_a) = 1$$

For simplicity we only keep the first non-zero term in the Taylor expansion and therefore assume that:

$$\ln(f_n) = aX_a \quad \forall n$$

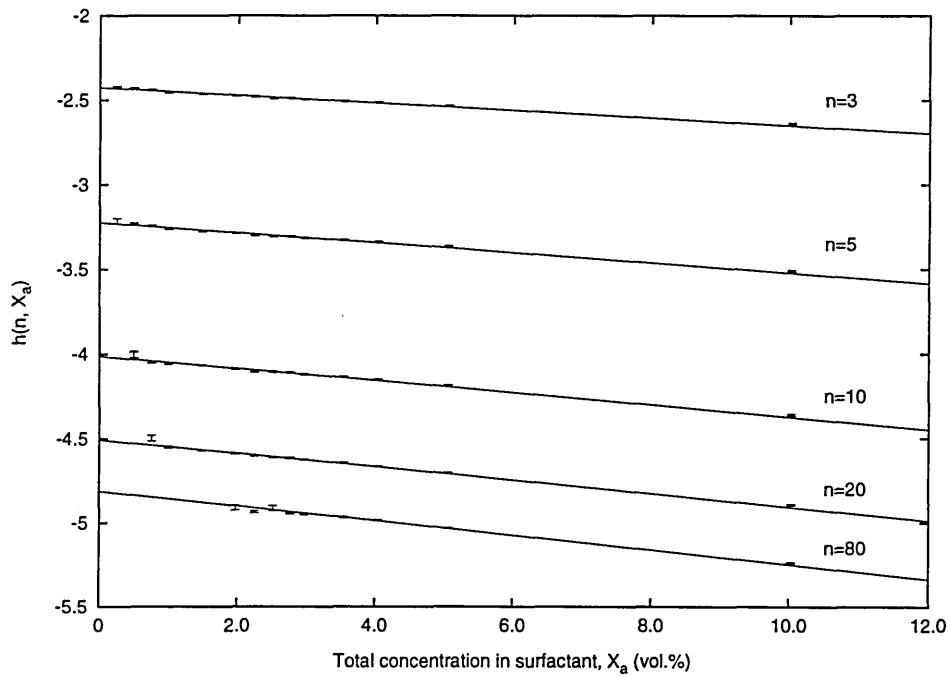
where  $a$  is independent of  $X_a$  and  $n$  and hence equ. 8.3 may be rewritten by separating the properties measured throughout the simulations (*i. e.*  $X_1$  and  $X_n$ ) from the others:

$$h(n, X_a) = \ln(X_1) - \frac{1}{n} \ln \left( \frac{X_n}{n} \right) = \beta(\mu_n^0 - \mu_1^0) + \left( -a + \frac{a}{n} \right) X_a \quad (8.4)$$

It is therefore possible to plot the function  $h(n, X_a)$  as a function of  $X_a$  from the measured cluster size distribution. This plot consists in a set of lines — one for each value of  $n$  — of slope  $m_n = -a + a/n$  and intercept for  $X_a \rightarrow 0$ ,  $\beta(\mu_n^0 - \mu_1^0)$ .

It is therefore possible to reformulate the expression of the concentration of monomers in clusters of size  $n$ , as a function of the total concentration in monomers  $X_a$ , as:

$$X_n(X_a) = nX_1^n \exp \left( -n \left( \beta fit(n) + \left( -a + \frac{a}{n} \right) X_a \right) \right) \quad (8.5)$$


 Figure 8.8:  $h(n, X_a)$ 

where  $fit(n)$  is the fit of  $(\mu_n^0 - \mu_1^0)$ .

Including this expression in the conservation relation for the total concentration in surfactant leads to a self consistent expression for  $X_a$ :

$$X_a = \sum_{n=1}^{n_0} X_n(X_a) \quad (8.6)$$

where  $n_0$  is the maximum cluster size considered. For the present work  $n_0 = 100$  because of statistically poor data for larger cluster sizes. It was therefore possible to compute the monomer concentration,  $X_1$ , using a Newton-Raphson technique [142] on equation 8.6. Results from this 'prediction' proved to be satisfactory (see figure 8.9). By inverting equation 8.5 it is also possible to get a 'complete predicted distribution'. Results from those distributions are presented in figure 8.10 together with data from the simulations. They appear to describe those latter reasonably well up to concentrations  $X_a \approx 5 \text{ vol.}\%$ .

The values of the slope,  $m_n$ , were determined by fitting a line using a standard

CHAPTER 8. SIMULATIONS IN THE MICELLAR REGION

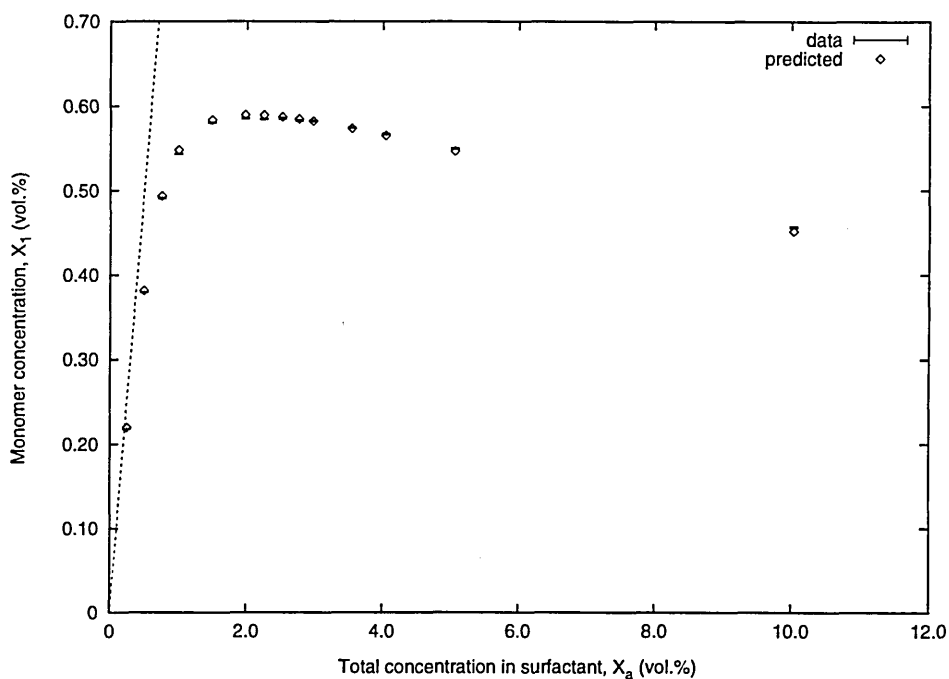


Figure 8.9: Monomer concentration,  $X_1$ , as a function of the total concentration in surfactant,  $X_a$ : simulation data and fit ( $\beta^{-1} = 1.18$ ,  $\gamma = -2.0$ )

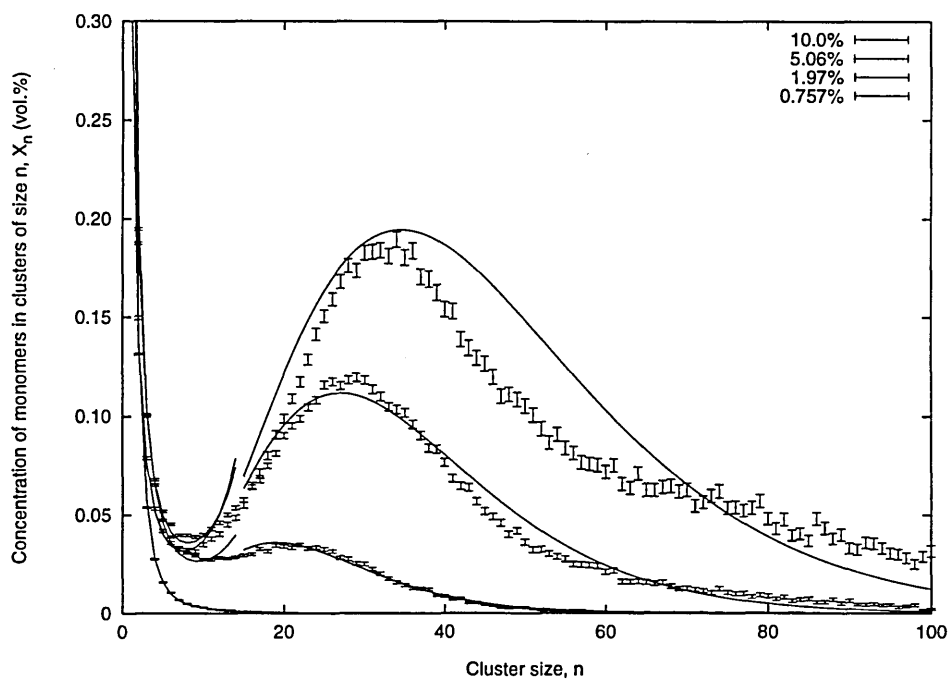


Figure 8.10: Concentration of monomers in clusters of size  $n$ ,  $X_n$ : pre-micellar and micellar distributions: simulation data and fit ( $\beta^{-1} = 1.18$ ,  $\gamma = -2.0$ )

linear regression technique for values of  $n$  having a minimum of 5 data points. It must be noted that as the size of the aggregate gets bigger, data for lower  $X_a$  become less frequent and have therefore a larger error associated. This is an obvious consequence of the absence — or strictly speaking of the very low statistical probability of occurrence — of large clusters at pre-micellar concentrations.

Both the slope and the intercept of  $h(n, X_a)$  were then plotted as a function of  $n$  (see figure 8.11) and fits were carried out using either downhill simplex or Levenberg-Marquardt methods [142].

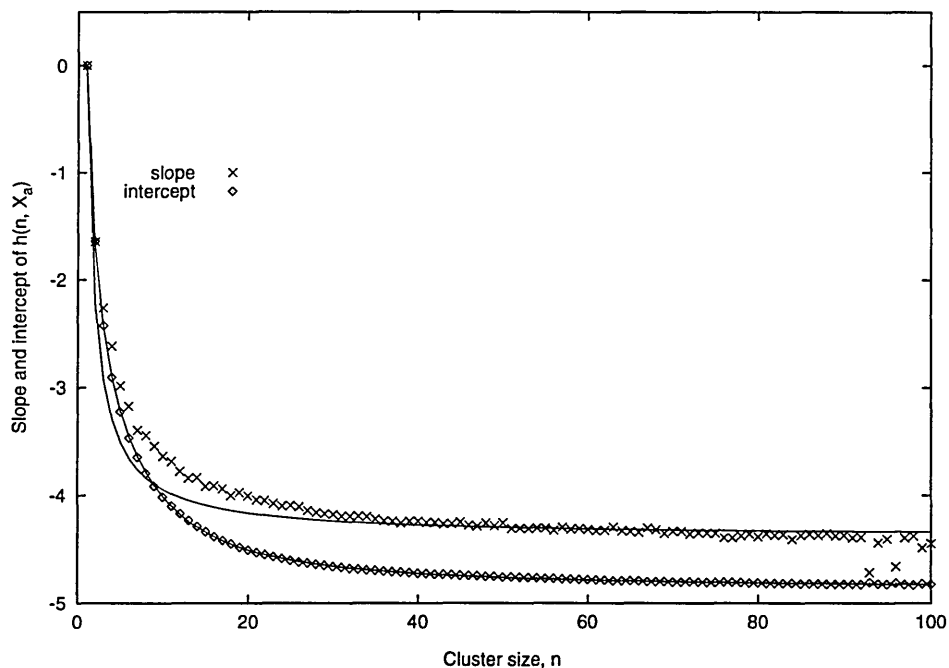


Figure 8.11: Slope and intercept of  $h(n, X_a)$ : data and fits

It must be noted that whereas the quality of the fit to  $m_n$  is not paramount since it is only a correction to the *dilute solution approximation*, the situation is completely different concerning the fit to the intercept. Indeed, the activity coefficients are only corrections to take into account the non-ideality arising from inter aggregate interactions, whereas  $(\mu_n^0 - \mu_1^0)$  being an exponent in equ. 8.3, the slightest deviation between the data

and the fit would cause serious discrepancies when using the above-mentioned equation to revert to a ‘predicted’ cluster size distribution.

The presence of discontinuities at  $n = 14$  on the fitted distribution functions stems from the decomposition of the fit on the excess chemical potential into two domains for small ( $n \leq 14$ ) and large ( $n > 14$ ) cluster size (see section 8.4).

## 8.4 Comparison with theory

Many theoretical models have been used to study micelles and microemulsions (see chapter 4). Amongst them, the one presented by Goldstein [71] appears the most suitable for comparison with the current results. This model is a phenomenological model for phase equilibria of nonionic surfactants in micellar solutions which includes both hydrophobic interactions and polymer chain like entropy effects. Its applicability is limited to spherical micelles only.

In this model, the free energy difference has been taken as arising from contributions of a bulk term,  $\delta_b$ , a surface term,  $\delta_s$ , and an entropic term  $\delta_e$ .

$$\delta = \delta_b + \delta_s + \delta_e \equiv (\mu_n^0 - \mu_1^0) \quad (8.7)$$

where  $\delta$  the free energy difference per surfactant molecule.

The bulk term,  $\delta_b$ , incorporates the favourable transfer of the hydrocarbon tail from the bulk to the interior of the micelle and the free energy change due to the proximity of the hydrophilic heads; it is proportional to the chain length and independent of the cluster size. This contribution is the main driving force for the aggregation process.

The surface term,  $\delta_s$ , reflects two competing factors: a loss of entropy due to the localisation of the surfactant chain, and a gain in free energy upon aggregation; it is

proportional to the aggregate surface area and to  $n^{-1/3}$ .

The entropic component,  $\delta_e$ , takes into account the conformational entropic loss arising from the elongation of the aliphatic tail as the radius of the spherical micelles is increased; it is made of the sum of a term proportional to  $n^{2/3}$  and a term independent of  $n$ .

Equation 8.7 can therefore be expressed as:

$$\delta = A + \frac{B}{n^{1/3}} + Cn^{2/3} \quad (8.8)$$

where  $A$ ,  $B$  and  $C$  do not depend upon the value of  $n$ .

Goldstein considers that in the absence of effects from the translational entropic terms, the optimum size of the micelles  $n_{max}$  will be that which minimises the free energy density  $\delta$ . However, it is essential to make clear that this statement does not constitute a prerequisite of micellisation as often assumed. Many authors (*e.g.* Israelachvili [3] or Wennerström [24]) have demonstrated that as long as  $\mu_n^0$  reaches its asymptotic value rapidly enough the micelles are stable although  $\mu_n^0$  decreases with increasing  $n$ . The excess chemical potential for the model ( $\mu_n^0 - \mu_1^0$ ) appears to follow such a behaviour and monotonically decreases as a function of the cluster size  $n$ .

Following simple geometric arguments, Israelachvili [3] (see chapter 3) proposed a simple expression to characterise the variation of the chemical potential for different simple structures:

$$\mu_n^0 = \mu_\infty^0 + \frac{\alpha kT}{n^p} \equiv A + \frac{B}{n^p} \quad \text{where} \quad \begin{cases} p = 1/3 & \text{for a sphere} \\ p = 1/2 & \text{for a disk} \\ p = 1 & \text{for a rod} \end{cases} \quad (8.9)$$

As the total concentration in surfactant increases, those small spherical micelles

disappear to the benefit of larger rod-like aggregates. Those latter are semi-flexible rods with constant radius and semi-spherical end caps. Since each new amphiphile joining such an aggregate increases only its length, one would expect the excess chemical potential to vary with  $1/n$ . It is thus possible to express the excess chemical potential as having components for the bulk term  $A$ , and to reflect the growth of small spherical micelles into rod-like micelles. One would expect it to be of the form:

$$(\mu_n^0 - \mu_1^0) = A + B/n^{f_n} \quad (8.10)$$

where  $f_n$  is a monotonically increasing function of  $n$  with limits:

$$f_n = \begin{cases} 1/3 & \text{for small } n \text{ (spherical micelles)} \\ 1 & \text{for large } n \text{ (rod-like micelles)} \end{cases}$$

Unfortunately, attempts to find such a function which would describe all the range of cluster size turned out to be unsuccessful and it was therefore necessary to use two different expressions for small and large  $n$ . Thus the form of the fit to  $(\mu_n^0 - \mu_1^0)$ :

$$fit(n) = \begin{cases} A_1 + B_1/n^{c_1} & \text{for } n \leq n_{limit} \\ A_2 + B_2/n^{c_2} & \text{otherwise} \end{cases} \quad (8.11)$$

where  $n_{limit}$  is the cluster size starting from which the driving force to grow cylindrical micelles becomes predominant. A value of  $n_{limit} = 14$  appeared to give the best fits (see figure 8.10). Larger values would yield unacceptable discontinuities in the distribution at  $n_{limit}$  whereas smaller values whilst decreasing the magnitude of these discontinuities would worsen the overall quality of the fit. The values of the parameters of the fit are presented in tables 8.2 and 8.4.

As was to be expected, the value taken by the exponent of the fit for large clusters,  $c_2$ , is consistent with the growth of rod-shaped aggregates whereas the values taken by

$c_1$  are more consistent with the growth of disk-like aggregates than spheres (see table 8.2 and 8.4). These conclusions are supported by Brindle [15] who reported a value of  $\approx 1/2$  for the ratio of the smallest to the largest principal moments of inertia at this region of the phase diagram.

The preferential formation of disk-like aggregates probably stems from the difficulty of forming spheres with such short chains (small hydrophilic head and length-to-width ratio) on an underlying cubic lattice.

## 8.5 Temperature and hydrophilic strength-dependencies

### 8.5.1 Temperature dependency

As this was previously emphasised, the determination of the cmc can yield different results depending on the criterion used. In the present work, both the the inflection point in the  $X_1$  vs  $X_a$  curves and the maximum concentration of monomers will be used. The critical micelle concentrations derived from those criteria will respectively be labelled  $cmc_1$  and  $cmc_2$ .

Regardless of the method used, the cmc appears to increase linearly with the temperature (see figure 8.12). This result appears to be in contradiction with experimental data [23] since the cmc of non-ionic surfactants such as  $C_iEO_j$  actually decreases (non-linearly) with temperature [143]. This behaviour can essentially be understood as arising from the endothermic enthalpy of micellisation (the heads become less hydrophilic as the temperature rises thus decreasing the probability of formation of H-bonds). In contrast, ionic surfactants such as *SDS* have a minimum cmc for temperature 20 – 30°C. Whereas the decrease at low temperatures can be attributed to the dehydration of monomers, the increase at higher temperatures stems from the disruption of the structured water around

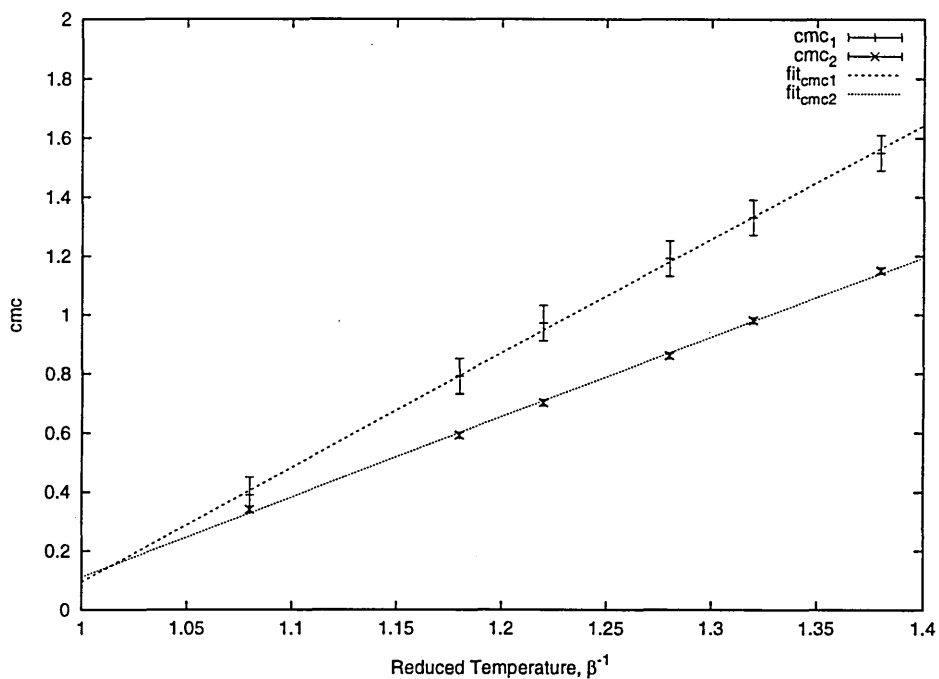


Figure 8.12: Temperature-dependence of the cmc ( $\gamma = -2.0$ )

the hydrophobic groups which opposes micellisation.

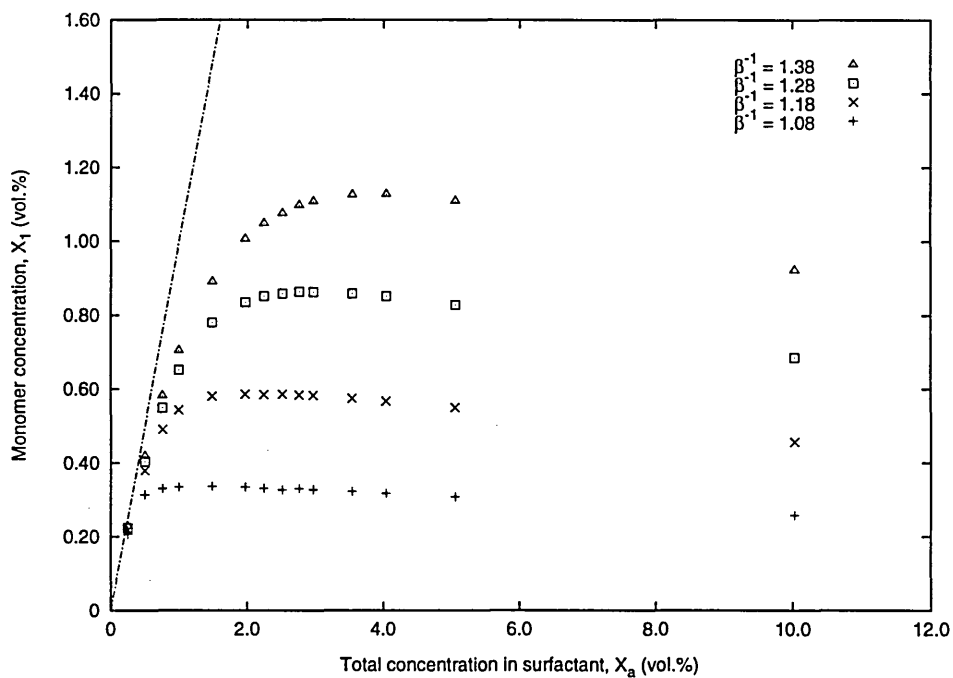


Figure 8.13: Temperature-dependence of the monomer concentration,  $X_1$ , as a function of the total concentration in surfactant,  $X_a$  ( $\gamma = -2.0$ )

## CHAPTER 8. SIMULATIONS IN THE MICELLAR REGION

The main influence of the temperature on the  $X_1$  vs  $X_a$  curve appears to be on the sharpness of the cmc (see figure 8.13) which decreases with increasing temperature. The unexpected negative slope for higher concentrations is still present with a similar magnitude.

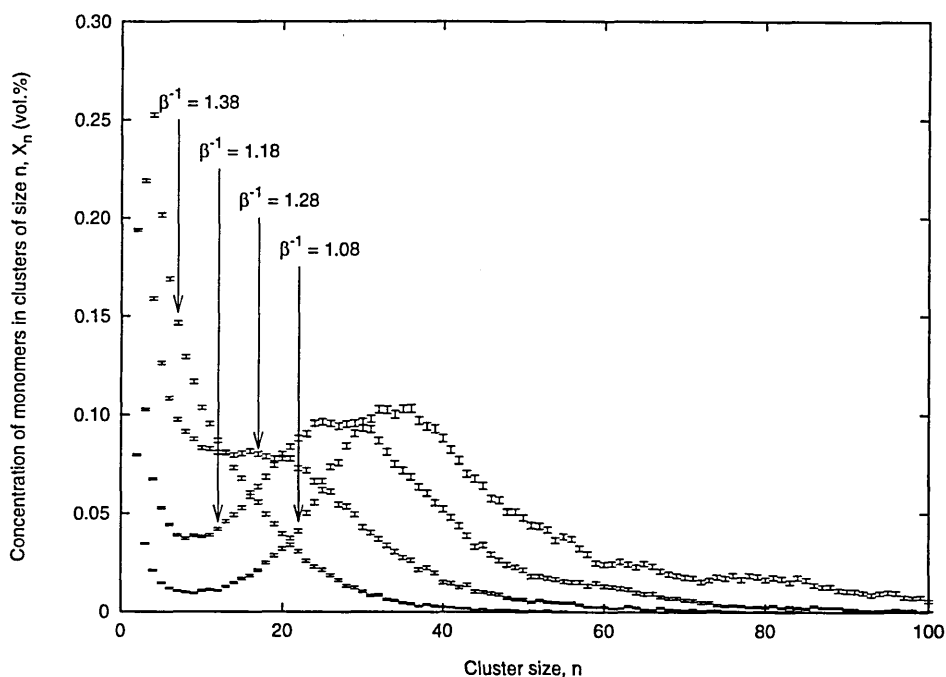


Figure 8.14: Temperature-dependence of the concentration of monomers in clusters of size  $n$ ,  $X_n$  ( $\gamma = -2.0$  and  $X_a = 4.04 \text{ vol. } \%$ )

The cluster size distributions themselves (see figure 8.14) appear to be sensitive to temperature as well. As this latter is raised, preferred aggregate sizes seem to become smaller which again is more consistent with the behaviour of ionic surfactants than that of non-ionic ones. Indeed, whereas a decrease of the micelle size of ionic surfactants with increase in temperature has been previously reported [144], micelles of many non-ionic surfactants increase rapidly in size with temperature [145, 146]. Israelachvili [3] uses geometric packing arguments to explain this behaviour. Indeed, both the critical chain length  $l_c$  and the optimal surface area occupied per head group  $a_0$  are sensitive to temperature: the areas of non-ionic *POE* groups decrease with increasing temperature because of their

increased hydrophobicity [147, 148], whereas that of ionic head groups usually increases due to the increased steric repulsion between them [149]. This particular behaviour emphasises the need for a more accurate modelling of water than the one currently used in this model.

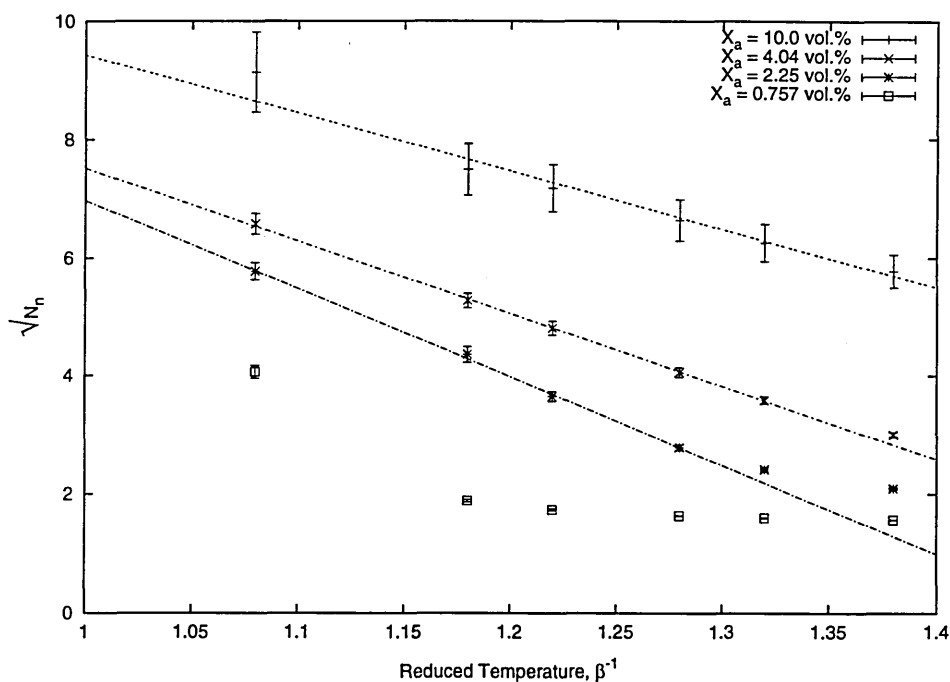
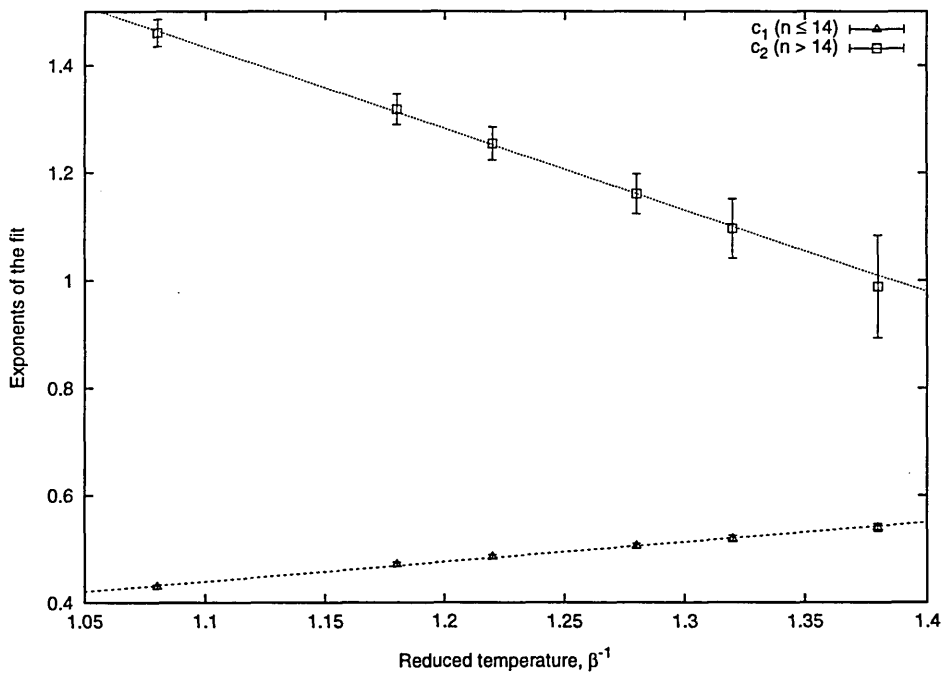


Figure 8.15: Temperature-dependence of  $\sqrt{N_n}$  ( $\gamma = -2.0$ )

The square root of the mean aggregation number  $\sqrt{N_n}$  has been reported as being linearly dependent upon the temperature for various surfactants (*e.g.* linear increase for  $C_{12}EO_6$  [150] and shallow pseudo-linear decrease for N-undecyl betaine [151]). The model exhibited such a pseudo-linear dependence for concentrations above the cmc. One may note that this linear dependence has got an upper temperature limit which increases with  $X_a$  as expected from the influence of the temperature on the cmc.

Both exponents of the fit,  $c_1$  and  $c_2$ , are also reported to be linearly dependent upon the temperature. This behaviour is not yet fully understood.

$\beta^{-1}$	1.08	1.18	1.22	1.28	1.32	1.38
$A_1$	-7.672 $\pm 0.038$	-7.152 $\pm 0.034$	-7.012 $\pm 0.034$	-6.827 $\pm 0.035$	-6.717 $\pm 0.042$	-6.576 $\pm 0.043$
$B_1$	7.691 $\pm 0.035$	7.170 $\pm 0.031$	7.030 $\pm 0.031$	6.845 $\pm 0.032$	6.736 $\pm 0.038$	6.596 $\pm 0.039$
$c_1$	0.4298 $\pm 0.0037$	0.4711 $\pm 0.0041$	0.4850 $\pm 0.0044$	0.5052 $\pm 0.0050$	0.5191 $\pm 0.0062$	0.5400 $\pm 0.0069$
$A_2$	-5.9158 $\pm 0.0033$	-5.7464 $\pm 0.0042$	-5.7077 $\pm 0.0049$	-5.6642 $\pm 0.0071$	-5.650 $\pm 0.013$	-5.669 $\pm 0.034$
$B_2$	35.4 $\pm 2.4$	22.2 $\pm 1.7$	18.6 $\pm 1.5$	14.3 $\pm 1.4$	12.1 $\pm 1.7$	9.6 $\pm 2.1$
$c_2$	1.460 $\pm 0.025$	1.318 $\pm 0.029$	1.255 $\pm 0.031$	1.161 $\pm 0.037$	1.097 $\pm 0.055$	0.989 $\pm 0.095$

 Table 8.2:  $\beta^{-1}$ -dependence of  $fit(n)$  ( $\gamma = -2.0$ )

 Figure 8.16: Temperature-dependence of the exponents of the fits,  $c_1$  and  $c_2$  ( $\gamma = -2.0$ )

### 8.5.2 Hydrophilic strength dependency

The effect of the hydrophilic strength on the micellisation process appears to be much more dramatic. Whereas the cmc and distributions (see figures 8.17 and 8.18) for  $\gamma = -3.0$  and  $\gamma = -4.0$  appear relatively close, a very sharp change occurs when

CHAPTER 8. SIMULATIONS IN THE MICELLAR REGION

decreasing the hydrophilic strength from  $\gamma = -2.0$  to  $\gamma = -1.0$  up to the point where no micellisation as such occurs for  $\gamma = -1.0$ . The saturation for the most negative  $\gamma$  stems from the saturation of the head groups which become fully hydrated.

This is similar to the arguments of Laughlin [4] which are that both upper and lower limits of hydrophilicity exist: the lower limit is determined by the requirement that a minimal thermodynamic strength of hydration must exist whereas the upper limit results from the intervention of chemical hydrolysis.

$\gamma$	-1.0	-2.0	-3.0	-4.0
<b>cmc<sub>1</sub></b> (vol. %)	0.44 $\pm 0.06$	0.79 $\pm 0.06$	0.94 $\pm 0.06$	1.08 $\pm 0.06$
<b>cmc<sub>2</sub></b> (vol. %)	0.38 $\pm 0.01$	0.59 $\pm 0.01$	0.67 $\pm 0.01$	0.70 $\pm 0.01$

Table 8.3:  $\gamma$ -dependence of the cmc ( $\beta^{-1} = 1.18$ )

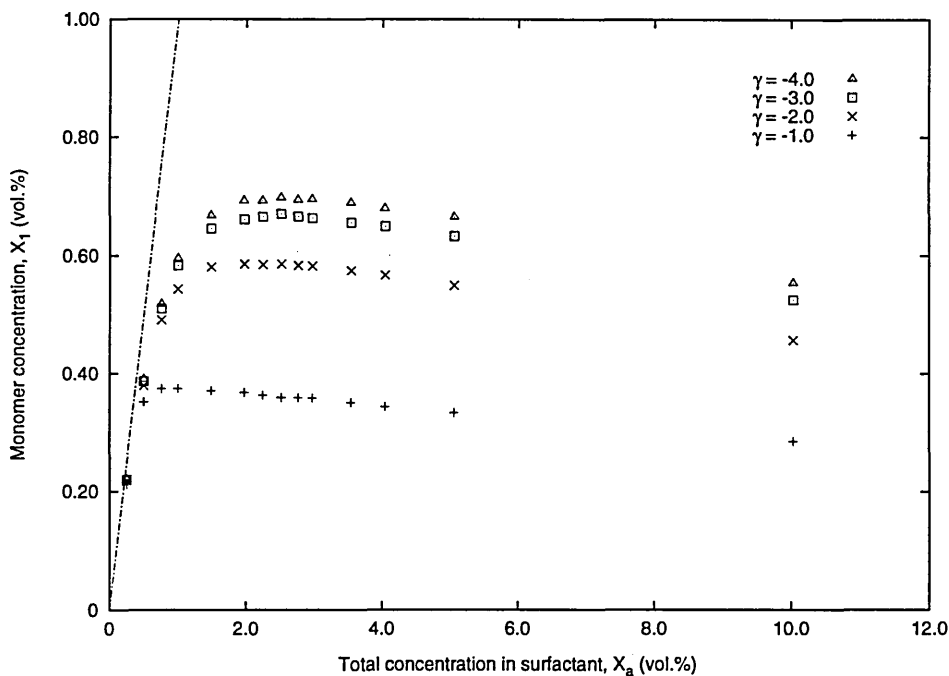


Figure 8.17: Hydrophilic strength-dependence of the monomer concentration,  $X_1$ , as a function of the total concentration in surfactant,  $X_a$  ( $\beta^{-1} = 1.18$ )

Unlike for the temperature, the parameters of the fit do not seem to follow any

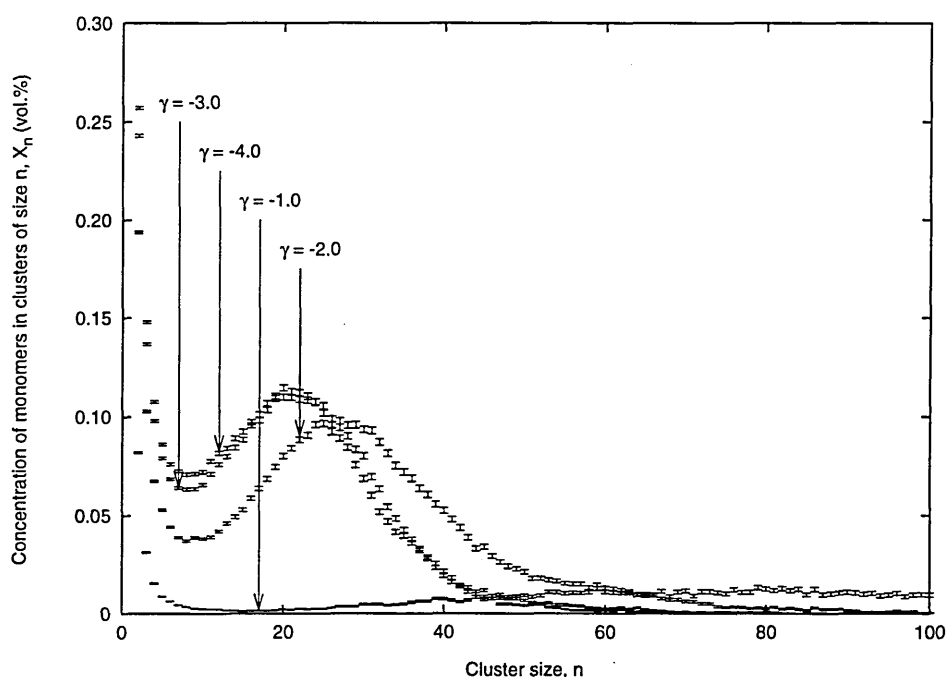


Figure 8.18: Hydrophilic strength-dependence of the concentration of monomers in clusters of size  $n$ ,  $X_n$  ( $\beta^{-1} = 1.18$  and  $X_a = 4.04 \text{ vol. } \%$ )

obvious dependence to the hydrophilic strength (see table 8.4).

$\gamma$	-1.0	-2.0	-3.0	-4.0
<b>A<sub>1</sub></b>	-7.952 $\pm 0.036$	-7.152 $\pm 0.034$	-6.904 $\pm 0.039$	-6.814 $\pm 0.046$
<b>B<sub>1</sub></b>	7.966 $\pm 0.033$	7.170 $\pm 0.031$	6.924 $\pm 0.036$	6.835 $\pm 0.042$
<b>c<sub>1</sub></b>	0.4359 $\pm 0.0035$	0.4711 $\pm 0.0041$	0.4807 $\pm 0.0050$	0.4844 $\pm 0.0061$
<b>A<sub>2</sub></b>	-6.5256 $\pm 0.0057$	-5.7464 $\pm 0.0042$	-5.5217 $\pm 0.0057$	-5.4156 $\pm 0.0071$
<b>B<sub>2</sub></b>	18.73 $\pm 0.73$	22.2 $\pm 1.7$	22.1 $\pm 2.7$	33.5 $\pm 6.5$
<b>c<sub>2</sub></b>	1.061 $\pm 0.015$	1.318 $\pm 0.029$	1.374 $\pm 0.046$	1.565 $\pm 0.072$

Table 8.4:  $\gamma$ -dependence of  $fit(n)$  ( $\beta^{-1} = 1.18$ )

## 8.6 Conclusion

This simple model appears to be successful in describing most of the features exhibited by mixtures of surfactants and solvent: its behaviour is in good agreement with both experimental data and theoretical studies. The expression of the excess chemical potential has been described satisfactorily by a unique functional form with different sets of parameters for small and large clusters. The values of the exponent of the fit appear to be consistent with the growth of disk-like micelles to rod-like micelles as the concentration in surfactant,  $X_a$ , is increased. This unexpected behaviour is reckoned to be a lattice effect — dimensionality of a sphere grown on a cubic lattice is  $\neq 3$  — since graphical observations actually confirm the smaller micelles as being spherical. Contrarily to an opinion commonly expressed in the literature, the micellisation process proves to take place in spite of the absence of any minimum in the excess chemical potential — indeed,  $(\mu_n^0 - \mu_1^0)$  is a monotonically decreasing function of  $n$ .

Clearly, this model also suffers from some serious limitations. First of all, it demonstrates an unrealistic linear-dependency of some of its properties (*e.g.* the cmc) on the temperature. Moreover, other properties appear to have a behaviour closer to that characteristic of ionic surfactants than the nonionic ones the model is supposed to be used for. This latter discrepancy may be partially overcome by considering that the model is also suitable for the modelling of ionic surfactants in the presence of electrolyte (hence with no long-range electrostatic interactions due to screening effects). Finally, the cluster size distribution is characterised adversely by too high a polydispersity, too weak a minimum and also too small a mean aggregation number,  $N_n$ . This is believed to be essentially due to lattice effects and the unrealistic 1 : 4 width/length ratio of the chains. Preliminary results for surfactant chains of length  $s = 6$  with  $t = 2$  head segments and bending energy parameter  $\epsilon = 1.0$  are presented in the conclusion to test this assumption.

## CHAPTER 8. SIMULATIONS IN THE MICELLAR REGION

Finally, another serious limitation of this model is its inability to give a good account of the immiscibility and thus to reproduce the cloud point phenomenon. The only solution is thought to be a more accurate modelling of the water by using a more refined Hamiltonian for the system.

## Chapter 9

# Conclusion

### 9.1 Concluding remarks

The current study allowed the characterisation of a lattice model of self-assembling chains. Despite its relative simplicity, this model exhibits behaviour in good agreement with experimental data and is well described by the multiple phase equilibria model for simulations in the micellar region.

The model exhibits a critical micelle concentration together with cluster size distributions consistent with experiment and theory. The dependence of the weight average aggregation number,  $N_w$ , on the total concentration in surfactant,  $X_a$ , is found to obey theoretical predictions. The dilute solution excess chemical potential ( $\mu_n^o - \mu_1^o$ ) is determined from the cluster size distribution. It is found to be a monotonically decreasing function of  $n$  with different functional forms for small and large clusters. A single analytical expression is found to describe the cluster size distribution and the  $X_1$  versus  $X_a$  curve on the concentration range from 0 to 5 vol.%. It is necessary to introduce an activity coefficient to accurately describe the behaviour of the model for amphiphile concentrations greater than 5 vol.%. .

## CHAPTER 9. CONCLUSION

As stated in chapter 8, two of the main causes responsible for the discrepancies observed in the cluster size distribution — such as too great a polydispersity or a very long tail in the distribution for total concentration in surfactant  $X_a > 5 \text{ vol.}\%$  — are linked to the the excessive width over length ratio and unrealistic folded conformations taken by the fully flexible chains. This hypothesis has been tested by running a similar set of simulations — *i. e.*  $\gamma = -2.0$  and  $\beta^{-1} = 1.18$  — with longer chains of length  $s = 6$  segments (including  $t = 2 H$ ) to correct the excessive width-to-length and hydrophobic section-to-hydrophilic section ratios, and some rigidity ( $\varepsilon = 1.0$ ), all the other simulation parameters being identical to those described in chapter 8. Preliminary observations of the cluster size distribution functions are illustrated in figure 9.1 and reference [152].

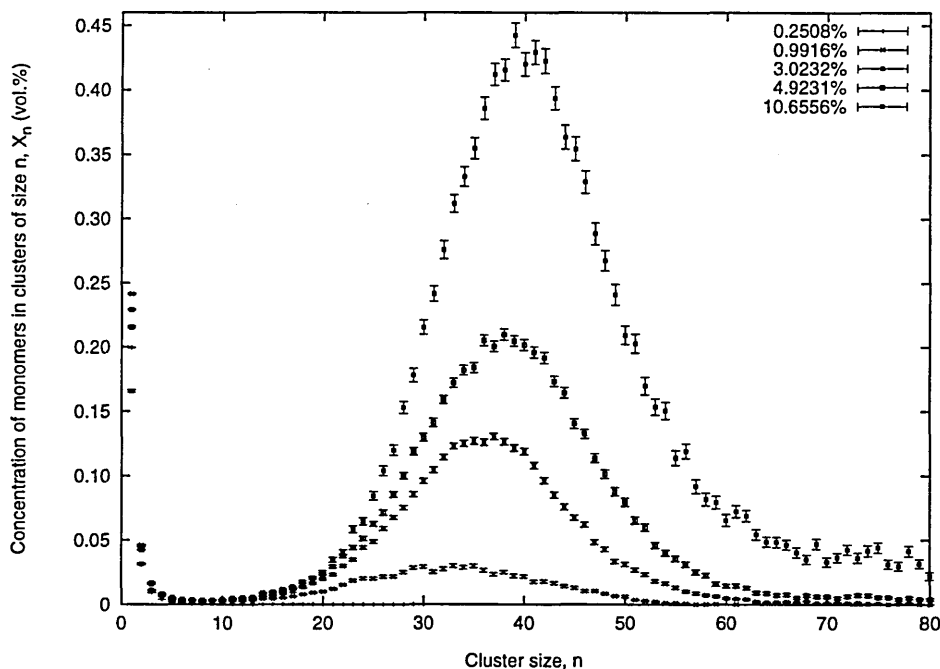


Figure 9.1: Concentration of monomers in clusters of size  $n$ ,  $X_n$ : pre-micellar and micellar distributions (preliminary results,  $\beta^{-1} = 1.18$  and  $\gamma = -2.0$ )

The correctness of this hypothesis can be simply checked by comparison with the results obtained for the fully flexible chains of length  $s = 4$  (see figure 8.3).

This comparison yields the following observations:

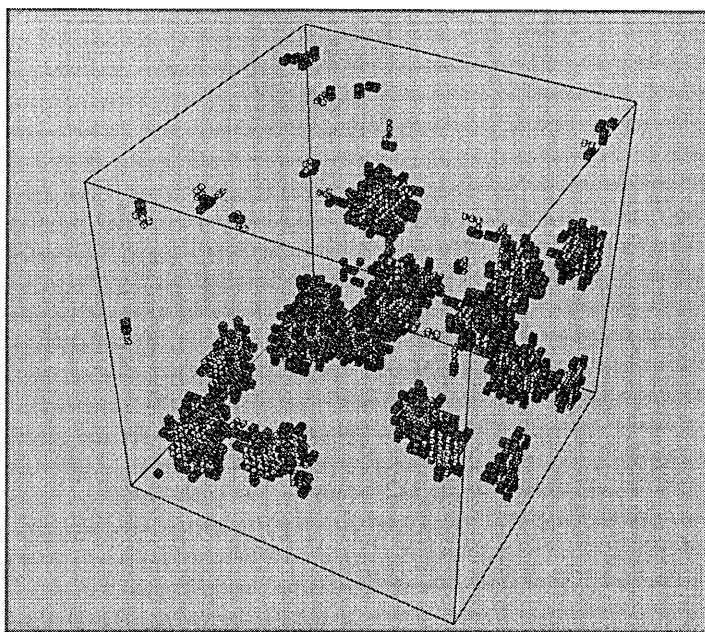


Figure 9.2: Micelles forming at  $X_a = 4.0 \text{ vol. } \%$  (preliminary results,  $\beta^{-1} = 1.18$  and  $\gamma = -2.0$ )

1. The cluster size distribution exhibits a much deeper minimum in the micellar region.
2. The cmc occurs at a lower total concentration in surfactant,  $X_a$ .
3. The cluster size distribution is still well behaved for total concentrations in surfactant  $5 \text{ vol. } \% < X_a < 10 \text{ vol. } \%$ .
4. The mean aggregation numbers,  $N_n$ , are larger.
5. The shape of the micelles is more spherical (compare figures 8.6 and 9.2).

This study of the micellar region will be pursued in more detail and is likely to lead to further publications [152–154].

The other simulations presented in chapter 7 aimed to investigate the formation of a vesicle reported by Brindle during a previous study. This latter has been demonstrated to be a metastable structure in equilibrium with structures resembling those thought to be formed in an asymmetric sponge phase. Both structures suffered from serious finite size

effects linked to the restriction on the system size imposed by current computer resources.

A phase diagram has been generated by plotting the average cavity size filled with entrapped solvent as a function of  $(\beta^{-1}, \gamma)$  in combination with information from other observables such as the average number of cavity, volume fraction of entrapped solvent and mean aggregation number. A number of regions, more or less well-characterised, have been successfully identified. The most interesting is that occurring for medium to low temperatures ( $1.30 < \beta^{-1}$ ) and moderately hydrophilic heads ( $-1.13 \leq \gamma \leq -0.80$ ) where metastable tubular vesicles and ‘spongy structures’ form. A succession of other structures such as spherical, discoid and rod-like micelles, a variety of ‘spongy structures’ exhibiting different degree of order with open and communicating cavities have also been observed. Although this piece of work is more qualitative, a few interesting similarities with both experimental and phenomenological studies have been found.

Finally, a novel sampling scheme applicable to models of chains lying on a lattice of high coordination number has been presented in chapter 6. Its theoretical foundation is provided together with a partial assessment of its efficiency, discussed with respect to that of the ‘classic’ CBMC and reptation schemes. A methodology aiming to achieve a better mapping of real molecules by using a cubic lattice of high coordination number is also briefly discussed in this section and applied to the particular case of polyoxyethylene surfactants.

## 9.2 Suggested improvements and further work

Although the features exhibited by the model went beyond initial expectations, the model still lacks some of the properties of real systems, the most noticeable of which being probably the absence of a cloud point. The following points ought to be implemented and their influence on the model behaviour carefully assessed:

## CHAPTER 9. CONCLUSION

- Perform a more accurate modelling of water (this should suppress the artificial ‘pseudo-linear’ temperature-dependency reported in chapter 8).
- Include long-range *HH* electrostatic repulsions (this should result in the formation of larger micelles and is known to play an important role in the mechanism involved in the most lyotropic phase transitions; it would also allow to mimic the influence of the screening resulting from the presence of an electrolyte by varying the interaction cut-off).
- Use a different lattice with a higher coordination number in order to achieve a better mapping of real molecules.
- Develop a more efficient sampling scheme to investigate the spongy phases with larger systems (say  $N = 16384$ ), and also for larger total concentration in surfactant. It could be interesting to simulate a dilution experiment to relate the data to existing experimental and phenomenological studies.

Other areas could also be looked at such as the simulation of mixtures of non-ionic surfactants in the micellar region or the study of the micellar to lamellar transition using the Gibbs ensemble [115].

### 9.3 Conclusion

The final comment has to be about the future of MC simulations of chains on a lattice. Indeed, although this type of simulations has proven so far to be more effective by allowing the use of lock-up tables and smart algorithm thus avoiding complex and costly calculations, properties inherent to this type of model lead to major difficulties in the development of efficient parallel — and vectorial — implementations. Since the use of parallel architectures is the only alternative for a gain in processing power, it is the

## CHAPTER 9. CONCLUSION

author's belief that MD simulations will therefore quickly become the way forward for the simulation of surfactant systems other than in the micellar region — where requirements on the system size are weaker — unless new more efficient sampling algorithms are designed.

# Bibliography

- [1] M P Allen and D J Tildesley. *Computer Simulation of Liquids*. Oxford University Press, 2nd edition, 1992.
- [2] D J Shaw. *Introduction to Colloid and Surface Chemistry*. Butterworths, 3rd edition, 1980.
- [3] J N Israelachvili. *Intermolecular and Surface Forces*. Academic Press, 2nd edition, 1992.
- [4] R G Laughlin. *The Aqueous Phase Behaviour of Surfactants*. Academic Press, 1994.
- [5] G J T Tiddy. Surfactant-water liquid crystal phases. *Physics Reports*, 57(1):1–46, 1980.
- [6] K Hatchman. *Kinetic Studies of Phase Transitions in Lyotropic Liquid Crystalline Systems*. PhD thesis, Department of Chemistry and Applied Chemistry, University of Salford, 1992.
- [7] G Porte, J Appell, P Bassereau, and J Marignan.  $L_\alpha$  to  $L_3$ : a topology driven transition in phase of infinite fluid membranes. *J. Phys. Paris*, 50(11):1335–1347, 1989.
- [8] J C Wheeler and B Widom. Phase transitions and critical points in a model three-component system. *J. Am. Chem. Soc.*, 60(12):3064–3071, 1968.

## BIBLIOGRAPHY

- [9] B Widom. Lattice model of microemulsions. *J. Chem. Phys.*, 84(12):6943–6954, 1986.
- [10] K A Dawson and Z Kurtovic. Lattice model of self-assembly. *J. Chem. Phys.*, 92(9):5473–5485, 1990.
- [11] J R Gunn and K A Dawson. A lattice model description of amphiphilic mixtures. 1. equilibrium properties. *J. Chem. Phys.*, 96(4):3152–3169, 1992.
- [12] G Gompper and M Schick. Microemulsion structure from a three-component lattice model. *Phys. Rev. Lett.*, 62(14):1647–1650, 1989.
- [13] K Chen, C Ebner, C Jayaprakash, and R Pandit. Microemulsions in oil-water-surfactant mixtures: Systematics of a lattice gas model. *Phys. Rev. A*, 38(12):6240–6254, 1988.
- [14] R G Larson. Monte Carlo simulation of microstructural transitions in surfactant systems. *J. Chem. Phys.*, 96(11):7904–7918, 1992.
- [15] D Brindle and C M Care. Phase diagram for the lattice model of amphiphile and solvent mixtures by Monte Carlo simulation. *J. Chem. Soc. Faraday Trans.*, 88(15):2163–2166, 1992.
- [16] B Smit, P A J Hilbers, and K Esselink. Computer simulations of simple oil/water/surfactants systems. *Tenside Surf. Det.*, 30(4):287–293, 1993.
- [17] D R Rector, F van Swol, and J R Henderson. Simulation of surfactant solutions: 1. micelle formation in the bulk phase. *Molecular Physics*, 82(5):1009–1031, 1994.
- [18] Y Zhan and W L Mattice. Self-assembly and adsorption of diblock copolymers from selective solvents. 1. self-assembly. *Macromolecules*, 27(3):677–682, 1994.

## BIBLIOGRAPHY

- [19] C M Care. A lattice model of the micellar phase of an amphiphile and solvent mixture in the quasi-chemical approximation. *J. Phys. C: Solid State Phys.*, 20(5):689–704, 1987.
- [20] D Frenkel, G C A M Mooij, and B Smit. Novel scheme to study structural and thermal properties of continuously deformable molecules. *J. Phys. : Condens. Matter*, 3(12):3053–3076, 1991.
- [21] J I Siepmann and D Frenkel. Configurational-bias Monte Carlo: a new sampling scheme for flexible chains. *Mol. Phys.*, 75(1):59–70, 1992.
- [22] R G Laughlin. *Advances in Liquid Crystals*, volume 3. Academic Press, 1978.
- [23] D Attwood and A T Florence. *Surfactant Systems: their chemistry, pharmacy and biology*. Chapman and Hall, 1983.
- [24] H Wennerström and B Lindman. Micelles, physical chemistry of surfactant association. *Physics Reports*, 52(1):1–86, 1979.
- [25] M Smnutzsky, A C Dianoux, C Gitler, and G Weber. *Biochemistry*, 10:2106, 1971.
- [26] J B Rosenholm, T Drakenberg, and B Lindman. A carbon-13 NMR shielding study of the water-sodium octanoate-pentanol, and water-sodium octanoate-decanol systems. *J. Colloid Interface Sci.*, 63(3):538–550, 1971.
- [27] A S Waggoner, A D Keith, and O H Griffith. Electron spin resonance of the solubilised long-chain nitroxides. *J. Phys. Chem.*, 72(12):4129–4132, 1968.
- [28] K S Birdi and T Magnusson. *Colloid and Polymer Sci.*, 254:1059, 1976.
- [29] H Umeyama and K Morokuma. *J. Am. Chem. Soc.*, 99:1316–1332, 1977.
- [30] M D Joesten and L J Schaad. *Hydrogen Bonding*. Marcel Dekker, Inc, 1974.

## BIBLIOGRAPHY

- [31] T A Bleasdale and G J T Tiddy. Surfactant liquid crystals. In D M Bloor and E Wyn-Jones, editors, *The Structure, Dynamics and Equilibrium Properties of Colloidal Systems*, pages 397–414. Kluwer Academic Publishers, 1990.
- [32] J Charvolin and J F Sadoc. Lyotropic liquid crystals: the common skeleton of their phase diagrams. *Physica A*, 176(1):138–150, 1991.
- [33] D Anderson, H Wennerström, and V Olsson. Isotropic bicontinuous solutions in surfactant solvent systems: the  $L_3$  phase. *J. Phys. Chem.*, 93(10):4243–4253, 1989.
- [34] L E Scriven. *Nature*, 93:123, 1976.
- [35] K D Lawson and T J Flaut. *J. Amer. Chem. Soc.*, 89:5489, 1967.
- [36] M E Cates. Isotropic phases of self-assembled amphiphilic aggregates. *Phil. Trans. R. Soc. Lond. A*, 344(1672):339–356, 1993.
- [37] L J Yu and A Saupe. Observation of a biaxial nematic phase in potassium laureate-1-decanol-water mixtures. *Phys. Rev. Lett.*, 45(12):1000–1003, 1980.
- [38] P A Winsor. Binary and multicomponent solutions of amphiphilic compounds. solubilisation and the formation, structure, and theoretical significance of liquid crystalline solutions. *Chem. Rev.*, 68(1):1–40, 1968.
- [39] J Ulmius, H Wennerström, G Lindblom, and G Arvidson. Deuteron nuclear magnetic resonance studies of phase equilibria in a lecithin-water system. *Biochemistry*, 16(26):5742–5745, 1977.
- [40] P Ekwall. *Advances in Liquid Crystals*, volume 1. Academic Press, 1975.
- [41] P Kekicheff and B Cabane. Between cylinders and bilayers: Structures of intermediate mesophases of the SDS-water system. *J. Phys.*, 48(9):1571–1583, 1987.

## BIBLIOGRAPHY

- [42] V Luzzati, H Mustacchi, A Skoulios, and F Husson. *Acta Cryst.*, 13:660, 1960.
- [43] P Ekwall, L Mandell, and K Fontell. Ternary systems of potassium soap, alcohol, and water: 1. phase equilibria and phase structures. *J. Colloid Interface Sci.*, 31(4):508–539, 1969.
- [44] A Jurgens. Microstructure and viscosity of liquid detergents. *Tenside Surf. Det.*, 26(3):222–226, 1989.
- [45] A Sein, J B F N Engberts, E van der Linden, and J C van de Pas. Salt-induced transition from a micellar to a lamellar liquid crystalline phase in dilute mixtures of anionic and nonionic surfactants in aqueous solution. *Langmuir*, 9(7):1714–1719, 1993.
- [46] J C van de Pas. Liquid detergents. *Tenside Surf. Det.*, 28(3):158–162, 1991.
- [47] J C van de Pas and C J Buytenhek. The effects of free polymers on osmotic compression, depletion flocculation and fusion of lamellar liquid-crystalline droplets. *Colloids and Surfaces*, 68(1):127–139, 1992.
- [48] A T Florence. Nonionic surfactant vesicles: Preparation and characterisation. In *Liposome Technology*, volume 1, chapter 10, pages 157–176. CRC Press, Inc., 2nd edition, 1993.
- [49] P Williams. *Liposomes in action*, pages 55–56, 1992.
- [50] A S C Lawrence. *Liquid Crystals 2*. Gordon and Breach, 1969.
- [51] C Tanford. *The hydrophobic effect: formation of micelles and biological membranes*. John Wiley & Sons, Inc., 2nd edition, 1980.
- [52] P Debye. Light scattering in soap solutions. *J. Phys. Chem.*, 53(1):1–8, 1949.

## BIBLIOGRAPHY

- [53] K Shinoda and E Hutchinson. *J. Phys. Chem.*, 66:557, 1962.
- [54] J E Desnoyers and G Perron. Thermodynamic methods. In R Zana, editor, *Surfactant Solutions: New Methods of Investigation*, pages 1–55. Marcel Dekker, Inc, 1990.
- [55] J E Desnoyers, G Caron, R DeLisi, R Roberts, A Roux, and G Perron. Thermodynamic properties of alkyldimethylamine oxides in water. application of a mass-action model for micellisation. *J. Phys. Chem.*, 87(8):1397–1406, 1983.
- [56] E M Wooley and T E Burchfield. Thermodynamics of ionic surfactant solutions containing added strong electrolyte. *Fluid Phase Equilib.*, 20:225–232, 1985.
- [57] J N Israelachvili. Thermodynamic and geometric aspects of amphiphile aggregation into micelles, vesicles and bilayers, and the interactions between them. In D Degiorgo and M Corti, editors, *Proceedings of the International School of Physics ‘Enrico Fermi’ - Physics of Amphiphiles: Micelles, Vesicles and Microemulsions*, pages 24–58. Italian Physical Society, 1985.
- [58] A Ben-Shaul, I Szleifer, and W M Gelbart. Amphiphile chain organisation in micelles of different geometries. In D Degiorgo and M Corti, editors, *Proceedings of the International School of Physics ‘Enrico Fermi’ - Physics of Amphiphiles: Micelles, Vesicles and Microemulsions*, pages 303–335. Italian Physical Society, 1985.
- [59] D G Hall and B A Pethica. *Nonionic Surfactants*, chapter 16. Marcel Dekker, New York, 1967.
- [60] T L Hill. *Thermodynamics of Small Systems*, volume 1 and 2. Benjamin, New York, 1964.

## BIBLIOGRAPHY

- [61] J N Israelachvili, D J Mitchell, and B W Ninham. Theory of self-assembly of hydrocarbon amphiphiles into micelles and bilayers. *J. Chem. Soc. Faraday Trans. 1*, 72(10):1525–1568, 1976.
- [62] C M Care, J-C Desplat, and D Brindle. Lattice models of surfactant systems. *Tenside Surf. Det.*, 30(4):281–286, 1993.
- [63] Y Talmon and S Prager. Statistical thermodynamics of phase equilibria in microemulsions. *J. Chem. Phys.*, 69(7):2984–2991, 1978.
- [64] P G De Gennes and C Taupin. Microemulsions and the flexibility of oil/water interfaces. *J. Phys. Chem.*, 86(12):2294–2304, 1982.
- [65] J Jouffroy, P Levison, and P G de Gennes. Phase-equilibria involving microemulsions (remarks on the talman-prager model). *J. Phys. (Paris)*, 43(8):1241–1248, 1982.
- [66] B Widom. A model microemulsion. *J. Chem. Phys.*, 81(2):1030–1046, 1984.
- [67] D Andelman, M E Cates, D Roux, and S A Safran. Structure and phase equilibria of microemulsions. *J. Chem. Phys.*, 87(12):7229–7241, 1987.
- [68] K S Sturgeon and H Reiss. Configurational entropy in a microemulsion: the error implicit in the use of a phenomenological lattice model. *J. Chem. Phys.*, 98(2):1493–1503, 1993.
- [69] G B Benedek. On the molecular basis for micellar formation and growth. In D Degiorgo and M Corti, editors, *Proceedings of the International School of Physics 'Enrico Fermi' - Physics of Amphiphiles: Micelles, Vesicles and Microemulsions*, pages 223–236. Italian Physical Society, 1985.

## BIBLIOGRAPHY

- [70] D Blankschtein, G M Thurston, and G B Benedeck. Phenomenological theory of equilibrium thermodynamic properties and phase separation of micellar solutions. *J. Chem. Phys.*, 85(12):7268–7288, 1986.
- [71] R E Goldstein. Model for phase equilibria in micellar solutions of nonionic surfactants. *J. Chem. Phys.*, 84(6):3367–3378, 1986.
- [72] B Widom. Lattice-gas model of amphiphiles and their orientation at interfaces. *J. Chem. Phys.*, 88(26):6508–6514, 1984.
- [73] B Widom. Correlation and scattering functions in a lattice model of oil-water-amphiphile solutions. *J. Chem. Phys.*, 90(4):2437–2443, 1989.
- [74] K A Dawson. Interfaces between phases in a lattice model of microemulsions. *Phys. Rev. A*, 35(4):1766–1773, 1987.
- [75] K A Dawson, B L Walker, and A Berera. Accounting for fluctuations in a lattice model of microemulsions. *Physica A*, 165(3):320–351, 1990.
- [76] K A Dawson. Lattice model of amphiphilic assembly. *Pure & Appl. Chem.*, 64(11):1589–1602, 1992.
- [77] D Stauffer and N Jan. Comment on ising-type models for microemulsions and micellar solutions. *J. Chem. Phys.*, 87(10):6210–6211, 1987.
- [78] K A Dawson, M D Lipkin, and B Widom. Reply to 'comment on ising-type models for microemulsions and micellar solutions'. *J. Chem. Phys.*, 87(10):6211–6212, 1987.
- [79] A Hansen, M Schick, and D Stauffer. Generalised widom model of amphiphilic systems. *Phys. Rev. A*, 44(6):3686–3691, 1991.

## BIBLIOGRAPHY

- [80] M Blume, V J Emery, and R B Griffiths. Ising model for the  $\lambda$  transition and phase separation in  $\text{He}^3$  -  $\text{He}^4$  mixtures. *Phys. Rev. A*, 4(3):1071–1077, 1971.
- [81] M Schick and W H Shih. Spin-1 model of a microemulsion. *Phys. Rev. B*, 34(3):1797–1801, 1986.
- [82] G Gompper and M Schick. Lattice model of microemulsions. *Phys. Rev. B*, 41(13):9148–9162, 1990.
- [83] M Laradji, H Guo, M Grant, and M J Zuckermann. Phase diagram of a lattice model for ternary mixtures of water, oil and surfactants. *Phys. Rev. A*, 44(12):8184–8188, 1991.
- [84] S Alexander. A lattice gas model for microemulsions. *J. Physique*, 39(1):L1–L3, 1978.
- [85] K Chen, C Ebner, C Jayaprakash, and R Pandit. Microemulsions in oil-water-surfactant mixtures: an ising lattice gas model. *J. Phys. C*, 20(17):L361–L366, 1987.
- [86] W Haan and R Pratt. Monte Carlo study of a simple model for micelle structure. *Chem. Phys. Lett.*, 79(3):436–440, 1981.
- [87] F T Wall and F Mandel. Macromolecular dimensions obtained by an efficient Monte Carlo method without sample attrition. *J. Chem. Phys.*, 63(11):4592–4595, 1975.
- [88] S Karaborni and J P O'Connell. *Surfactants in Solution*, volume 11, pages 83–94. Plenum Press, New York, 1991.
- [89] S Karaborni and J P O'Connell. Molecular dynamics simulations of model chain molecules and aggregates including surfactants and micelles. *Tenside Surf. Det.*, 30(4):235–242, 1993.

## BIBLIOGRAPHY

- [90] R G Larson, L E Scriven, and H T Davis. Monte Carlo simulations of model amphiphile-oil-water systems. *J. Chem. Phys.*, 83(5):2411–2420, 1985.
- [91] H Tompa. *Polymer Solutions*. Academic Press, New York, 1956.
- [92] R G Larson. Monte Carlo lattice simulation of amphiphilic systems in two and three dimensions. *J. Chem. Phys.*, 89(3):1642–1650, 1988.
- [93] R G Larson. Self-assembly of surfactant liquid crystalline phases by Monte Carlo simulation. *J. Chem. Phys.*, 91(4):2479–2488, 1989.
- [94] P Kekicheff and G J T Tiddy. Structure of the intermediate phase and its transformation to lamellar phase in the lithium perfluorooctanoate/water system. *J. Phys. Chem.*, 93(6):2520–2526, 1989.
- [95] A T Bernardes, V B Henriques, and P M Bisch. Monte Carlo simulation of a lattice model for micelle formation. *J. Chem. Phys.*, 101(1):645–650, 1994.
- [96] B Smit, P A J Hilbers, K Esselink, L A M Ruppert, N M van Os, and A G Schlijper. Computer simulations of a water/oil interface in the presence of micelles. *Nature*, 348(6302):624–625, 1990.
- [97] B Smit, P A J Hilbers, K Esselink, L A M Ruppert, N M van Os, and A G Schlijper. Structure of a water/oil interface in the presence of micelles: A computer simulation study. *J. Phys. Chem.*, 95(16):6361–6368, 1991.
- [98] B Smit, K Esselink, P A J Hilbers, N M van Os, L A M Ruppert, and I Szleifer. Computer simulations of surfactant self-assembly. *Langmuir*, 9(1):9–11, 1993.
- [99] D Kramer, D Ben-Shaul, Z Y Chen, and W M Gelbart. Monte Carlo and mean field studies of successive phase transitions in rod monolayers. *J. Chem. Phys.*, 96(3):2236–2252, 1992.

## BIBLIOGRAPHY

- [100] J Harris and S A Rice. A lattice model of a supported monolayer of amphiphile molecules: Monte Carlo simulations. *J. Chem. Phys.*, 88(2):1298–1306, 1988.
- [101] L Steehuizen, D Kramer, and A Ben-Shaul. Statistical thermodynamics of molecular organisation in the inverse hexagonal phase. *J. Phys. Chem.*, 95(19):7477–7483, 1991.
- [102] K A Dill, D E Koppel, R S Cantor, J D Dill, D Bendedouch, and S H Chen. Molecular conformations in surfactant micelles. *Nature*, 309(5963):42–45, 1984.
- [103] T Haliloglu and W L Mattice. Monte Carlo lattice simulation of the interchange of chains between micelles of diblock copolymers. *Chem. Eng. Sci.*, 49(17):2851–2857, 1994.
- [104] C M Care. Cluster size distribution in a Monte Carlo simulation of the micellar phase of an amphiphile and solvent mixture. *J. Chem. Soc. Faraday Trans. 1*, 83(9):2905–2912, 1987.
- [105] A J C Ladd. Molecular dynamics. In C R A Catlow, S C Parker, and M P Allen, editors, *Computer Modelling of Fluids, Polymers and Solids*, pages 55–82. Kluwer Academic Publishers, 1990.
- [106] N Metropolis, A W Rosenbluth, M N Rosenbluth, A H Teller, and E Teller. Equation of state calculations by fast computing machines. *J. Chem. Phys.*, 21(6):1087–1092, 1953.
- [107] D Chandler. *Introduction to Modern Statistical Mechanics*. Oxford University Press, 1987.
- [108] D Frenkel. Monte Carlo simulations. In C R A Catlow, S C Parker, and M P Allen, editors, *Computer Modelling of Fluids, Polymers and Solids*, pages 83–123. Kluwer Academic Publishers, 1990.

## BIBLIOGRAPHY

- [109] J C Owicki and H A Scheraga. Preferential sampling near solutes in Monte Carlo calculations on dilute solutions. *Chemical Physics Letters*, 47(3):600–602, 1977.
- [110] J C Owicki. Optimisation of sampling algorithms in Monte Carlo calculations on fluids. *ACS Symposium Series: Computer Modelling of Matter*, 86:159–171, 1978.
- [111] K Binder and D W Heermann. *Monte Carlo Simulation in Statistical Physics: an Introduction*. Springer-Verlag, 1988.
- [112] I Carmesin and K Kremer. The bond fluctuation model: a new effective algorithm for the dynamics of polymers in all spatial dimensions. *Macromolecules*, 21(9):2819–2823, 1988.
- [113] A L Rodriguez, H P Wittmann, and K Binder. Orientational ordering in two-dimensional polymer solutions: Monte Carlo simulations of a bond fluctuation model. *Macromolecules*, 23(19):4327–4335, 1990.
- [114] N Madras and A D Sokal. The pivot algorithm: a highly efficient Monte Carlo method for the self-avoiding walk. *J. Stat. Phys.*, 50(1):109–188, 1988.
- [115] A Z Panagiotopoulos. Direct determination of phase coexistence properties of fluid by Monte Carlo simulations in a new ensemble. *Mol. Phys.*, 61(4):813–826, 1987.
- [116] K K Mon and K Binder. Finite size effects for the simulation of phase co-existence in the Gibbs ensemble near the critical point. *J. Chem. Phys.*, 96:6989–6995, 1992.
- [117] A Baumgärtner. Simulation of polymer motion. *Ann. Rev. Phys. Chem.*, 35:419–435, 1984.
- [118] K Kremer and K Binder. Monte Carlo simulations of lattice models for macromolecules. *Computer Physics Reports*, 7(6):259–312, 1988.

## BIBLIOGRAPHY

- [119] K Kremer and G S Grest. Simulations for structural and dynamic properties of dense polymer systems. *J. Chem. Soc. Faraday Trans.*, 88(13):1707–1717, 1992.
- [120] M N Rosenbluth and A W Rosenbluth. Monte Carlo calculation of the average extension of molecular chains. *J. Chem. Phys.*, 23(2):356–359, 1955.
- [121] J I Siepmann. A method for the direct calculation of chemical potentials for dense chain systems. *Mol. Phys.*, 70(6):1145–1159, 1990.
- [122] B Widom. Some topics in the theory of fluids. *J. Chem. Phys.*, 39(11):2808–2812, 1963.
- [123] P J Flory. *Statistical Mechanics of Chain Molecules*. Oxford University Press, 2nd edition, 1988.
- [124] J-P Hansen and I R McDonald. *Theory of Simple Liquids*. Academic Press, 2nd edition, 1990.
- [125] M Bishop and S Frinks. Error analysis in computer simulations. *J. Chem. Phys.*, 87(6):3675–3676, 1987.
- [126] P R Bevington. *Data Reduction and Error Analysis for the Physical Sciences*. McGraw-Hill, inc, 1969.
- [127] D Frenkel and G C A M Mooij. How to optimise configurational-bias Monte Carlo. *Information Quarterly for Computer Simulation of Condensed Phases (Daresbury Laboratory)*, February(40):15–23, 1994.
- [128] R F Rapold and W L Mattice. New high-coordination lattice model for rotational isomeric state polymer chains. *J. Chem. Soc. Faraday Trans.*, 91(16):2435–2441, 1995.

## BIBLIOGRAPHY

- [129] D Brindle. *Lattice Models of Amphiphile and Solvent Mixtures*. PhD thesis, School of Science, Sheffield City Polytechnic, 1991.
- [130] D Frenkel. The simulation of entropic phase transitions. *J. Phys. : Condens. Matter*, 6:A71–A78, 1994.
- [131] J N Israelachvili and H Wennerström. Entropic forces between amphiphilic surfaces in liquids. *J. Phys. Chem*, 96(2):520–531, 1992.
- [132] I F Uchegbu, J A Bouwstra, and T Florence. Large disk-shaped structures (discomes) in nonionic surfactant vesicle to micelle transitions. *J. Phys. Chem.*, 96(25):10548–10553, 1992.
- [133] G Gompper, J Goos, and M Kraus. Internal structure of microemulsions and sponge phases. *Ber. Bunsenges. Phys. Chem.*, 98(3):501–503, 1994.
- [134] D Roux, C Coulon, and M E Cates. Sponge phases in surfactant solutions. *J. Phys. Chem.*, 96(11):4174–4187, 1992.
- [135] B D Simons and M E Cates. Vesicles and onion phases in dilute surfactant solutions. *J. Phys. II France*, T2(7):1439–1451, 1992.
- [136] J-M Drouffe, A C Maggs, and S Leibler. Computer simulations of self-assembled membranes. *Science*, 254(5036):1353–1356, 1991.
- [137] P Mukerjee. The size distribution of small and large micelles: a multiple equilibrium analysis. *J. Phys. Chem.*, 76(4):565–570, 1972.
- [138] N Kamenka, G Haouche, B Faucompré, B Brun, and B Lindman. Dodecylbetaine micelle formation from fourier-transform H1-NMR and tracer self-diffusion studies. *J. Colloid Interface Sci.*, 108(2):451–456, 1985.

## BIBLIOGRAPHY

- [139] G Gunnarsson, B Jönsson, and H Wennerström. Surfactant association into micelles. an electrostatic approach. *J. Phys. Chem.*, 84(23):3114–3121, 1980.
- [140] B Lindman, M-C Puyal, N Kamenka, Brun B, and G Gunnarsson. Micelle formation of ionic surfactants. tracer self-diffusion studies and theoretical calculations for sodium p-octylbenzenesulfonate. *J. Phys. Chem.*, 86(9):1702–1711, 1982.
- [141] W M Gelbart, A Ben-Shaul, A Masters, and W E McMullen. Effects of interaggregate forces on micellar size in isotropic and aligned phases. In D Degiorgo and M Corti, editors, *Proceedings of the International School of Physics ‘Enrico Fermi’ - Physics of Amphiphiles: Micelles, Vesicles and Microemulsions*, pages 394–403. Italian Physical Society, 1985.
- [142] W H Press, S A Teukolsky, W T Vetterling, and B P Flannery. *Numerical Recipes in Fortran — The Art of Scientific Programming*. Cambridge University Press, 2nd edition, 1992.
- [143] V Degiorgio. Nonionic micelles. In D Degiorgo and M Corti, editors, *Proceedings of the International School of Physics ‘Enrico Fermi’ - Physics of Amphiphiles: Micelles, Vesicles and Microemulsions*, pages 303–335. Italian Physical Society, 1985.
- [144] K Kumiyama, H Inoue, and T Nakagawa. *Kolloid-Z-n-Z Polymere*, 183:68, 1962.
- [145] D Attwood. A light-scattering study of the effect of temperature on the micellar size and shape of a nonionic detergent in aqueous solution. *J. Phys. Chem.*, 72(1):339–345, 1968.
- [146] R H Ottewill, C C Storer, and T Walker. Ultracentrifugal study of a non-ionic surface-active agent in D<sub>2</sub>O. *Trans. Faraday Soc.*, 63:2796–2802, 1967.

## BIBLIOGRAPHY

- [147] S Puvvada and D Blanckstein. Molecular-thermodynamic approach to predict micellisation: Phase behaviour and phase separation of micellar solutions: 1. application to nonionic surfactants. *J. Chem. Phys.*, 92(6):3710–3724, 1990.
- [148] T M Herrington and S S Sahi. Temperature-dependence of the micellar aggregation number of n-dodecylpolyethyleneoxide surfactants. *J. Colloid Interface Sci.*, 121(1):107–120, 1988.
- [149] P J Missel, N A Mazer, G B Benedeck, C Y Young, and M C Carey. Thermodynamic analysis of the growth of sodium dodecyl sulfate micelles. *J. Phys. Chem.*, 84(9):1044–1057, 1980.
- [150] D Attwood, P H Elworthy, and S B Kayne. Membrane osmometry of aqueous micellar solutions of pure nonionic and ionic surfactants. *J. Phys. Chem.*, 74(19):3529–3534, 1970.
- [151] J Swarbrick and J Daruwala. Micellar aggregation properties of some zwitterionic betaines. *J. Phys. Chem.*, 74(6):1293–1296, 1970.
- [152] J-C Desplat, T Dalby, and C M Care. A study of micelle formation by Monte Carlo simulation, 1995. Poster presented at the annual meeting of the Institute Of Physics.
- [153] J-C Desplat and C M Care. A Monte Carlo simulation of the micellar phase of an amphiphile and solvent mixture. *Mol. Phys.*, 87(2):441–453, 1996.
- [154] C M Care and J-C Desplat. Micelle formation in a lattice model of an amphiphile and solvent mixture. In American Chemical Society, editor, *American Chemical Society, Division of Colloid & Surface Chemistry, 210 ACS National Meeting*, 1995.

# Appendix A

## Appendix

This appendix contains ancilliary figures related to the study in the 'vesicle region' (see chapter 7).

### A.1 Average number of cavity

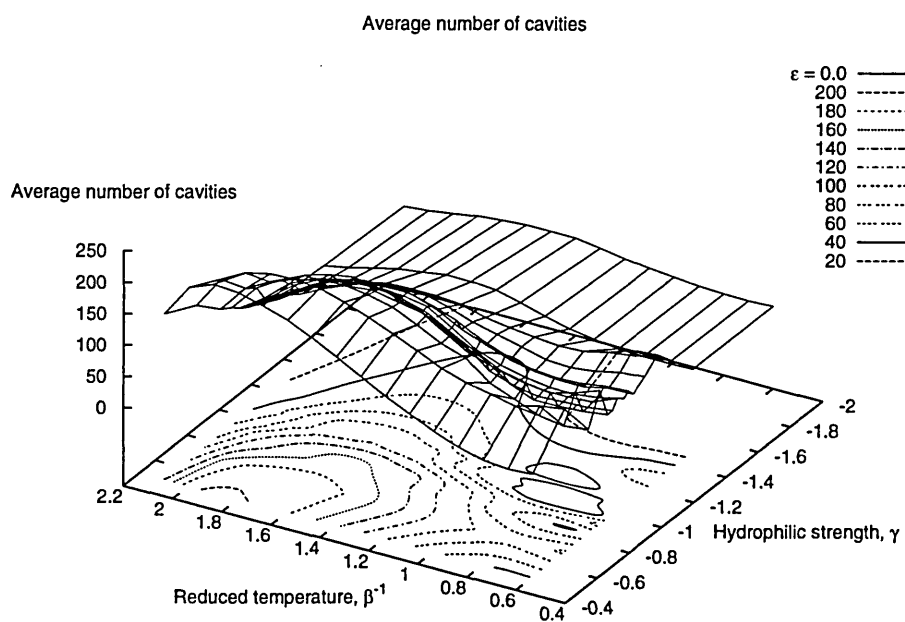


Figure A.1: Average number of cavity ( $\epsilon = 0.0$ )

APPENDIX A. APPENDIX

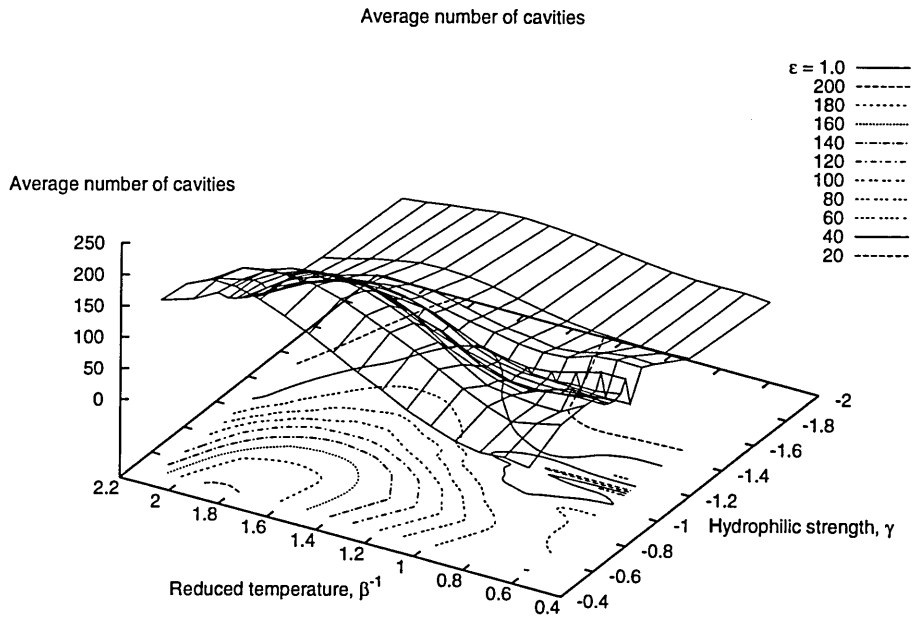


Figure A.2: Average number of cavity ( $\epsilon = 1.0$ )

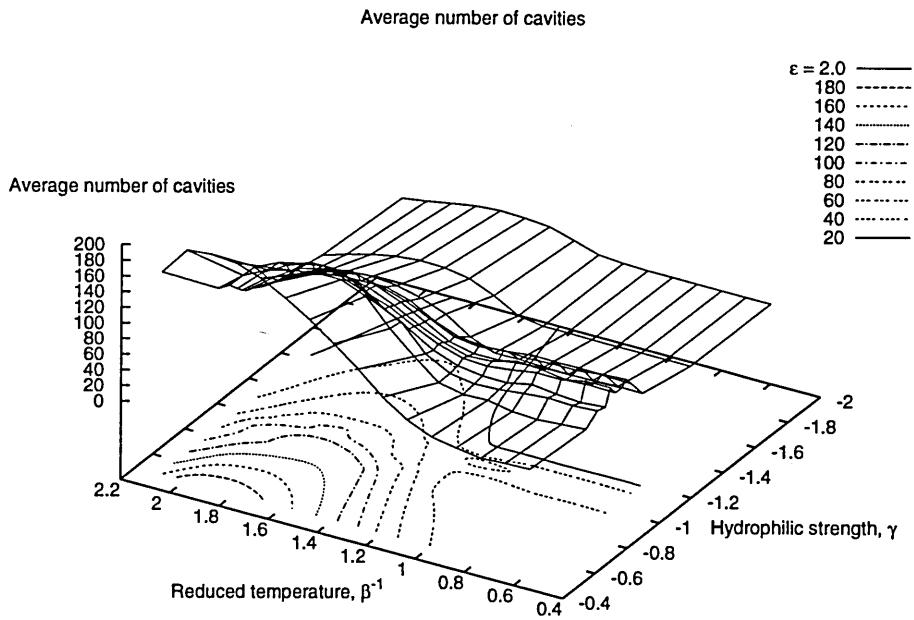


Figure A.3: Average number of cavity ( $\epsilon = 2.0$ )

## A.2 Average cavity size

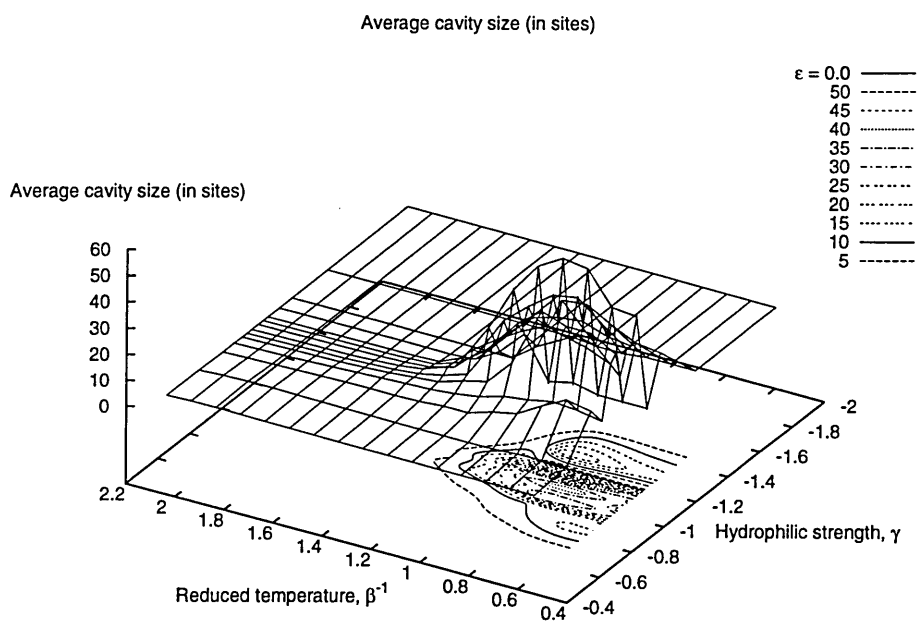


Figure A.4: Average cavity size ( $\epsilon = 0.0$ )

APPENDIX A. APPENDIX

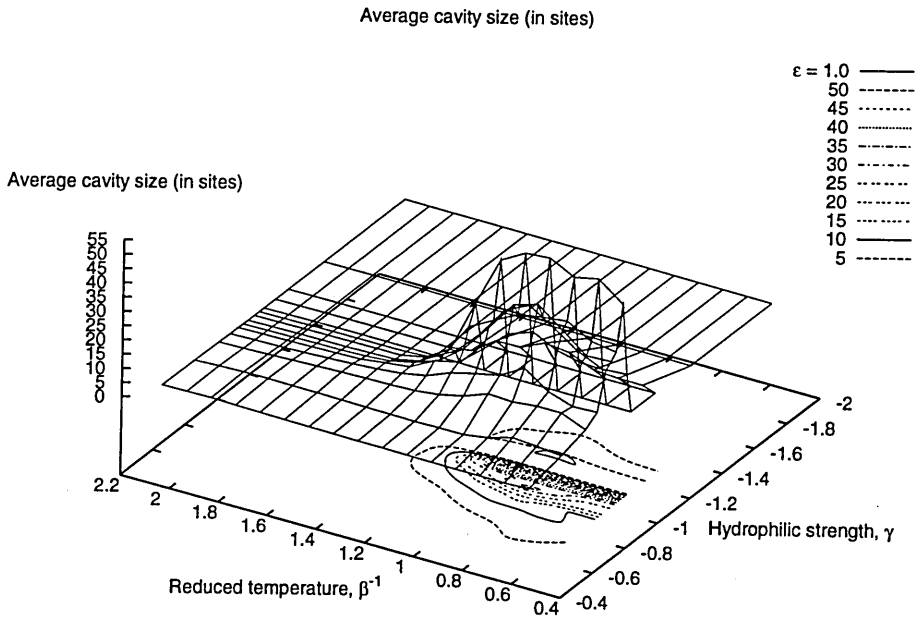


Figure A.5: Average cavity size ( $\epsilon = 1.0$ )

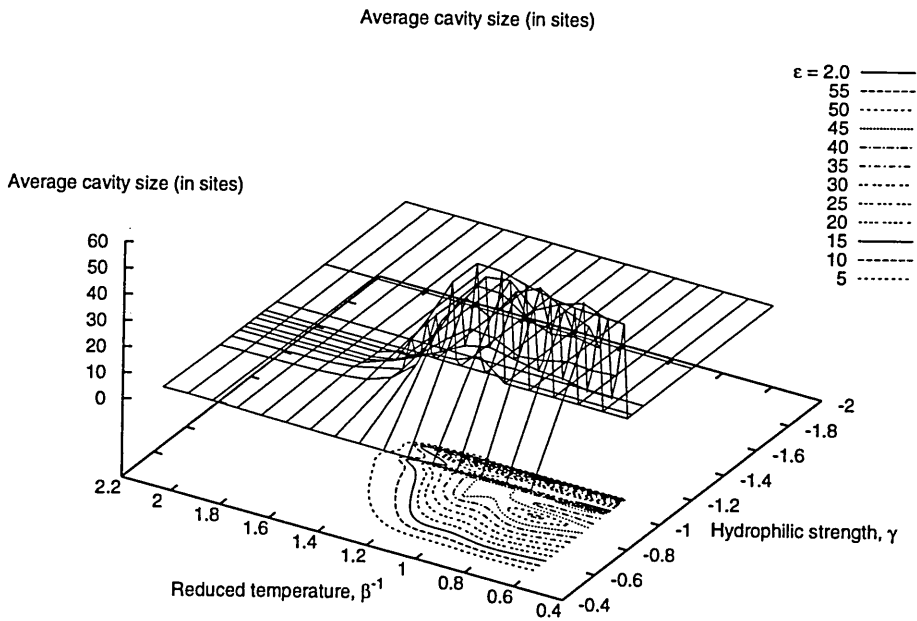


Figure A.6: Average cavity size ( $\epsilon = 2.0$ )

### A.3 Average volume fraction of enclosed solvent

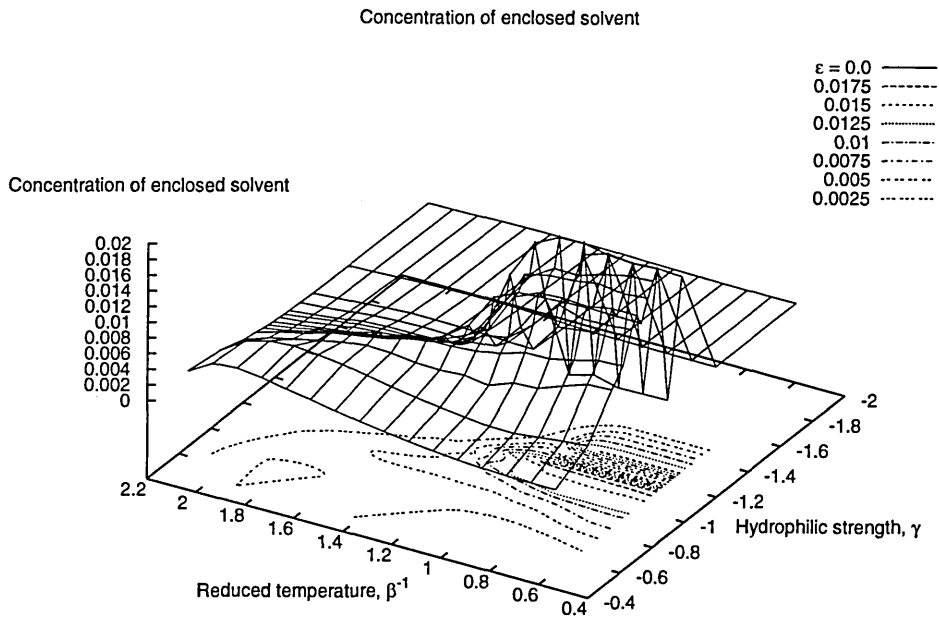


Figure A.7: Average volume fraction of enclosed solvent ( $\varepsilon = 0.0$ )

APPENDIX A. APPENDIX

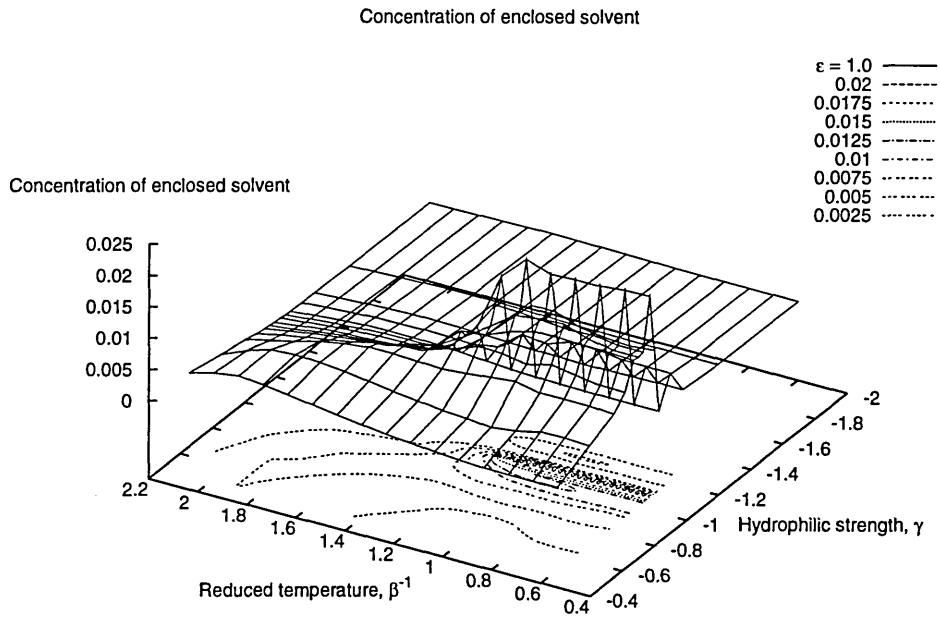


Figure A.8: Average volume fraction of enclosed solvent ( $\epsilon = 1.0$ )

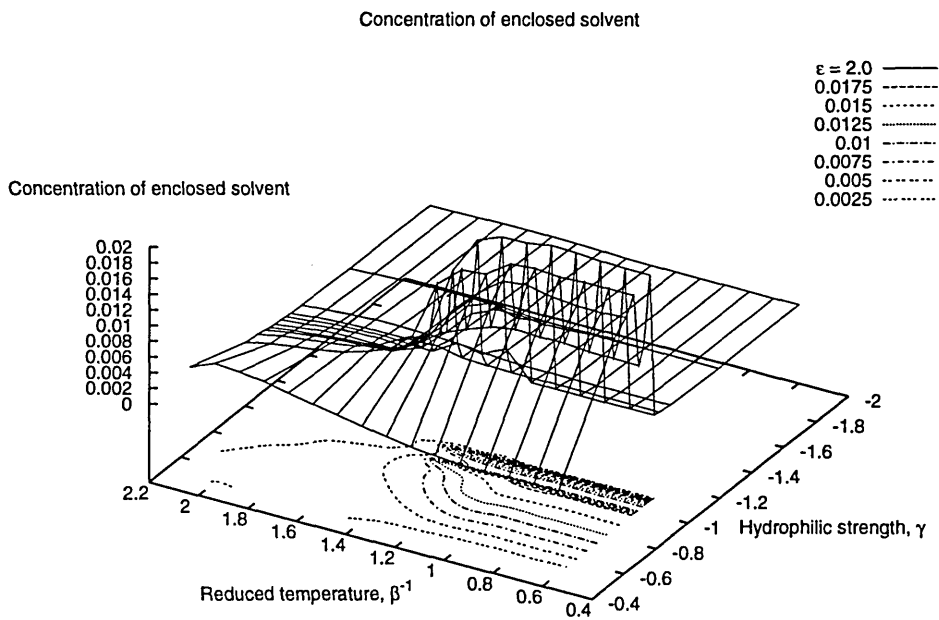


Figure A.9: Average volume fraction of enclosed solvent ( $\epsilon = 2.0$ )

### A.4 Normalised average number of external interactions

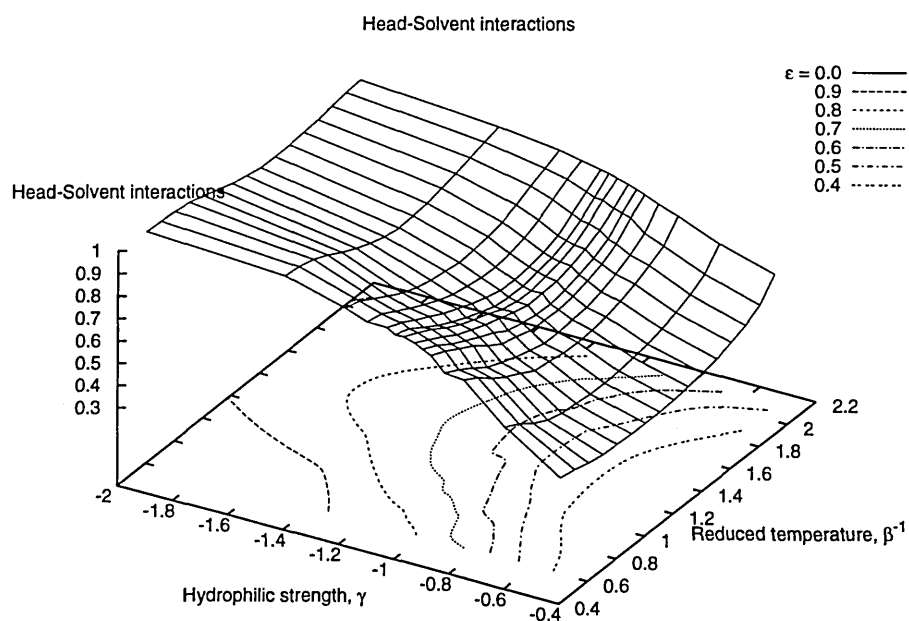


Figure A.10: Normalised average number of *HS* interactions ( $\epsilon = 0.0$ )

APPENDIX A. APPENDIX

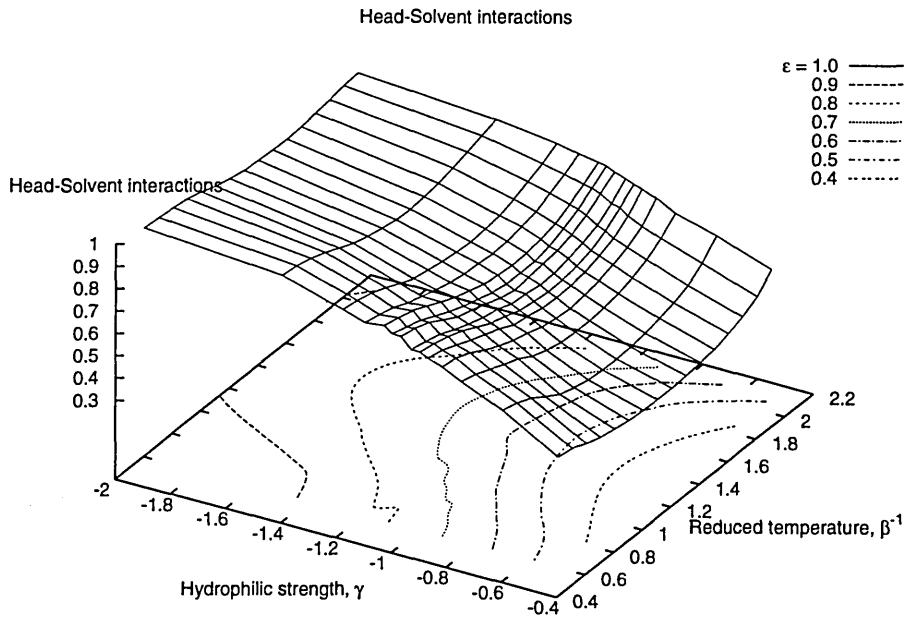


Figure A.11: Normalised average number of *HS* interactions ( $\epsilon = 1.0$ )

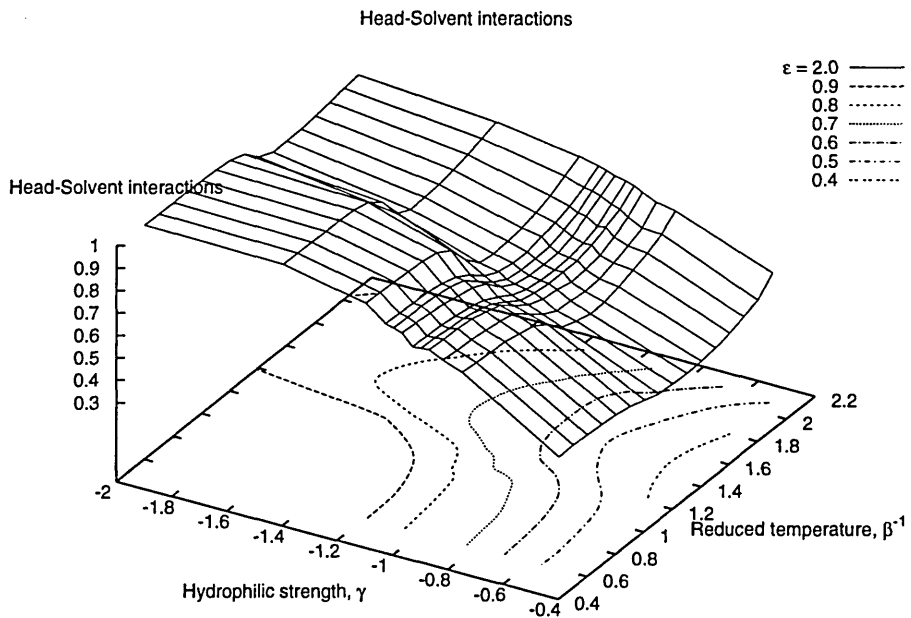


Figure A.12: Normalised average number of *HS* interactions ( $\epsilon = 2.0$ )

APPENDIX A. APPENDIX

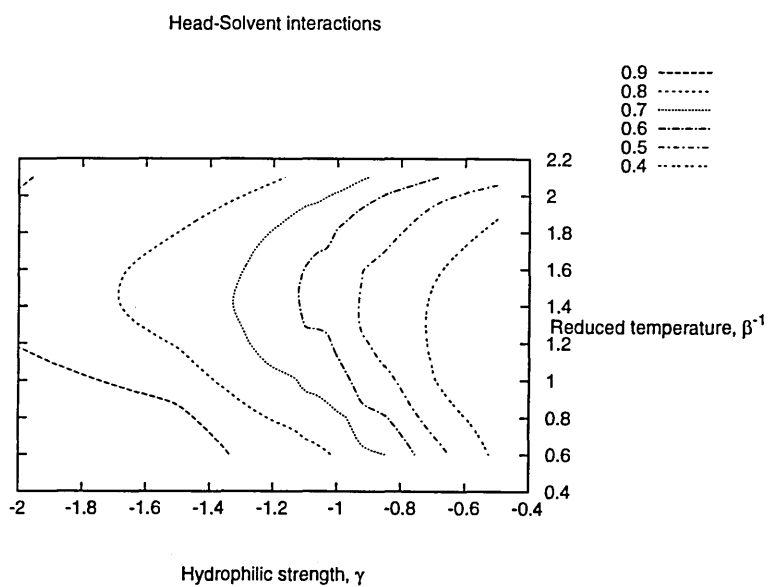


Figure A.13: Normalised average number of *HS* interactions ( $\epsilon = 0.0$ )

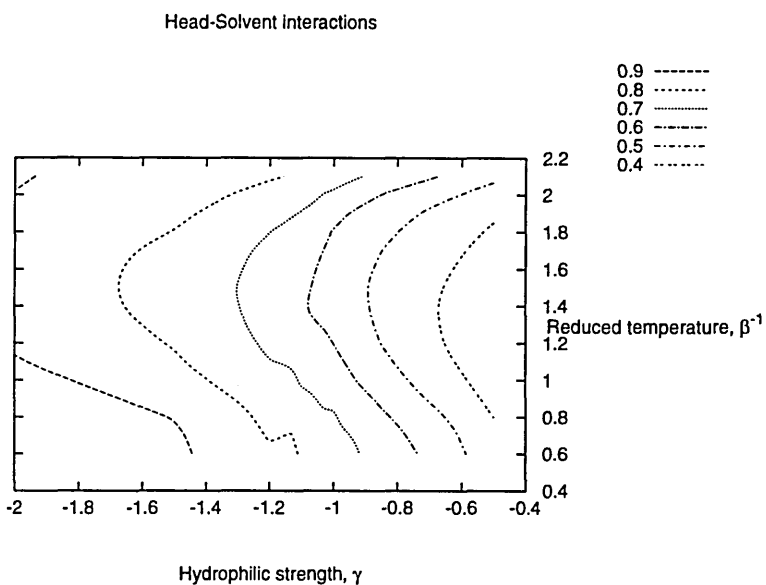


Figure A.14: Normalised average number of *HS* interactions ( $\epsilon = 1.0$ )

APPENDIX A. APPENDIX

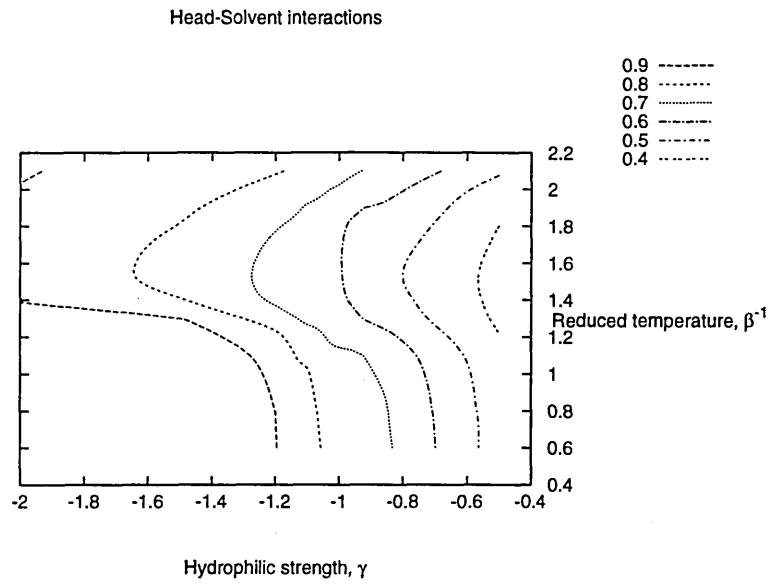


Figure A.15: Normalised average number of *HS* interactions ( $\epsilon = 2.0$ )

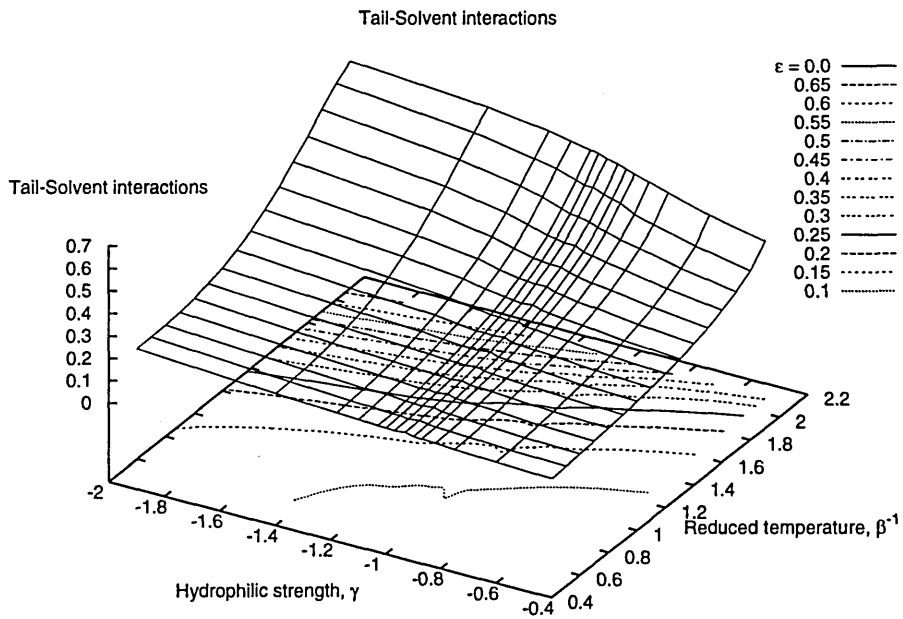


Figure A.16: Normalised average number of *TS* interactions ( $\epsilon = 0.0$ )

# APPENDIX A. APPENDIX

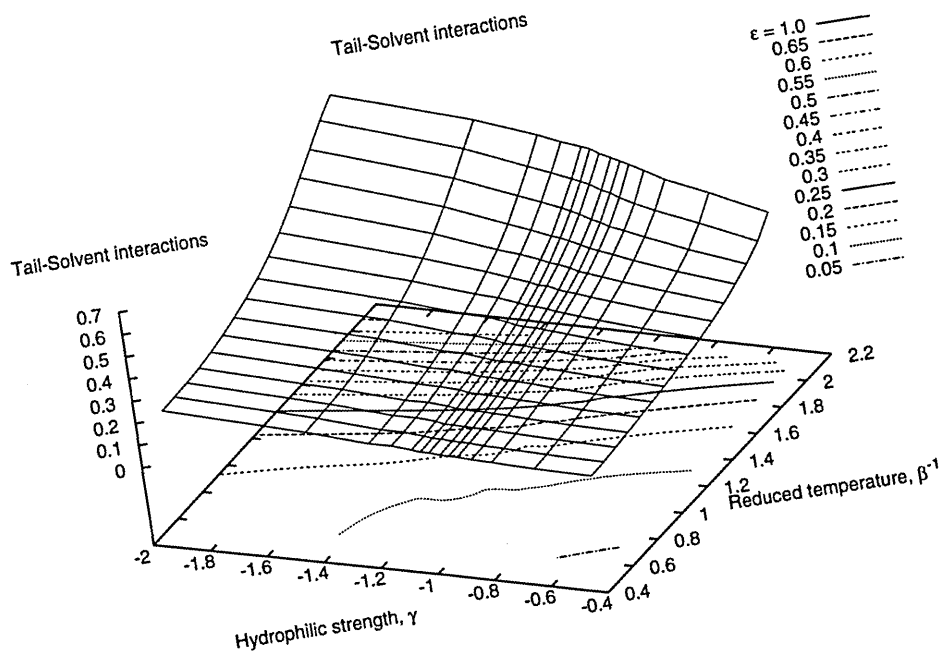


Figure A.17: Normalised average number of *TS* interactions ( $\epsilon = 1.0$ )

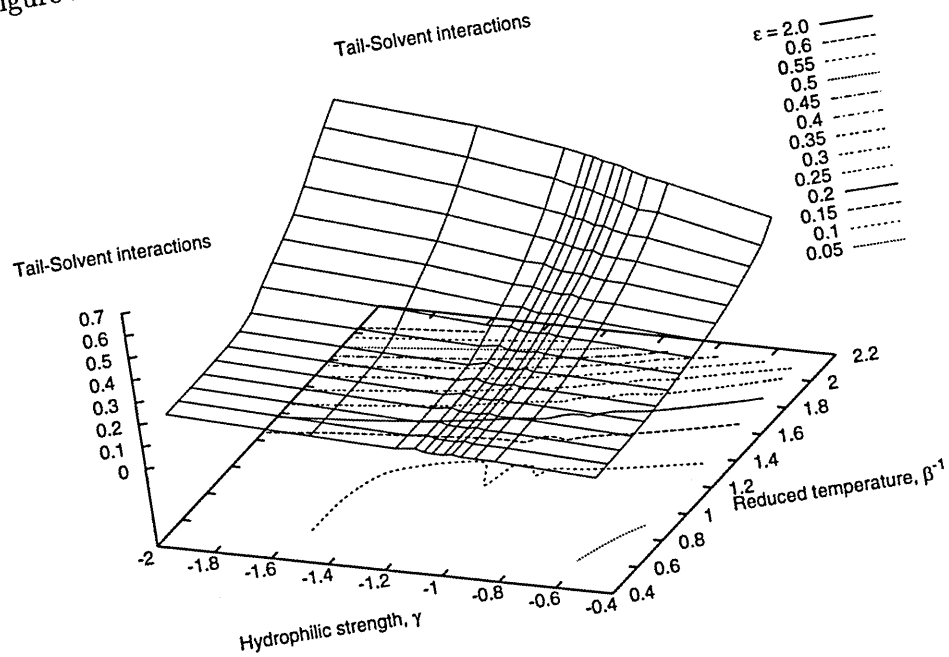


Figure A.18: Normalised average number of *TS* interactions ( $\epsilon = 2.0$ )

APPENDIX A. APPENDIX

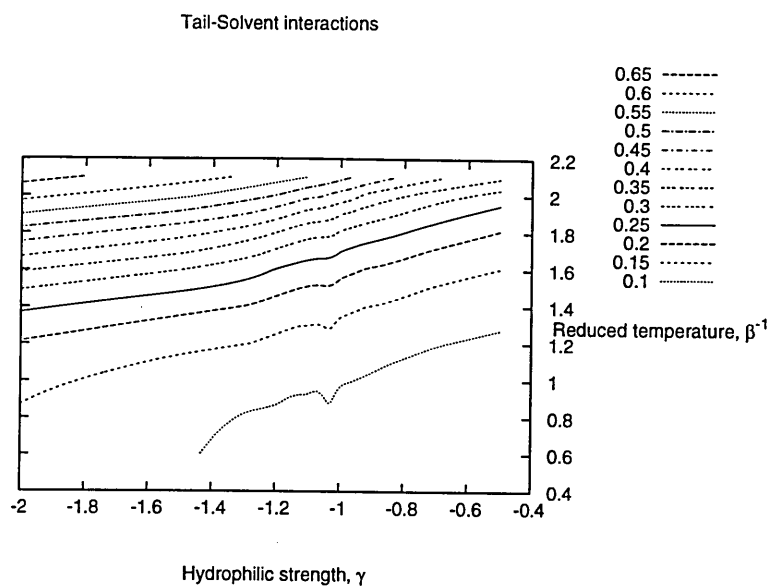


Figure A.19: Normalised average number of *TS* interactions ( $\epsilon = 0.0$ )

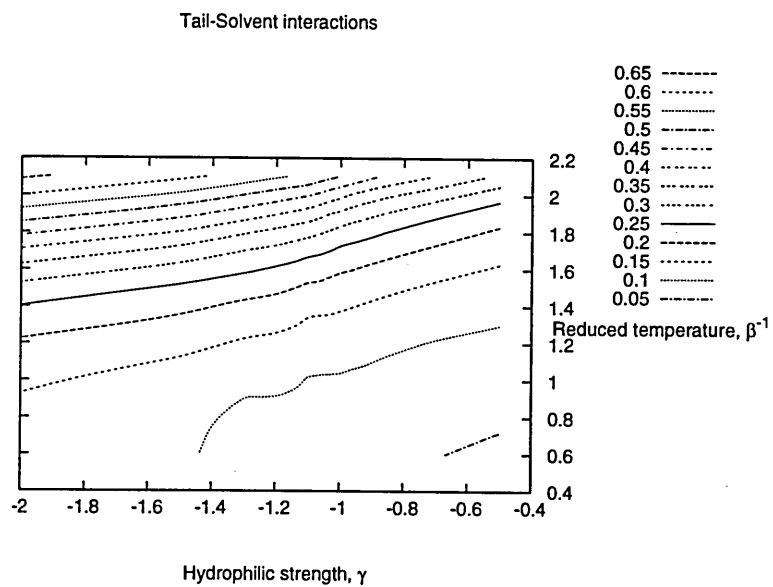


Figure A.20: Normalised average number of *TS* interactions ( $\epsilon = 1.0$ )

APPENDIX A. APPENDIX

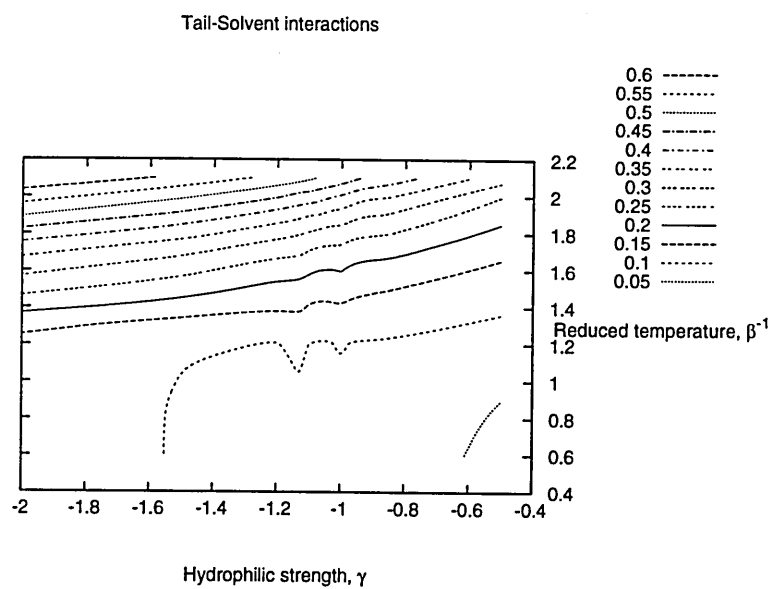


Figure A.21: Normalised average number of *TS* interactions ( $\epsilon = 2.0$ )

### A.5 Mean aggregation number

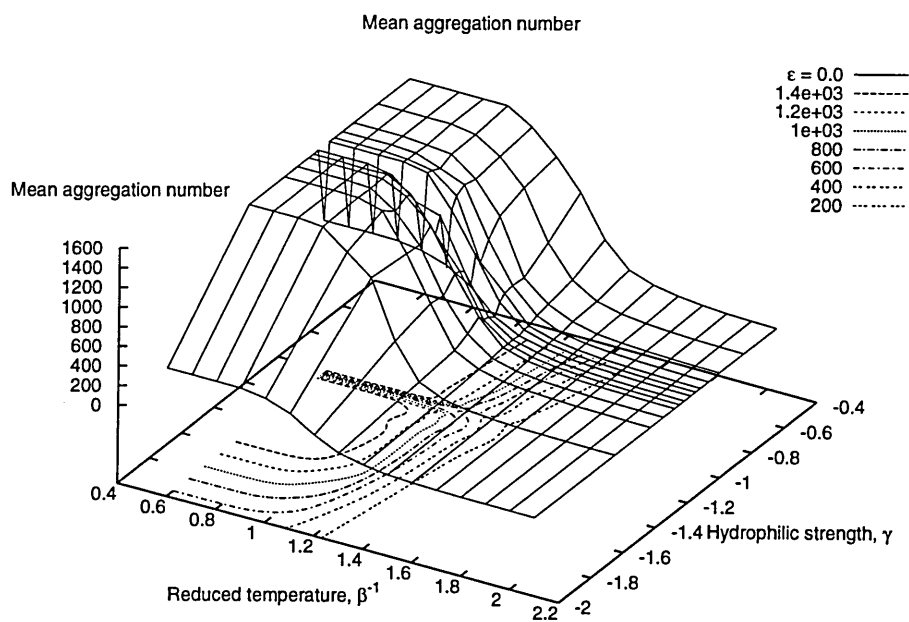


Figure A.22: Mean aggregation number,  $N_n(\epsilon = 0.0)$

APPENDIX A. APPENDIX

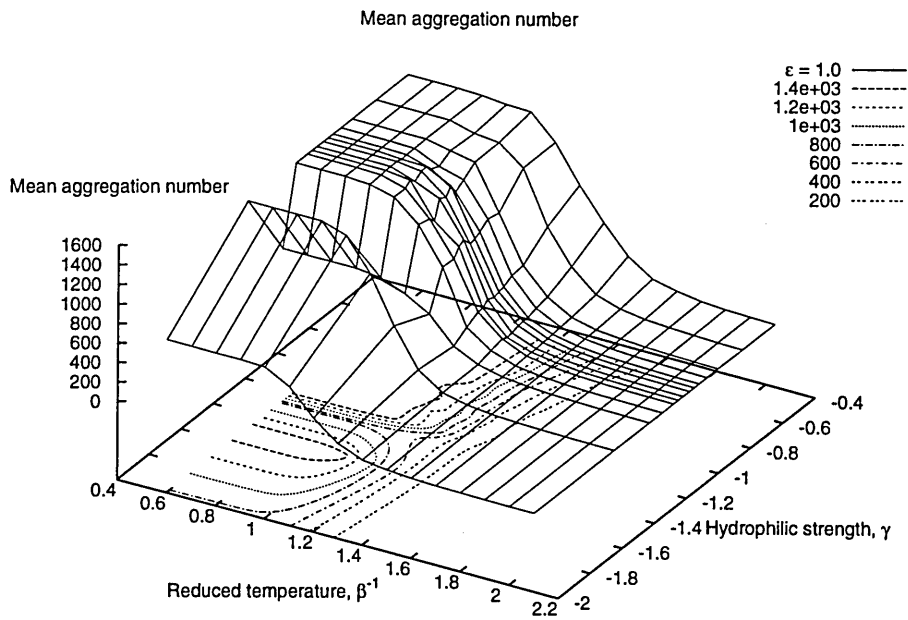


Figure A.23: Mean aggregation number,  $N_n(\epsilon = 1.0)$

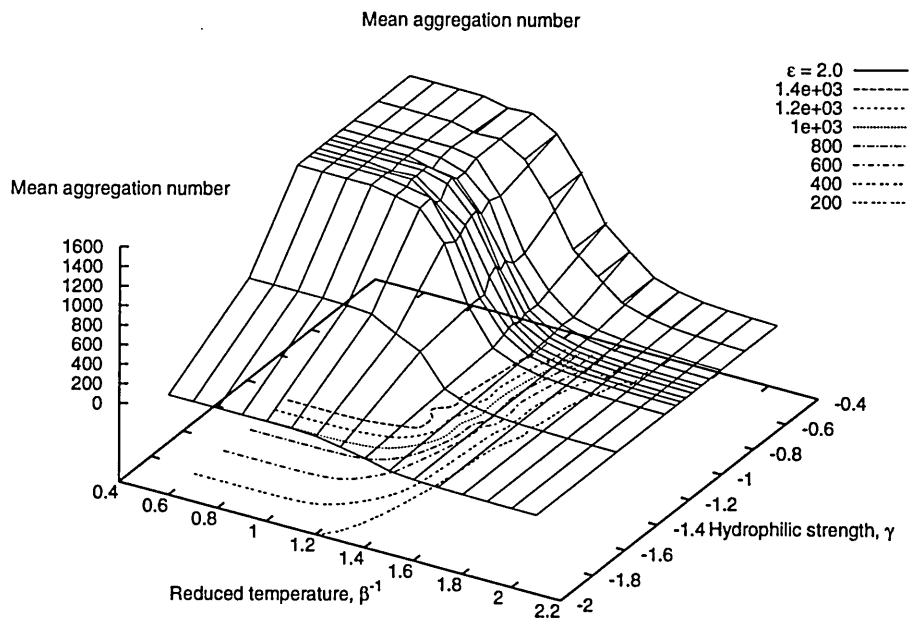


Figure A.24: Mean aggregation number,  $N_n(\epsilon = 2.0)$

APPENDIX A. APPENDIX

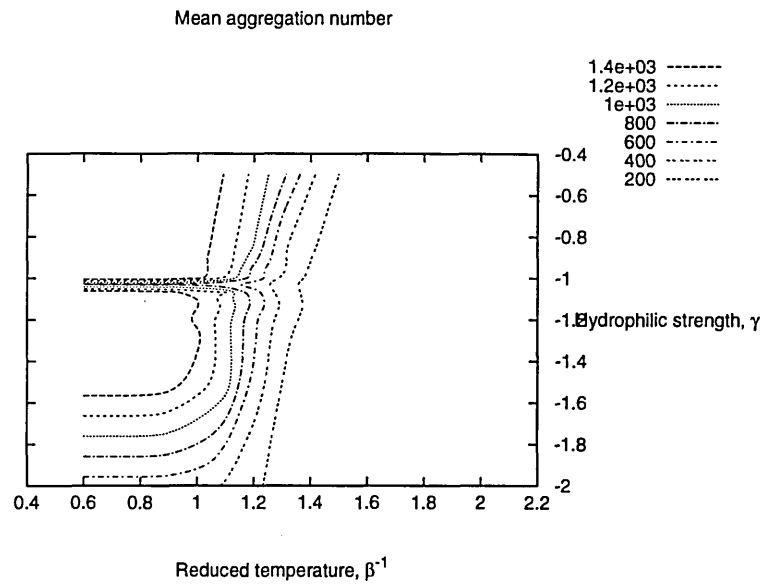


Figure A.25: Mean aggregation number,  $N_n(\epsilon = 0.0)$

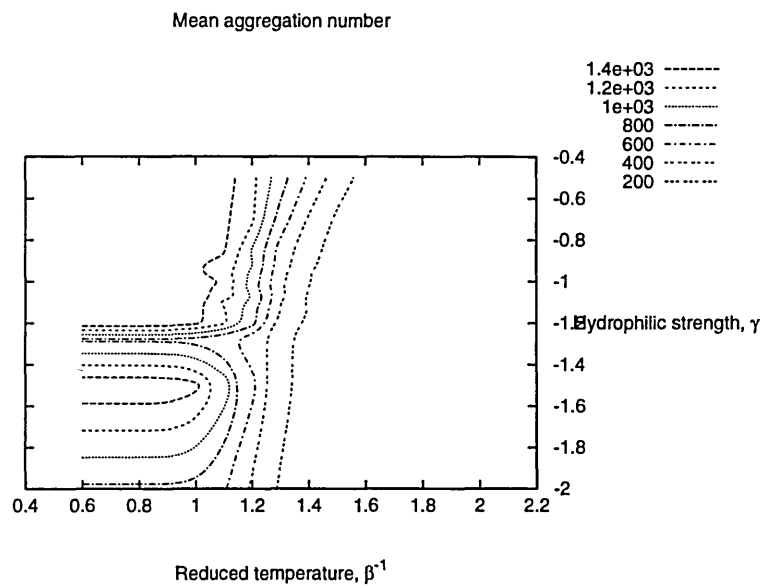


Figure A.26: Mean aggregation number,  $N_n(\epsilon = 1.0)$

APPENDIX A. APPENDIX

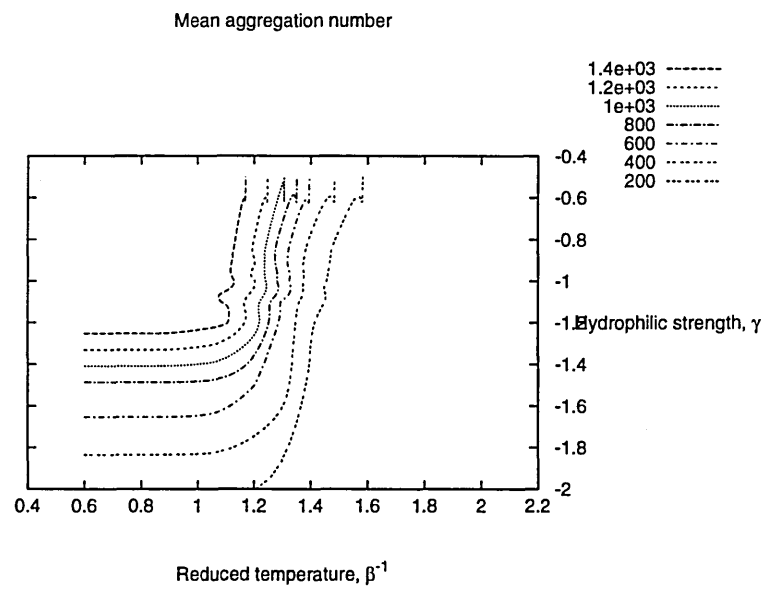


Figure A.27: Mean aggregation number,  $N_n(\varepsilon = 2.0)$